

**University of Alberta**

2-D Modeling of Freeze-up Processes on the Athabasca River downstream  
of Fort McMurray, Alberta

by

Agata Maria Wojtowicz

A thesis submitted to the Faculty of Graduate Studies and Research  
in partial fulfillment of the requirements for the degree of

Master of Science

in

Water Resources Engineering

Department of Civil and Environmental Engineering

©Agata Maria Wojtowicz  
Spring, 2010  
Edmonton, Alberta

Permission is hereby granted to the University of Alberta Libraries to reproduce single copies of this thesis and to lend or sell such copies for private, scholarly or scientific research purposes only. Where the thesis is converted to, or otherwise made available in digital form, the University of Alberta will advise potential users of the thesis of these terms.

The author reserves all other publication and other rights in association with the copyright in the thesis and, except as herein before provided, neither the thesis nor any substantial portion thereof may be printed or otherwise reproduced in any material form whatsoever without the author's prior written permission.

## **Examining Committee**

Faye Hicks, Civil and Environmental Engineering

Peter Steffler, Civil and Environmental Engineering

Paul Myers, Earth and Atmospheric Sciences

## **Abstract**

This study is part of a three year project aimed to assess the effects of industrial water withdrawals on the ice regime of the Athabasca River. A 2-D numerical model was used to provide quantitative data for this effort. Freeze-up monitoring was carried out over two years along 80-km of the river from Fort McMurray to Bitumont. Summer bathymetric and winter ice surveys were conducted along with discharge measurements on a 5-km long detailed study reach that exhibited the full range of ice cover initiation processes. The data collected was used to build a *CRISSP2D* river ice process model for the simulation of freeze-up processes. An extensive parametric assessment was carried out to evaluate the capabilities of the model. Although it was not possible to simulate bridging, the simulated border ice agreed very well with field observations. Limitations of the model are addressed and future research recommendations are included.

## **Acknowledgements**

The author would like to thank Dr. Faye Hicks for all of her support and guidance. Thanks are also extended to the entire river ice group: Robyn Andrishak, Chris Krath, Josh Maxwell, Julia Blackburn, Brett Howard, Wendy Howard, and Perry Fedun. For all of their help in the field, thank you to Michael Brayall, Jennifer Nafziger, and David Watson.

The author acknowledges Dr. Peter Steffler from the Water Resources group and Dr. Paul Myers from the Earth and Atmospheric Sciences group. Their participation in such short notice is greatly appreciated.

Funding for this project was provided by the Natural Sciences and Engineering Research Council of Canada, AMEC Earth and Environmental, Alberta Ingenuity Centre for Water Research, and the Cumulative Environmental Management Association; this support is truly appreciated.

For all of their love and support, the author would like to thank her family and her fiancé, Neil Hall.

## Table of Contents

1.	Introduction .....	1
1.1	River Ice Processes.....	2
1.2	Previous Studies .....	4
1.3	Current Study Objectives .....	5
2.	Field Program .....	9
2.1	Introduction .....	9
2.2	Description of Study Reach.....	10
2.3	Summer Field Program .....	10
2.3.1	Bathymetric Surveys .....	12
2.3.2	Water Level Surveys .....	13
2.3.3	Discharge Measurements .....	13
2.4	Freeze-Up Monitoring.....	15
2.4.1	Discharge Data .....	15
2.4.2	Meteorological Data.....	16
2.4.3	Water Temperature Data .....	18
2.4.4	Ice Cover Observations .....	19
2.4.5	Water Level Data.....	23
2.5	Winter Field Program.....	23
2.5.1	Top of Ice Surveys .....	24
2.5.2	Ice Thickness Measurement .....	25
2.5.3	Snow Depth Measurement .....	25
2.5.4	Underwater Video .....	26
2.5.5	Velocity Measurements .....	26
2.5.6	Depth of Water under Ice .....	28
2.5.7	Discharge Measurements .....	29
3.	2-D Ice Process Modeling .....	59
3.1	Introduction .....	59
3.2	Model Description .....	61
3.2.1	Hydrodynamics .....	62

3.2.2	Ice Dynamics .....	66
3.2.3	Thermal Processes .....	67
3.3	Model Testing.....	74
3.3.1	Critical Velocities related to Border Ice Formation .....	75
3.3.2	Channel Constriction .....	77
3.3.3	Channel Constriction with a Steeper Slope .....	78
3.4	Model Application to the Athabasca River .....	79
3.4.1	Geometry and Computational Mesh.....	80
3.4.2	Hydrodynamic Calibration.....	81
3.4.3	Thermal Calibration .....	83
3.4.4	Sensitivity Analysis.....	84
3.4.4.1	Hydrodynamic Parameters .....	85
3.4.4.2	Coupling Time Step.....	86
3.4.4.3	Initial Water Temperature .....	87
3.4.4.4	Border Ice Formation Parameters.....	88
3.4.4.5	Water Temperature and Thermal Growth and Decay of Ice Parameters .....	91
3.4.4.6	Ice Input Parameters .....	93
3.4.4.7	Frazil Rise Velocity Parameter.....	97
3.4.4.8	Ice Cover Formation Parameters .....	98
3.4.5	Border Ice Simulation .....	100
3.4.6	Validation .....	101
4.	Summary and Recommendations .....	136
5.	References .....	141
Appendix A – Summer Discharge Measurement Output from the Acoustic Doppler Current Profiler .....		144
Appendix B – Winter Discharge Measurement Output from the Acoustic Doppler Current Profiler .....		147

## List of Tables

Table 2.1. Water Levels measured during the July 2008 survey.....	13
Table 2.2. Water Levels measured during the August 2008 survey.....	13
Table 2.3. Summary of location, orientation and duration of digital time lapse cameras, 2008. ....	20
Table 2.4. Ice concentration measured during the freeze-up period at M268.1.....	22
Table 2.5. Average values of the ‘top of ice’ elevation survey.....	25
Table 3.1. Details of border ice formation parameter testing in a simple channel.....	75
Table 3.2. Border ice formation parameter defaults, values tested and final values used.....	89
Table 3.3. Water temperature and thermal growth and decay of ice parameter defaults, values tested and final values used.....	92
Table 3.4. Ice input parameter defaults, values tested and final values used. ....	95
Table 3.5. Ice cover formation parameter defaults, values tested and final values used. ....	99

## List of Figures

Figure 1.1.	Mean monthly flows on the Athabasca River at Fort McMurray, Alberta (Data Source: Water Survey of Canada, available record from 1957 to 2008). .....	7
Figure 1.2.	Border ice, pans and rafts on the Athabasca River in Fort McMurray, November 17 <sup>th</sup> , 2008. ....	7
Figure 1.3.	Bridging point at Suncor Bridge on the Athabasca River below Fort McMurray, November 19 <sup>th</sup> , 2008. ....	8
Figure 1.4.	Juxtaposed ice cover on the Athabasca River below Fort McMurray, November 19 <sup>th</sup> , 2008. ....	8
Figure 2.1.	Map of the full study reach from Fort McMurray to Bitumont (adapted from Robichaud, 2003). ....	32
Figure 2.2.	Map of the 5-km detailed study reach. ....	33
Figure 2.3.	Dune bed forms at km 276 on the Athabasca River in the reach downstream of Fort McMurray, November 8, 2008. ....	34
Figure 2.4.	Defining sketch for calculation of bed point elevation (adapted from Meliefste and Hicks, 2005). ....	34
Figure 2.5.	Channel Bathymetry in the detailed study reach (m). ....	35
Figure 2.6.	Discharges reported by Water Survey of Canada (Station 07DA001) throughout freeze-up for the years 2006 to 2008. ....	35
Figure 2.7.	Mean daily air temperatures for 2006 to 2008, as compared to historical (Environment Canada, Fort McMurray Airport). ....	36
Figure 2.8.	Accumulated degree-days of freezing for 2006 to 2008, as compared to historical (Environment Canada, Fort McMurray Airport). ....	36
Figure 2.9.	Water temperatures measured during freeze-up 2007 at M268.1 and M288.1. ....	37
Figure 2.10.	Photograph showing the approximate location of water temperature sensor at M288.1 in 2007. ....	37
Figure 2.11.	Photograph showing the approximate location of water temperature sensor at M268.1 in 2007. ....	38
Figure 2.12.	Water temperatures measured during freeze-up 2008 at M268.1. ....	38

Figure 2.13. Digital time lapse camera placement and orientation in the full study reach (a) 2007, (b) 2008.....	39
Figure 2.14. Examples of photographs taken on November 17, 2008 to document freeze-up in the study reach (a) remote camera (268.1), (b) aerial observations.....	40
Figure 2.15. Ice map based on aerial flight observations made on November 1, 2007.....	41
Figure 2.16. Ice map based on aerial flight observations made on November 9, 2007.....	42
Figure 2.17. Ice map based on aerial flight observations made on November 10, 2007.....	43
Figure 2.18. Ice map based on aerial flight observations made on November 16, 2007.....	44
Figure 2.19. Ice map based on aerial flight observations made on November 8, 2008.....	45
Figure 2.20. Ice map based on aerial flight observations made on November 16, 2008.....	46
Figure 2.21. Ice map based on aerial flight observations made on November 17, 2008.....	47
Figure 2.22. Ice map based on aerial flight observations made on November 19, 2008.....	48
Figure 2.23. Surface ice concentrations measured in the study reach (a) 2007, (b) 2008.....	49
Figure 2.24. Water levels measured during freeze-up 2008 at M268.1.....	50
Figure 2.25. Ice thickness measurements at Site 3 (km 265.7; 110.9 m from left edge of water to right edge of water).....	51
Figure 2.26. Ice thickness measurements at Site 4 (km 265.7; 134.1 m from left edge of water to right edge of water).....	51
Figure 2.27. Ice thickness measurements at Site 5 (km 267.7; 202.9 m from left edge of water to right edge of water).....	52
Figure 2.28. Ice thickness measurements at Site 6 (km 268.7; 309.9 m from left edge of water to right edge of water).....	52
Figure 2.29. Snow depth measurements at Site 3 (km 265.7; 110.9 m from left edge of water to right edge of water).....	53

Figure 2.30. Snow depth measurements at Site 4 (km 265.7; 134.1 m from left edge of water to right edge of water).	53
Figure 2.31. Snow depth measurements at Site 5 (km 267.7; 202.9 m from left edge of water to right edge of water).	54
Figure 2.32. Snow depth measurements at Site 6 (km 268.7; 309.9 m from left edge of water to right edge of water).	54
Figure 2.33. Velocity measurements at Site 3 (km 265.7; 110.9 m from left edge of water to right edge of water).	55
Figure 2.34. Velocity measurements at Site 4 (km 265.7; 134.1 m from left edge of water to right edge of water).	55
Figure 2.35. Velocity measurements at Site 5 (km 267.7; 202.9 m from left edge of water to right edge of water).	56
Figure 2.36. Velocity measurements at Site 6 (km 268.7; 309.9 m from left edge of water to right edge of water).	56
Figure 2.37. Depth of water under ice measurements at Site 3 (km 265.7; 110.9 m from left edge of water to right edge of water).	57
Figure 2.38. Depth of water under ice measurements at Site 4 (km 265.7; 134.1 m from left edge of water to right edge of water).	57
Figure 2.39. Depth of water under ice measurements at Site 5 (km 267.7; 202.9 m from left edge of water to right edge of water).	58
Figure 2.40. Depth of water under ice measurements at Site 6 (km 268.7; 309.9 m from left edge of water to right edge of water).	58
Figure 3.1. Average channel velocity for a flow of 388.0 m <sup>3</sup> /s in a simple trapezoidal channel.	103
Figure 3.2. Border ice formed in a simple trapezoidal channel with critical velocity above which skim ice will not form set to 0.05 m/s	103
Figure 3.3. Border ice formed in a simple trapezoidal channel with critical velocity above which skim ice will not form set to 0.08 m/s	104
Figure 3.4. Border ice formed in a simple trapezoidal channel with critical velocity above which skim ice will not form set to 0.10 m/s	104
Figure 3.5. Ice parcel velocity magnitude for a flow of 25.2 m <sup>3</sup> /s in a simple rectangular channel.	105

Figure 3.6.	Water velocity magnitude for a flow of 25.2 m <sup>3</sup> /s in a simple rectangular channel.....	105
Figure 3.7.	Ice parcel velocity magnitude for a flow of 90.0 m <sup>3</sup> /s in a simple rectangular channel with a steep slope, stopping criterion velocity of 0.1 m/s .....	106
Figure 3.8.	Ice concentration for a flow of 90.0 m <sup>3</sup> /s in a simple rectangular channel with a steep slope, stopping criterion velocity of 0.1 m/s.....	106
Figure 3.9.	Geometry mesh showing boundaries, nodes, triangulation and breaklines.....	107
Figure 3.10.	Computational mesh, showing finer node spacing at narrow and shallow areas.....	108
Figure 3.11.	Water surface elevation profiles for <i>River2D</i> and <i>CRISSP2D</i> .....	109
Figure 3.12.	Velocity comparisons for open water conditions surveyed in July 2008 (a) Site 2 and (b) Site 3.....	110
Figure 3.13.	Velocity comparisons for ice covered conditions surveyed in February 2009 (a) Site 3, (b) Site 4 and (c) Site 5.....	111
Figure 3.14.	Air and water temperatures for the Athabasca River at Fort McMurray, $h_{wa}=10 \text{ W/m}^2/\text{°C}$ (a) 2006, (b) 2007 and (c) 2008.....	112
Figure 3.15.	Ice formation in the channel at 72 hours after ice pans with an ice concentration of 35% have been introduced using a coupling time step of 60 s ( $T_a = -30\text{°C}$ ). .....	113
Figure 3.16.	Ice formation in the channel at 72 hours after ice pans with an ice concentration of 35% have been introduced using a coupling time step of 5 s ( $T_a = -30\text{°C}$ ). .....	113
Figure 3.17.	Frazil concentration present in channel when initial water temperature is set to 0°C. ....	114
Figure 3.18.	Frazil concentration present in channel when initial water temperature is set to -0.1°C.....	114
Figure 3.19.	Water temperature throughout the channel when initial water temperature is set to 0°C. ....	115
Figure 3.20.	Water temperature throughout the channel when initial water temperature is set to -0.1°C.....	115
Figure 3.21.	Ice formation in the channel at 65 hours after ice pans with an ice concentration of 35% have been introduced with the	

critical velocity above which skim ice will not form set to 0.25 m/s ( $T_a = -30^\circ\text{C}$ ).....	116
Figure 3.22. Ice formation in the channel at 65 hours after ice pans with an ice concentration of 35% have been introduced with the critical velocity above which skim ice will not form set to 0.30 m/s ( $T_a = -30^\circ\text{C}$ ).....	116
Figure 3.23. Ice formation in the channel at 65 hours after ice pans with an ice concentration of 35% have been introduced with the critical velocity above which skim ice will not form set to 0.35 m/s ( $T_a = -30^\circ\text{C}$ ).....	117
Figure 3.24. Ice formation in the channel at 65 hours after ice pans with an ice concentration of 35% have been introduced with the critical velocity above which skim ice will not form set to 0.40 m/s ( $T_a = -30^\circ\text{C}$ ).....	117
Figure 3.25. Ice formation in the channel with the coefficient of heat flux for water to air set to $10 \text{ W/m}^2/\text{C}$ ( $T_a \sim$ of $-5^\circ\text{C}$ for 56 hours).....	118
Figure 3.26. Ice formation in the channel with the coefficient of heat flux for water to air set to $15 \text{ W/m}^2/\text{C}$ ( $T_a \sim$ of $-5^\circ\text{C}$ for 56 hours).....	118
Figure 3.27. Ice formation in the channel with the coefficient of heat flux for water to air set to $20 \text{ W/m}^2/\text{C}$ ( $T_a \sim$ of $-5^\circ\text{C}$ for 56 hours).....	119
Figure 3.28. Ice formation in the channel with the coefficient of heat flux for water to air set to $25 \text{ W/m}^2/\text{C}$ ( $T_a \sim$ of $-5^\circ\text{C}$ for 56 hours).....	119
Figure 3.29. Ice thickness in the channel at 1 hour after ice pans with an ice concentration of 5% have been introduced. ....	120
Figure 3.30. Ice thickness in the channel at 1 hour after ice pans with an ice concentration of 35% have been introduced. ....	120
Figure 3.31. Ice thickness in the channel at 1 hour after ice pans with an ice concentration of 70% have been introduced. ....	121
Figure 3.32. Ice formation in the channel at 30 hours after ice pans with an ice concentration of 35% have been introduced ( $T_a = -30^\circ\text{C}$ ).....	121
Figure 3.33. Ice formation in the channel at 30 hours after ice pans with an ice concentration of 70% have been introduced ( $T_a = -30^\circ\text{C}$ ).....	122

Figure 3.34. Ice velocity magnitude in the channel at 30 hours after ice pans with an ice concentration of 70% have been introduced ( $T_a = -30^{\circ}\text{C}$ ).....	122
Figure 3.35. Ice thickness in the channel at 30 hours after ice pans with an ice concentration of 70% have been introduced ( $T_a = -30^{\circ}\text{C}$ ).....	123
Figure 3.36. Ice formation on the Athabasca River after 12 hours.....	123
Figure 3.37. Modeled ice formation on the Athabasca River after 24 hours.....	124
Figure 3.38. Modeled ice formation on the Athabasca River after 36 hours.....	124
Figure 3.39. Modeled ice formation on the Athabasca River after 48 hours.....	125
Figure 3.40. Modeled ice formation on the Athabasca River after 60 hours.....	125
Figure 3.41. Modeled ice formation on the Athabasca River after 72 hours.....	126
Figure 3.42. Modeled ice formation on the Athabasca River after 84 hours.....	126
Figure 3.43. Modeled ice formation on the Athabasca River after 96 hours.....	127
Figure 3.44. Modeled ice formation on the Athabasca River after 108 hours.....	127
Figure 3.45. Modeled ice formation on the Athabasca River after 120 hours.....	128
Figure 3.46. Modeled ice formation on the Athabasca River after 132 hours.....	128
Figure 3.47. Modeled ice formation on the Athabasca River after 144 hours.....	129
Figure 3.48. Annotated ice map based on field observations made on November 16, 2009.....	130
Figure 3.49. Annotated ice map based on field observations made on November 17, 2009.....	131
Figure 3.50. Aerial photograph of Site A, view from west to east, November 17, 2008.....	132
Figure 3.51. Aerial photograph of Site B, view from west to east, November 17, 2008.....	132
Figure 3.52. Aerial photograph of Site C, view northeast, November 17, 2008.....	133
Figure 3.53. Aerial photograph of Site D, view north, November 17, 2008.....	133

Figure 3.54. Aerial photograph of Site E, view from east to west, November 17, 2008.....	134
Figure 3.55. Aerial photograph of Site F, view from east to west, November 17, 2008.....	134
Figure 3.56. Aerial photograph of Site G, view south, November 17, 2008. ....	135

## List of Symbols

$H$	=	depth of flow ( $m$ )
$U$	=	depth averaged velocity in the x-direction ( $m/s$ )
$V$	=	depth averaged velocity in the y-direction ( $m/s$ )
$q_x, q_y$	=	discharge intensity in the x- and y-directions ( $m^3/s$ )
$g$	=	acceleration due to gravity ( $m/s^2$ )
$\rho$	=	density of water ( $kg/m^3$ )
$S_{0x}, S_{0y}$	=	bed slope in the x- and y-directions ( <i>dimensionless</i> )
$S_{fx}, S_{fy}$	=	friction slope in the x- and y-directions ( <i>dimensionless</i> )
$\tau_{xx}, \tau_{xy}, \tau_{yx}, \tau_{yy}$	=	components of the horizontal turbulent stress tensor ( $N/m^2$ )
$\tau_{xy}$	=	bed shear stress ( $N/m^2$ )
$\nu_t$	=	eddy viscosity coefficient ( $m^2/s$ )
$\varepsilon_1, \varepsilon_2, \varepsilon_3$	=	eddy viscosity components ( $m^2/s$ , <i>dimensionless</i> , <i>dimensionless, respectively</i> )
$C_s$	=	Chezy coefficient ( <i>dimensionless</i> )
$k_b$	=	bed roughness height ( $m$ )
$T_{xy}, T_{yx}, T_{xy}$	=	bed shear stress over the flow depth ( $N/m$ )
$\varepsilon_{xy}, \varepsilon_{yx}, \varepsilon_{xy}$	=	generalized eddy viscosity coefficients ( $m^2/s$ )
$T$	=	groundwater transmissivity ( $m^2/s$ )
$S$	=	groundwater storativity of the artificial aquifer ( <i>dimensionless</i> )
$z_b$	=	ground surface elevation ( $m$ )
$M_i$	=	ice mass per unit area ( $kg/m^2$ )
$\frac{D\vec{V}_i}{Dt}$	=	acceleration of ice ( $m/s^2$ )
$\vec{V}_i$	=	velocity of ice ( $m/s$ )
$\bar{R}$	=	internal ice resistance ( $N/m^2$ )
$\bar{F}_a$	=	wind drag force ( $N/m^2$ )

$\bar{F}_w$	=	water drag force ( $N/m^2$ )
$\bar{G}$	=	gravitational force component due to water surface slope ( $N/m^2$ )
$F_f$	=	frictional force between ice and solid boundary ( $N$ )
$F_c$	=	ice cohesive force ( $N$ )
$F_N$	=	normal component of the ice force against the boundary ( $N$ )
$\phi_B$	=	dynamic friction angle ( $^\circ$ )
$\phi^*$	=	total surface heat flux between air-water and/or air-ice ( $W/m^2$ )
$\phi_R$	=	net solar radiation (shortwave radiation) ( $W/m^2$ )
$\phi_T$	=	effective back radiation (terrestrial radiation) ( $W/m^2$ )
$\phi_E$	=	heat transfer due to evaporation ( $W/m^2$ )
$\phi_H$	=	conductive, or sensible, heat transfer ( $W/m^2$ )
$\phi_S$	=	heat transfer due to precipitation ( $W/m^2$ )
$\phi_{wa}^*$	=	net rate of heat loss at the water surface ( $W/m^2$ )
$\phi_{Rw}$	=	net shortwave solar radiation reaching the water surface ( $W/m^2$ )
$\alpha'$	=	a linear heat transfer constant ( $W/m^2$ )
$\beta'$	=	a linear heat transfer coefficient ( $W/m^2/^\circ C$ )
$T_w$	=	water temperature ( $^\circ C$ )
$T_a$	=	air temperature ( $^\circ C$ )
$T_{ws}$	=	water surface temperature ( $^\circ C$ )
$T_{cr}$	=	critical surface water temperature for border ice formation ( $^\circ C$ )
$v_b$	=	buoyant velocity of suspended frazil ( $m/s$ )
$v_z'$	=	vertical turbulence velocity ( $m/s$ )
$ \bar{V} $	=	the magnitude of the local depth averaged velocity ( $m/s$ )
$V_{cr}$	=	the critical depth averaged velocity for border ice formation ( $m/s$ )
$e_T$	=	thermal energy of the ice-water mixture in suspended layer ( $J/m^3$ )

$\phi_{ss}$	=	rate of heat gain on unit area through top/bottom boundary ( $W/m^2$ )
$\phi_{sk}$	=	rate of heat loss on unit area through top/bottom boundary ( $W/m^2$ )
$\rho_i$	=	density of ice ( $kg/m^3$ )
$L_i$	=	latent heat of fusion of ice ( $J/kg$ )
$E$	=	net volumetric rate of loss of frazil due to mass exchanges with the surface layer and at the bed ( $m^3/s/m^2$ )
$C_p$	=	specific heat of water ( $J/kg/^\circ C$ )
$C_v$	=	volumetric ice concentration ( $m^3/m^3$ )
$h_i$	=	thickness of the ice cover ( $kg/m^2$ )
$\alpha$	=	a linear heat transfer constant ( $W/m^2$ )
$\beta$	=	a linear heat transfer coefficient ( $W/m^2/^\circ C$ )
$T_s$	=	temperature of snow ( $^\circ C$ )
$n_b$	=	Manning's resistance coefficient ( <i>dimensionless</i> )
$C_r$	=	Courant number ( <i>dimensionless</i> )
$V_x$	=	velocity in the x-direction ( $m/s$ )
$\Delta t$	=	time step increment ( $s$ )
$\Delta x$	=	mesh spacing (m)

## **1. Introduction**

With the large growth of population and industry in Fort McMurray, AB, the issue of adequate water supply arises as the demand for water increases. Currently, 349 million cubic meters of water per year ( $11.1 \text{ m}^3/\text{s}$ ) are approved for withdrawal from the Athabasca River, while planned oil sand projects will increase these withdrawals to 529 million cubic meters per year ( $16.8 \text{ m}^3/\text{s}$ ). The latter value reflects a figure that is greater than the amount used by the City of Toronto. However, unlike water used for municipal purposes, only about 10% of the water used will return to the watershed which it came from (Woynillowicz, 2006). Of particular interest are the flows during the winter months since the Athabasca River is unregulated and naturally experiences low flows during this time. Figure 1.1 displays a graph of the mean monthly flows on the Athabasca River downstream of Fort McMurray (1957-2008) to illustrate this. The mean monthly values from December to March show discharges between 159 and  $200 \text{ m}^3/\text{s}$ , with minimum monthly flows for these months being around  $100 \text{ m}^3/\text{s}$ . This suggests that it is possible for current approved withdrawals to take up over 10% of the flow in certain cases.

Although extensive efforts are being undertaken by various organizations, such as Alberta Environment, the Department of Fisheries and Oceans (DFO) and the Cumulative Environmental Management Association (CEMA), to assess the potential implications of water demand on the ecology of the lower Athabasca River, one significant outstanding question involves the issue of river ice. The nature and extent of ice cover development on large rivers is highly dependent upon flow rates and thus a key question arises as to whether substantial flow withdrawals will have a significant impact on the ice regime of the river. If the flow hydrodynamics change substantively with discharge, then this has the potential to produce thicker or thinner ice covers. This suggests that future demands on the winter water supply of the Athabasca River have the potential to change the relative proportions of ice and liquid water during winter. This may

result in a future winter water supply that is significantly less than indicated by past records. This in turn has implications for winter water supply, water quality and fish habitat.

In order to address the issues surrounding river ice, a good understanding of the winter ice regime on the Athabasca River must be developed. One-dimensional modeling has been undertaken (Abarca, 2007) along a substantial length of the river. However, it is necessary to develop a detailed 2-D model of ice cover formation in order to fully assess the potential impacts of flow withdrawals.

### **1.1 River Ice Processes**

In order to understand the impact that withdrawals may have on the ice regime of the river, knowledge of river ice processes is important. Over the winter season, the cycle of a northern river includes the formation, growth and eventual removal of an ice cover. This evolution involves various thermal and mechanical processes and is distinctive for each river. This section serves to provide the general background information of these processes, with a focus on ice cover formation.

Border ice is usually the first type of ice to form in a river. It forms thermally from the river banks, as the water loses heat to the surrounding air, and grows outwards where the velocities are low enough to permit it. As a result, its formation is greatest on the inside of river bends as well as around large boulders and bridge piers. The amount of this ice that is created is highly dependent on the flow conditions and geometry of the river.

Skim ice is another type of ice that forms thermally. However, instead of being attached to the banks of the river, it produces sheets of ice that travel downstream with the velocity of the river. Low wind and flow velocities are ideal for the formation of skim ice; however, it has been observed to form at flow velocities of up to 1.0 m/s when air temperatures are very low (Beltaos, 1995). This type of ice is very rare.

Away from banks and in the areas of turbulent flow, small ice particles called frazil ice begin to form as soon as temperatures drop below 0°C. A decrease in water temperature of 0.01°C causes supercooling and once it occurs, frazil ice appears to form spontaneously throughout the flow depth. Frazil production is greatest when there is a strong net heat flux, thus its formation tends to follow a diurnal cycle with most production occurring at night and even ceasing throughout the day (Beltaos, 1995). Frazil particles are highly adhesive and easily come together to form a frazil slush. Once the frazil rise velocity is able to overcome the turbulence of the river, particles reach the water surface and freeze together to create frazil pans, or pancake ice, as can be seen in Figure 1.2. Frazil pans move freely at the water surface and frequently come into contact with other pans and border ice. When pans freeze together, they form rafts. Ice pans can also accumulate near the banks to form border ice dynamically. Supercooling can only occur in areas that are not covered in ice, thus frazil production decreases as rafts and pans increase in surface concentration.

As surface ice concentrations increase, ice becomes congested and eventually bridging, or consolidation, occurs and an ice cover begins to form. This commonly takes place in areas where the channel is narrow or makes tight bends. Bridge and border ice constrictions the most likely places for this to occur (Figure 1.3). Once ice is stopped at a bridging point, the stopping front begins to propagate upstream. If pans and rafts accumulate edge to edge, a juxtaposed ice cover is formed, as can be seen in Figure 1.4. Eventually, the spaces between the pans and rafts freeze and a full ice cover begins to form. If the drag force on the underside of the ice cover is high enough to collapse the juxtaposed ice cover, a hummocky ice cover is formed. This cover has much more roughness and tends to slow water flow and raise the stage. Throughout the winter, low air temperatures cause the ice cover originally formed to thicken thermally in long vertically oriented crystals known as columnar ice.

In the spring, when air temperatures increase, the ice cover slowly begins to deteriorate and may undergo either a thermal or dynamic break-up. A thermal

break-up occurs when the ice melts in place steadily throughout the spring. As the ice cover begins to melt, the albedo of the snow is reduced which allows more heat to be absorbed and this continues until all of the ice has melted away. A dynamic break-up can occur when a high flow event, usually a large snowmelt runoff, raises the water levels and lifts the ice cover causing it to break into many pieces and be carried downstream. This ice run will continue until stopped by an intact ice cover downstream which will form an ice jam. Ice jams are often associated with flooding and may form several times along the length of the river throughout break-up.

## **1.2 Previous Studies**

Abarca (2007) reported that several hydrologic and hydraulic studies have been conducted on the Athabasca River downstream of Fort McMurray. The focus of each of these studies has been on the environmental impact of the oil sands; however, in some of the studies information regarding ice covered hydraulics can be found. Beltaos (1979) examined mixing under ice covered conditions from Fort McMurray to Lake Athabasca and this study included information about ice thicknesses and various geomorphic characteristics throughout the reach. Van der Vinne (1993) performed winter low flow dye tracer studies from Fort McMurray to Bitumont and this study contained information about times-of-travel and the variation of Manning's roughness coefficient. Unfortunately, neither of the studies contains information about ice cover formation processes.

In order to examine and address potential cumulative effects of industrial development, the Regional Aquatics Monitoring Program (RAMP) was initiated in 1997 and the Cumulative Environmental Management Association (CEMA) was established in 2000. As a result, several reaches along the Athabasca River have been selected and private consultants have been hired to conduct winter ice surveys which include obtaining winter bathymetry and ice cover characteristics. CEMA has helped fund the development of the ice cover component of *River2D*, a two dimensional depth averaged finite element hydrodynamic model, in order to

better understand the effects of an ice cover on river hydraulics. Using the ice survey data with *River2D*, several 2-D simulations of ice-covered channel hydraulics were developed by Katopodis and Ghamry (2005) of the Department of Fisheries and Oceans (DFO).

In 2006, a three-year program was established investigate the potential of flow withdrawals on the ice regime and the effect on future water supply in the Athabasca River through the collection of data and the application of river ice process models. In the first year of this study, Abarca (2007) established the main conditions describing the winter ice regime of the 80 km section of the Athabasca River from Fort McMurray to Bitumont. This was accomplished through an extensive field program that included freeze-up monitoring, winter ice surveys and discharge measurements as well as break-up monitoring. Preliminary modeling of freeze-up over the entire 80 km reach was conducted using *River1D*. It was established from this study that the ice regime of the reach is highly two-dimensional and thereby limiting the effectiveness of the 1-D model. Flows measured in the winter of 2007 were used to run a *River2D* model supplied by CEMA; however, it was found that the model results did not correlate will with measurements and that additional data collection was recommended. These efforts helped to direct the following two years of field programs and model development.

### **1.3 Current Study Objectives**

The primary objectives of the current study were two-fold. First of all, a detailed reach that experienced an adequate range of ice cover initiation processes was found and data was gathered at this site in order to build a 2-D numerical ice process model. In order to accomplish this, an extensive field program which included freeze-up monitoring, summer bathymetric surveys and discharge measurements and winter ice surveys was carried out. Data gathered from the previous year of this study was used to direct this effort. Second, using all of the data collected, parameters were calibrated and a 2-D model was used to simulate

border ice formation in the detailed study reach. An extensive sensitivity analysis was carried out in order to understand the function of each model component, including bridging and ice cover formation. Through this process, an insight was gained into the capabilities of 2-D ice process models.

Field work was conducted over the freeze-up periods of 2007 and 2008 along 80 km of the Athabasca River and in the summer of 2008 and the winter of 2009 focusing on a 5-km long detailed study reach. Chapter 2 introduces the study site selected and presents all the details of the field programs carried out. The various data collection methods are described and the information gained from each piece of equipment is discussed and analyzed. Freeze-up processes are compared for the two years of data collected, as well as with data from the previous year of this study.

A 2-D model of the detailed study reach was built using *River2D* and *CRISSP2D* modeling software. Chapter 3 begins by describing the principles of hydrodynamics and the thermal processes that govern the equations being solved by the 2-D models. Preliminary model testing is carried out on simple trapezoidal and rectangular channels in order to understand how various components of the model behave. The full details of the Athabasca River model construction are presented, including the calibration and sensitivity analysis performed. Border ice simulation is carried out and compared with field observations.

Recommendations are made on how to use this data to conduct future studies in order to continue this effort of the evaluation of potential impacts of winter water withdrawal.

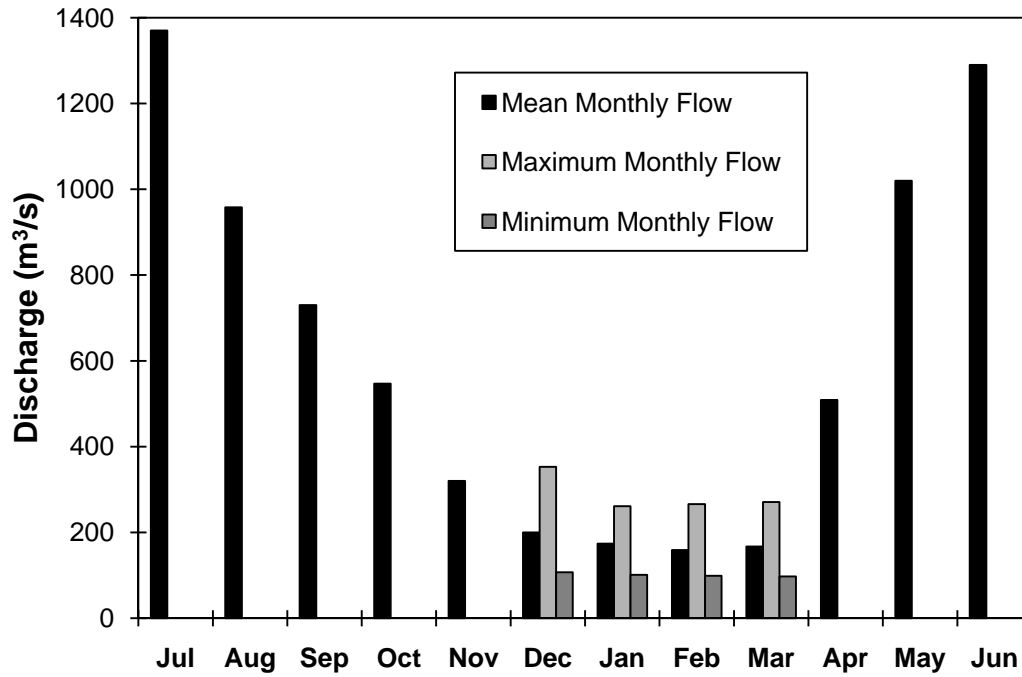


**Figure 1.1. Mean monthly flows on the Athabasca River at Fort McMurray, Alberta (Data Source: Water Survey of Canada, available record from 1957 to 2008).**

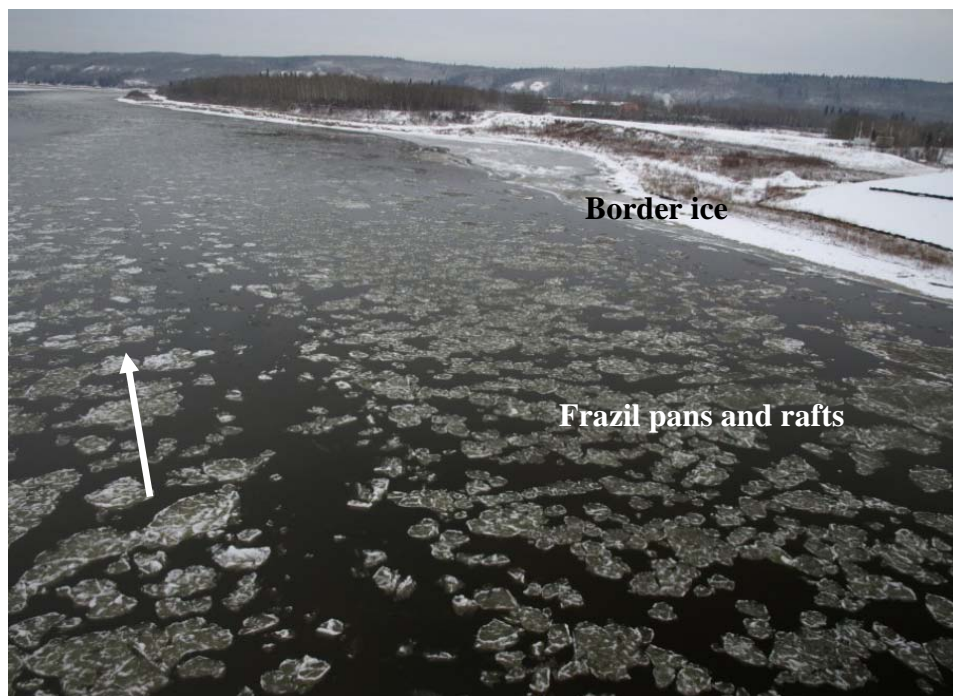


**Figure 1.2. Border ice, pans and rafts on the Athabasca River in Fort McMurray, November 17<sup>th</sup>, 2008.**

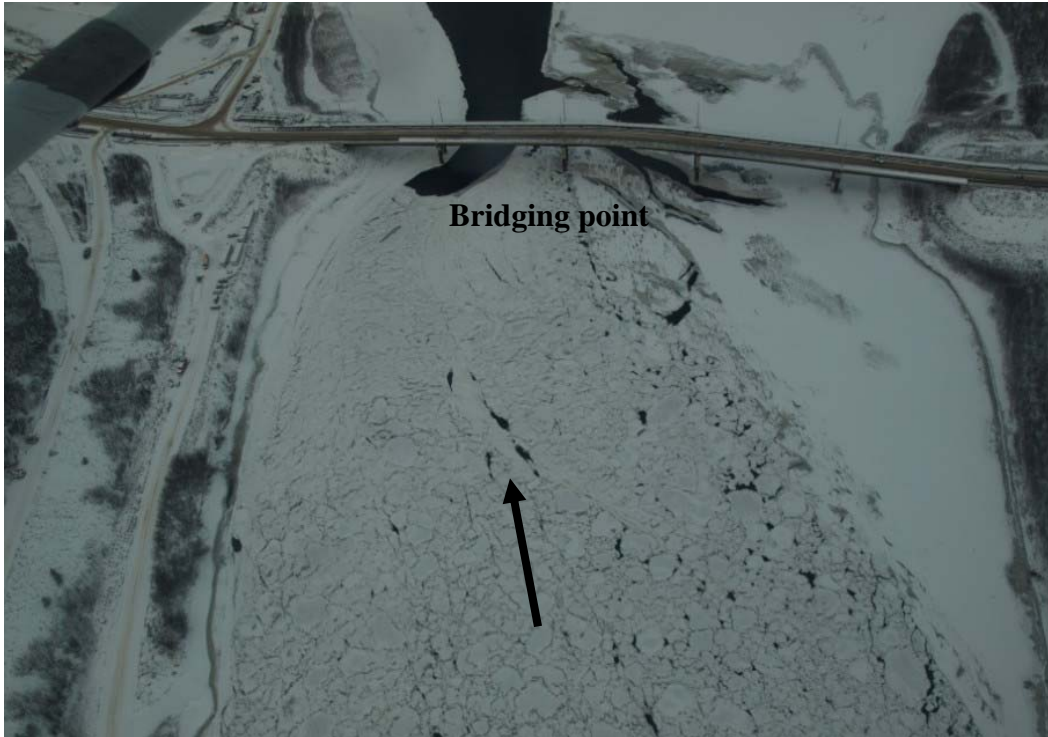


**Figure 1.3. Bridging point at Suncor Bridge on the Athabasca River below Fort McMurray, November 19<sup>th</sup>, 2008.**



**Figure 1.4. Juxtaposed ice cover on the Athabasca River below Fort McMurray, November 19<sup>th</sup>, 2008.**

## 2. Field Program<sup>1,2</sup>

### 2.1 Introduction

Field programs were conducted along the Athabasca River in 2007 and 2008 to obtain data for numerical modeling. In order to validate a 1-D model created based on data acquired in the fall of 2006 (Abarca, 2007), a field program to observe freeze-up along 80 km the Athabasca River, from Fort McMurray to Bitumont, was conducted in the fall of 2007. Based on the freeze-up observations of 2006 and 2007, a comprehensive field program was developed around a 5 km long sub-reach of the 80 km section for 2008. This sub-reach was identified as a suitable model validation study site for a 2-D model, since it encompassed an area that experienced a full range of ice cover initiation processes. The upstream and downstream boundaries were carefully chosen to contain the least amount of influence from factors such as sandbars, river bends and bridges.

Figure 2.1, shows a view of the entire reach from Fort McMurray to Bitumont, with the 5-km sub-reach highlighted. Figure 2.2 gives a more detailed view of the sub-reach, with various stations and sites labeled. The 2008 field program included detailed bathymetric and water level surveys as well as discharge measurements in the summer, freeze-up monitoring in late fall and winter ice surveys. This chapter provides details of the field programs conducted and the data obtained.

---

<sup>1</sup> A version of this chapter referring to the summer survey has been submitted for the field summary report entitled, "Report on the Ice Process Model Validation Reach Survey, Athabasca River, 2008" by Agata Wojtowicz, Faye Hicks and Robyn Andrishak for the Cumulative Environmental Management Association Instream Flow Needs Technical Task Group.

<sup>2</sup> A version of this chapter referring to the winter survey has been submitted for the conference paper entitled, "2-D Modeling of Ice Cover Formation Processes on the Athabasca River, AB" by Agata Wojtowicz, Faye Hicks, Robyn Andrishak, Michael Brayall, Julia Blackburn and Joshua Maxwell for the 15<sup>th</sup> Workshop on River Ice in St. John's Newfoundland and Labrador, June 15-17, 2009.

## **2.2 Description of Study Reach**

The 80 km long reach of the Lower Athabasca River chosen for the study extending from Fort McMurray to Bitumont is shown in Figure 2.1. Fort McMurray is located at the confluence of the Clearwater and Athabasca Rivers. At this site, the Athabasca River has an effective drainage area of 130,000 km<sup>2</sup>, as reported by the Water Survey of Canada. The major tributaries located further along the reach include the Steepbank, Beaver, Muskeg and MacKay Rivers, which together drain approximately 8220 km<sup>2</sup> and contribute approximately 4% to the total flow of the river in this reach (Doyle, 1977).

In the study reach, the Athabasca River flows north through the Athabasca tar sands deposits, on an average slope of 0.13 m/km (Kellerhals, *et al.*, 1972). The bed material is predominantly sand, with local gravel over limestone, and the channel is entrenched (Kellerhals, *et al.*, 1972). The river is laterally stable and deeply entrenched in its valley, flowing in a relatively straight planform pattern, with many islands and large sand bars (Conly *et al.*, 2002). The range of Manning's roughness values reported by Kellerhals *et al.* (1972) is between 0.018 and 0.030 for the entire reach at various flood frequencies. Downstream of Fort McMurray, it is reported that the thalweg shifts year to year in much of the reach (Doyle, 1977). A Manning's roughness of 0.017 was determined for the entire reach under ice-covered conditions by Van der Vinne and Andres (1993); however, this value was regarded as low due to inadequate establishment of the under ice top width. Aerial observations, as part of this study, show distinct dune bed forms in the reach downstream of Fort McMurray, as can be seen in Figure 2.3.

## **2.3 Summer Field Program**

Summer topography survey work in 2008 included: depth sounding (for below water portions), ground surveys (for the above water portions), water profiling and discharge measurement. This work involved the use of various types of

instruments, including: an acoustic depth sounder; a Real Time Kinematic Global Positioning System (RTK-GPS) for control surveys, bank surveys and boat tracking; a basic rod and level for water level measurements; and an Acoustic Doppler Current Profiler (ADCP) for flow measurement.

Summer surveys were carried out during two trips to the study site. The first trip was conducted during the week of July 21 – 25, 2008 and concentrated on the downstream section of the reach (Figure 2.2). The second trip took place from August 25 – 29, 2009 and focused on the upstream section. Horizontal and vertical positioning was achieved in this survey using a RTK-GPS consisting of one base station communicating by radio with two mobile ‘rover’ units. The Universal Transverse Mercator Zone 12 North (UTM12N) co-ordinate system was used for the projection of the horizontal plane and the North American Datum 1983 (NAD83) was the vertical datum for the elevations. The Geodetic Survey Datum 1995 (GSD95) geoid model was used as a reference for the co-ordinate system in the surveys. As there are no Geodetic Survey of Canada (GSC) benchmarks accessible in the vicinity of the study site, the survey was conducted using a ‘local’ co-ordinate system. This was achieved by driving a 1m length of re-bar into the ground to establish a centralized temporary benchmark (TBM) and then using this same TBM as the location for the RTK-GPS base station during all surveys (TBM ISL2, shown in Figure 2.2). The base station was allowed to self locate on the first day (by accessing global positioning satellites) and the co-ordinates obtained were then adopted as the ‘known’ location of the base station on each subsequent day of the survey, for consistency. The self-locating procedure provides a local co-ordinate system which is within about  $\pm 2\text{m}$ , relative to GSC. However, the relative accuracy of all points surveyed within this local co-ordinate system (i.e. between the rovers and the base station) was within  $\pm 2\text{ cm}$ .

### 2.3.1 Bathymetric Surveys

The bathymetric survey was comprised of two parts: a bank survey for the above water portion of the channel, extending high enough to enable channel definition for high water conditions, and a channel bed survey for the portion below the water. The style of surveying required for 2-D hydrodynamic modeling is known as a ‘feature based’ survey. Specifically, rather than measuring widely spaced cross section transects (as is typically done for 1-D surveys), a feature based survey captures the details of the topography of the channel by capturing the definitive features of a river. To achieve this, break-line surveys are run along the top of bank, the bottom of the bank, around islands and bars, along the edge of water, and in a variety of line patterns within the channel itself.

The above water portion of the survey was conducted by two person crews (one crew on each bank) using the RTK-GPS rovers. Points were measured for ~1 second duration along the edge of water (EOW), bottom of bank (BOB) and top of bank (TOB) at intervals of approximately 30 m. Any other topographic features of interest were noted and measured as well. In total, 1650 ground points were surveyed. Over 1000 photographs were taken during the bank surveys as well, and handheld GPS units were carried by each crew to facilitate automated geo-referencing of these photos.

The channel bed survey was conducted from a boat by synchronizing an RTK-GPS rover unit with a depth sounder. For this survey, the transducer was fixed to a bracket on the boat, and positioned at a depth approximately 0.3 m below the water level. The RTK-GPS antenna was then positioned a known offset distance directly above this transducer (Figure 2.4). From this the bed elevation could be determined for each point as the RTK-GPS antenna elevation, minus the offset, minus the depth sounder reading. In total, 6200 discrete bed points were measured and recorded over this 5-km reach, averaging to about 5 meter spacing. Figure 2.5 shows the resulting bathymetry map obtained from this survey.

### 2.3.2 Water Level Surveys

Additional TBMs were set up at various points throughout the study site to facilitate additional measurements of water levels during the survey (as shown in Figure 2.2). The co-ordinates of these points were obtained by positioning one of the RTK-GPS rovers on the TBM for at least 5 minutes, so as to reduce the measurement error to about  $\pm 1.0$  to 1.5 cm. Water levels were then surveyed from these points using a rod and level. Table 2.1 presents a summary of the water levels obtained during the July field trip. Table 2.2 contains two water levels that were measured in August. It was found that these were in good agreement with the edge of water profiles surveyed with the RTK GPS “on-the-fly”. Therefore, extra profiling was not conducted for the survey in August, as it was clear that the time would be more appropriately spent obtaining topography and bathymetry data instead.

**Table 2.1. Water Levels measured during the July 2008 survey.**

<b>TBM</b>	<b>Station (km)</b>	<b>Water Level (m)</b>
0801	263.4	234.31
0802	264.9	234.52
ISL1	265.7	234.47
0803	266.8	234.77

**Table 2.2. Water Levels measured during the August 2008 survey.**

<b>TBM</b>	<b>Station (km)</b>	<b>Water Level (m)</b>
0801	263.4	234.54
ISL1	265.7	234.80

### 2.3.3 Discharge Measurements

A SonTek Acoustic Doppler Current Profiler (ADCP) was used to measure the local velocities and total discharge across Sites 1, 2 and 3 within the study reach (as indicated in Figure 2.2). The ADCP sensor was mounted in a trimaran and

then deployed from a boat. Endpoints were established near the edge of water at the minimum depth traversable by the boat, and the coordinates of these points were surveyed with the RTK-GPS. In addition, the distance from the endpoint to the edge of water was measured in each case. A minimum of 4 passes were made across each section, with survey crew members positioned at each endpoint to guide the boat path across the channel and to ensure the straight path was maintained in the last few meters of travel into the endpoints. Instrument control and quality control monitoring was done via computer from the river bank.

Unfortunately, the conditions at Site 1 were not conducive to discharge measurement. A large bar on the left side of the channel resulted in depths too shallow to traverse safely with the boat, and on the right side, the maximum depth exceeded 7m (beyond the range of the ADCP). Nevertheless, velocity profiles were obtained over a portion of the section, which were very useful for model validation purposes. According to the manufacturer's specifications, the error in velocity measurement for this instrument was  $\pm 1\%$  or  $\pm 0.5$  cm/s; however, it is likely that this error is increased because of the difficulties in measurement.

On July 24<sup>th</sup>, 2008, four passes were conducted at Site 2, with the resulting discharges ranging from 602 to 617 m<sup>3</sup>/s. The error in velocity measurement for this instrument was  $\pm 1\%$  or  $\pm 0.5$  cm/s. The estimated error for the discharge measurements was  $\pm 10\%$ . The average of the recorded values for this section (609 m<sup>3</sup>/s) was within 10% of the preliminary discharge reported by WSC for July 24<sup>th</sup>, 2008. Appendix A provides the detailed records for this discharge measurement.

At Site 3, discharge measurements were carried out on July 24<sup>th</sup>, 2008. Nine passes were conducted with the discharge ranging from 318 to 398 m<sup>3</sup>/s. Extra passes were conducted, since there was a small section of the channel over which the sensor was unable to track the bed (again, depths were in excess of 6 m in this region). Because of the difficulty in traversing this section, the error in velocity measurement for this instrument was greater than  $\pm 1\%$  or  $\pm 0.5$  cm/s and the estimated error for the discharge measurements was greater than  $\pm 10\%$ . The

average discharge measurement during these nine passes ( $370 \text{ m}^3/\text{s}$ ) represents approximately 60% of the total flow. Measurements were attempted at Site 4; however, it was too shallow over the entire width of the channel on the right side of this island for the boat to traverse. Appendix A provides the detailed records for this discharge measurement.

## **2.4 Freeze-Up Monitoring**

Freeze-up work in 2007 and 2008 included monitoring of ice cover development as well as measurements of water temperature, water depth and meteorological conditions. This work was performed using a variety of equipment such as automated stationary cameras for remote ice monitoring, high quality cameras for detailed aerial photography, water temperature sensors for water temperature measurement, pressure transducers for water depth measurements and a meteorological station for air temperature measurements. Water discharge data was obtained from Water Survey of Canada's gauge station 07DA001 (Athabasca River below McMurray), as shown in Figure 2.1.

On November 5, 2007, frazil was present in the 80 km reach of the Athabasca River between Fort McMurray and Bitumont, signifying the start of freeze-up. After bridging occurred at M264.9 (Figure 2.2), the ice front propagated upstream and moved through Fort McMurray on November 16, 2007. In 2008, freeze-up began on November 14, 2008, bridging occurred at the Suncor Bridge and the stopping front reached Fort McMurray by November 20, 2008.

### **2.4.1 Discharge Data**

The discharges experienced throughout the freeze-up period were similar throughout the years of study. Figure 2.6 shows the discharges in the Athabasca River as reported by the WSC for station 07DA001 from the day ice was first observed (first ice) to the day the ice stopping front moved through Fort McMurray (completion) for the years 2006 to 2008. The discharges experienced

over these three years are below average when comparing to historical flows from 1957 to 2008 during the freeze-up period, as can be seen in the graph.

Since the models were run using steady flow hydrodynamics, a single flow was determined to represent each year of record. The freeze-up period in 2007 lasted for 12 days and the average discharge was 277 m<sup>3</sup>/s. However, the majority of freeze-up, including bridging, occurred when the discharge was approximately 260 m<sup>3</sup>/s, thus this value was used for model validation efforts. In 2008, the average flow over the freeze-up period was 254 m<sup>3</sup>/s, with a range from 280 m<sup>3</sup>/s to 210 m<sup>3</sup>/s. Since bridging occurred when the river flow was 250 m<sup>3</sup>/s, this value was chosen as representative of the freeze-up period for the year.

#### **2.4.2 Meteorological Data**

Air temperature is the primary meteorological parameter of interest for the freeze-up period. In 2006, air temperature data was measured at three distinct sites. These included (1) the University of Alberta's (UA) meteorological station located in Fort McMurray at the city services compound at the northwest corner of McKenzie Boulevard and MacAlpine Crescent, (2) Environment Canada's (EC) meteorological station at the Fort McMurray Airport and (3) with an additional air temperature sensor that was installed along the river at M216.7 (Abarca, 2007); this location is shown in Figure 2.1. According to the manufacturer's specifications, the error in air temperature data measurement was  $\pm 0.2^{\circ}\text{C}$  for temperatures between  $0^{\circ}\text{C}$  and  $70^{\circ}\text{C}$  and up to  $\pm 0.5^{\circ}\text{C}$  at  $-50^{\circ}\text{C}$ .

Good correlation was established between the measurement records at all three stations. Robichaud (2003) found that there was excellent correlation between the air temperature records at the UA station and the EC station, with a coefficient of determination ( $R^2$ ) value of 0.991. Abarca (2007) found that there was good correlation between the UA meteorological station and the sensor installed at the river level at M216.7, resulting in a  $R^2$  value of 0.957. There appeared to be some seasonal variation between these two stations during the months of December and

January as air temperatures decreased to values below zero. This suggests that the UA meteorological station in town does not accurately represent temperatures experienced at the river level during colder periods. However, the period of interest for freeze-up involved the months of October and November, thus the relationship between the three stations was valid. Since data was recorded at the UA meteorological station and EC meteorological stations, it was not necessary to install the additional air temperature sensor along the river at M216.7 in 2007 and 2008.

Figure 2.7 shows the air temperature throughout the freeze-up period for 2006-2008, as recorded at Fort McMurray from Environment Canada's meteorological station at the airport. From this graph, it can be seen that air temperatures during the freeze-up period in 2008 were lower than air temperatures during the freeze-up period in 2007. This is the reason that the duration of freeze-up was shorter in 2008. While air temperatures were slightly lower in 2008, they were above average throughout the majority of both of the 2007 and 2008 freeze-up periods, as compared with historical data.

The calculated degree days of freezing were determined and compared for freeze-up in the years 2006 through 2008. Degree days of freezing are calculated by adding up all of the consecutive average daily temperatures, in degrees Celsius, when the temperatures are below 0°C. If a positive average daily temperature is experienced after several days of negative temperatures, the calculation begins again. Figure 2.8, adapted from Andrishak *et al.*, 2008, shows the calculated degree days of freezing ( $ADD_F$ ) at Fort McMurray (EC station at the airport) in comparison with the historical averages at the same station (1971-2000). This figure also shows the dates of first ice present in the channel and the date of complete ice cover up to Fort McMurray. It is interesting to note that there is some consistency between the three years of observations for both first ice ( $ADD_F = 8.8, 10.2$  and  $13.3^\circ\text{C-days}$ , respectively) and the complete ice cover ( $ADD_F = 50.4, 50.6$  and  $62.1^\circ\text{C-days}$ , respectively).

Solar insolation is another parameter that is considered important for ice process modeling. This parameter is recorded at the University of Alberta's meteorological station. Typically, during freeze-up in Fort McMurray, the weather tends to be very cloudy and snowfall is often experienced. The effect of the specific cloud cover experienced in this area at this time is that a very minimal amount of solar insolation is recorded. Since the effect of this parameter is so small, it was neglected in the 2-D model.

### **2.4.3 Water Temperature Data**

In 2006, water temperature was measured at 4 stations along the study reach: M288.1, M268.1, M245.6, and M216.7 (Abarca, 2007); these locations are shown in Figure 2.1. It was found that “water temperatures essentially cooled simultaneously at all four stations,” thus subsequent water temperature recordings did need not to be taken at many sites along the 80 km river reach (Andrishak *et al.*, 2008).

In 2007, water temperature probes connected to dataloggers were installed at river stations M288.1 and M268.1 (Figure 2.1). The water temperature probe installed at M288.1 was connected to a cellular modem, which allowed for the transmission of real-time water temperature data. Figure 2.9 displays the data collected at both stations. According to the manufacturer's specifications, the error in the water temperature measurement was  $\pm 0.2^{\circ}\text{C}$ . Unfortunately, low battery problems occurred at station M288.1, so data collected has missing values from October 21, 2007 to November 1, 2007 at that station. As can be seen in the figure, water temperatures reached  $0^{\circ}\text{C}$  on November 5, 2007, indicating the start of freeze-up. The water temperature data at station M288.1 was more sensitive to diurnal temperature fluctuations, displaying lower temperatures throughout the night than in the day. This may be due to the placement of the sensor at M288.1 in an area that just downstream of a side channel that meanders through a series of sandbars (Figure 2.10). The sensor at M268.1 was placed in the main channel (Figure 2.11).

In 2008, a water temperature probe was connected to a datalogger and deployed at river station M268.1. The water temperature probe was connected to a cellular modem which allowed for the transmission of real-time temperature data. A 75-Watt solar panel was used to generate power for the system. Low battery problems occurred throughout the freeze-up period, making the data from November 13, 2008 to November 17, 2008 discontinuous. Figure 2.12 shows water temperature readings during freeze-up in 2008. Again, to the manufacturer's specifications, the error in the water temperature measurement was  $\pm 0.2^{\circ}\text{C}$ . The water temperature probe indicated that the water temperature was near zero on November 14<sup>th</sup>, 2008. This was the first day that frazil was spotted in the river, marking the start of freeze-up.

#### **2.4.4 Ice Cover Observations**

In 2007, four digital time lapse cameras were installed prior to the start of freeze-up in order to observe ice cover development. These cameras were placed at M288.1, M250.6, M245.5, and M216.7, each oriented to face the downstream direction (Figure 2.13). Each of the automated camera stations mounted in 2007 provided useful data throughout the entire freeze-up period.

In addition to automated cameras, six aerial flights were carried out between November 10 and November 30 in order to document the freeze-up process along the entire 80 km from Fort McMurray to Bitumont. Georeferenced photographs were taken with digital cameras. An example of photographs taken by automated cameras and during aerial flights is provided in Figure 2.14. It was from these photographs that a set of detailed maps showing the ice cover development process was created, as can be seen in Figures 2.15 through 2.18.

It was noted that while being a relatively complex process, the development of the freeze-up in 2007 was very consistent to that of observed in 2006 (Abarca, 2007). Border ice formed in the slow moving shallow areas and side channels. Bridging occurred in the same two locations along the 80 km reach approximately 2 km

upstream of the Suncor Bridge at M264.9 (see Figure 2.18). A juxtaposed ice cover formed in the main part of the channel upstream of the bridging points, with the remaining uncovered areas mainly freezing thermally. One contrast noted was that a hummocky area was observed over the first 8.5 km of the study reach, downstream of station M288.1 (Figure 2.1) in 2006 (Abarca, 2007), while no hummocky ice cover formed in this reach in 2007.

In October of 2008, nine digital time lapse cameras were installed (Figure 2.13). Observations from 2006 and 2007 showed that bridging was observed near the same area, thus five of these cameras were installed at M264.9 and M264.8 to try to gain a better understanding of the bridging process. Two cameras were installed at M268.1, a location near the upstream boundary of the detailed 5-km reach study reach. The remaining two cameras were installed at M288.1. Each camera was programmed to take pictures either every 15 or every 30 minutes. Five of the nine cameras installed in 2008 provided useful data. Some of the stations could not withstand the cold air temperatures and stopped working before freeze-up had even begun. Table 2.3 describes the location, orientation and the final date that each camera was able to take and record photographs.

**Table 2.3. Summary of location, orientation and duration of digital time lapse cameras, 2008.**

Location (km)	Orientation	Camera	Last Date
288.1	Across	Campbell	12/24/2008
288.1	Downstream	CamTrakker	12/27/2008
268.1	Downstream	Campbell WebCam	11/25/2008
268.1	Across	CamTrakker	10/3/2008
264.8	Upstream	Campbell	12/28/2008
264.8	Downstream	Campbell	no data
264.8	Across	CamTrakker	11/1/2008
264.9	Downstream	Campbell	1/2/2009
264.9	Across	CamTrakker	10/18/2008

In 2008, ten flights were conducted from November 16, 2008 to November 29, 2008, as permitted by weather conditions. Georeferenced photographs were taken using both a digital single-lens reflex camera and a digital camera with mounted

GPS unit. Using this data, a set of detailed maps showing the ice cover development process was created, as can be seen in Figures 2.19 through 2.22.

In 2008, a bridging spot formed at the Suncor Bridge, an area 2 km downstream of where it occurred the year before (Figure 2.22). Despite bridging occurring in different areas, the freeze-up process in 2008 was very similar to freeze-up in 2007. Border ice developed in the same way, forming in the shallow and slow moving areas along the reach. After bridging occurred, a juxtaposed ice cover formed in the main part of the channel, with no areas of hummocky ice observed. In both 2007 and 2008, it can be seen that constrictions were created at the upstream-most sandbar and the downstream-most sandbar in the detailed study reach (Figures 2.18 and 2.22).

The differences in the way ice was formed and the fact that in bridging occurred at a bend in 2007 and at the Suncor Bridge in 2008 is likely because sand bed rivers tend to shift each year. As seen in Figure 2.18, in 2007, the sandbar located just downstream of the island affected the formation of a bridging point. It can be seen in Figure 2.22 that a larger sandbar, created by the flow patterns in the river, is located further downstream in 2008. Also, in 2007, the sandbar to the right of the island caused a blockage and pans filled the channel creating a juxtaposed ice cover shortly after freeze-up began. In 2008, it was not evident that a juxtaposed cover formed in the area until the stopping front passed through. Another major difference between the two years is that a sandbar was located upstream of the island in 2008 (Figure 2.22), while in 2007, it existed farther upstream and was much smaller (Figure 2.18).

Surface ice concentrations were measured from aerial flight photographs for both 2007 and 2008. Graphs containing this data can be seen in Figure 2.23. Straight sections, in which the ice pans were evenly distributed across the channel and where there were no islands, sandbars or sharp bends to create a channel narrowing, were selected for this analysis. The stations along the x-axis of the graph in Figure 2.23 correspond with the stationing in the site map in Figure 2.1. A representative portion of the river was chosen from each photograph and

computer software was used to determine the percentage of white areas (ice pans) that existed within the dark area (water). The estimated error for these measurements was less than 5% given the method used. From the figures it can be seen that ice concentration is variable throughout the reach. This can be attributed to the fact that river cross sections can vary in width. Considering a simple conservation of mass, a wider section will allow pans to spread out and create an area of lower ice concentration, while a narrow section will push pans together to create an area of higher ice concentration. Also, higher ice concentrations are noted near Fort McMurray and ice concentrations decrease slightly as ice pans travel downstream. This may be attributed to the fact that ice pans are created throughout several sections of rapids that exist just upstream of Fort McMurray. As these pans travel downstream, they accumulate in slow moving areas to form dynamic border ice or fill side channels to create a juxtaposed ice cover.

Data collected at the remote station located at the upstream boundary of the detailed 5-km reach was necessary for inflow surface ice concentration data for the numerical model. Surface ice concentrations were measured from photographs taken from the remote station at M268.1. The results of this analysis are contained in Table 2.4. It can be seen that there was a gradual increase in ice concentration throughout the freeze-up period.

**Table 2.4. Ice concentration measured during the freeze-up period at M268.1.**

<b>Date</b>	<b>Ice Concentration (%)</b>
14-Nov-08	5
15-Nov-08	20
16-Nov-08	20
17-Nov-08	30
18-Nov-08	50
19-Nov-08	100

### **2.4.5 Water Level Data**

In 2008, a pressure transducer connected to a datalogger was deployed at river station M268.1, in order to record the water level rise associated with the ice stopping front passing through. The pressure transducer was also connected to a cellular modem, allowing for the transmission of real-time water level data. Similarly as for water temperature, water level data from November 13, 2008 to November 17, 2008 was discontinuous due to low battery problems. Figure 2.24 shows the water level readings recorded over the freeze-up period. The estimated error for these measurements consisted of a ~1% water level sensor error plus the error due to not correcting for barometric pressure. From this information, it can be seen that bridging occurred sometime between the evening of November 18 and the morning of November 19, 2008, since the water levels rose 1.1 m during this time.

### **2.5 Winter Field Program**

Winter work in early 2009 consisted of ‘top of ice’ profiling, water depth, ice thickness and snow thickness measurements as well as velocity and discharge measurement. This involved using the RTK-GPS for control surveys and top of ice measurements, an underwater camera for observing under ice roughness and frazil conditions, a handheld digital sonar for measuring water depth, an ice thickness gauge, a rod for measuring snow thickness as well as an Acoustic Doppler Velocimeter (ADV) and an Acoustic Doppler Current Profiler (ADCP) for velocity and flow measurements. Ice core samples were to be taken at several locations; however, due to equipment malfunction, this was not possible.

The ADV and ADCP were used at the same sites in order to test out which piece of equipment is more effective for winter measurements. Each unit has benefits and disadvantages associated with its use. The ADV is able to record velocities at various depths and that information can be used to manually calculate the discharge across a section. The ADV requires much less preparation time;

however, it does not allow the user to view results in real time and the quality of the data is not known until it is processed later. The ADCP requires a more extensive set-up and must be connected to a computer via a modem to work. The user can always view results and all velocity as well as discharge measurements are shown; however, if the connection between the computer and ADCP is lost, work on a particular transect must be restarted.

Winter surveys were carried out during the week of February 23 through 27, 2009 at Sites 3 through 6 (Figure 2.2). These sites were identified as significant for the winter survey. Obtaining under ice discharge measurements at Sites 3 and 4 is important for gathering flow split information. Site 5 crosses the narrowest and the deepest section of the channel, thus it was thought to be the easiest site to carry out a full channel discharge measurement. Similar to the surveys conducted in the summer, horizontal and vertical positioning was achieved in this survey using the RTK-GPS with a 'local' co-ordinate system. The same TBM (ISL2) was used throughout the program.

### **2.5.1 Top of Ice Surveys**

Top of ice measurements were completed at Sites 3 through 6 (Figure 2.2). Upon conducting a thorough safety assessment, specified co-ordinates were flagged along each transect using a handheld GPS and holes were augured in the ice cover. Extra holes were also augured to locate the edge of water at each bank. The RTK-GPS was then used to accurately record the location and top of ice elevation at every augured hole across each section. Additional top of ice measurements were taken at station 0801, the downstream boundary of the detailed 5-km reach. The relative accuracy of all points surveyed within this local co-ordinate system was, again, within  $\pm 2$  cm. The results of the average top of ice level at each section are contained in Table 2.5.

**Table 2.5. Average values of the ‘top of ice’ elevation survey.**

<b>Site Number/TBM</b>	<b>Station (km)</b>	<b>Water Level (m)</b>
6	268.7	234.20
5	267.7	233.98
4	265.7	233.68
3	265.7	233.62
0801	263.4	233.42

### **2.5.2 Ice Thickness Measurement**

Ice thickness measurements were completed at each augured hole at Sites 3 through 6 (Figure 2.2). Ice thickness measurement data shows that there was some variation in ice thicknesses throughout each cross section, as can be seen in Figures 2.25 through 2.28. The range of values extended from 0.45 m at Site 6 to 0.76 m at Site 5. The estimated error for each measurement is  $\pm 0.05$  m. The average thicknesses calculated at Sites 3 through 6 were 0.56 m, 0.57 m, 0.60 m and 0.61 m, respectively. The overall average value of all the thicknesses measured was 0.58 m. This average value was used for the ice covered modeling efforts.

### **2.5.3 Snow Depth Measurement**

Snow depth measurements were completed at each augured hole at Sites 3 through 6 (Figure 2.2). Each measurement was conducted using a rod with centimeter markings. The results can be seen in Figures 2.29 through 2.32. The estimated error for each measurement is  $\pm 0.10$  m. The sources of error include possible variability in the amount of compaction of the snow and difficulty in locating the exact level of the bottom of the snow as well as the top of the snow with a simple rod. It was found that values at Sites 3, 5 and 6 were very scattered and ranged between 0.15 m and 0.48 m. The average values at Sites 3, 5 and 6 were 0.34 m, 0.37 m and 0.34 m, respectively. This uneven snow cover is likely caused by winds that blew across the sections. At Site 4, values were consistent

at each hole (Figure 2.30). At this site, it was found that the snow cover varied between 0.15 m and 0.28 m with snow that was approximately 0.10 m thicker in the middle of the channel than at the sides. The average snow depth at Site 4, 0.25 m, was approximately 0.10 m lower than the averages at the three other sites. This falls within the estimated measurement error.

#### **2.5.4 Underwater Video**

At Sites 3 and 6, video was recorded of the underside of the ice (Figure 2.2). This was done to gain an understanding of the nature of the underside of the ice cover and to determine if any frazil was being transported below the ice cover. Video was taken at Sites 3 and 6 in relatively deep sections and at Site 6 in a relatively shallow section. The results showed that the underside of the ice is very smooth and confirmed that no frazil ice was present below the ice surface.

#### **2.5.5 Velocity Measurements**

Velocity measurements were conducted on the Athabasca River in each augured hole at Sites 3 through 6 with an ADV and Site 3 through 5 with an ADCP (Figure 2.2). For each measurement with the ADV, the sensor was submerged just below the ice surface in the augured hole for a 5-minute interval. Such a time interval was necessary due to the uncertainty of results as they were not able to be viewed instantly. Upon completion of all measurements across a section, the data was downloaded and processed in order to view results. At Sites 3, 4 and 5, the ADCP was used in a similar fashion to the ADV with each measurement conducted over a 1-minute interval. Due to the ability to perform quality control as results of flow depths and velocities were viewed instantly, measurements could be carried out over a shorter time interval. Also, measurement carried out by the ADCP needed to be done quickly because of the difficulties experienced with maintaining a stable connection with the computer due to battery power issues in the extreme cold weather. As mentioned previously, once a connection

is lost, measurements for the entire section need to be repeated. The velocity measurement error for both of these instruments, as specified by the manufacturers, is  $\pm 1\%$  or 0.5 cm/s.

The velocity measurements recorded by the ADV and the ADCP were compared for each cross section. At Site 3, two passes were carried out with an ADCP and one set of measurements were completed with an ADV (Figure 2.33). It was found that the first pass of the ADCP produced one erroneous velocity reading at a point 96 m away from the left bank. In the second pass of the ADCP, this point was measured correctly. Aside from the error encountered in the first pass, the two sets of ADCP readings were very similar. When comparing the readings from the ADV, it can be seen that most of the values reported were slightly higher than those of the ADCP. In the part of the cross section located near the right bank where values start to decrease, the measurements are considerably higher than those recorded by the ADCP.

At Site 4, two passes were carried out with the ADCP and one set of measurements were completed with the ADV (Figure 2.34). It can be seen that both passes of the ADCP resulted in very similar readings. The ADV produced an unreasonable reading of 1.4 m/s at a point 46 m away from the left bank. Apart from this error, it can be seen that the values of the measurements recorded by the ADV were considerably higher than those of the ADCP. It is possible that the ADV is less sensitive at lower velocities than the ADCP.

At Site 5, one pass of the ADCP and the ADV were completed along the cross section (Figure 2.35). It can be seen that results from both instruments are similar; however, it can be seen that the values given by the ADV are slightly higher than those given by the ADCP. This is most apparent in the middle of the section and near the left and right banks. At Site 6, the only velocity measurements carried out were those of the ADV (Figure 2.36). The results show that velocities are highest at the sides of the channel and decrease towards the middle. This section is very wide and straight and it is possible that the deeper and faster flowing sections are located closer to the edges of the channel.

When comparing the measurements made by the ADCP and those made by the ADV, it can be seen that the values from the ADV are higher than values measured by the ADCP. This is especially evident in areas of lower velocities, where ADCP readings are below 0.3 m/s. This suggests that the ADCP has a greater resolution than the ADV in the lower velocity range. Testing carried out on other cross sections is needed in order to investigate this further.

### **2.5.6 Depth of Water under Ice**

The depth of water under the ice cover was measured at each augured hole at Sites 3 through 6 (Figure 2.2). Water depths were obtained by using a hand-held digital sonar and compared with the depth readings measured by the ADV and the ADCP. The results of these readings are displayed in Figures 2.37 through 2.40. The estimated error in measurement is 2 to 5 cm for all three instruments.

At Site 3 (Figure 2.37), an erroneous ADCP depth measurement occurred at a distance of 96 m from the left bank, which corresponds with the erroneous velocity measurement noted earlier (Figure 2.33). Apart from this point, it can be seen that all of the remaining values obtained by the three different pieces of equipment are very similar. Similarly, Site 4 (Figure 2.38), water depth measurements taken by all three instruments were quite consistent, with the exception of one hand-held sonar reading at a distance of 46 m from the left bank which was approximately 50% high.

At Site 5, water depth measurements were taken by an ADCP, an ADP and a hand-held digital sonar (Figure 2.39). It appears that the data recorded by the ADV is very similar to the digital sonar data; however, the measurements taken by the ADCP at this site are both higher and lower than the other two instruments throughout the middle of the cross section. The accuracy of this measurement is questioned since the differences between readings from this instrument and all the others were up to 1.4 m. This also demonstrates the importance of taking more than one discharge measurement across the section. At Site 6, water depth

measurements were taken by an ADP and a hand-held digital sonar (Figure 2.40). From the figure, it can be seen the readings from the two pieces of equipment are very similar.

When comparing all of the depth measurements made with an ADCP, an ADV and a hand-held sensor, it was found that the results were mostly very similar. The one exception is the ADCP readings taken at Site 5. It appears that these were not accurate when comparing with the other two sets of data. The reason for this error is unknown, but it is possible that it was caused by ice forming on the bottom of the sensors as they were being taken in and out of the augured holes.

### **2.5.7 Discharge Measurements**

Discharges measurements were determined from the ADCP velocity measurements at Sites 3 through 5, and from the velocity measurements conducted by an ADV at Sites 3 through 6 (Figure 2.2). The estimated error for the readings from each of the instruments is  $\pm 10\%$  plus there is an additional error associated with only taking measurements at 5 to 10 stations (augured holes) as compared to at 20 stations. Hicks *et al.* (1995) showed that this error can cause the discharge to be underestimated by 8-9%. Measurements across a full section were compared with the WSC measurements for Station 07DA001 (Athabasca River below Fort McMurray). Throughout the winter, when the water gauges are affected by ice conditions and cannot provide discharge data, the WSC conducts several manual discharge measurements. Prior to the commencement of the winter field program, the last measurement was carried out on February 5, 2009 and reported a value of  $149 \text{ m}^3/\text{s}$ .

Discharge measurements were carried out at Site 3 in order to gain an understanding of the flow in the channel on the left side of the island (Figure 2.2). The results of these measurements carried out by the ADCP were  $152 \text{ m}^3/\text{s}$  on the first pass and  $144 \text{ m}^3/\text{s}$  on the second pass. The estimated error on these values is  $15 \text{ m}^3/\text{s}$  and  $14 \text{ m}^3/\text{s}$ , respectively. The value calculated for the ADV was 148

$\text{m}^3/\text{s}$  at this site, with an estimated error of  $15 \text{ m}^3/\text{s}$ . These values are all similar; however, the value of the second pass of the ADCP,  $144 \text{ m}^3/\text{s}$ , was selected as representative of the section. This choice was based on the results of the velocity and depth measurements (Figures 2.33 and 2.37). The graphical output of all of the ADCP discharge measurements is contained in Appendix B.

Discharges measurements were carried out at Site 4 in order to get an idea of the flow split in the channel at the island (Figure 2.2). The results of the discharge measurements carried out at this site were quite different for the ADCP and the ADV. The first and second passes of the ADCP reported discharges across the section of  $14 \text{ m}^3/\text{s}$  and  $15 \text{ m}^3/\text{s}$ , respectively. The estimated error on these values is  $1.5 \text{ m}^3/\text{s}$  and  $1.4 \text{ m}^3/\text{s}$ , respectively. Based on velocity data collected by the ADV, the calculated discharge across the section was  $32 \text{ m}^3/\text{s}$ , with an estimated error of  $3.2 \text{ m}^3/\text{s}$ . This reflects the higher water velocity readings obtained using the ADV (Figure 2.34). The results from discharge measurements taken at Sites 3 and 4 indicate that only a very small percentage of water flows on the right side of the island under low flow conditions. The addition of the discharges at Sites 3 and 4 represents the total discharge in the river. Using the ADCP measurements, this value is  $158 \text{ m}^3/\text{s}$  and within 10% of the value reported by WSC. This value is  $178 \text{ m}^3/\text{s}$  using the ADV values, which 20% higher than the value reported by WSC. Because of this, more confidence is placed in the values obtained by the ADCP and the value of  $14 \text{ m}^3/\text{s}$  was selected as representative of this section. The graphical output of all of the ADCP discharge measurements is contained in Appendix B.

Discharge measurements were carried out at Site 5 to obtain a value of the total discharge experienced by the river (Figure 2.2). The discharge obtained by the ADCP was  $153 \text{ m}^3/\text{s}$  and the value calculated from the velocity readings made by the ADV was  $154 \text{ m}^3/\text{s}$ . These values are very similar and are within 3% of the value of  $149 \text{ m}^3/\text{s}$ , as reported by the WSC. It is interesting to note that the depth measurements made by the ADCP were different from those made by both the ADV and the digital sensor (Figure 2.39); however, the resulting discharge is

within 1 m<sup>3</sup>/s. The graphical output of all of the ADCP discharge measurements is contained in Appendix B.

The discharge at Site 6 was calculated from the velocity measurements made by the ADV (Figure 2.2). This value was determined to be 125.0 m<sup>3</sup>/s. This value is 17% lower than the previously calculated discharges and the value reported by the WSC. This is most likely due to the fact that velocity measurements were only made at 8 holes across a 300 m wide cross section, causing areas of higher velocity to be overlooked. An increase in the number of holes augured would likely have improved results; however, this was not known in the field because ADV data needs to be post-processed before viewing.

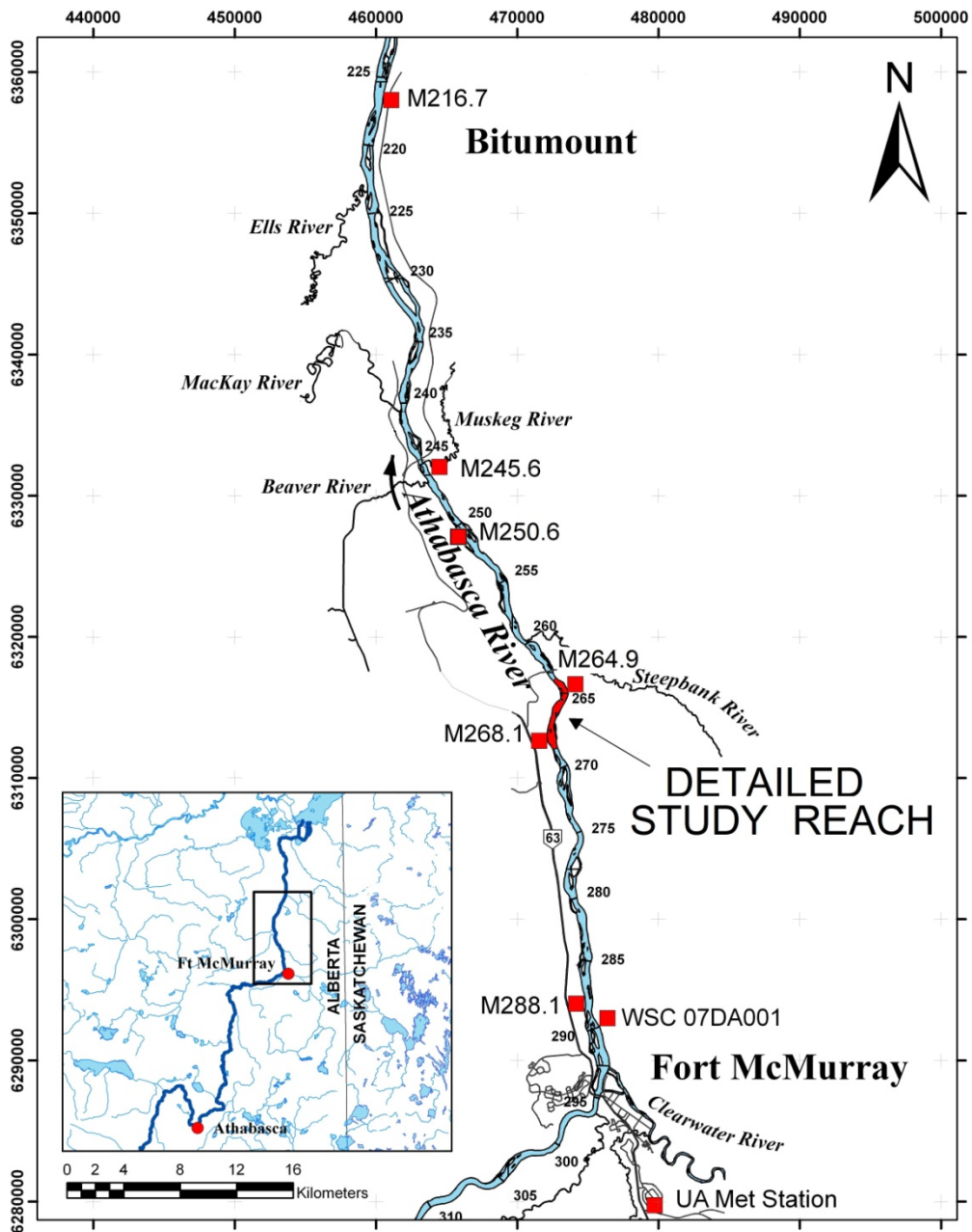


Figure 2.1. Map of the full study reach from Fort McMurray to Bitumont (adapted from Robichaud, 2003).

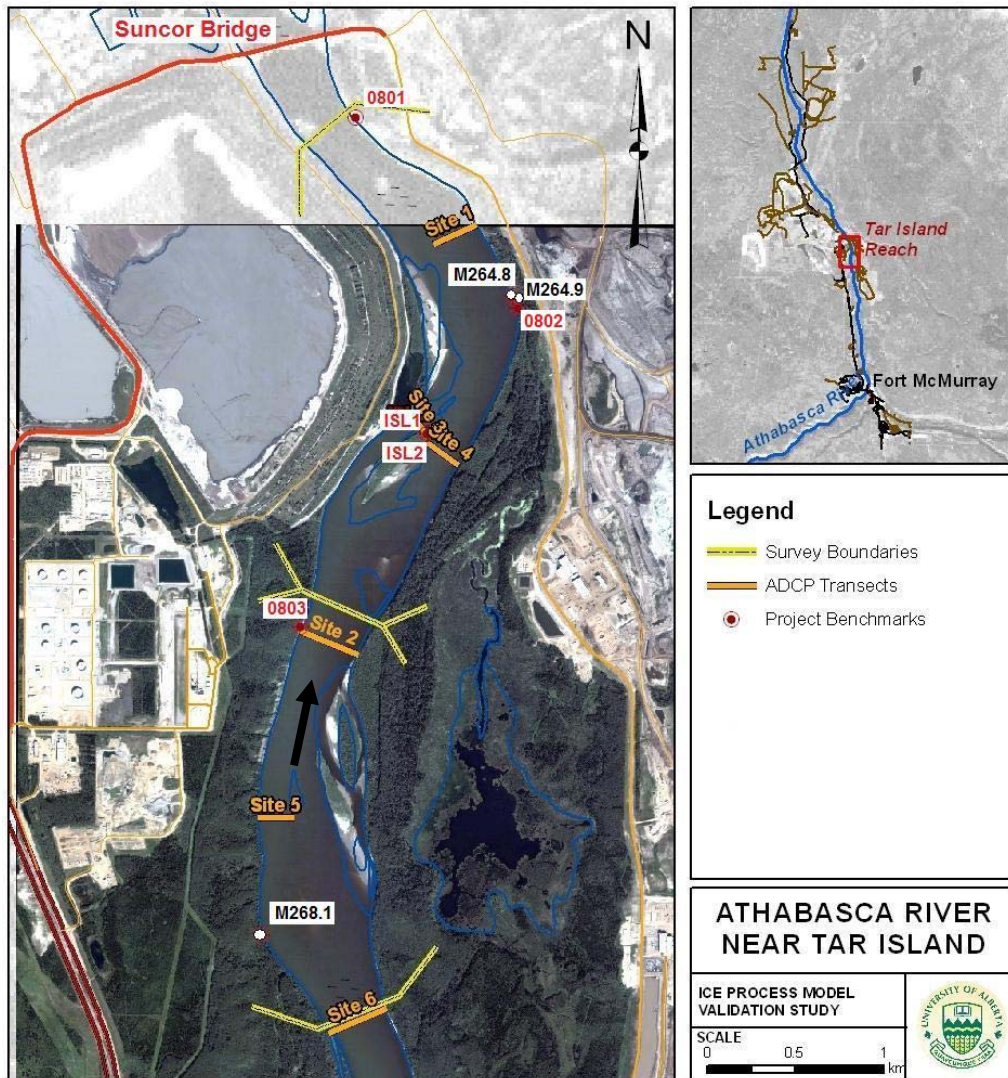
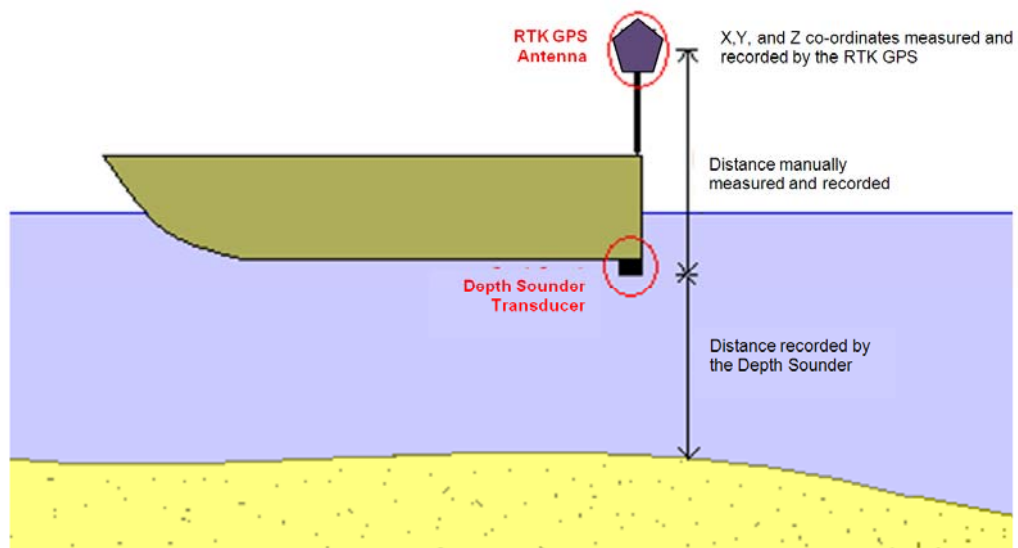


Figure 2.2. Map of the 5-km detailed study reach.



**Figure 2.3. Dune bed forms at km 276 on the Athabasca River in the reach downstream of Fort McMurray, November 8, 2008.**



**Figure 2.4. Defining sketch for calculation of bed point elevation (adapted from Meliefste and Hicks, 2005).**

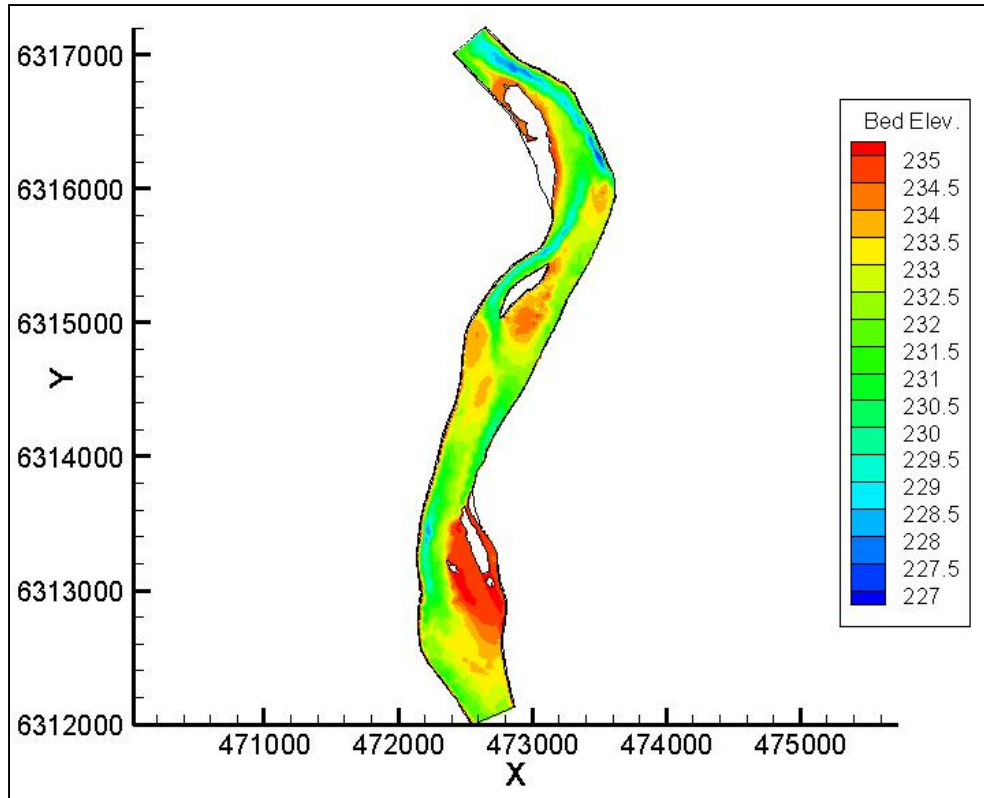


Figure 2.5. Channel Bathymetry in the detailed study reach (m).

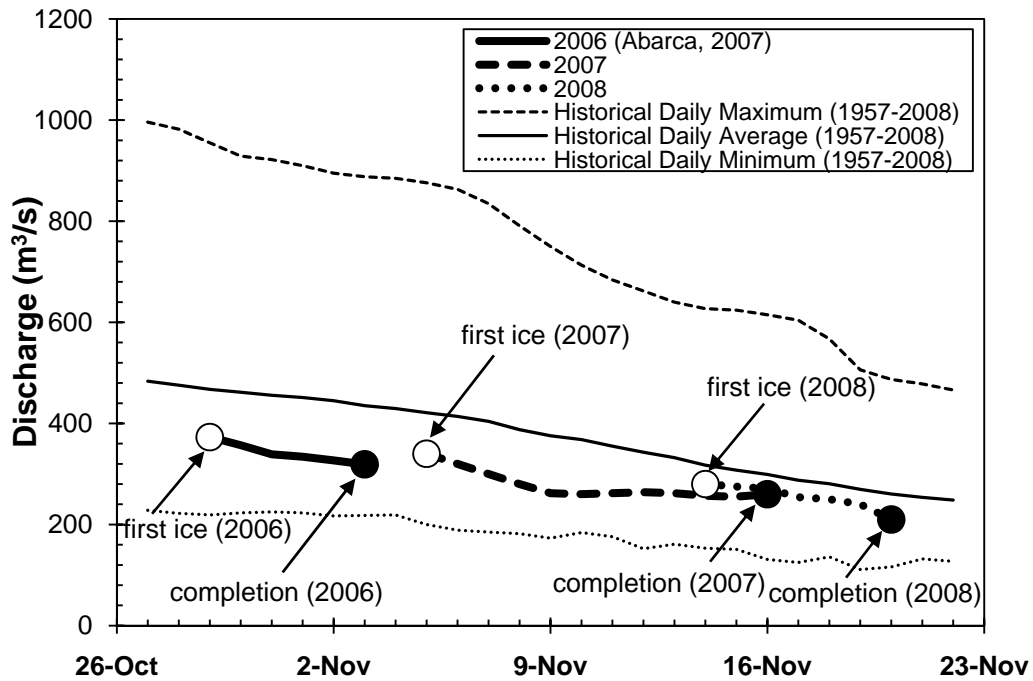
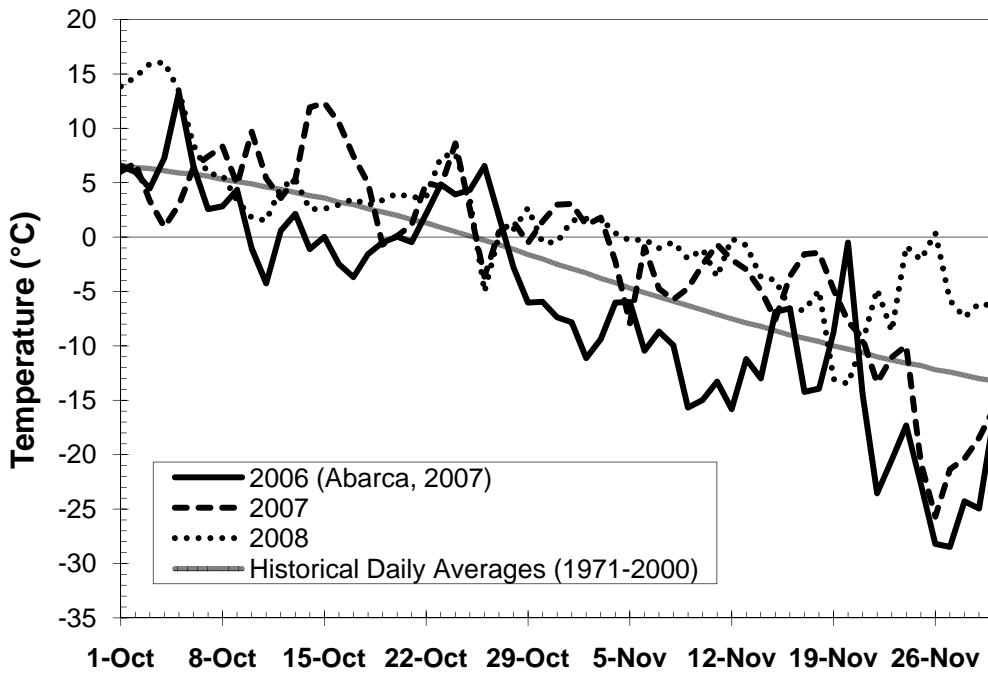
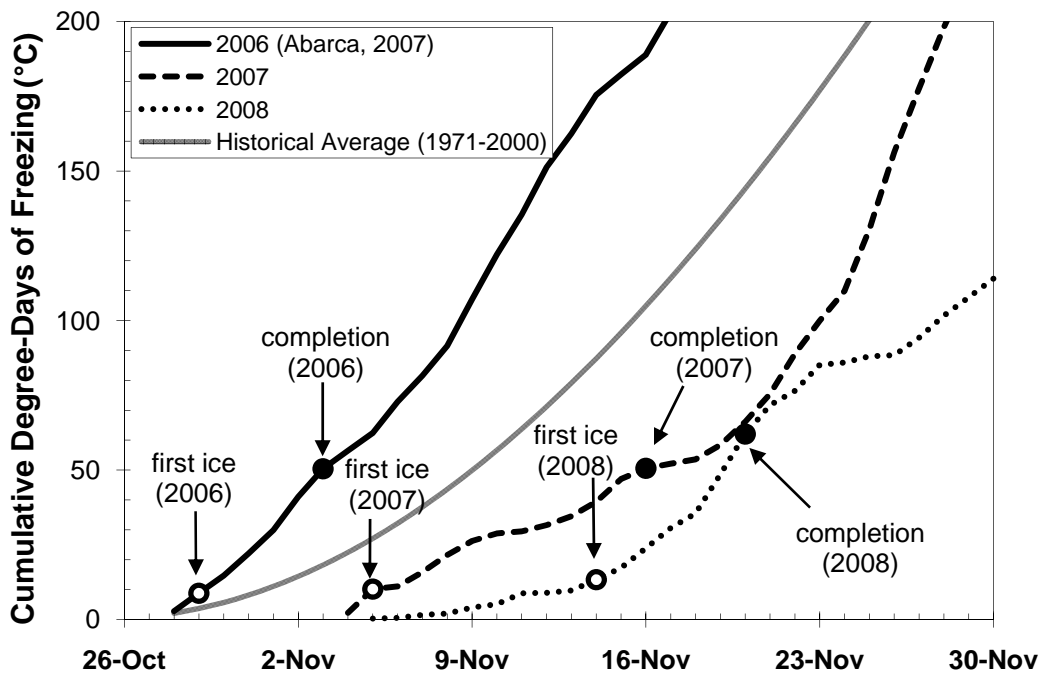


Figure 2.6. Discharges reported by Water Survey of Canada (Station 07DA001) throughout freeze-up for the years 2006 to 2008.



**Figure 2.7. Mean daily air temperatures for 2006 to 2008, as compared to historical (Environment Canada, Fort McMurray Airport).**



**Figure 2.8. Accumulated degree-days of freezing for 2006 to 2008, as compared to historical (Environment Canada, Fort McMurray Airport).**

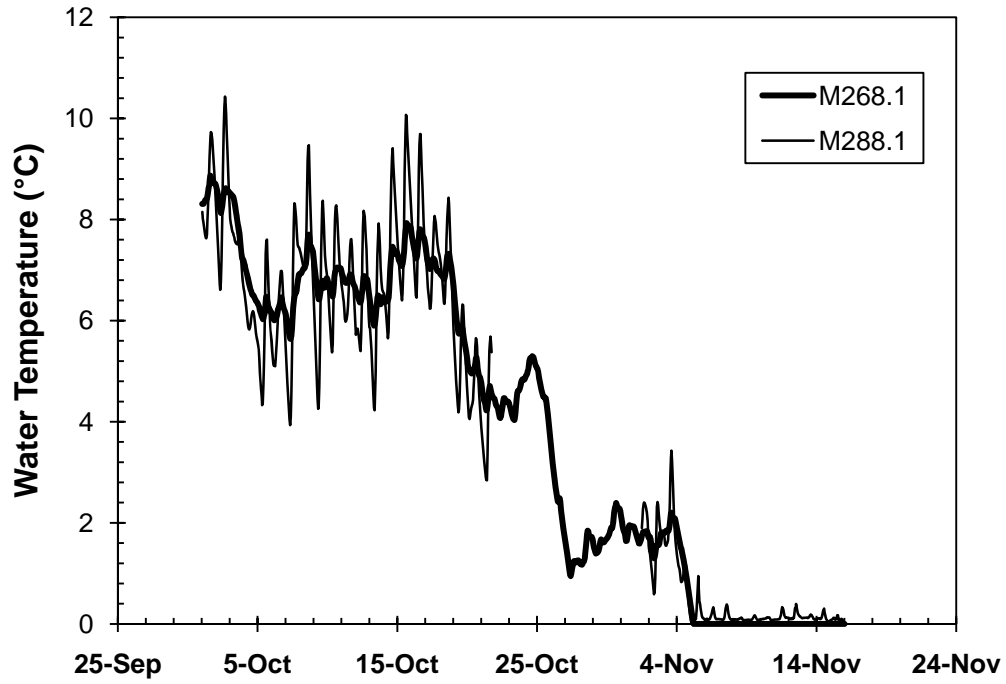


**Figure 2.9. Water temperatures measured during freeze-up 2007 at M268.1 and M288.1.**



**Figure 2.10. Photograph showing the approximate location of water temperature sensor at M288.1 in 2007.**

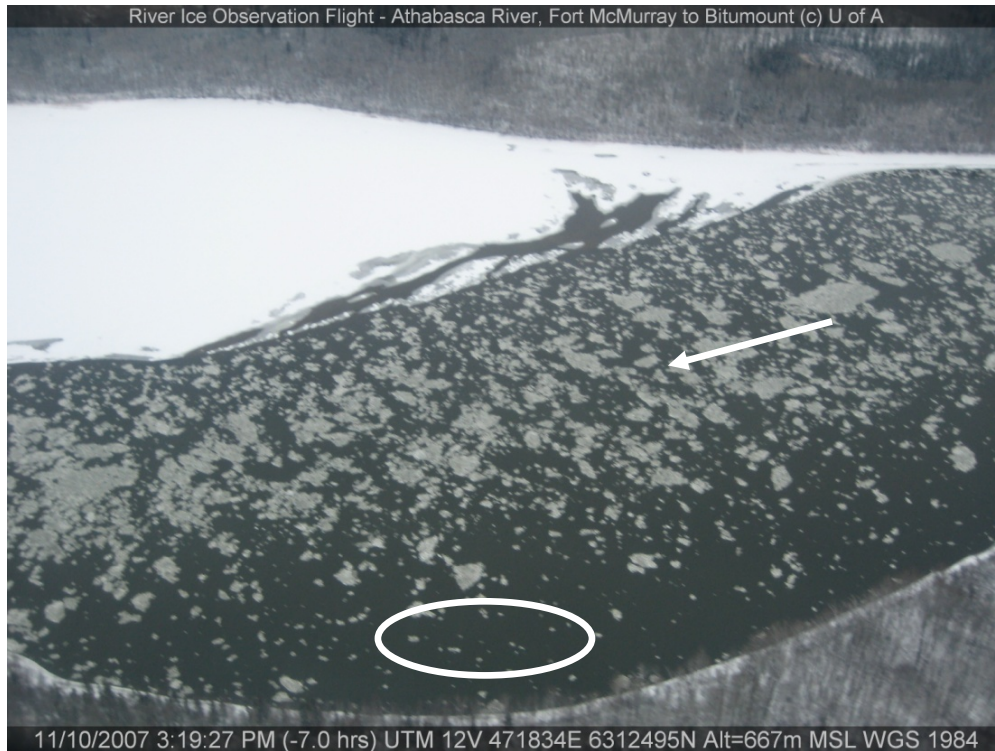


**Figure 2.11. Photograph showing the approximate location of water temperature sensor at M268.1 in 2007.**

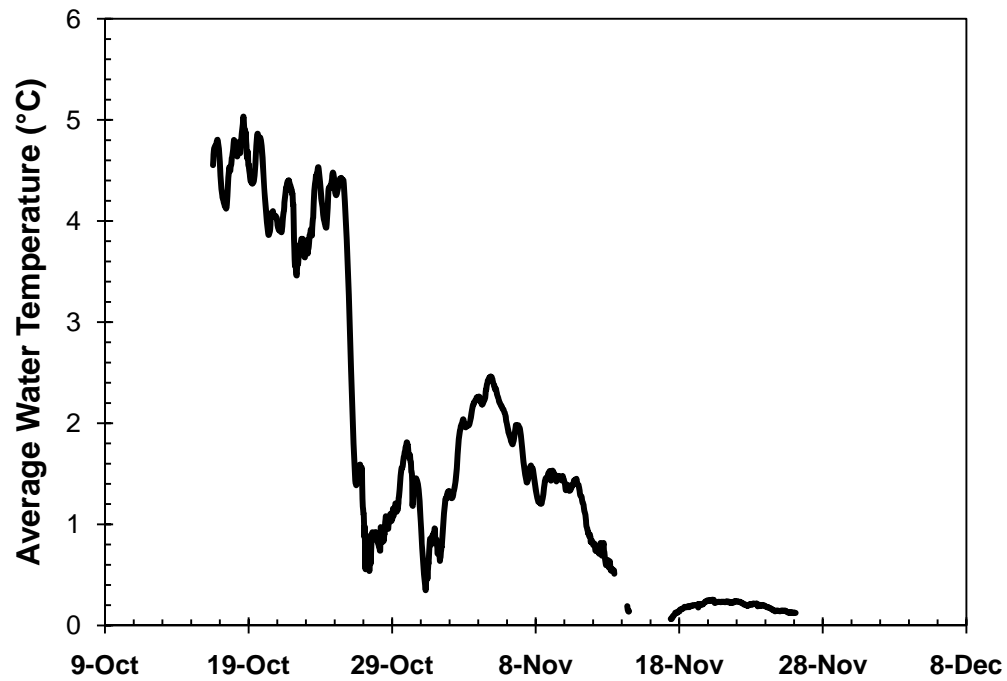


**Figure 2.12. Water temperatures measured during freeze-up 2008 at M268.1.**

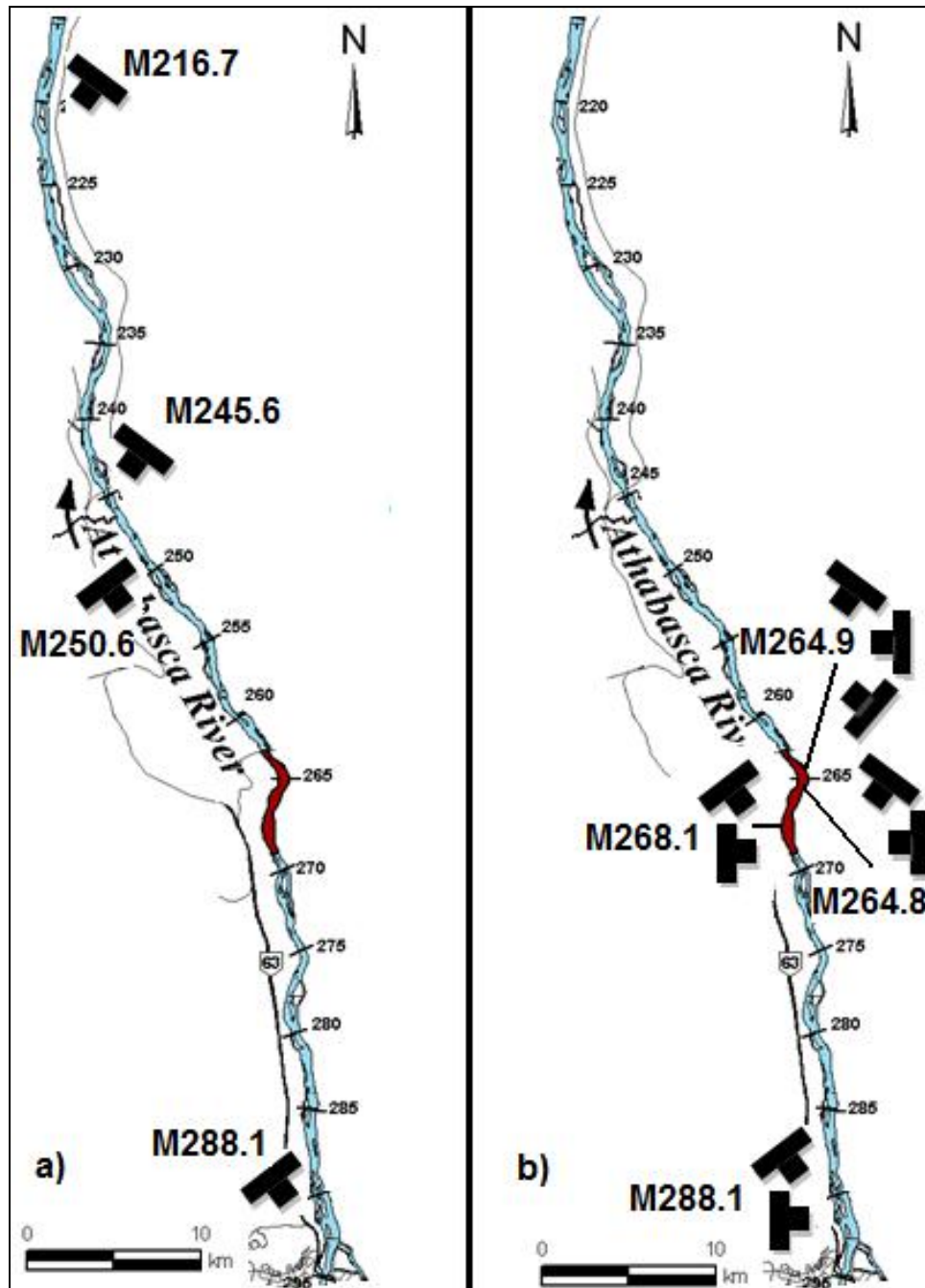
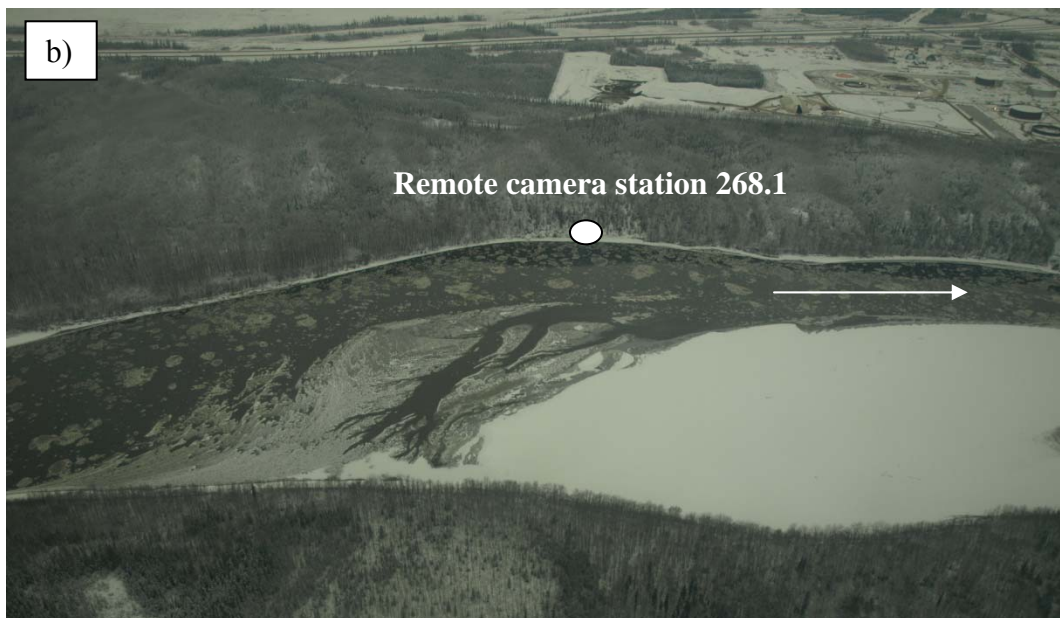
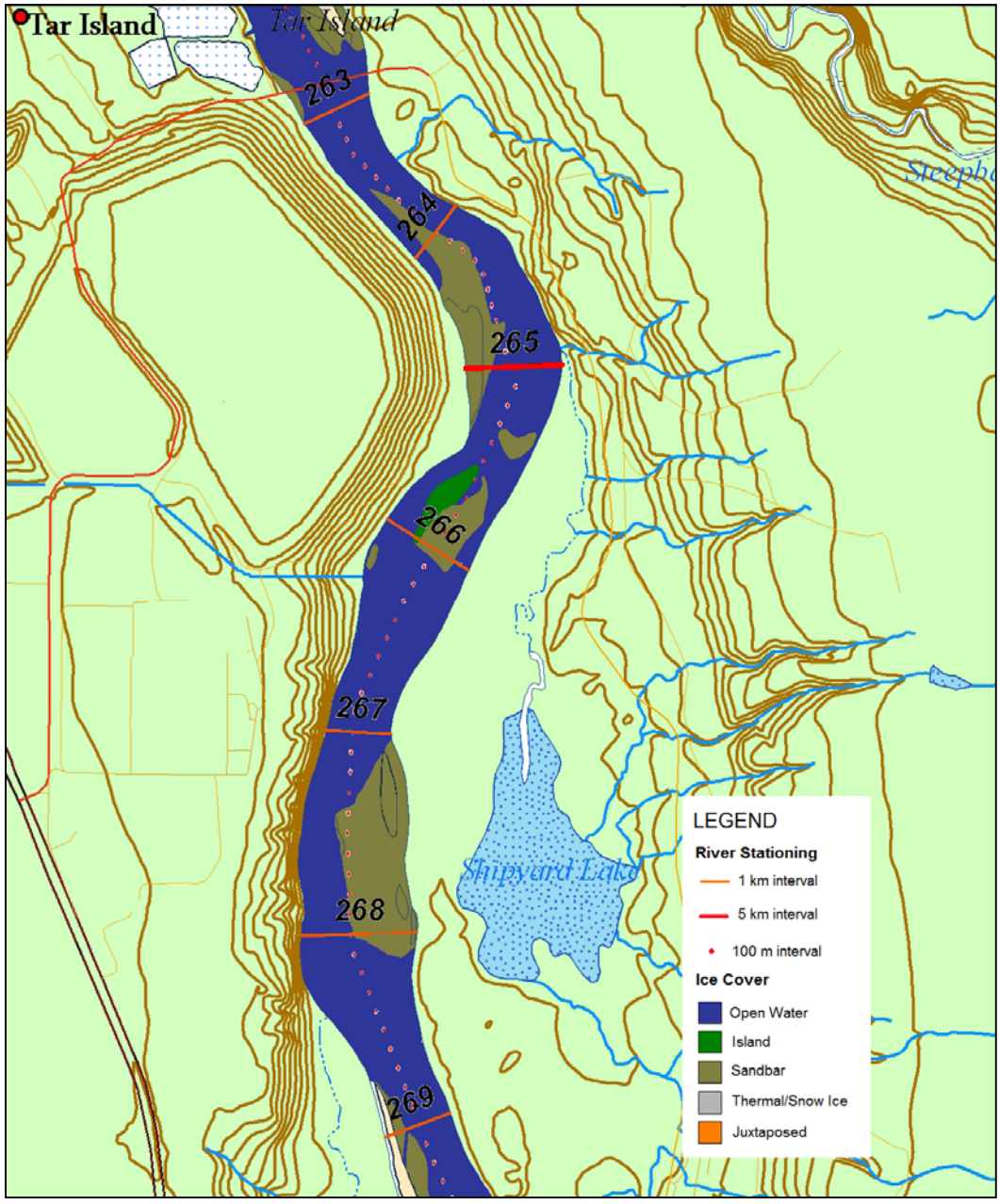


Figure 2.13. Digital time lapse camera placement and orientation in the full study reach (a) 2007, (b) 2008.



**Figure 2.14. Examples of photographs taken on November 17, 2008 to document freeze-up in the study reach (a) remote camera (268.1), (b) aerial observations.**



**Figure 2.15. Ice map based on aerial flight observations made on November 1, 2007.**

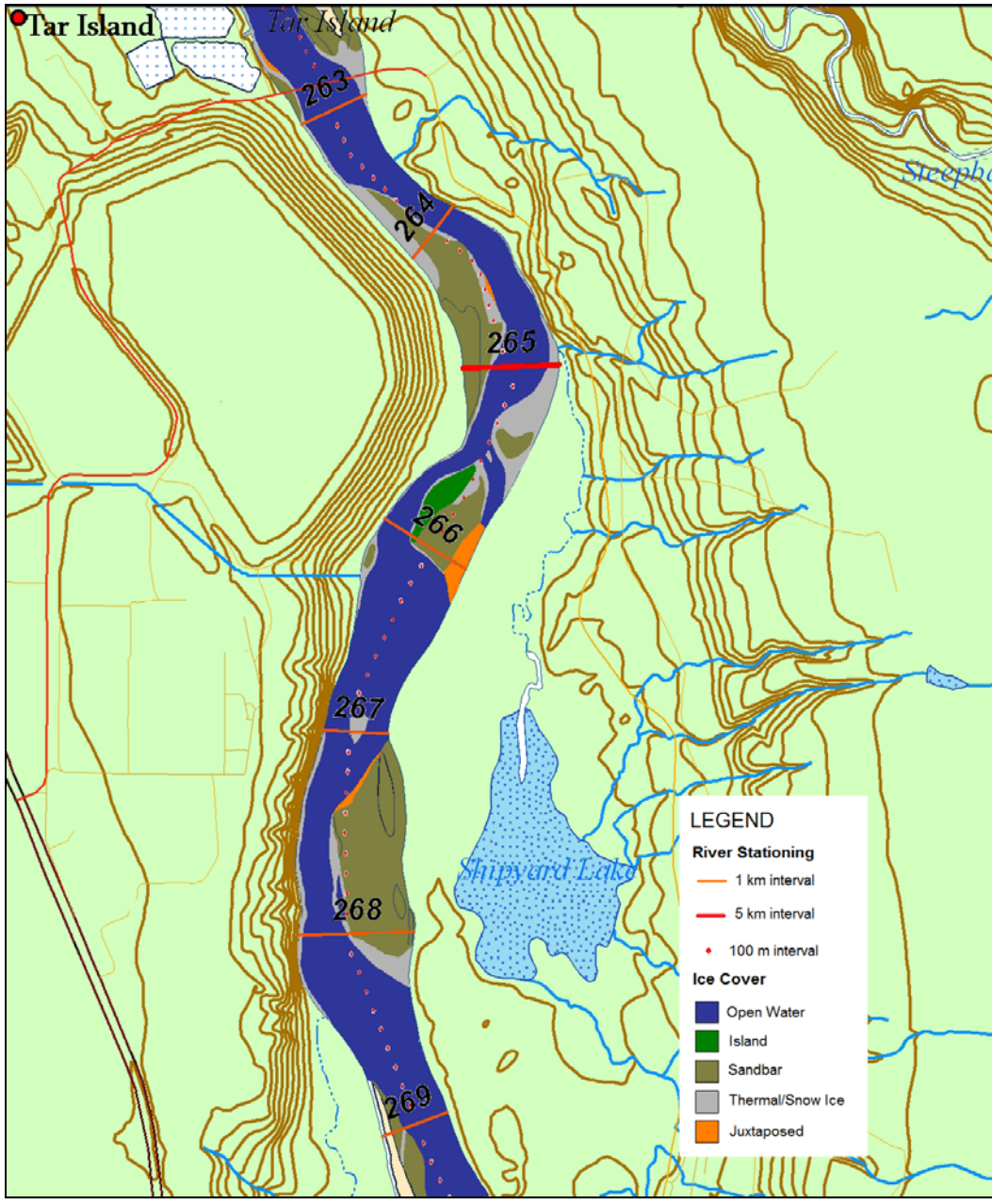


**Figure 2.16. Ice map based on aerial flight observations made on November 9, 2007.**

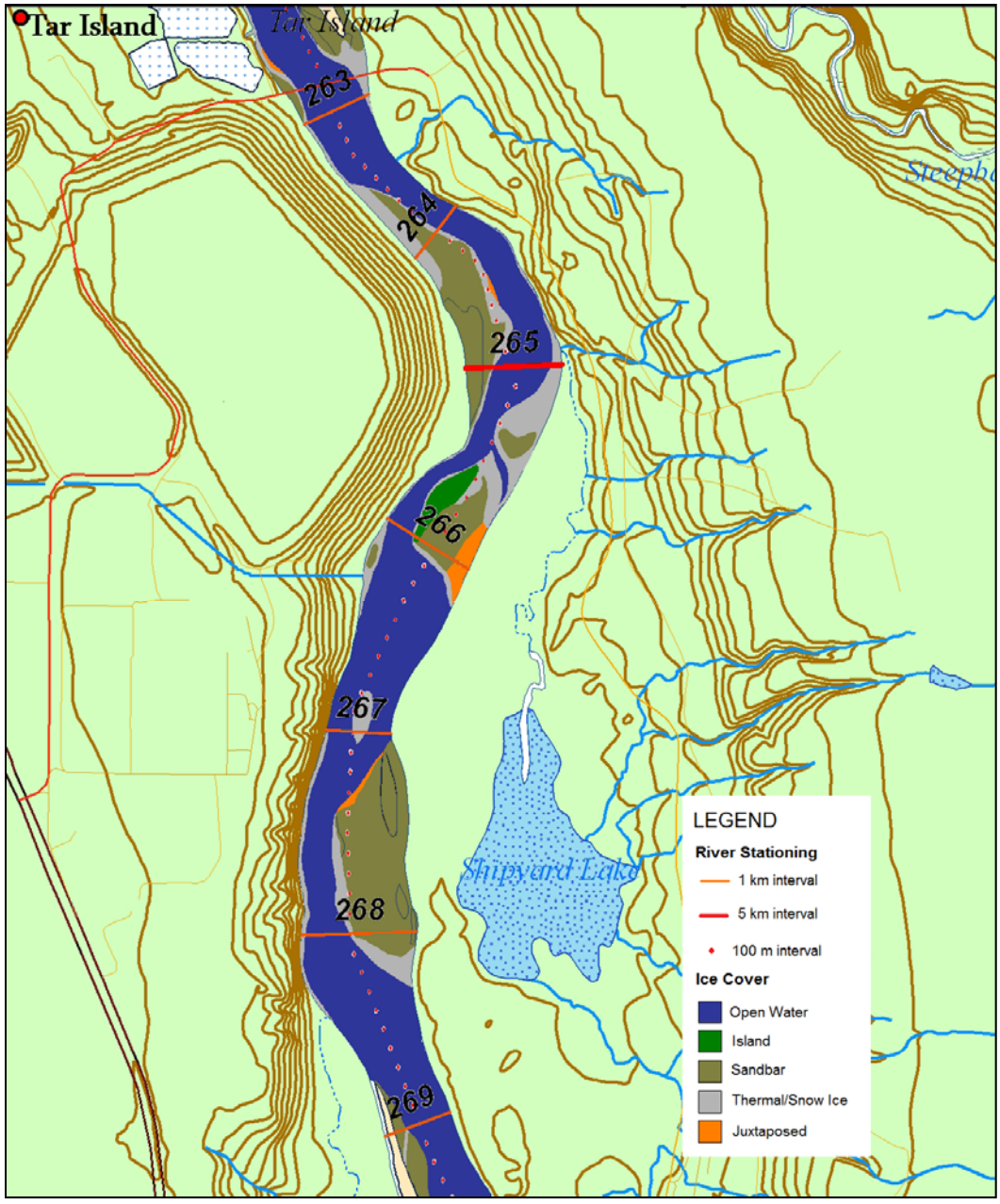


**Figure 2.17. Ice map based on aerial flight observations made on November 10, 2007.**

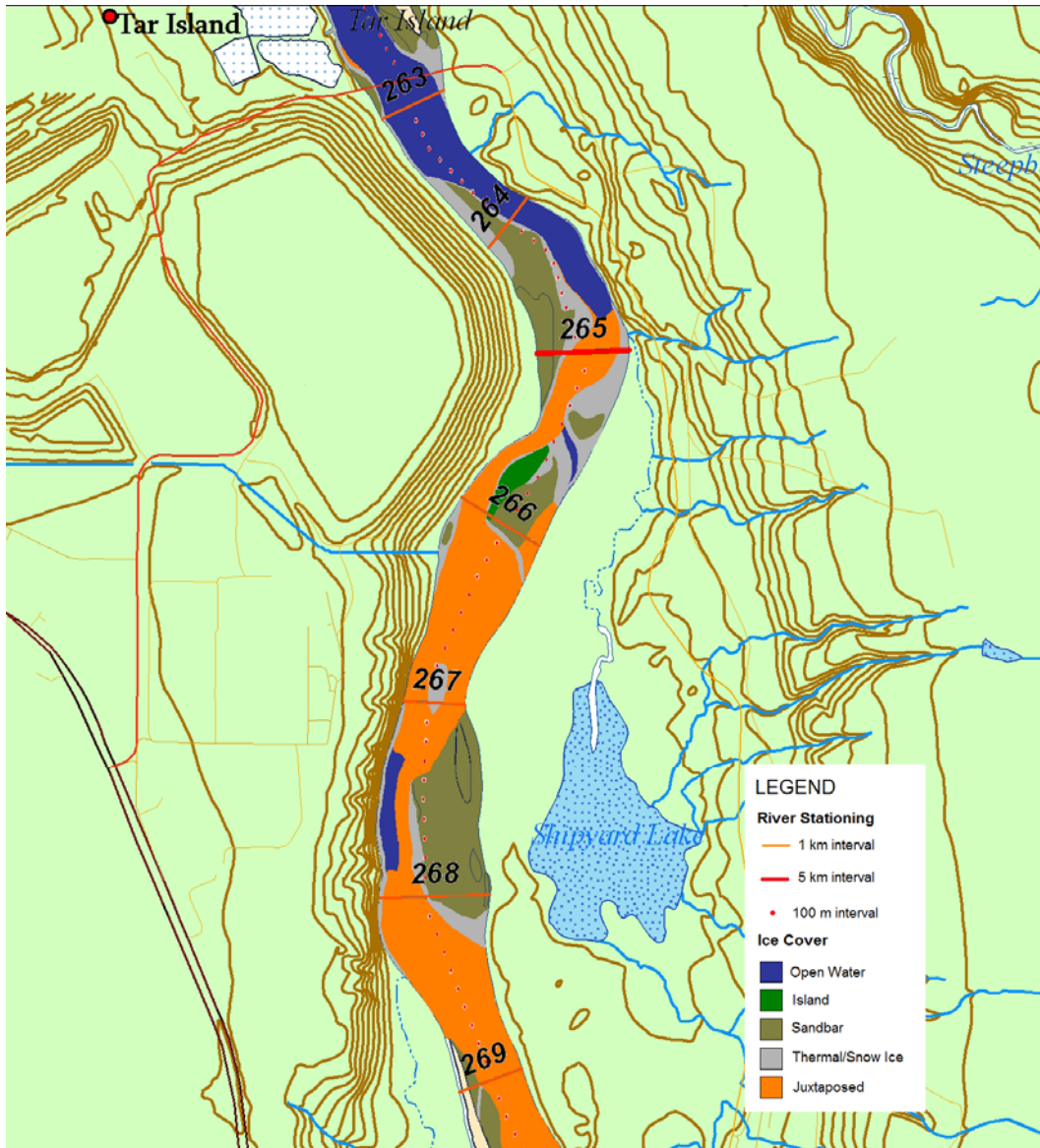


**Figure 2.18. Ice map based on aerial flight observations made on November 16, 2007.**

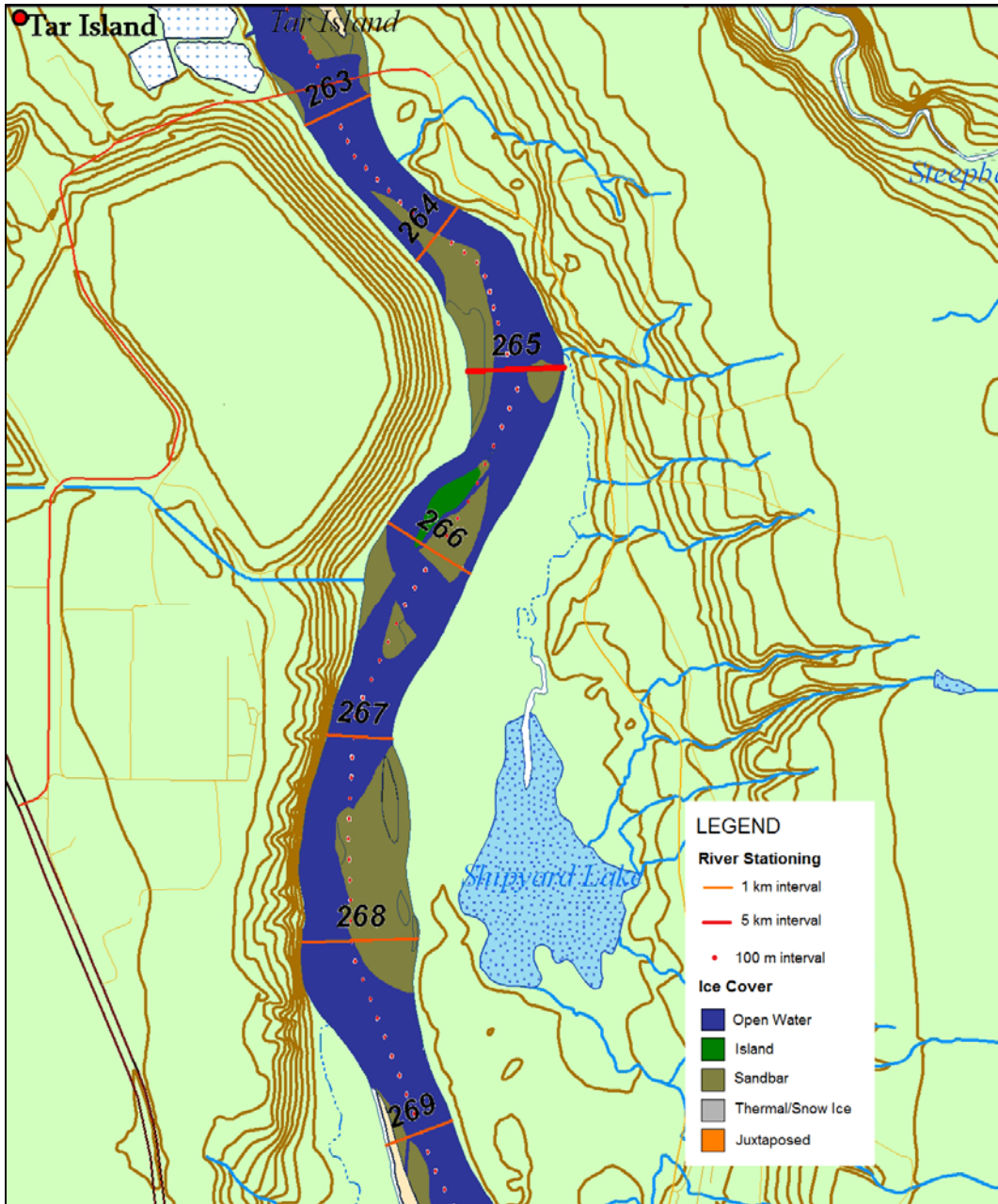


**Figure 2.19. Ice map based on aerial flight observations made on November 8, 2008.**

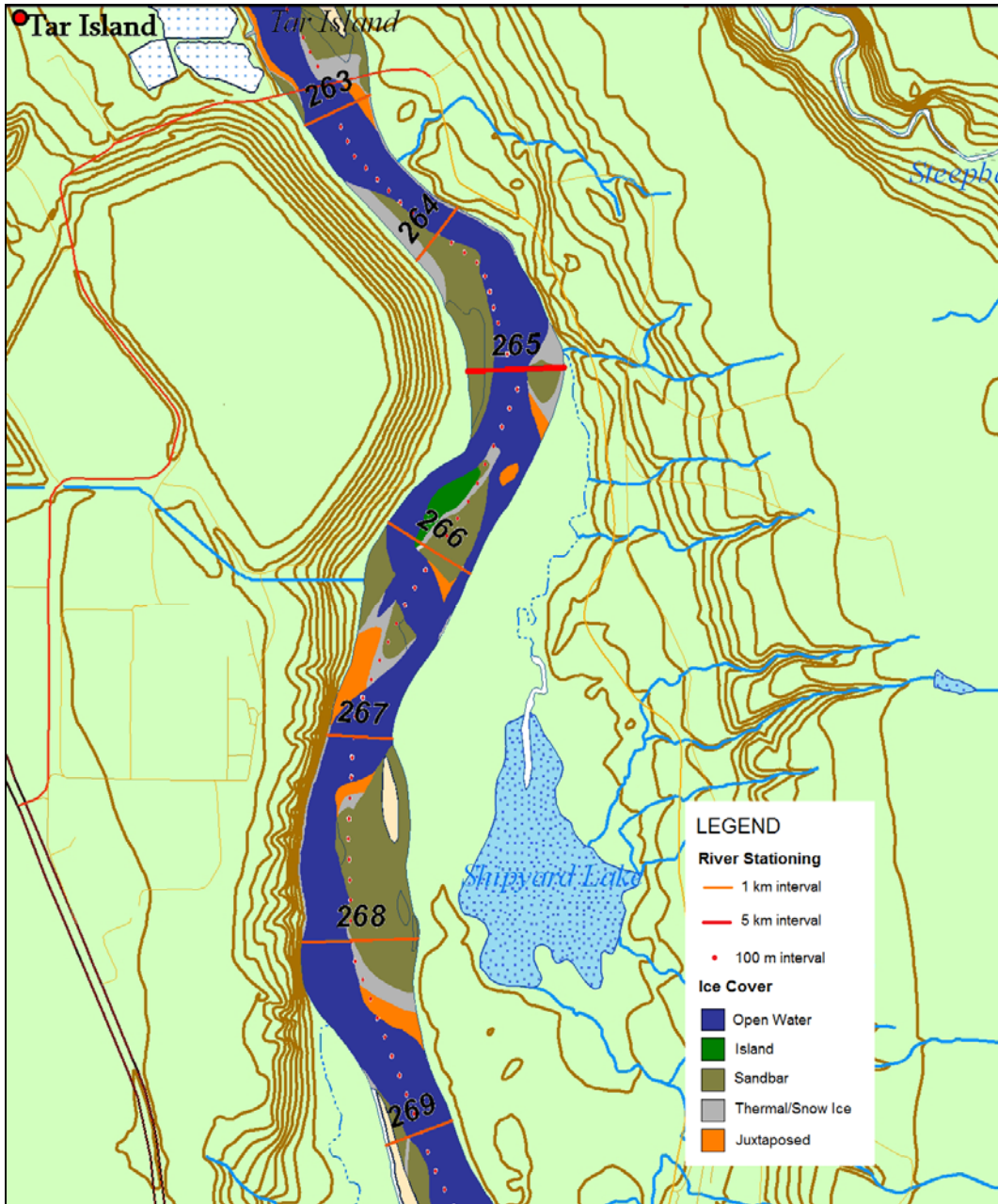


**Figure 2.20. Ice map based on aerial flight observations made on November 16, 2008.**

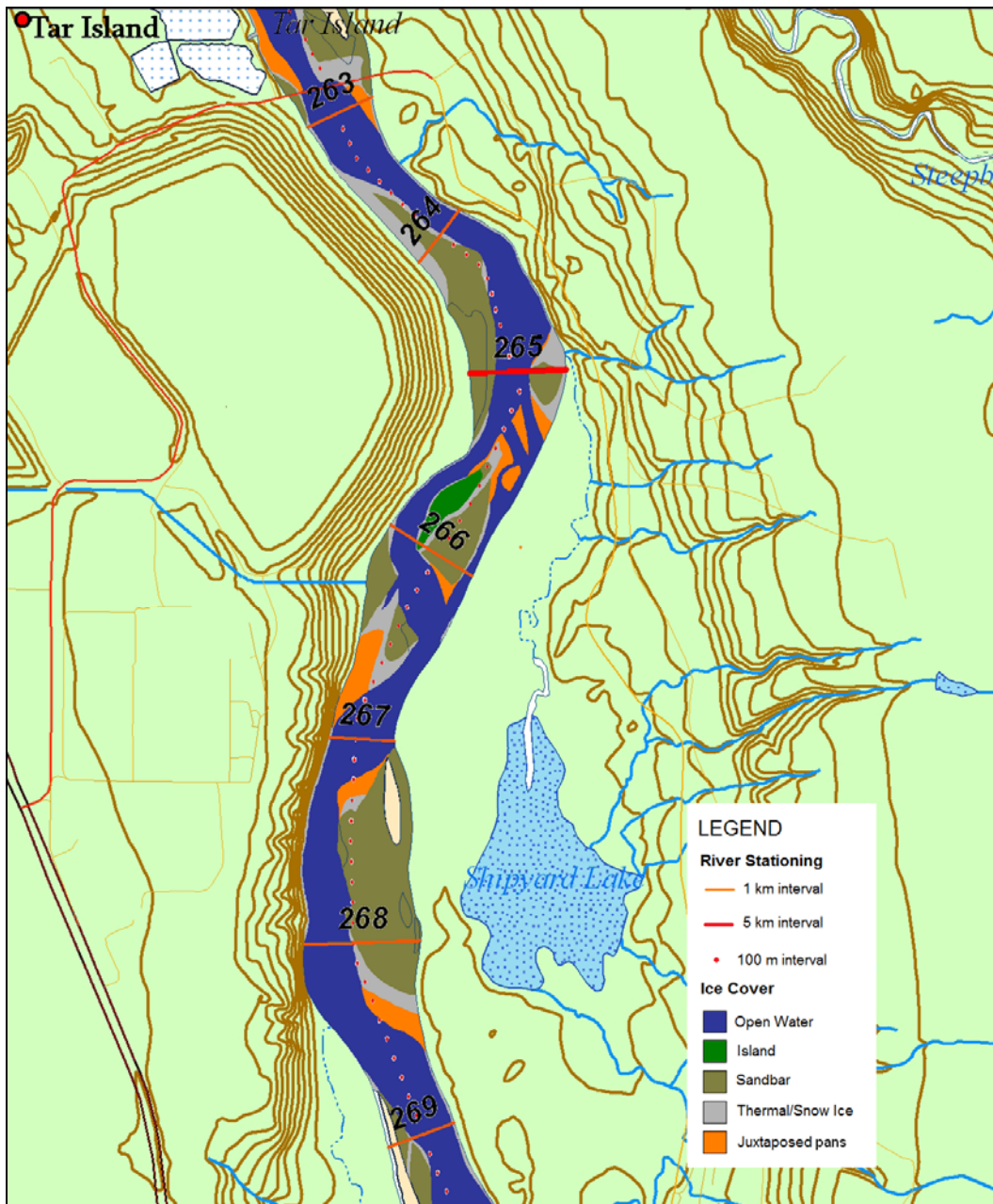


**Figure 2.21. Ice map based on aerial flight observations made on November 17, 2008.**

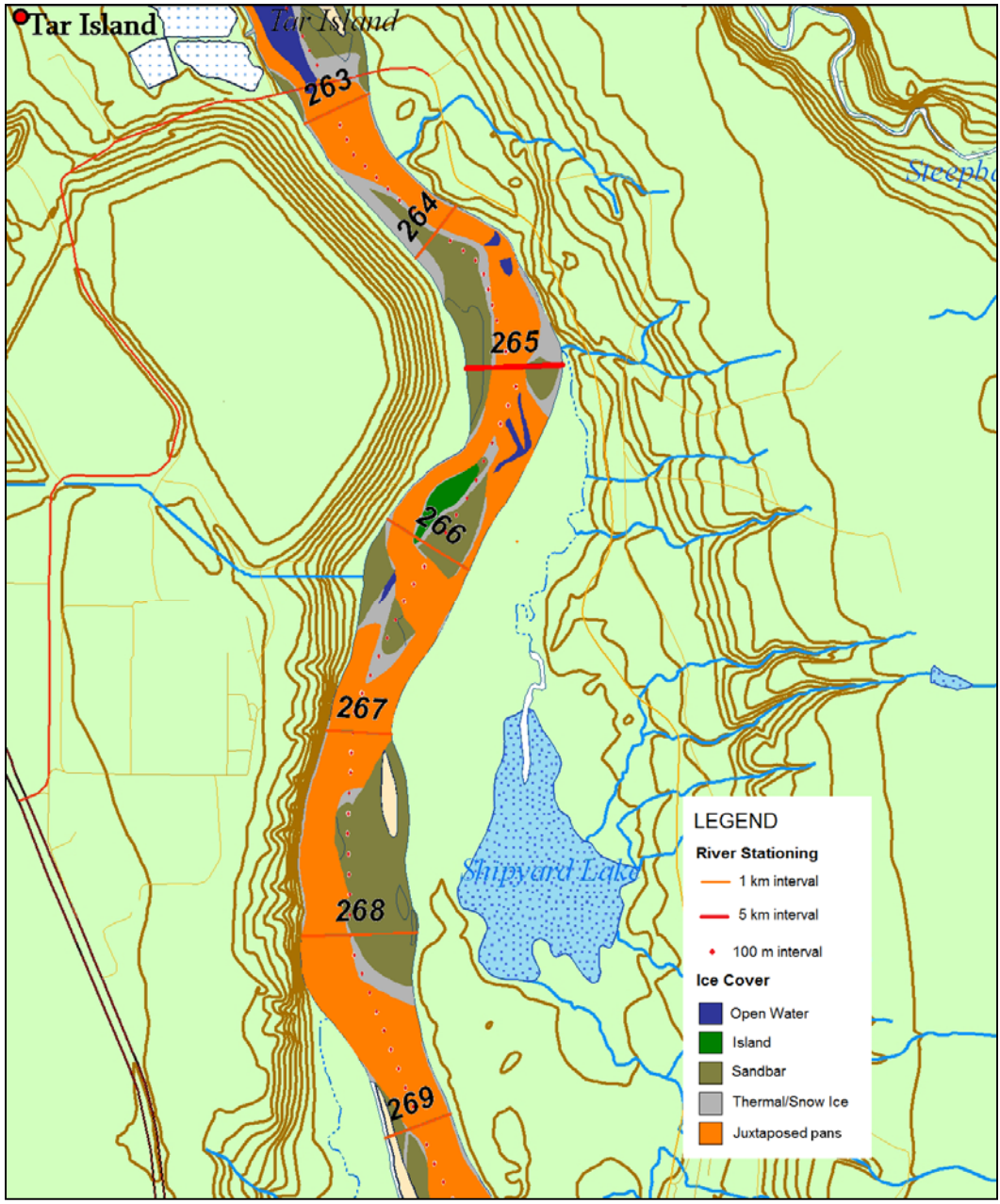
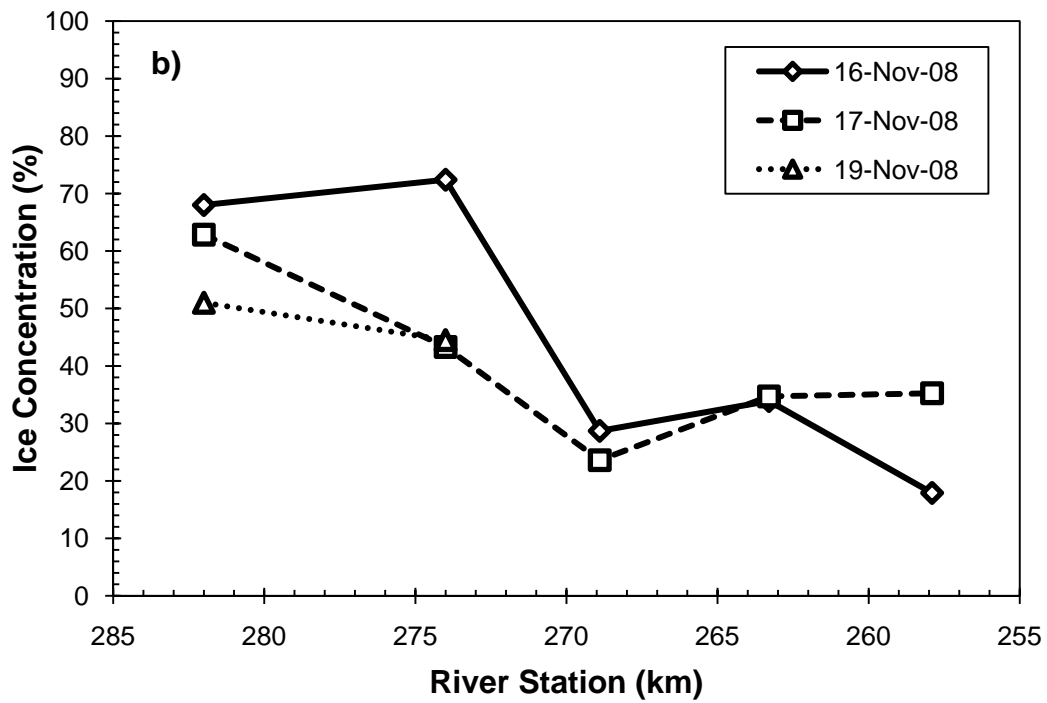
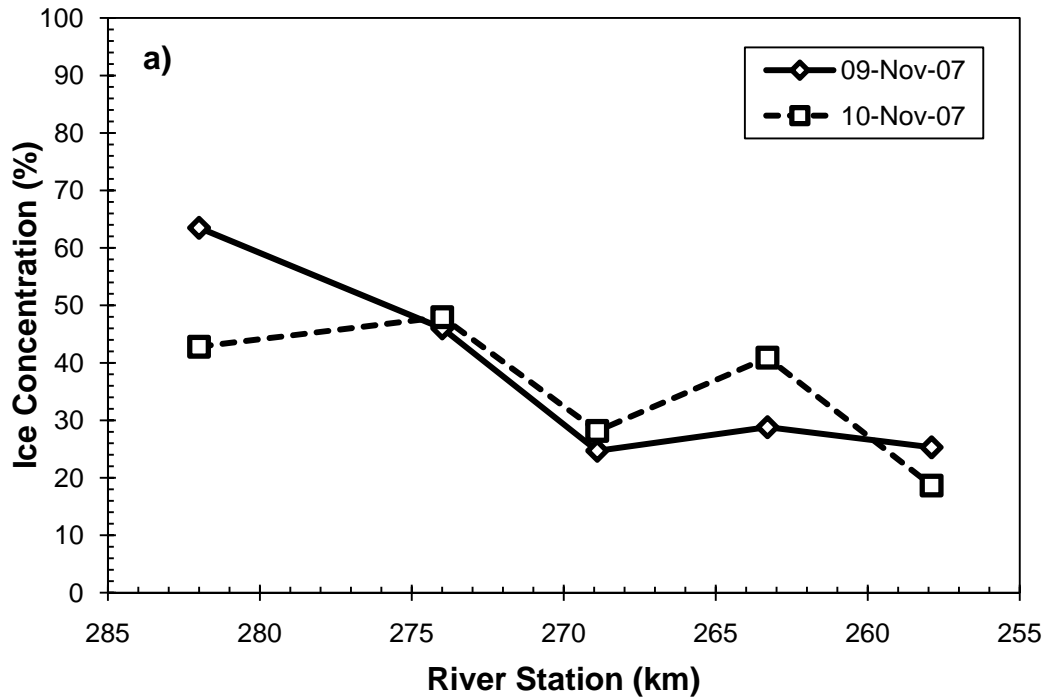
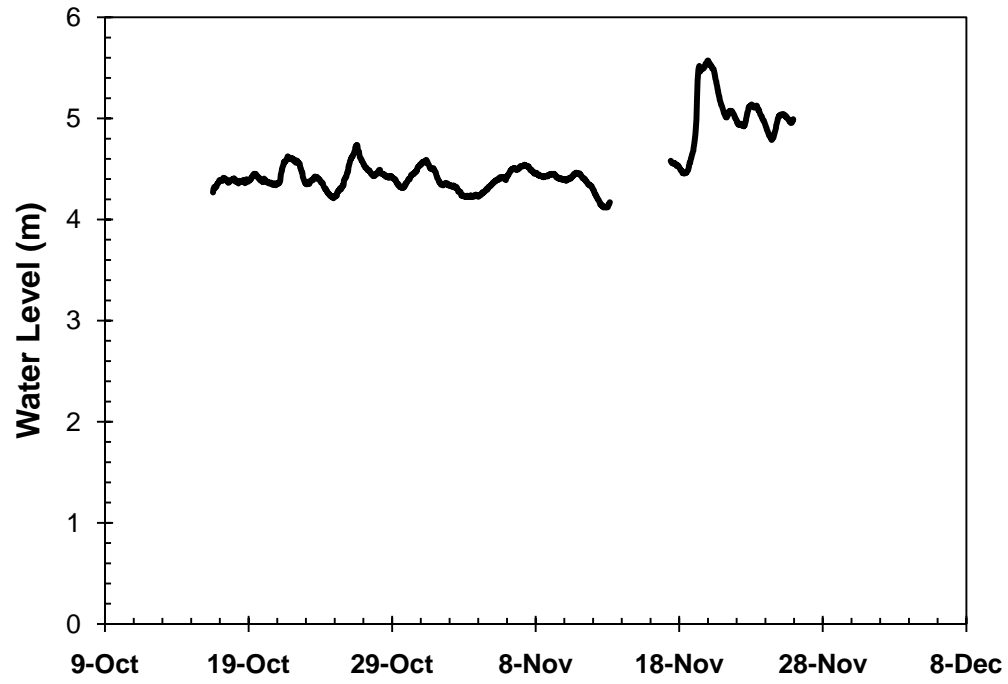


Figure 2.22. Ice map based on aerial flight observations made on November 19, 2008.



**Figure 2.23. Surface ice concentrations measured in the study reach (a) 2007, (b) 2008.**



**Figure 2.24. Water levels measured during freeze-up 2008 at M268.1.**

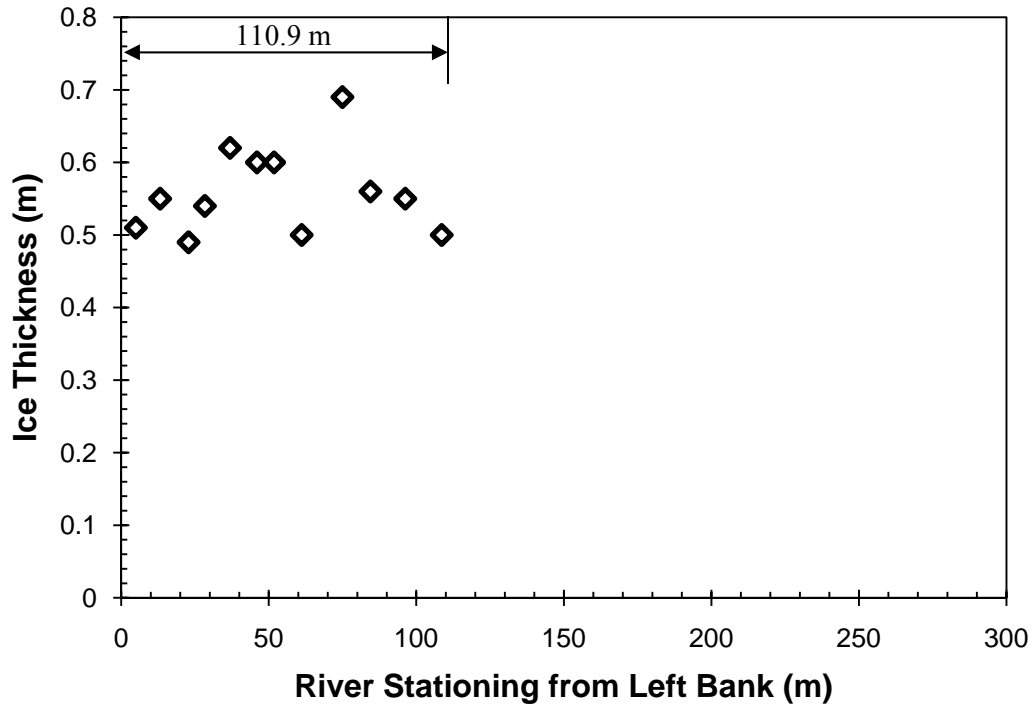


**Figure 2.25. Ice thickness measurements at Site 3 (km 265.7; 110.9 m from left edge of water to right edge of water).**

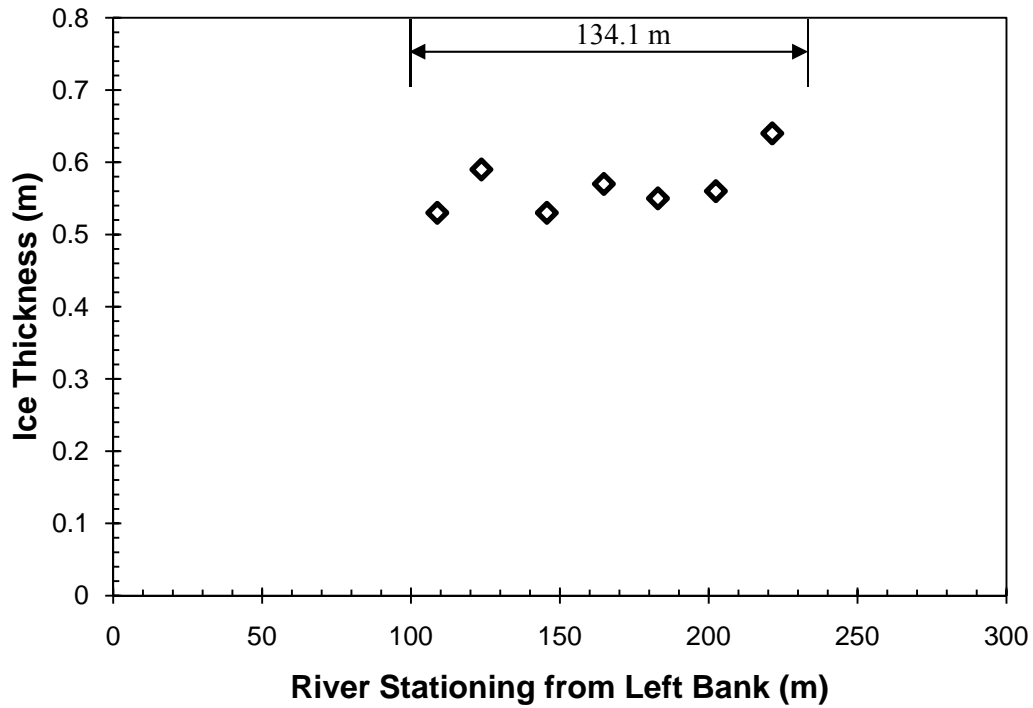


**Figure 2.26. Ice thickness measurements at Site 4 (km 265.7; 134.1 m from left edge of water to right edge of water).**

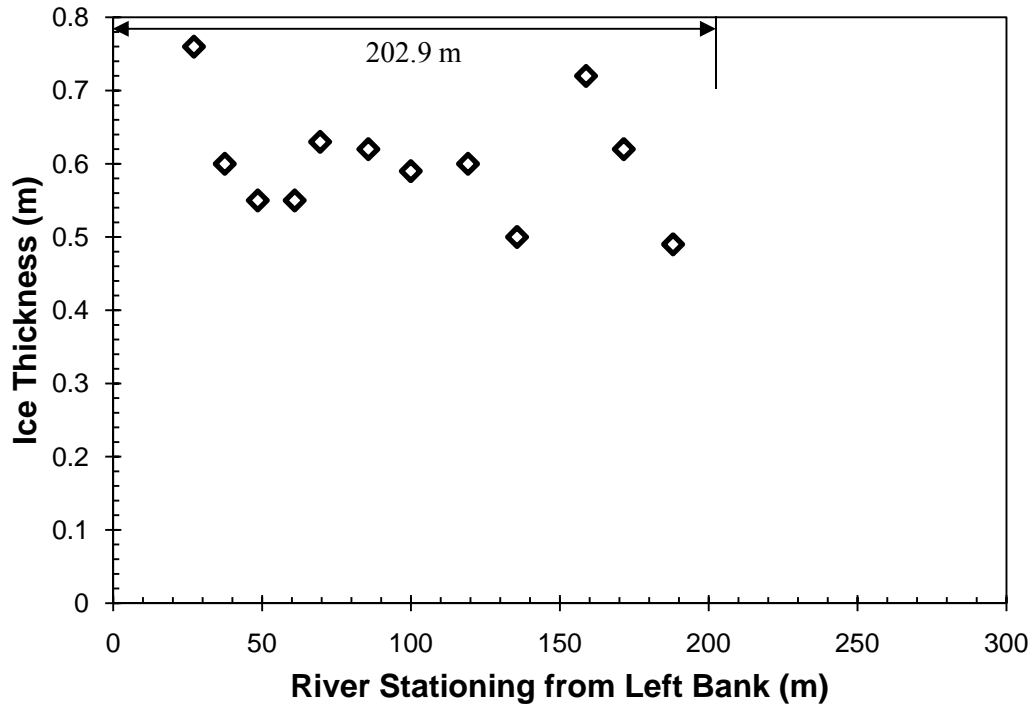


Figure 2.27. Ice thickness measurements at Site 5 (km 267.7; 202.9 m from left edge of water to right edge of water).

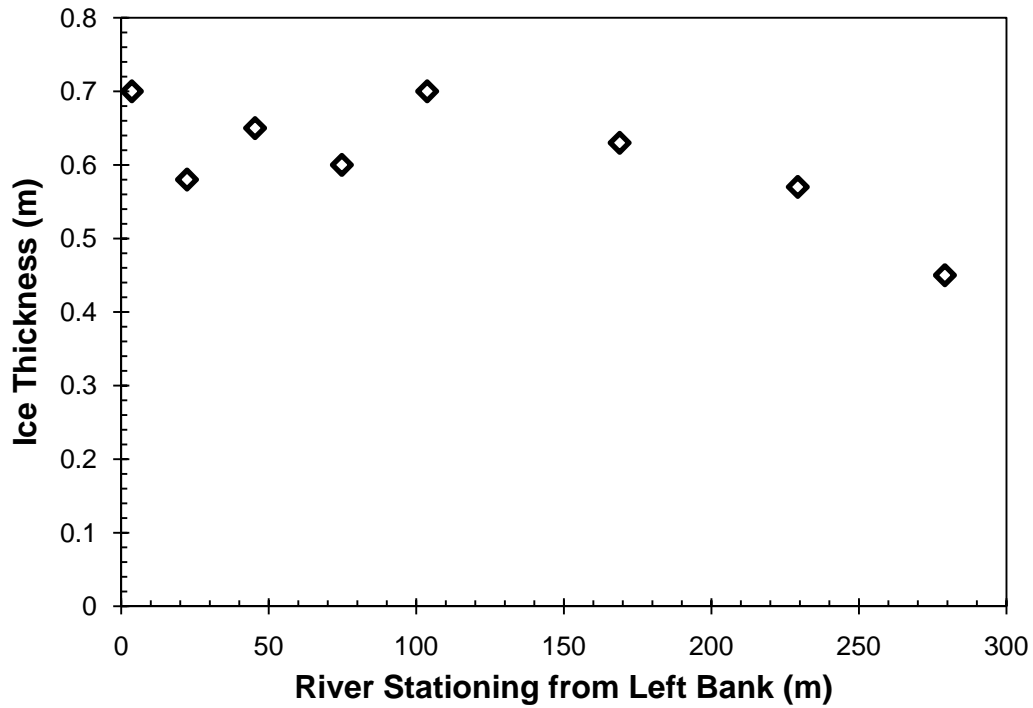


Figure 2.28. Ice thickness measurements at Site 6 (km 268.7; 309.9 m from left edge of water to right edge of water).

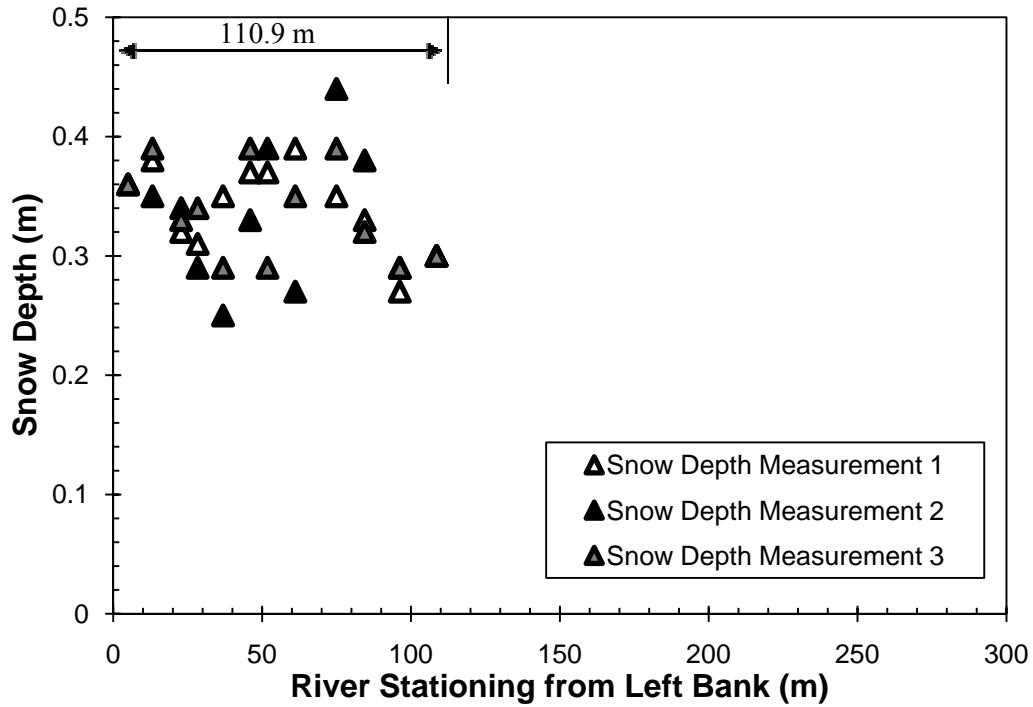


Figure 2.29. Snow depth measurements at Site 3 (km 265.7; 110.9 m from left edge of water to right edge of water).

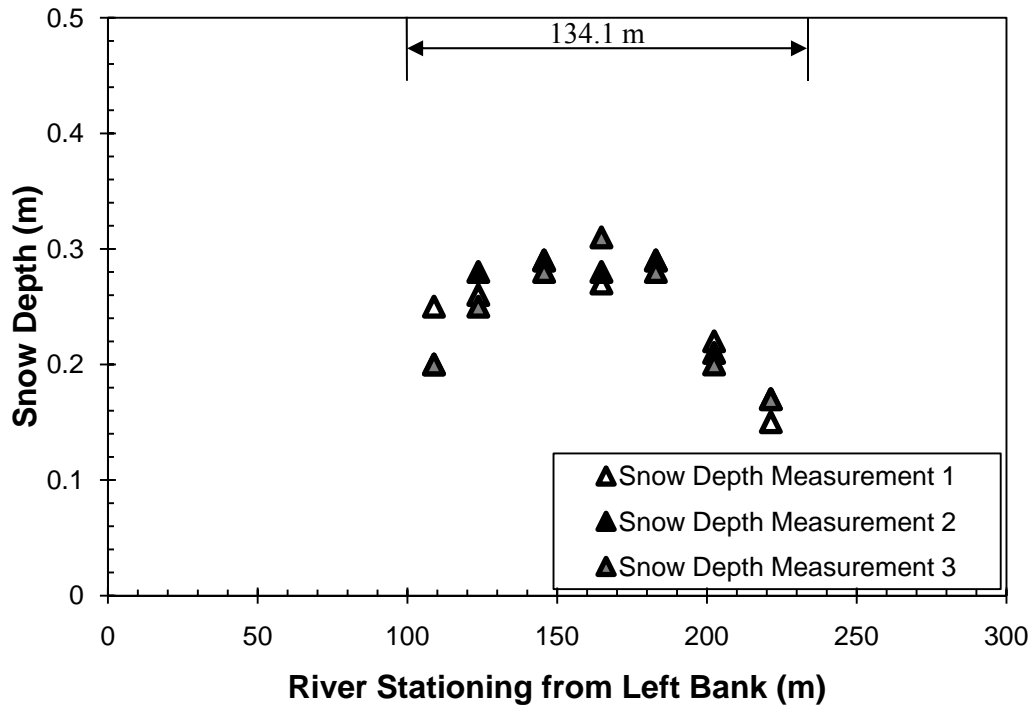


Figure 2.30. Snow depth measurements at Site 4 (km 265.7; 134.1 m from left edge of water to right edge of water).

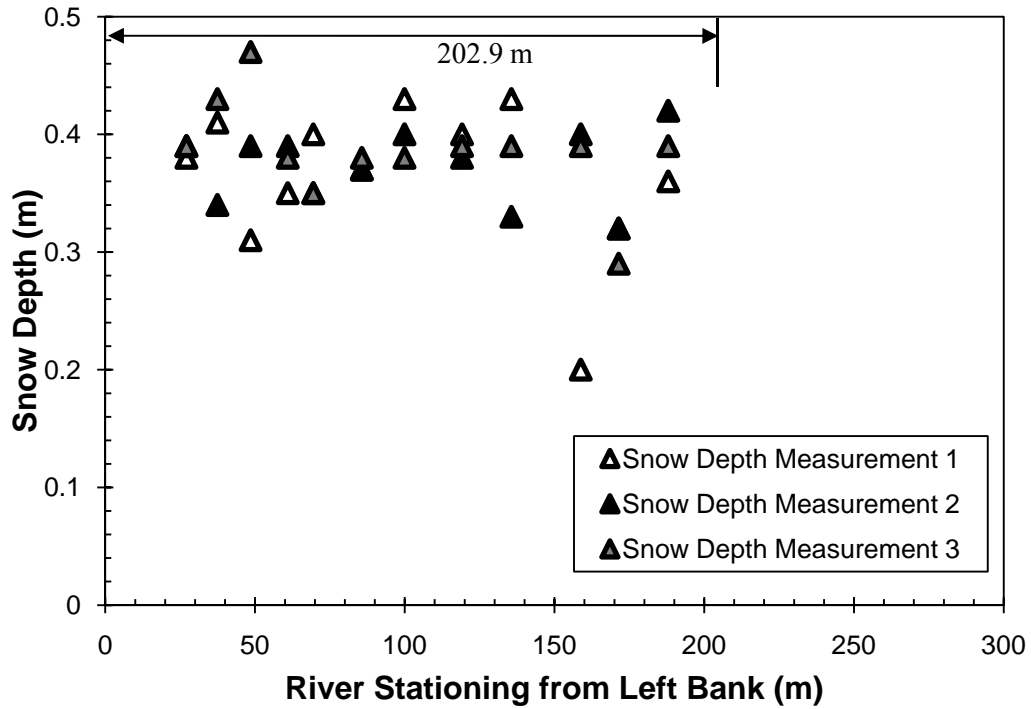


Figure 2.31. Snow depth measurements at Site 5 (km 267.7; 202.9 m from left edge of water to right edge of water).

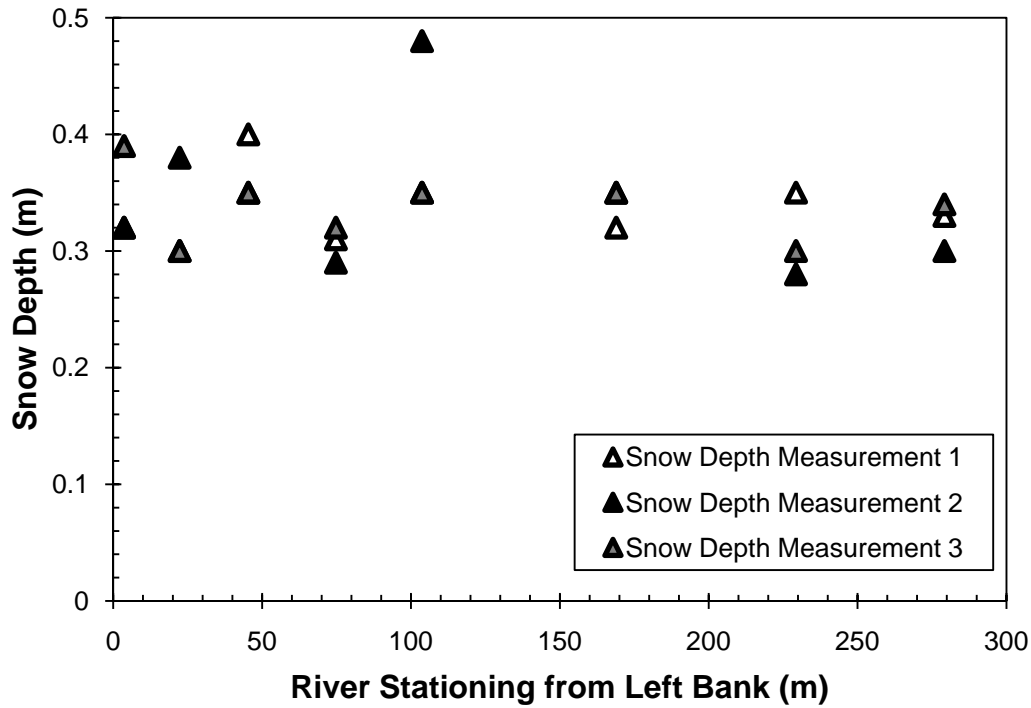


Figure 2.32. Snow depth measurements at Site 6 (km 268.7; 309.9 m from left edge of water to right edge of water).

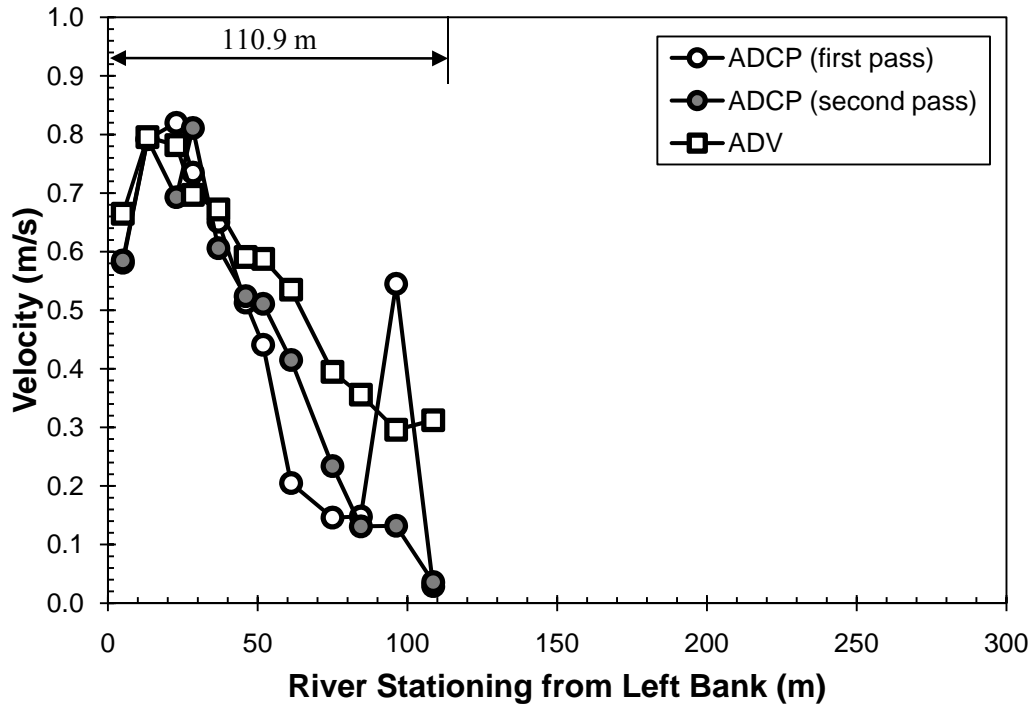


Figure 2.33. Velocity measurements at Site 3 (km 265.7; 110.9 m from left edge of water to right edge of water).

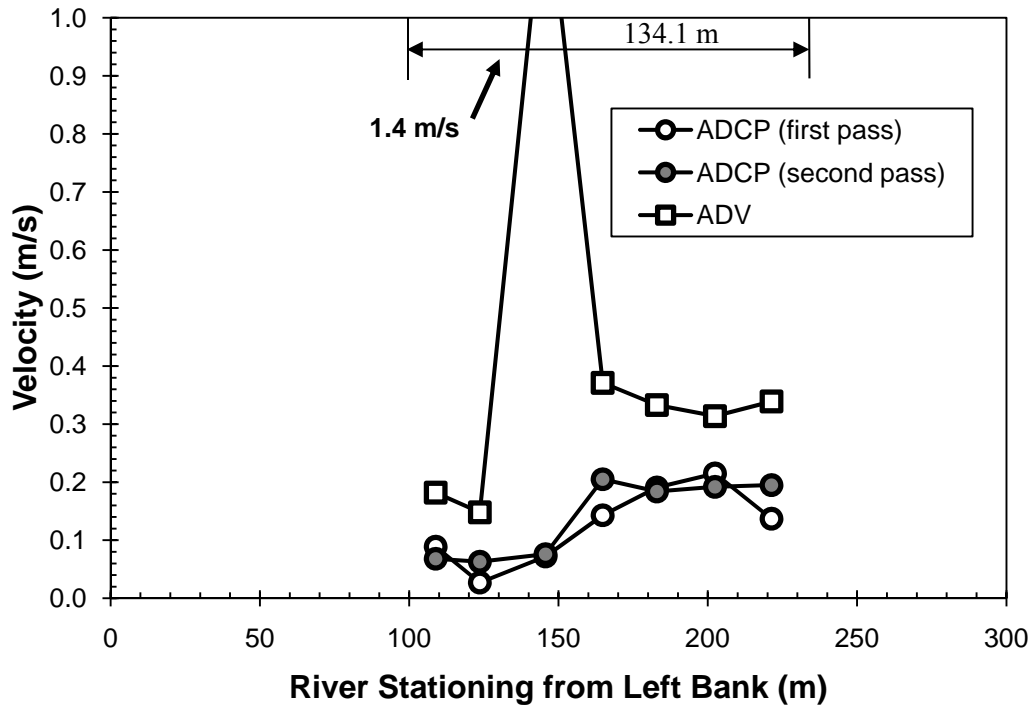


Figure 2.34. Velocity measurements at Site 4 (km 265.7; 134.1 m from left edge of water to right edge of water).

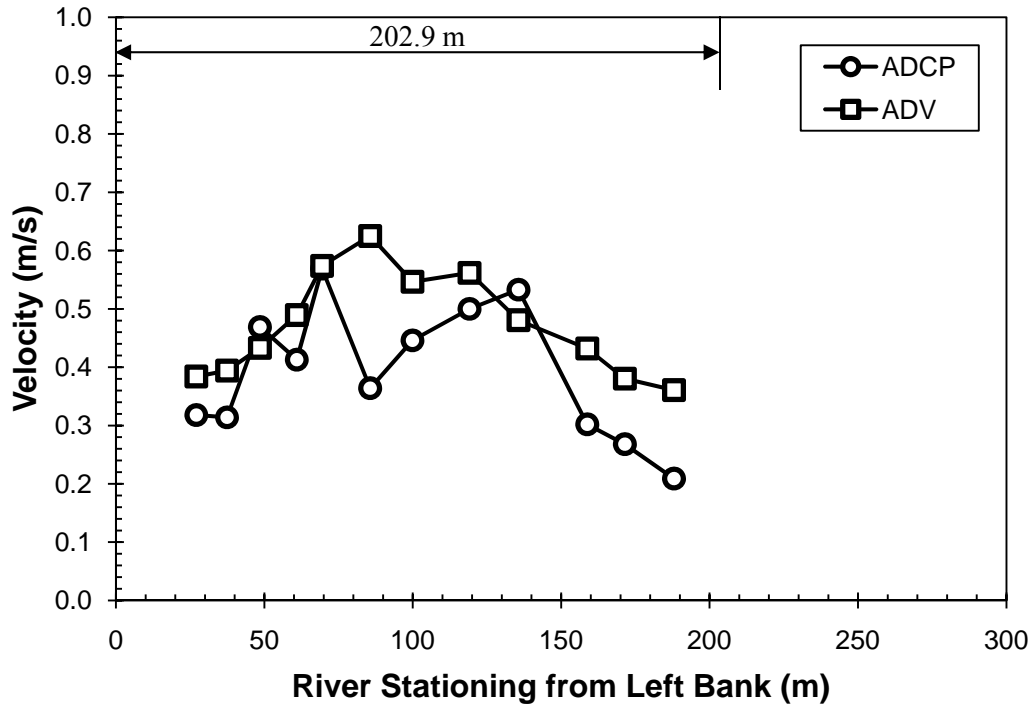


Figure 2.35. Velocity measurements at Site 5 (km 267.7; 202.9 m from left edge of water to right edge of water).

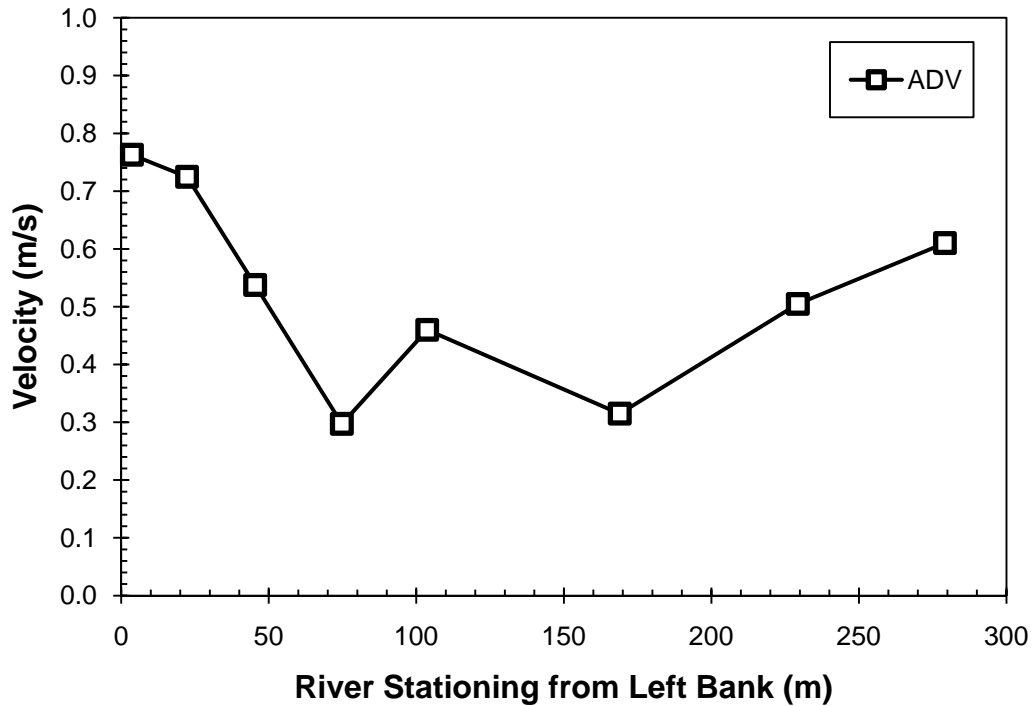


Figure 2.36. Velocity measurements at Site 6 (km 268.7; 309.9 m from left edge of water to right edge of water).

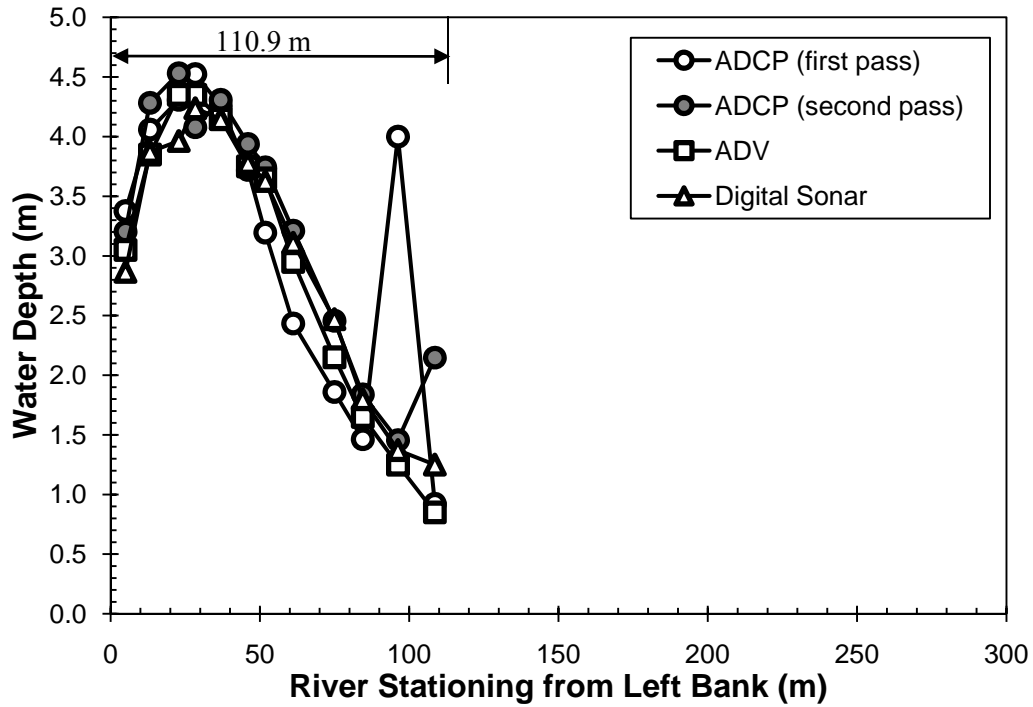


Figure 2.37. Depth of water under ice measurements at Site 3 (km 265.7; 110.9 m from left edge of water to right edge of water).

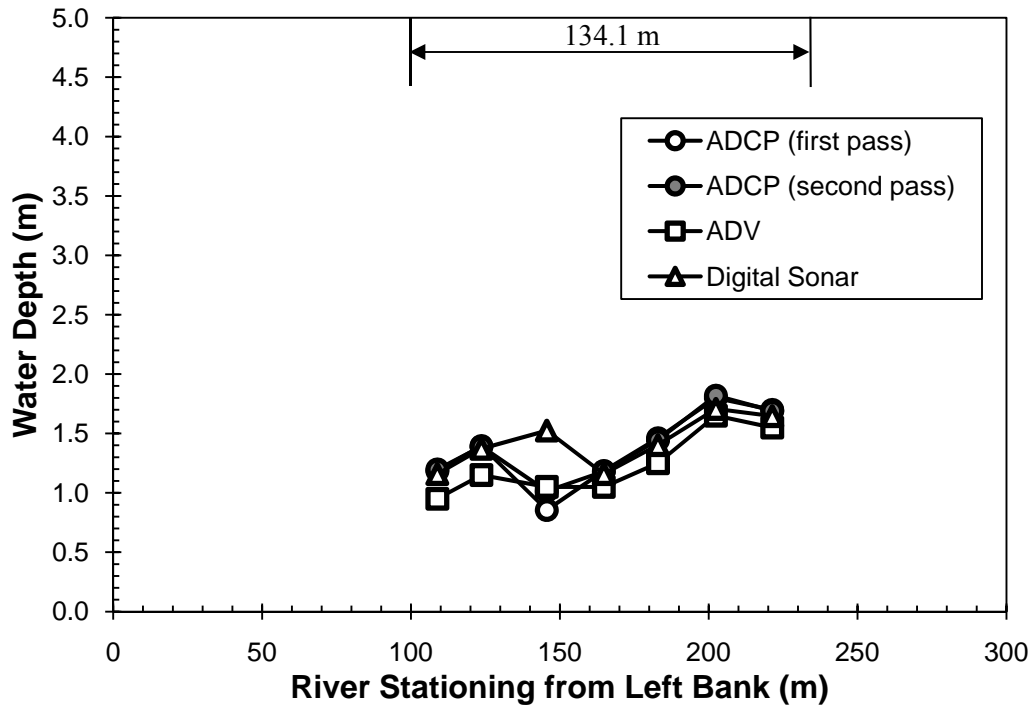


Figure 2.38. Depth of water under ice measurements at Site 4 (km 265.7; 134.1 m from left edge of water to right edge of water).

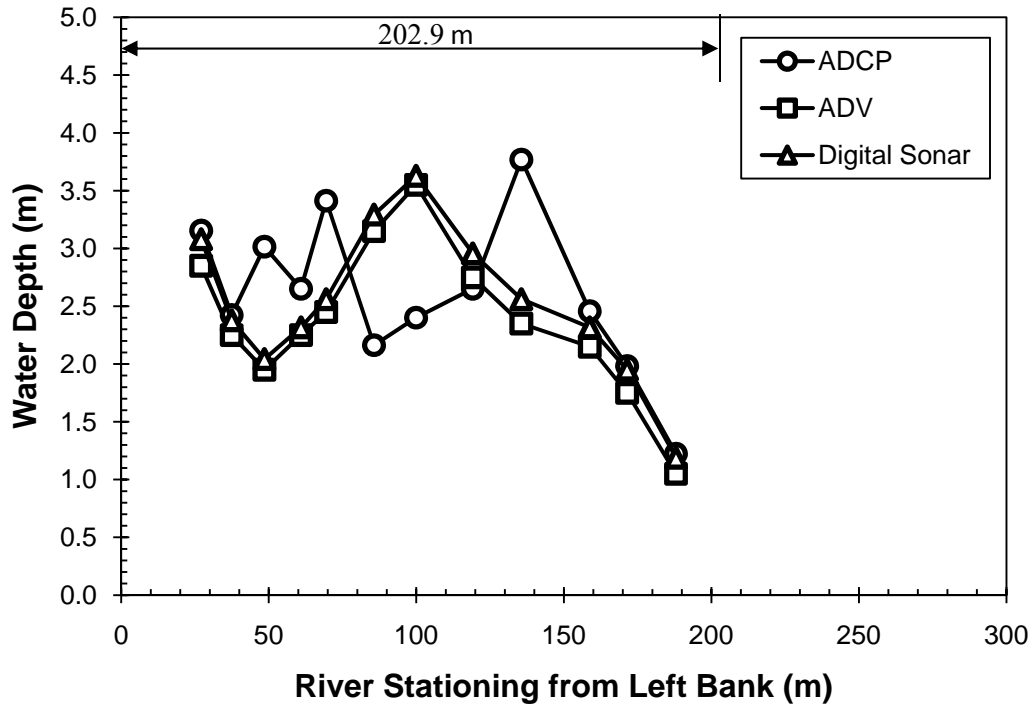


Figure 2.39. Depth of water under ice measurements at Site 5 (km 267.7; 202.9 m from left edge of water to right edge of water).

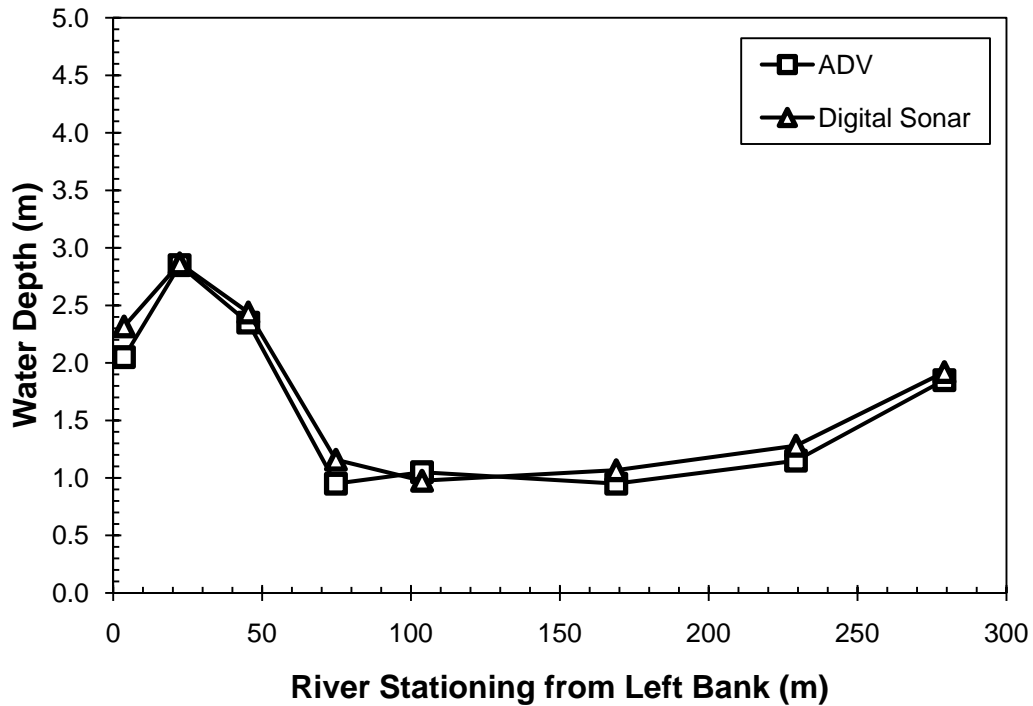


Figure 2.40. Depth of water under ice measurements at Site 6 (km 268.7; 309.9 m from left edge of water to right edge of water).

### 3. 2-D Ice Process Modeling<sup>3</sup>

#### 3.1 Introduction

In order to be able to assess the potential impacts of flow withdrawals on the Athabasca River, the use of a numerical model was necessary. A numerical model solves differential equations that represent various physical processes. Its application is a valuable predictive tool for complex physical problems. The objectives of this modeling effort were to test the ability of the most comprehensive ice process models available in simulating the formation of border ice, bridging and the formation of an ice cover. This chapter explores all of the steps taken to achieve these goals. The theory of how an ice process model operates, including some of the governing equations it is used to solve, is explained. Simple test cases were created and used to explore the function of various model parameters. Construction of the 2-D model is documented, along with calibration, sensitivity analysis of various physical parameters and validation. The results of the modeling effort are discussed, along with recommendations for future studies.

Using *River1D*, 1-D modeling was carried out on the 80 km long section of the lower Athabasca extending from Fort McMurray to Bitumont, as seen in Figure 2.1 (Abarca, 2007). *River1D* is a hydraulic flood routing model developed at the University of Alberta, which uses the characteristic-dissipative-Galerkin (CDG) finite element method to solve a conservation formulation for the Saint-Venant equations for rectangular channels of varying width (Hicks and Steffler, 1990, 1992). The latest version of the model incorporates thermal ice related processes, including water temperature, suspended and surface frazil ice, surface ice concentrations and solid surface ice, as well as ice front location (Andrishak

---

<sup>3</sup> A version of this chapter referring to model calibration has been submitted for the conference paper entitled, “2-D Modeling of Ice Cover Formation Processes on the Athabasca River, AB” by Agata Wojtowicz, Faye Hicks, Robyn Andrishak, Michael Brayall, Julia Blackburn and Joshua Maxwell for the 15<sup>th</sup> Workshop on River Ice in St. John’s Newfoundland and Labrador, June 15-17, 2009.

and Hicks, 2008). The model was calibrated with data collected in 2006 (Abarca, 2007) and validated with data collected in 2007 (Andrishak *et al.*, 2008).

1-D modeling was a successful first step into investigating the effects of river ice formation on the availability of water. It was learned that the quality of water temperature and ice concentration inflow boundary conditions are very significant to the accuracy of the freeze-up process simulation (Andrishak *et al.*, 2008). However, it was observed that the winter ice regime is highly two-dimensional. 1-D modeling was not able to take into account the complex processes that occurred during ice formation, such as border ice growth, multiple bridging points and ice cover consolidation (Abarca, 2007). In order to fully assess the potential impacts of flow withdrawals on the ice regime of the Athabasca River, the use of a 2-D model was necessary.

Initially, 2-D modeling of freeze-up was to be conducted using two different hydrodynamic models: *River2D* and *CRISSP2D*. The University of Alberta's public domain *River2D* model uses the CDG finite element scheme to solve the 2-D depth averaged hydrodynamic equations. The model simulates the hydraulics of open water and ice covered flow conditions, with a focus on fish habitat assessment, and is currently being adapted to model ice formation processes in a purely Eulerian frame of reference. These ice formation processes include: water cooling/supercooling; border ice formation; frazil production, transport and rise; surface ice transport, bridging and frontal progression. The ice process model components are still being tested and validated, and so the application of *River2D* to date has been limited to modeling open water and winter ice cover conditions.

Since *River2D* was still being developed at the time of thesis writing, it could not be used to simulate any freeze-up ice processes. Instead, *CRISSP2D*, a 2-D comprehensive ice river simulation program developed by Hung Tao Shen and colleagues at the University of Clarkson, NY, was the only model used to simulate freeze-up. *CRISSP2D* is a proprietary model that employs the CDG Eulerian finite element model to simulate hydrodynamics and a Lagrangian discrete parcel method to simulate the transport and dynamics of surface ice

(Shen, 2005a). *CRISSP2D* has comprehensive ice process modeling components and has been successfully applied in a number of practical cases (e.g. Liu *et al.*, 2006; Malenchak *et al.*, 2006).

Two-dimensional ice process modeling presents unique practical problems, most notably because of the limited reach lengths that can reasonably be considered. It is neither economical to measure, nor computationally feasible to model extended domain lengths in 2-D. However, in this river at least, the processes of frazil formation, flocculation and floatation develop over many kilometers and consequently, until bridging occurs, the inflow and outflow ice concentrations for short reaches (such as the 5-km 2-D study reach) are not measurably different. Essentially this means that whatever ice concentration is specified as the inflow boundary condition is simply translated through the domain and out the downstream boundary. Furthermore, since the bridging phenomenon is highly dependent upon border ice formation in this reach, it is essential to have this component of the model working well before the rest of the ice cover formation processes can be correctly modeled. Therefore, border ice growth modeling was the primary ice process modeling focus. The ability of these models to simulate border ice development is also interesting, because of the limited models available for this particular process, combined with the fact that the edges of the domain (where the border ice tends to form) present the greatest modeling challenges in 2-D.

### **3.2 Model Description**

The following section describes the fundamental principles which govern the function of both *River2D* and *CRISSP2D*. This includes equations specific to hydrodynamics, ice dynamics and thermal processes. The information in this section paraphrases the contents of the *River2D* User's Manual and the *CRISSP2D* Programmer's Manual. Specifically, Sub-Section 3.2.1 references both of these manuals (where appropriate), while Sub-Sections 3.2.2 and 3.2.3 reference information contained in the *CRISSP2D* Programmer's Manual.

### 3.2.1 Hydrodynamics

Both the *River2D* and *CRISSP2D* models can be used to simulate a variety of regimes in natural streams and rivers, including supercritical, sub-critical and mixed flow. The hydrodynamic component of both the *River2D* and *CRISSP2D* models is based on a conservative form of the Saint Venant equations. The first equation represents the conservation of mass and the second two equations represent the conservation of momentum in the longitudinal and transverse directions, respectively.

$$\frac{\partial H}{\partial t} + \frac{\partial q_x}{\partial x} + \frac{\partial q_y}{\partial y} = 0 \quad [1]$$

$$\begin{aligned} \frac{\partial q_x}{\partial t} + \frac{\partial}{\partial x}(Uq_x) + \frac{\partial}{\partial y}(Vq_x) + \frac{g}{2} \frac{\partial}{\partial x} H^2 \\ = gH (S_{0x} - S_{fx}) + \frac{1}{\rho} \left( \frac{\partial}{\partial x} (H\tau_{xx}) \right) + \frac{1}{\rho} \left( \frac{\partial}{\partial y} (H\tau_{xy}) \right) \end{aligned} \quad [2]$$

$$\begin{aligned} \frac{\partial q_y}{\partial t} + \frac{\partial}{\partial x}(Uq_y) + \frac{\partial}{\partial y}(Vq_y) + \frac{g}{2} \frac{\partial}{\partial y} H^2 \\ = gH (S_{0y} - S_{fy}) + \frac{1}{\rho} \left( \frac{\partial}{\partial x} (H\tau_{yx}) \right) + \frac{1}{\rho} \left( \frac{\partial}{\partial y} (H\tau_{yy}) \right) \end{aligned} \quad [3]$$

where

- $H$  = depth of flow ( $m$ )
- $U$  = depth averaged velocity in the x-direction ( $m/s$ )
- $V$  = depth averaged velocity in the y-direction ( $m/s$ )
- $q_x, q_y$  = discharge intensity in the x- and y-directions ( $m^3/s$ )

where  $q_x = HU$

and  $q_y = HV$

- $g$  = acceleration due to gravity ( $m/s^2$ )  
 $\rho$  = density of water ( $kg/m^3$ )  
 $S_{0x}, S_{0y}$  = bed slope in the x- and y-directions (*dimensionless*)  
 $S_{fx}, S_{fy}$  = friction slope (slope of the energy grade line) in the x- and y-directions (*dimensionless*)  
 $\tau_{xx}, \tau_{xy}, \tau_{yx}, \tau_{yy}$  = components of the horizontal turbulent stress tensor ( $N/m^2$ )

A relationship with side shear stresses must be specified to solve the governing equations in a 2-D model. Transverse eddy viscosity distributions may be significant for stability in some finite difference and finite element models. *River2D* and *CRISSP2D* handle shear stresses in a slightly different way. *River2D* uses a Bousinessq type eddy viscosity formulation. For the transverse shear, the equation is:

$$\tau_{xy} = \rho v_t \left( \frac{\partial U}{\partial y} + \frac{\partial V}{\partial x} \right) \quad [4]$$

and

$$v_t = \varepsilon_1 + \varepsilon_2 \frac{H\sqrt{U^2 + V^2}}{C_s} + \varepsilon_3^2 H^2 \sqrt{2\left(\frac{\partial U}{\partial x}\right)^2 + \left(\frac{\partial U}{\partial x} + \frac{\partial V}{\partial y}\right)^2 + 2\left(\frac{\partial V}{\partial y}\right)^2} \quad [5]$$

- where  $\tau_{xy}$  = bed shear stress ( $N/m^2$ )  
 $v_t$  = eddy viscosity coefficient ( $m^2/s$ )  
 $\varepsilon_1, \varepsilon_2, \varepsilon_3$  = eddy viscosity components ( $m^2/s$ , *dimensionless*, *dimensionless*, *respectively*)

$C_s$  = Chezy coefficient (*dimensionless*)

$$\text{defined as: } C_s = 5.75 \log \left( 12 \frac{H}{k_b} \right) \quad [6]$$

where  $k_b$  = bed roughness height (*m*)

The equations for shear in the x and y directions are very similar.  $\varepsilon_1$  is the eddy viscosity constant and is useful in stabilizing the solution in very shallow flows.  $\varepsilon_2$ , usually the most important term, is the eddy viscosity bed shear parameter and is analogous to the transverse dispersion coefficients in rivers.  $\varepsilon_3$  is the eddy viscosity horizontal shear parameter and is important in flows with high transverse velocity outlet gradients (Steffler and Blackburn, 2002). For all the modeling efforts carried out in *River2D*, the defaults of  $\varepsilon_1 = 0 \text{ m}^2/\text{s}$ ,  $\varepsilon_2 = 0.5$  and  $\varepsilon_3 = 0$  were used. Using these default values, an upper bound value of the eddy viscosity coefficient,  $\nu_t$ , for this section of the Athabasca River would be  $0.2 \text{ m}^2/\text{s}$ .

The treatment of eddy viscosity by the *CRISSP2D* model is different than that of *River2D*. Instead of only relating bed shear stress to an eddy viscosity coefficient, bed shear stress multiplied by the depth of flow is related to a generalized eddy viscosity coefficient:

$$T_{xy} = \rho \varepsilon_{xy} \left( \frac{\partial q_x}{\partial y} + \frac{\partial q_y}{\partial x} \right); T_{xx} = 2\rho \varepsilon_{xx} \left( \frac{\partial q_x}{\partial x} \right); T_{yy} = 2\rho \varepsilon_{yy} \left( \frac{\partial q_y}{\partial y} \right) \quad [7]$$

where  $T_{xy}, T_{xy}, T_{xy}$  = bed shear stress over the flow depth (*N/m*)

$\varepsilon_{xy}, \varepsilon_{xy}, \varepsilon_{xy}$  = generalized eddy viscosity coefficients ( $\text{m}^2/\text{s}$ )

In *CRISSP2D*, the eddy viscosity coefficient is not a single value made up of various components, but rather three separate eddy viscosity coefficients exist and are used individually to calculate bed shear stress in each of the three directions. For all the model runs carried out using *CRISSP2D*, the defaults of  $\varepsilon_{xx} = 1.0 \text{ m}^2/\text{s}$ ,  $\varepsilon_{yy} = 1.0 \text{ m}^2/\text{s}$  and  $\varepsilon_{xy} = 1.0 \text{ m}^2/\text{s}$  were used. In comparison with the upper bound

value of the eddy viscosity coefficient in the *River2D* model of 0.2 m<sup>2</sup>/s, these values of eddy viscosity coefficients are five times greater.

When a 2-D model encounters an area of transition between the wet and dry, as in an area of shallow depth or of no depth at all, significant computational difficulties occur. It is unknown how *CRISSP2D* manages such a situation; however, the *River2D* model changes the surface flow equations into groundwater flow equations in that area. This allows the program to calculate a continuous free surface with positive and negative depths, and to continue without the need to change boundary conditions. In such a case, the water mass conservation equation is replaced by:

$$\frac{\partial H}{\partial t} = \frac{T}{S} \left( \frac{\partial^2}{\partial x^2} (H + z_b) + \frac{\partial^2}{\partial y^2} (H + z_b) \right) \quad [8]$$

where  $T$  = groundwater transmissivity ( $m^2/s$ )  
 $S$  = groundwater storativity of the artificial aquifer  
 (*dimensionless*)  
 $z_b$  = ground surface elevation ( $m$ )

*CRISSP2D* can simulate an array of ice processes. When surface ice and seepage flow are incorporated, the *CRISSP2D* model follows a slightly modified form of the hydrodynamic equations, in which the conservation of mass equation accommodates the mass of ice and the two remaining momentum equations incorporate ice thickness and shear stresses at the ice-water interface.

While *River2D* cannot yet simulate thermal ice dynamics, it is able to model flow under a floating ice cover with a known ice thickness and ice roughness. In such cases, the basic surface water equations are adapted to accommodate for various ice effects. The conservation of mass equation stays the same; however, the momentum equations are adapted to include ice thickness terms. Also, one

further assumption is made in the *River2D* model: the ice cover is fixed in space so that the ice will not react to any shear force applied by the water.

### 3.2.2 Ice Dynamics

*CRISSP2D* uses a Lagrangian discrete-parcel method (DPM) coupled with flow hydrodynamics to simulate the movement of surface ice. Based on the theory of smoothed particle hydrodynamics (SPH), the main concept of the DPM is that ice is represented by an adequately large number of parcels which carry mass, momentum and energy. The ice run is considered as a two-dimensional continuum, with ice pieces of variable size. While the ice dynamics are simulated using Lagrangian discrete parcels, the results are later interpolated and exhibited on Eulerian finite element nodes. The momentum equation for surface ice is written in the following form:

$$M_i \frac{D\vec{V}_i}{Dt} = \vec{R} + \vec{F}_a + \vec{F}_w + \vec{G} \quad [9]$$

- where
- $M_i$  = ice mass per unit area ( $kg/m^2$ )
  - $\frac{D\vec{V}_i}{Dt}$  = acceleration of ice ( $m/s^2$ )
  - $\vec{V}_i$  = velocity of ice ( $m/s$ )
  - $\vec{R}$  = internal ice resistance ( $N/m^2$ )
  - $\vec{F}_a$  = wind drag force ( $N/m^2$ )
  - $\vec{F}_w$  = water drag force ( $N/m^2$ )
  - $\vec{G}$  = gravitational force component due to water surface slope ( $N/m^2$ )

Along solid boundaries, such as river banks, the boundary resistance to the ice dynamics is considered. The method of images is used to implement the partial-slip solid boundary condition. In order to calculate the boundary frictional force, the model applies a dynamic Mohr-Coulomb yield criterion:

$$F_f = F_c + F_N \tan \phi_B \quad [10]$$

where

$F_f$	=	frictional force between ice and solid boundary ( $N$ )
$F_c$	=	ice cohesive force ( $N$ )
$F_N$	=	normal component of the ice force against the boundary ( $N$ )
$\phi_B$	=	dynamic friction angle ( $^\circ$ )

A constitutive law relating stresses with the motion of ice is required to quantify the internal ice resistance. The viscoelastic-plastic (VEP) model is used to calculate the internal stresses and then another form of the Mohr-Coulomb criterion is applied.

### 3.2.3 Thermal Processes

River ice thermodynamic processes are guided by energy exchanges that are present between the atmosphere, ice cover, water and riverbed. The main energy fluxes considered are those between water and air, ice and air, water and ice. Each of these energy fluxes, particularly those that occur at the surface of the river, must be quantified and accounted for when simulating thermal ice processes. The equation that represents the overall energy budget is as follows:

$$\phi^* = -\phi_R + \phi_T + \phi_E + \phi_H + \phi_S \quad [11]$$

where	$\phi^*$	=	total surface heat flux between air-water and/or air-ice ( $W/m^2$ )
	$\phi_R$	=	net solar radiation (shortwave radiation) ( $W/m^2$ )
	$\phi_T$	=	effective back radiation (terrestrial radiation) ( $W/m^2$ )
	$\phi_E$	=	heat transfer due to evaporation ( $W/m^2$ )
	$\phi_H$	=	conductive, or sensible, heat transfer ( $W/m^2$ )
	$\phi_S$	=	heat transfer due to precipitation ( $W/m^2$ )

This equation is appropriate for the study site based on the given conditions. The difficulty that arises is that several of these heat exchange components are very difficult to determine. Some components require meteorological data that is not readily available and others contain non-linear functions. Thus, a simplified linear formulation is useful. While linearized surface heat exchange formulas cannot accurately take into account the diurnal variation of heat exchange, they can give good results when applied to long-term simulations with calibrated heat exchange coefficients (Shen 2005b). The following linear equation, which includes a constant, a component proportional to the difference between air and water temperatures and a temperature independent shortwave radiation, is used to approximate the heat exchange per unit area between water and air:

$$\phi_{wa}^* = -\phi_{Rw} + \alpha' + \beta'(T_w - T_a) \quad [12]$$

where	$\phi_{wa}^*$	=	net rate of heat loss at the water surface ( $W/m^2$ )
	$\phi_{Rw}$	=	net shortwave solar radiation reaching the water surface ( $W/m^2$ )

$\alpha'$	=	a linear heat transfer constant ( $W/m^2$ )
$\beta'$	=	a linear heat transfer coefficient ( $W/m^2/^\circ C$ )
$T_w$	=	water temperature ( $^\circ C$ )
$T_a$	=	air temperature ( $^\circ C$ )

In this equation,  $\alpha'$  is a constant value that is used to compensate for an exposure effect that would be experienced at the study site and not in the measurement area. For example, if the site is located in a deep valley, measurements taken at the top of the valley wall (e.g. at an airport rather than at river level) may receive more sunlight exposure and may not fully represent the conditions experienced at the site. The use of this parameter allows for such a correction. Alternatively, it may simply be used as a calibration constant.

When an ice cover is present, similar linearized equations can be written for the heat transfer through the air-ice interface and the water-ice interface. Both the detailed thermal budget method and the linearized approximation formulations for surface heat exchange are included in *CRISSP2D* and the user is able to decide which to employ based on available weather data.

Border ice is usually the first type of ice to develop during freeze-up. This ice, which forms along the river's edge, can be divided into two categories: static border ice and dynamic border ice. The first of these, static border ice, develops when the water surface temperature has decreased to a point low enough to form ice crystals and when the turbulence is not strong enough to entrain the ice crystals into the water column. In *CRISSP2D*, these thermal and mechanical conditions translate into a set of four criteria used to determine the presence of border ice. The first criterion is that the temperature of the water surface must be less than some critical water surface temperature.

$$T_{ws} < T_{cr} < 0^\circ C$$

where  $T_{ws}$  = water surface temperature ( $^{\circ}C$ )

$T_{cr}$  = critical surface water temperature for border ice formation ( $^{\circ}C$ )

The second criterion is that the buoyant velocity must be greater than the vertical turbulence velocity.

$$v_b > v_z'$$

where  $v_b$  = buoyant velocity of suspended frazil ( $m/s$ )

$v_z'$  = vertical turbulence velocity ( $m/s$ )

If this criterion is not met, ice crystals are entrained into the depth of the flow and subject to either melting if the temperature of the water is above zero or transportation as frazil suspension. The third criterion is the magnitude of the local depth averaged velocity must be less than a critical velocity.

$$|\vec{V}| < V_{cr}$$

where  $|\vec{V}|$  = the magnitude of the local depth averaged velocity ( $m/s$ )

$V_{cr}$  = the critical depth averaged velocity for border ice formation ( $m/s$ )

Finally, the fourth criterion is that the node must be either a land boundary node or have two contiguous border ice nodes around it, since border ice requires a fixed boundary to grow from. The velocity of the surface ice at this node is then set to zero so that the ice formed at this node will not move. It is given a concentration of 1.0 and an initial solid ice thickness. From this point on, the node will be subject to thermal growth or decay.

Skim ice forms thermally in areas with relatively low flow velocity and low wind. The formation of a large thin sheet of ice not attached to the shore, known as a skim ice run, is governed by low water surface turbulence relative to the rise velocity of ice crystals. In *CRISSP2D*, there are three criteria that must be met for skim ice to form. The first is that the water surface temperature is less than 0°C.

$$T_{ws} < 0^{\circ}C$$

where  $T_{ws}$  = water surface temperature ( $^{\circ}C$ )

The second criterion is that the buoyant velocity must be greater than the vertical turbulence velocity (same as for border ice growth).

$$v_b > v_z'$$

where  $v_b$  = buoyant velocity of suspended frazil ( $m/s$ )

$v_z'$  = vertical turbulence velocity ( $m/s$ )

Finally, the third criterion is that the water surface must not already be covered by a stationary ice cover. When the three criteria are satisfied, two possibilities exist at the finite element: either there is no parcel in the element, or there are ice parcels with an ice concentration of less than 1.0. In the case where no parcel is present, a new ice parcel is created and subsequently given a concentration of 1.0, an initial solid ice thickness, an area, and a mass. The velocity of the parcel is set equal to the flow velocity at the centre of the finite element unit. For the second case, where ice parcels are already present, a calculation is performed to obtain the total mass of new skim ice which can be created in the element unit. This mass is then distributed to the existing parcels in the element according to the ratio of open water area of calculated parcels to the total open water area of all parcels in the element unit. The thickness of the ice parcel is then recalculated as a solid ice thickness, while the ice concentration of each ice parcel is reset to 1.0.

When the water temperature in a turbulent river decreases to the point of super-cooling, frazil ice production commences. This is simulated in *CRISSP2D* by solving the energy equation for the ice-water mixture using the finite element method. Water temperature and frazil ice transport simulations take into account the transport of thermal energy of the mixture due to advection and diffusion, heat exchanges at the water surface and bottom, heat exchanges between suspended ice and water, mass exchange between suspended layer and surface ice and at the bed as well as heat and mass exchanges related to the frazil ice suspension. Whenever there is a mass exchange between layers, ice parcel thickness is recalculated, and the concentration of ice is reset accordingly. The conservation of thermal energy of the ice-water mixture in the suspended layer in the Lagrangian form can be written as:

$$\frac{De_T}{Dt} = \phi_{ss} - \phi_{sk} + \rho_i L_i E \quad [13]$$

and

$$e_T = \rho C_p (1 - C_v) T_w - \rho_i C_v L_i \quad [14]$$

where

$e_T$	=	thermal energy of the ice-water mixture in suspended layer ( $J/m^3$ )
$\phi_{ss}$	=	rate of heat gain on unit area through top/bottom boundary ( $W/m^2$ )
$\phi_{sk}$	=	rate of heat loss on unit area through top/bottom boundary ( $W/m^2$ )
$\rho_i$	=	density of ice ( $kg/m^3$ )

$L_i$	=	latent heat of fusion of ice ( $J/kg$ )
$E$	=	net volumetric rate of loss of frazil due to mass exchanges with the surface layer and at the bed ( $m^3/s/m^2$ )
$\rho$	=	density of water ( $kg/m^3$ )
$C_p$	=	specific heat of water ( $J/kg/^\circ C$ )
$C_v$	=	volumetric ice concentration ( $m^3/m^3$ )
$T_w$	=	water temperature ( $^\circ C$ )

Frazil that is produced in the river joins together with other frazil particles to create ice pans and rafts of various shapes and sizes. The simulation of these ice parcels, which are assumed to be square in shape, is achieved in *CRISSP2D* through an even distribution input at the upstream boundary. Parcels move freely through the domain, simulating ice pans and rafts, and change shape and size through interactions with other particles and reach boundaries. When these moving ice particles are able to accumulate along the leading edge of the existing border ice, they establish dynamic border ice. In the *CRISSP2D* model, dynamic border ice is governed by a critical depth averaged velocity separate from the one that governs static border ice formation. When these pans come to a channel narrowing such that they become constricted and form bridging point, an ice cover is initiated. In *CRISSP2D*, this thermal dynamic process involves the use of a specified velocity as a stopping criterion for ice parcels. This process can also be artificially created through the use of a fictitious barrier, called a boom, to stop the ice parcels.

Once full ice cover is established, frazil is no longer formed in the river. At this point, the growth and decay of that ice cover is modeled using another linearized heat exchange equation. The heat transfer from air to ice and that of water to ice,

as well as the heat exchange with the atmosphere are all considered in calculating ice thickness.

$$\rho_i L_i \frac{dh_i}{dt} = -\phi_R + \alpha + \beta(T_s - T_a) - h_{wi}(T_w - T_m) \quad [15]$$

where

$h_i$	=	thickness of the ice cover ( $kg/m^2$ )
$\alpha$	=	a linear heat transfer constant ( $W/m^2$ )
$\beta$	=	a linear heat transfer coefficient ( $W/m^2/^\circ C$ )
$T_s$	=	temperature of snow ( $^\circ C$ )

The processes of anchor ice formation, undercover ice transport, and ice jams are other simulations that can be achieved using *CRISSP2D*. However, the details and theory behind their function will not be discussed in this thesis as they are not relevant to the present study.

### 3.3 Model Testing

Before a model can be applied to a given study area, it must first be tested on a simple channel in order to understand how various parameters behave. Since the objective of this study is to model border ice, form a bridging point and initiate an ice cover, the parameters related to these processes were investigated. The first test involved gaining an understanding of the critical velocities leading to border ice formation. *CRISSP2D* is able to model the formation of two types of border ice: static border ice and dynamic border ice. Static border ice forms thermally and grows out from the river banks, while dynamic border ice is created from moving ice particles adhering to the static border ice. *CRISSP2D* can also model skim ice formation. This type of ice is formed thermally in areas of low velocity, but unlike border ice, it does not attach itself to the river banks. The second test investigated the effect of constricting a channel to slow down ice pan velocities and eventually form a bridging point. The third test was similar to the second

test; however, included the effects of a change in the channel bed slope and the use of the stopping velocity criterion. This section describes the details of the three test cases that were investigated.

### 3.3.1 Critical Velocities related to Border Ice Formation

In the *CRISSP2D* model, there are two critical velocities that affect border ice formation. The first of these is the critical velocity above which skim ice will not form, *VCRSKM*. This parameter relates to the third criteria for static border ice formation which states that border ice will only form where the magnitude of the local depth averaged velocity is less than a critical velocity. The second parameter is the critical velocity above which shore ice accumulation does not occur, *VCRBOM*. This parameter affects the formation of dynamic border ice.

The effect of these two critical velocities was tested in a simple trapezoidal channel that was 10000 m long, 1000 m wide, 5.5 m deep, with side slopes 5.5V:200H, and a bed slope of 6.00E-7. A flow of 388.0 m<sup>3</sup>/s was input at the upstream boundary and it was found that the maximum average velocity in the channel was 0.095 m/s (Figure 3.1). The values of both critical velocities tested ranged from 0 m/s to 0.10 m/s. Table 3.1, below, contains the details of each test carried out.

**Table 3.1. Details of border ice formation parameter testing in a simple channel.**

Run	Inflow Ice Concentration (%)	VCRSKM (m/s)	VCRBOM (m/s)	Figure
1	0	0	0	n/a
2	0	0.05	0	3.2
3	0	0.08	0	3.2
4	0	0.1	0	3.4
5	0	0.05	0.05	n/a
6	0	0.05	0.08	n/a
7	0	0.05	0.1	n/a
8	50	0.05	0.1	n/a
9	100	0.05	0.1	n/a

Runs 1 through 4 were conducted without any ice parcels entering the domain at the upstream boundary. It was found that the critical velocity above which skim ice will not form ( $V_{CRSKM}$ ) had a direct effect on the amount of border ice formed. When the value of this parameter was set to 0 m/s, no border ice formed and skim ice was present everywhere in the reach. As the value of the critical velocity above which skim ice will not form was increased, border ice formation increased along the sides of the channel, with skim ice remaining present everywhere else in the reach. Figures 3.2 through 3.4 show the results of setting this parameter equal to 0.05 m/s, 0.08 m/s and 0.10 m/s. When the value of this parameter was set to 0.10 m/s, border ice filled the entire channel (Figure 3.4). This suggests that the model allows border ice to form everywhere that skim ice is present as long as the flow velocity is below the critical velocity above which skim ice will not form ( $V_{CRSKM}$ ).

In Runs 5 through 7, several values of the critical velocity above which shore ice accumulation does not occur ( $V_{CRBOM}$ ) were tested with the critical velocity above which skim ice will not form set to 0.05 m/s. This was done so that a small amount of static border ice would form to allow dynamic border ice to adhere to it. However, it was found that this parameter had no effect on the amount of border ice formed. The reason for this may have been the fact that this parameter does not form dynamic border ice out of skim ice, but out of ice pans. Thus, in the next set of tests conducted, ice concentrations were incorporated into the domain.

In Run 8, ice pans with a concentration of 50% were input at the upstream boundary in order to test the effects of the parameter that controls the velocity above which shore ice accumulation does not occur ( $V_{CRBOM}$ ). For this test, the value of the critical velocity above which skim ice will not form ( $V_{CRSKM}$ ) was set to 0.05 m/s and the value of critical velocity above which shore ice accumulation does not occur ( $V_{CRBOM}$ ) was set to 0.1 m/s. Again, it was found that this value had no effect on the amount of border ice formed. Specifically, this parameter was supposed to affect the formation of dynamic border ice;

however, not a single parcel of this ice type was formed. The test was repeated with an ice concentration of 100% at the upstream boundary (Run 9), but this also showed that there was no effect on border ice formation by this parameter.

### 3.3.2 Channel Constriction

In addition to being able to form border ice adequately, a 2-D ice process model needs to be able to create a bridging point in order to initiate ice cover formation. For high surface ice concentrations in the field, it is observed that ice pans congest and decelerate as they approach a narrowing in the channel. If the narrowing becomes too small to let ice pans pass through (e.g. due to border ice encroachment or channel width reduction), then a bridging point is formed. In *CRISSP2D*, a bridging point is formed though the use of a stopping velocity criterion. However, before this can be applied, it must be seen if the model can reproduce congestion effects at a channel narrowing. A rectangular channel 1000 m long, 1 m deep and 100 m at the upstream boundary narrowing to 60 m at the downstream boundary was created in order to test *CRISSP2D*'s ability to model the behavior of ice pans at a constriction. The channel slope was maintained at a constant slope of 1.00E-4. A flow of 25.2 m<sup>3</sup>/s was input at the upstream boundary and ice parcels were injected at a concentration of 90%.

The results of this test showed that *CRISSP2D* does not simulate the behavior of ice pans as it was observed in the field. Upon approaching the constriction, it was found that ice parcels did not slow down, but rather they sped up with the velocity of the water in order to pass through the narrowing (Figure 3.5). It can even be seen that ice velocity magnitude was greater than the water velocity magnitude by 20% in the downstream end of the channel (Figures 3.6). This may be attributed to the fact that the model is approximating a velocity distribution in the vertical direction where the surface water velocity is 20% greater than the average velocity. Since the ice parcels are located at the surface of the water, they travel with this increased water surface velocity.

A similar test was repeated in another simple rectangular channel that was 100 m at the upstream boundary narrowing to 20 m at the downstream boundary. The channel length, depth, and slope remained the same. A flow of  $8.0 \text{ m}^3/\text{s}$  was input at the upstream boundary along with ice parcels at a concentration of 90%. The results of this test showed the same patterns as the previous test. Ice parcels did not slow down, but increased in velocity as they approached the narrowing. Further adjustments had to be made to the channel in order to simulate ice pans congesting at a narrowing.

### **3.3.3 Channel Constriction with a Steeper Slope**

In order to understand what conditions cause ice pans to congest at a channel narrowing, further testing was carried out with *CRISSP2D* on a slightly different simple channel. In this case, the channel created narrowed in width from 100 m to 60 m, while a slope change from  $1.00\text{E-}4$  to  $2.24\text{E-}3$  allowed the channel depth to increase from 2.6 m to 3.6 m over the length. With this arrangement, depth averaged water velocities were maintained, as opposed to the increasing average channel velocities seen with maintaining a constant slope. It can be shown through a simple constant volume analysis that if water velocities remain constant through the section and if ice parcels travel with the velocity of the water, the ratio of the ice concentration at the upstream boundary to the downstream boundary is equal to the ratio of the water depth at the upstream boundary to the downstream boundary. This means the concentration of ice at the downstream boundary is a function of water depths and the initial ice concentration.

A flow of  $90.0 \text{ m}^3/\text{s}$  was input at the upstream boundary and ice parcels were injected at a concentration of 90%. It was found that a constricting channel with an increasing depth caused the ice parcels to congest and slow down through the channel narrowing. This shows that the model can simulate the behavior that is seen in the field.

Upon successfully simulating the congestion of ice parcels through a channel narrowing, the use of a stopping velocity criterion (*STPV*) to create a bridging point was explored. Tests were conducted using values of 0.001 m/s, 0.01 m/s and 0.1 m/s for this parameter. It was found that setting this value equal to 0.001 m/s and 0.01 m/s did not cause ice parcels to stop. However, using a value of 0.1 m/s, it was possible to achieve ice parcel stoppage halfway through the constriction (Figure 3.7). Results show ice concentrations upstream of the bridging point are 100%, while downstream of this point virtually no ice exists (Figure 3.8). This test suggests that it is possible for this model to achieve bridging; however, this can only be done in areas where ice parcel velocities do not increase while the channel is being constricted (ie: areas that deepen as they become more narrow). It is interesting to note that after ice velocities have stopped in the channel, ice parcels continue to enter the domain and build up at the upstream boundary. Eventually, this leads to a stability error due to an ice jam blockage and causes the program to stop.

### **3.4 Model Application to the Athabasca River**

This section presents the steps taken to create a 2-D model using both *River2D* and *CRISSP2D*. The geometry and computational meshes were initially created. Hydrodynamic calibration was completed for both the *River2D* and *CRISSP2D* models in open water and ice covered conditions. Thermal calibration was completed for a heat flux coefficient, as a starting point for physical parameter selection. This was followed by a detailed sensitivity analysis involving many of the physical parameters. The resulting model was tested for its ability to form border ice, create a bridging point and form an ice cover.

### 3.4.1 Geometry and Computational Mesh

The geometry and computational mesh for both the *River2D* and *CRISSP2D* models was constructed using *River2D*. This was done both because of its ease of use, and so as to ensure identical meshes were used for the hydrodynamic model comparisons. The model geometry and computational mesh were constructed using the detailed bathymetric data that was collected in the summer of 2008.

Using all of the points collected in the field, a data mesh was created to represent the bed and bank geometry. The Triangulated Irregular Network (TIN) methodology was used to take the irregularly distributed data points, or nodes, and arrange them in a network of non-overlapping triangles (Steffler and Blackburn, 2002). Breaklines were inserted in the longitudinal direction in order to link together common features and allow for accurate interpolation of field data points. Boundaries were created in at the upstream and downstream sections of the reach, as well as around the island. A detail of this file showing the area around the island can be seen in Figure 3.9, where the points represent nodes, the solid lines show triangulation and the dotted lines represent breaklines.

2-D models require a method of discretization, which is the reduction of an infinite number of equations for an infinite number of unknowns to a finite number of equations at a finite number of mesh or grid points in space and time. Both *River2D* and *CRISSP2D* employ the finite element method for solving the governing equations (Steffler and Blackburn, 2002; Shen, 2005b). Based on the weighted residual method, this method offers great geometrical flexibility. Since elements are not restricted to any specific sizes or shapes, very complex boundaries can be traced and refinements can be made in critical areas (Steffler and Blackburn, 2002). When creating a mesh, it is important to find a balance between time and accuracy. If node spacing is too large, there is a danger of losing accuracy; however, a very small spacing may result in excessive computing time (Steffler and Blackburn, 2002).

Using the results of the geometry mesh, the computational mesh with node spacing varying between 15 m and 30 m, was created using *River2D*. As can be seen in Figure 3.10, finer spacing was employed in narrow areas where there are higher anticipated velocities and in wide shallow areas where the wet-dry transition would be used. The narrowest section in the reach, located on the left side of the island, is approximately 100 m wide. Employing a mesh spacing of 15 m distributes approximately 6 nodes across the section. This is better than the minimum of 4 nodes as guided by the *River2D* user's manual; however, not up to the recommended 10 nodes (Steffler and Blackburn, 2002). The initial mesh was smoothed by moving each point to a more central position with respect to neighboring points. Manual adjustments were made to several triangles that were found to be the most unlike equilateral triangles by the mesh editor. While *River2D* has an unlimited amount of nodes and elements available, special care was taken not to exceed the limited amount of nodes and elements available for the *CRISSP2D* model.

### **3.4.2 Hydrodynamic Calibration**

Both boundary conditions and initial conditions must be appropriately applied in order to calibrate the bed resistance in the reach. For a flow regime that is subcritical, the boundary conditions are specified as total discharge at the inflow or upstream section and a fixed water surface elevation at the outflow, or downstream section. The initial condition is an estimate of the inflow elevation. It is important to choose initial conditions well, since they are used as the initial guess in the iterative solution procedure and may make the difference between a stable run and an unstable run.

The *River2D* model was first used for calibration of open water and intact ice cover conditions. Since the summer survey data was collected in both July and August at various stages and discharges, data was available for both calibration and validation of bed roughness,  $k_b$ . A value of  $k_b = 0.15$  m was found to be appropriate. Using the *River2D* model calibrations, an equivalent *CRISSP2D*

model was constructed. This necessitated conversion of the bed roughness height,  $k_b$ , to a Manning's resistance coefficient,  $n_b$ , which was achieved using the following equations (Steffler and Blackburn, 2002):

$$k_b = \frac{12H}{e^m} \quad [16]$$

and

$$m = \frac{H^{1/6}}{2.5n_b\sqrt{g}} \quad [17]$$

where        H        =        flow depth ( $m$ )  
                   g        =        acceleration due to gravity ( $m/s^2$ )  
                    $n_b$     =        Manning's resistance coefficient (*dimensionless*)

The equivalent Manning's roughness coefficient was found to be  $n_b = 0.028$ . Figure 3.11 shows the calibrated profiles for both models. Figure 3.12 shows a comparison between modeled and measured velocities at the measurement transects for the calibration inflow discharge of  $685 \text{ m}^3/\text{s}$ . In July, the average flow measured with the ADCP was  $609 \text{ m}^3/\text{s}$ , whereas  $685 \text{ m}^3/\text{s}$  was the value reported at the Water Survey of Canada (WSC) gauge just upstream of the study reach. The average measured flow in the left channel around the island was  $370 \text{ m}^3/\text{s}$ , whereas the flow modeled in this channel by *River2D* was  $425 \text{ m}^3/\text{s}$  and by *CRISSP2D* was  $435 \text{ m}^3/\text{s}$ . The difference in values was within 10% of the total discharge.

For the ice covered case, both models were calibrated for the conditions observed during winter 2009. In this case, the inflow discharge used was  $150 \text{ m}^3/\text{s}$ . Based on the ice thickness survey, a constant value of 60 cm was found to be appropriate throughout the domain. Based on this, the ice roughness height for the *River2D* model was calibrated to be  $k_i = 0.000001 \text{ m}$ . The equivalent Manning's roughness coefficient for the *CRISSP2D* model was found to be  $n_b = 0.01$ . This

suggests a very smooth ice underside, which is consistent with the underwater video obtained. Reasonable correlation was also found when comparing the velocity data collected with the ADV and ADCP to the velocities output from the model (Figure 3.13). In February, the WSC measurement of discharge at the Athabasca River below Fort McMurray was 149 m<sup>3</sup>/s. The average flows measured at the site with the ADCP were 144 m<sup>3</sup>/s and 14 m<sup>3</sup>/s in the left and right channels (Sites 3 and 4, Figure 2.2), respectively. Using a flow of 150 m<sup>3</sup>/s, the corresponding modeled values were 120 and 30 m<sup>3</sup>/s, respectively, for the *River2D* model and 125 and 25 m<sup>3</sup>/s, respectively, for the *CRISSP2D* model. The difference in values was within 10% of the total discharge.

Since it would have been too difficult and dangerous, discharge and downstream water elevation data were not measured during the freeze-up period. Discharge was obtained from WSC and a value of 250 m<sup>3</sup>/s was found to be a good representation of the average discharge experienced in 2008 over the freeze-up period (Figure 2.6). However, the problem of obtaining a downstream water surface elevation remained. Using the known geometry at the downstream boundary, Manning's n for the channel, the slope and discharge, a downstream water level was estimated using a uniform flow approximation. A value of 233.0 m was used at the downstream boundary in all freeze-up simulations.

### **3.4.3 Thermal Calibration**

A simple linear heat transfer model based on observations of the water cooling phase at the study site was created in order to attempt to quantify the heat exchange between the air and the water during ice formation. Using the relationship in Equation 12, which *CRISSP2D* employs to approximate the heat exchange per unit area between water and air, the value for the coefficients  $\alpha'$  and  $\beta'$  were determined. Solar radiation was neglected at the site since it was found that the weather was consistently heavily overcast at the site during freeze-up, resulting in a very minimal amount of solar radiation being recorded. The constant  $\alpha'$  was also taken as zero, as there was no direct evidence for any

exposure effect that would warrant assigning a value. This left only  $\beta'$ , and based on air and water temperature data collected from 2006 to 2008, a value of  $10 \text{ W/m}^2/\text{°C}$  was found to be the most consistently appropriate. Figure 3.14 shows the modeled water temperatures based on recorded air temperatures and is compared with recorded water temperatures at the study site.

When looking at the results of 1-D water temperature modeling conducted with *River1D* for the water cooling phase of freeze-up in 2006 and 2007, a value of  $10 \text{ W/m}^2/\text{°C}$  for  $\beta'$  was also found to be most suitable (Andrishak *et al.*, 2008). *River1D* uses the linear heat transfer relationship in Equation 12. In this analysis, solar radiation effects were neglected and no appropriate value was found for the constant  $\alpha'$ . The 1-D modeling results showed that there was little sensitivity for values of the heat transfer coefficient between air and water ranging from 10 to  $20 \text{ W/m}^2/\text{°C}$ . It was found that the quality of the water temperature boundary condition was far more significant than the ambient cooling effect within the simulation (Andrishak *et al.*, 2008).

From a simple linear heat transfer model and the results of 1-D water temperature modeling, it was found that  $\alpha' = 0 \text{ W/m}^2$  and  $\beta' = 10 \text{ W/m}^2/\text{°C}$  during the water cooling phase at the study site. These values served as a starting point for the selection of the constant and coefficient of heat exchange between the air and water for the 2-D model. The sensitivity analysis carried out on these values is reported in the following section.

#### **3.4.4 Sensitivity Analysis**

In addition to providing channel geometry, a discrete mesh, roughness and transverse eddy viscosity coefficients, boundary conditions and initial flow conditions, a series of physical parameters are required for ice process modeling. Some of these inputs, such as ice concentration and size of ice parcels, can be quantified from observations made in the field during the time of freeze-up. However, the values for other parameters, such as various critical temperatures

and velocities, are often more difficult to quantify due to the lack of such detailed data. The effect of each ice process input must be investigated in detail. Since calibrations are often not possible, a sensitivity analysis can be conducted to aid in the final choice of parameters.

The process of freeze-up was intended to be modeled from the time that water temperatures were first observed to reach 0°C to the time of bridging. The *CRISSP2D* model requires an extremely small time step to maintain stability ( $\Delta t_h = 0.5$  s in this case), which means that it takes ~2 hours of actual time for ~3 hours of simulation time. Therefore, to reduce the computational time required to test different scenarios, the initial air temperature was set to a constant value of -30°C. In the testing of the effect of each parameter, only one variable was changed at a time while keeping all others constant. As previously mentioned, the most important ice process to model correctly in the context of this study is the border ice formation. Testing of the various upstream boundary ice inputs and physical parameters was aimed at facilitating this.

#### **3.4.4.1 Hydrodynamic Parameters**

In *CRISSP2D*, the physical parameters file contains a minimum depth parameter (*HTMIN*) which directly affects the quality of the hydrodynamic simulation. This parameter is of particular interest because of its relation to the way the model manages wet-dry transitions. As discussed in Section 3.2.1, difficulties in computation are encountered when the water depth is very shallow (Steffler and Blackburn, 2002). This means that there is a minimum depth in which the model can accurately perform hydrodynamic calculations. As in the case of discretization, the smaller the value for this parameter, the more accurate the solution becomes. Therefore it is optimal to choose the smallest value for this parameter that does not produce unstable results.

This parameter was examined at 0.5 m (the default), 0.2 m, and 0.1 m. When the minimum depth was set to 0.1 m, unstable results were produced. When it was

set to 0.5 m or 0.2 m, the results were not significantly different. Since more accuracy can be achieved when this number is set to the lowest value possible, all subsequent tests were carried out with the value of this parameter set to 0.2 m.

### 3.4.4.2 Coupling Time Step

The *CRISSP2D* model requires the input of a time step for the hydrodynamic simulation, the ice dynamic simulation and the coupling between the ice dynamics and the hydrodynamics. The values of the time step for the hydrodynamic simulation and the ice dynamic simulation are chosen such that stability can be maintained. As mentioned in the introduction, the hydrodynamic time step used was 0.5 s in order to maintain stability. This value was used also for the ice dynamic time step to maintain stability. Both values were determined by trial and error. The Courant number is used as a measure of stability in hydrodynamic modeling and should not exceed the value of one. It is defined as (Steffler and Blackburn, 2002):

$$C_r = \frac{V_w \Delta t}{\Delta x} \quad [18]$$

where

$C_r$	=	Courant number ( <i>dimensionless</i> )
$V_x$	=	velocity in the x-direction ( <i>m/s</i> )
$\Delta t$	=	time step increment ( <i>s</i> )
$\Delta x$	=	mesh spacing ( <i>m</i> )

The Courant number varies throughout the domain at a given point in time due to varying velocities and mesh spacing (Steffler and Blackburn, 2002). The Courant number was calculated for the 2-D model of the Athabasca River. Since a time step of 0.5 s must be used, a reasonably high value calculated for this number is 0.0167. This number is much smaller than one.

The value of the coupling time is chosen based on the type of process being modeled. For highly dynamic cases, such as an ice jam release simulation, a smaller interval in the order of a few seconds should be used. For slow processes in which ice thickness and hydrodynamic changes are small, a larger value, such as the default value of 900 s, is appropriate (Shen, 2005b). Thus, for simulations of border ice formation where ice pans were not incorporated at the upstream boundary of the domain, a coupling time step of 900 s was used. This value was considered suitable since very little change was occurring between each time step. For the simulations where ice pans were introduced, a coupling time step of 60 s was used. The ratio of the hydrodynamic time step to the coupling time step in this case was 1:120. A smaller coupling time step of 5 s, which results in a ratio of 1:10 was also tested in order to test the effects of the coupling time step value. As in the choice of mesh discretization, the choice of a coupling time is once again a matter of balancing time and accuracy. Results show that there is a small difference in ice cover extent between using a coupling time step of 60 s and 5 s (Figures 3.15 and 3.16). However, this difference is small enough to justify the use of a larger value to save computational time.

#### **3.4.4.3 Initial Water Temperature**

One of the initial conditions that must be set for an ice process model is the water temperature of the upstream boundary. Modeling on the Athabasca River was carried out from the point that the water temperature in the river was at the freezing point; however, tests were carried out in order to determine the effect of lowering the water temperature on the model's behavior. Testing involved two sets of runs with the upstream boundary water temperatures set to 0°C, the freezing point of freshwater, and -0.1°C, a temperature below the freezing of freshwater.

By changing the water temperature from 0°C to -0.1°C, it was found that there was no significant difference made to the extent and thickness of border ice formed. However, it is interesting to note that changes were seen to various other

components of the model. When the water temperature was set to  $-0.1^{\circ}\text{C}$ , a higher concentration of frazil ice was present throughout the channel, especially at the upstream end of the reach (Figures 3.17 through 3.18). It was also noted that frazil ice concentration formed in the first quarter of the reach when the water temperature was set to  $-0.1^{\circ}\text{C}$ , while frazil formed mostly in the second quarter of the reach when the water temperature was set to  $0^{\circ}\text{C}$ . Warmer water temperatures were also observed throughout the first half of the reach when the inflow water temperature was set to  $-0.1^{\circ}\text{C}$ , which is likely due to the increased frazil formation (Figures 3.19 and 3.20). Through a series of tests, it was seen that when the water temperature was set to  $-0.1^{\circ}\text{C}$ , problems occasionally occurred near the upstream boundary where unreasonable ice thicknesses were produced. Due to this, the upstream boundary water temperature was set to  $0^{\circ}\text{C}$ .

#### **3.4.4.4 Border Ice Formation Parameters**

In *CRISSP2D*, the physical parameters file contains a series of parameters that are directly related to the formation of border ice. These parameters include the critical water surface temperature for border ice formation ( $TC$ ), the critical velocities for static and dynamic border ice formation ( $VCRSKM$ ;  $VCRBOM$ ) and the maximum concentration for border ice formation ( $ANMAXBORDER$ ). Each of these parameters was explored in detail. Table 3.2 contains the default values given in the *CRISSP2D* manual for each input parameter, the values tested, and the final values assigned to each variable. Tests were conducted over a 72 hour length of time with the initial ice concentration at the upstream boundary set to a constant value of 35%.

The critical water surface temperature for border ice formation,  $TC$ , is an important parameter since it directly affects the first criterion for static border ice formation. When surface water temperatures are above this value, no border ice can be created. The value of this parameter was initially set to the default value of  $-0.5^{\circ}\text{C}$ . While air temperature remained  $-30^{\circ}\text{C}$ , values of this parameter ranging between  $-1.0^{\circ}\text{C}$  and  $-0.05^{\circ}\text{C}$  made no difference to the model output. In

tests where actual air temperatures ( $T_a \sim$  of  $-5^\circ\text{C}$ ) were used, it was found that this parameter did affect the amount of border ice that was formed. In such a case, the higher air temperature values did not facilitate as much cooling of the water surface, making it more difficult to achieve the critical temperature necessary for border ice formation. In order to mitigate this, the value of the critical water surface temperature for border ice formation was adjusted to  $-0.05^\circ\text{C}$ .

**Table 3.2. Border ice formation parameter defaults, values tested and final values used**

Physical Parameter	Units	Default value	Tested values	Final value used
Critical water surface temperature for border ice formation, TC	$^\circ\text{C}$	-0.5	-0.05, -0.1, -1.0	-0.05
Critical velocity above which skim ice will not form, VCRSKM	m/s	0.25	0.3, 0.35, 0.4	0.35
Critical velocity above which shore ice will not accumulate, VCRBOM	m/s	0.4	1.2	0.4
Maximum concentration for border ice formation, ANMAXBORDER	dimensionless	1.0	0.5	1.0

The parameter which had the greatest effect on border ice formation was the critical velocity above which skim ice will not form, *VCRSKM*. Referring back to the four criteria for border ice formation, the third criteria states that border ice will only form where the magnitude of the local depth averaged velocity is less than a critical velocity. This parameter was investigated in model testing (Section 3.3) and it was found that border ice formation increased significantly with the increase of this parameter.

Preliminary tests with the Athabasca River model were carried out with the default value of 0.25 m/s assigned to this parameter (Figure 3.21). However, this did not produce as much border ice as was observed in the field, therefore, the values of 0.30 m/s, 0.35 m/s and 0.40 m/s were also explored. The results of

these tests after 65 hours can be seen in Figures 3.22 through 3.24. A greater amount of border ice was formed with each increase in this parameter. Values of this parameter equal to or greater than 0.30 m/s caused border ice to form around the sandbar located just upstream and to the left of the island, as it was observed in the field (see Figures 2.20 and 2.21). When the value of this parameter was equal of greater than 0.35 m/s, the extent of ice formed around the upstream-most sandbar was very similar to what was observed in the field. However, the modeling results also showed that the right side of the channel filled in with border ice for values equal to or greater than 0.35 m/s and this was not observed in the field. Since the border ice formation was simulated very well throughout the upstream part of the reach, the value of this parameter was set to 0.35 m/s.

The parameter *VCRBOM*, which represents the critical velocity above which shore ice accumulation does not occur, did not seem to have any effect on border ice formation. This parameter is responsible for creating dynamic border ice. This was investigated in for the idealized model test cases (Section 3.3) and it was found to have no effect on the amount of border ice formed. When tested on the Athabasca River model, the same results occurred. As indicated by the output files, this parameter was not successful in creating even one fragment of dynamic border ice, even when set to a high value. Since the value of this parameter made no apparent difference, it was set to the default of 0.4 m/s.

The maximum concentration for border ice formation, *ANMAXBORDER*, is another parameter that exists in the border ice formation group. The default sets this parameter to 1.0, or 100%; however, the value of 0.5, or 50%, was also explored. It was found that while this value dictated the initial concentration of the border ice that was formed, there were no significant differences to the extent of border ice or any other ice process detail. Thus, this parameter remained set to 1.0 for all other runs.

#### 3.4.4.5 Water Temperature and Thermal Growth and Decay of Ice Parameters

In *CRISSP2D*, the physical parameters file contains a series of parameters that directly affect the simulation of water temperature as well as thermal growth and ice decay. This group of parameters includes heat exchange coefficients for water to air, ice to air and water to ice as well as the thermal conductivity of black ice, white ice and snow. Of particular interest in this group were the values of the coefficient of heat flux for water to air (*HWA*), the coefficient of heat flux for ice to air (*HIA*) and constant of heat flux for ice to air (*ALP*). Since there was not enough data to justify changing values any of the other values, default values were assigned.

Table 3.3 contains the default values given in the *CRISSP2D* manual for each parameter, the values tested, and the final values assigned to each variable. Each of these parameters was assessed for its effect on border ice formation. Two sets of tests were conducted over a 72 hour length of time. In the first, air temperatures were set to  $-30^{\circ}\text{C}$  and in the second, actual air temperatures were used ( $T_a \sim$  of  $-5^{\circ}\text{C}$ ).

For the initial set of tests, the values of the heat flux coefficients were based on the thermal calibration carried out in Section 3.4.3. The value of the coefficient of heat flux for water to air (*HWA*), is equivalent to  $\beta'$  in Equation 12 and a value of  $10 \text{ W/m}^2/^{\circ}\text{C}$  was determined to be appropriate for this coefficient. This value served as a starting point for the sensitivity analysis. The value for the coefficient of heat flux for ice to air (*HIA*) is typically less than or equal to the value of the coefficient of heat flux for air to water, thus it was set to  $10 \text{ W/m}^2/^{\circ}\text{C}$ . In a linearized heat transfer equation, the constant of heat flux for ice to air (*ALP*) is used to adjust the value of the net rate of heat loss at the water surface by a specific amount. Without any justification of assigning a value to it before knowing how the other parameters affect the model, it was set to  $0 \text{ W/m}^2$ .

**Table 3.3. Water temperature and thermal growth and decay of ice parameter defaults, values tested and final values used**

Physical Parameter	Units	Default value	Tested values	Final value used
Coefficient of heat flux for water-air, HWA	W/m <sup>2</sup> /°C	20.0	10, 15, 20, 25	25
Coefficient of heat flux for ice-air, HIA	W/m <sup>2</sup> /°C	12.189	10, 12, 15	12
Constant of heat flux for ice-air, ALP	W/m <sup>2</sup>	32.547	0, 100, 300, 500	0
Component of heat transfer coefficient for water-ice, CWI1	W·s <sup>0.8</sup> /m <sup>2.6</sup> /°C	1477.25	---	1477.25
Component of heat transfer coefficient for water-ice (supercooled), CIW1	W·s <sup>0.8</sup> /m <sup>2.6</sup> /°C	1433.45	---	1433.45
Nusselt number for heat transfer coefficient water-ice (laminar flow), ATA	dimensionless	2.47	---	2.47
Thermal conductivity of black ice, XKI	W/m <sup>2</sup> /°C	2.24	---	2.24
Thermal conductivity of white ice, XKW	W/m <sup>2</sup> /°C	1.12	---	1.12
Thermal conductivity of snow, XKS	W/m <sup>2</sup> /°C	0.3	---	0.3
Coefficient of heat flux for water-ice, CWI	W·s <sup>0.8</sup> /m <sup>2.6</sup> /°C	900.0	---	900.0

Two sets of tests were carried out with coefficient of heat flux for water to air, the coefficient of heat flux for ice to air and the constant of heat flux for ice to air. In the first set of tests, air temperatures were set to -30°C and in the second set of tests, actual air temperatures from the 2008 freeze-up period were applied ( $T_a \sim$  of -5°C for 120 hours). Results from the first set of tests showed that, when the air temperature was set to -30°C, the extent of border ice did not change with increasing values of any of these three parameters. However, it was found that considerably more skim ice was present in the channel for cases where the coefficient of heat flux for air to water was increased over the range indicated in Table 3.3. When actual air temperatures from the 2008 freeze-up period were used, it was found that much less border ice formed in this case than when air

temperatures were  $-30^{\circ}\text{C}$ . When considering the four criteria necessary to create border ice, it is easy to understand why this would be so. The first criterion is that the surface water temperature must be below the critical temperature for freezing. The rate of heat flux from the water to air was not high enough to decrease the water surface temperature to a low enough point. From this, it was evident that it was necessary to increase the value of the heat flux coefficients in order to form more border ice.

Each of the heat flux parameters was examined to see what effect it had on the formation of border ice at higher air temperatures. Testing showed that increasing the values of the constant of heat flux for ice to air and coefficient of heat flux for ice to air affected the growth of ice thickness. That is, wherever ice was present, an increase in either of these parameters aided in thickening it faster; however, it did not help to extend ice farther out into the channel. Since there was no justification in setting it to any other value, the constant of heat flux for ice to air was set to  $0 \text{ W/m}^2$  and the coefficient of heat flux for ice to air was left at the default value of  $12 \text{ W/m}^2/^{\circ}\text{C}$ . Test results also showed that border ice formation was very sensitive to coefficient of heat flux for water to air. Figures 3.25 through 3.28 show border ice formation with this parameter varying from  $10 \text{ W/m}^2/^{\circ}\text{C}$  to  $25 \text{ W/m}^2/^{\circ}\text{C}$  when real air temperatures ( $T_a \sim$  of  $-5^{\circ}\text{C}$ ) were used for 56 hours. This length of time corresponded with November 16, 2008 and model results were compared with observations made on that day (Figure 2.20). The coefficient of heat flux for water to air was set to  $25 \text{ W/m}^2/^{\circ}\text{C}$  in order to produce results that were most like those observed in the field.

#### **3.4.4.6 Ice Input Parameters**

In *CRISSP2D*, the boundary ice input file contains a series of parameters that relate to the dynamic ice processes in the program. These parameters are divided into groups containing information about ice islands and ice parcels, including the location, timing and quantity of ice input along the upstream boundary. Values for these parameters were selected based on the knowledge from the field and

their effects on border ice formation were investigated. Where there was not enough data to justify varying values, default values were assigned.

Table 3.4 contains the default values given in the *CRISSP2D* manual for each input parameter, the values tested, and the final values assigned to each variable. Of particular interest in this group were the values for the inflow surface ice concentration (*ANB*), surface ice thickness (*THIO*), frazil ice thickness (*THIOF*), size of ice parcels (*HPIO*), the initial concentration of each parcel (*ANO*), the maximum concentration of each parcel (*ANMAX*), Manning's n roughness coefficient for ice (*CNI*), and the internal friction angle of ice (*PHI*). Each of these parameters was assessed for its effect on border ice formation. Tests were conducted over a 5 hour length of time with the initial ice concentration at the upstream boundary set to a constant value of 35%.

It was found that problems were encountered when the inflowing ice was distributed at nodes that were near the edge of the channel. To mitigate this effect, an increased amount of ice concentration was distributed over the central portion of the channel. It was found that limiting the inflowing ice to the central 70% of the channel width was the maximum practical. This meant that, if an inflow ice concentration of 35% was required, an inflow ice concentration of 50% was input over this central 70% width (i.e.  $0.5 \times 0.7 = 0.35$ ).

Through the examination of various concentrations of inflow surface ice concentration, it was found that regardless of the inflow surface ice concentration introduced into the channel, the ice concentration visible in the domain remained relatively constant at approximately 85-95%. The difference is that the ice thickness increased substantially with the increase of ice concentration. Figure 3.29 (ice concentration input of 5%) Figure 3.30 (ice concentration input of 35%) and Figure 3.31 (ice concentration input of 70%) demonstrate the ice thickness at 1 hour after ice pans have been introduced into the domain. Note the differences in ice thickness in the upstream half of the reach. The reason that ice concentration cannot be distinguished in the output is likely due to the fact that ice

dynamics are carried out on a Lagrangian frame and then put into an Eulerian frame.

**Table 3.4. Ice input parameter defaults, values tested and final values used**

Physical Parameter	Units	Default value	Tested values	Final value used
Manning's n of ice islands or border ice, CNISLD	dimensionless	0.02	---	0.02
Darcy's coefficient for seepage flow in ice islands, DARCYILD	dimensionless	0.02	---	0.02
Darcy's coefficient for seepage flow in rubble ice, DARCYRUB	dimensionless	0.02	---	0.02
Maximum concentration of ice parcels, ANMAX	dimensionless	0.6	0.99	0.99
Initial concentration of each parcel, AN0	dimensionless	0.6	0.5	0.5
Surface ice thickness, THIO	m	0.2	0.05, 0.10	0.05
Frazil ice thickness, THIOF	m	0	0.10, 0.20, 0.30	0.2
Ice parcel length, HPIO	m	10	15, 20	15
Friction coefficient between ice and bank, FRIC1	dimensionless	1.04	---	1.04
Friction coefficient between ice and bed, FRIC2	dimensionless	1.04	---	1.04
Wind-ice stress coefficient, CA	dimensionless	0.0015	---	0.0015
Manning's n coefficient of single layer of ice, CNI	dimensionless	0.02	0.01	0.02
Maximum Manning's n coefficient of ice jam, CNIMAX	dimensionless	0.06	---	0.06
Internal angle of friction, PHI	°	46	45	45
Empirical constant, PJ	dimensionless	15	---	15

Upon looking at longer simulations with various quantities of inflow surface ice concentration, it was observed that higher concentrations of inflow surface ice concentration at the upstream boundary contributed to a slightly greater extent of border ice cover. Figure 3.32 shows the border ice after 30 hours with a constant input ice concentration of 35%, while Figure 3.33 shows the border ice with an input ice concentration of 70%. This suggests the formation of dynamic border ice; however, from the output files, it can be seen that this ice type was never created.

Simulation with an inflow surface ice concentration of 70% was shown to affect the velocity and thickness of the ice parcels in narrow areas. Figure 3.34 shows that the ice velocity magnitude decreases to a value of 0.2 m/s in the downstream portion of the reach where the border ice formed has caused a constriction. It can also be seen that where the velocity magnitude decreases, ice thickness in the channel increases (Figure 3.35).

The next set of tests conducted looked at the effects of changing the values of thickness for surface ice and frazil ice in each ice parcel. Based on qualitative field observations, the values for the thickness of surface ice and frazil ice were 0.05 m and 0.20 m, respectively. This compares to 0.3 m which was used for the ice thickness in the 1-D model of the 80 km section of the Athabasca River from Fort McMurray to Bitumont (Andrishak *et al.*, 2008). From the test results, it can be seen that changing the values of surface ice and frazil ice thickness tested had no significant effect on border ice formation.

The next set of tests carried out tested the effects of changing the ice parcel length. In *CRISSP2D*, it is assumed that all ice parcels are squares and the input value needed for the model is the edge length of these squares. In order to determine values for testing, the computational mesh and the width of the narrowest section in the model were considered. Since the smallest computational mesh spacing used was 15 m and the narrowest section in the channel was approximately 100 m wide, values of 15 m and 20 m were selected as reasonable values for this parameter. It was found that there was negligible difference in the

extent of border ice formation between the runs conducted using these two values, so without any justification to set it to a higher value, the length of ice parcels was set to 15 m.

The values of the initial concentration of each parcel (*AN0*) and the maximum concentration of each parcel (*ANMAX*) were adjusted to those that were found to be more relevant to the given study. The default values for both of these parameters were 0.60. Lal and Shen (1991) used the values of 0.50 and 0.99 for the initial and maximum concentrations of each parcel when modeling ice cover formation in 1-D on the upper Saint Lawrence River using *RICE*, a predecessor to *CRISSP2D*. Therefore, a value of 0.5 was used for the initial concentration of each parcel and a value of 0.99 was used for the maximum concentration of each parcel.

The value of Manning's roughness coefficient of ice parcels was explored. It was found that changing its value from 0.02 to 0.01 produced some unreasonably thick ice at the downstream end of the channel. Therefore, the value of Manning's roughness coefficient of ice parcels remained at the default value of 0.02. This value was also used by Andrishak and Hicks (2008) in a 1-D ice process model on the Peace River.

The default value for the internal angle of friction (*PHI*) in *CRISSP2D* is 46°; however, the value of 45° was used in this study. It is not possible to measure this parameter in the field, thus knowledge gained in laboratory experiments must be applied. Healy and Hicks (2006) found values ranging from 42° to 46° for synthetic ice. Lal and Shen (1991) also used a value of 45° when modeling ice cover formation in 1-D.

#### **3.4.4.7 Frazil Rise Velocity Parameter**

In the *CRISSP2D* model, another parameter that can affect the formation of border ice is the frazil rise velocity, *VBB*. This parameter is contained in the geometry file. This parameter is of interest because it affects the second criterion

of static border ice formation. This criterion requires the buoyant velocity of frazil,  $v_b$  or  $VBB$ , to be greater than the vertical turbulent velocity. The default value of this parameter 0.001 m/s; however, several other values were found in the literature. Ye and Doering, 2003, deduced a frazil rise velocity of 7.83 cm/s through laboratory experiments. Morse et al, 2008, measured a mean frazil rise velocity of 0.92 cm/s on the St. Lawrence River at Quebec City, Canada. Andrishak and Hicks (2008) calibrated a value of 0.1 mm/s for a 1-D model of the Peace River in Canada.

Tests were conducted over a 72 hour length of time with a frazil rise velocity value of 0.1 m/s, 0.01 m/s, 0.0001 m/s as well as the default value of 0.001 m/s. It was found in each case that changing this parameter did not lead to any significant change in border ice extent; therefore, the default value was employed hereafter. It was noticed that at 0.1 m/s, there was a slight decrease of frazil ice concentration in the channel and a slight increase in frazil ice thickness along the surface.

#### **3.4.4.8 Ice Cover Formation Parameters**

In *CRISSP2D*, the physical parameters file contains a series of parameters that relate to ice cover formation. These parameters include the ice parcel stoppage criterion (*STPV*), the critical Froude number for ice parcels to submerge (*CRIFR*), the erosion velocity of ice parcels (*UEROS*), and the critical velocity for freezing calculation (*VCRFRZ*). As modeling undercover ice transport and ice jams was not the intent of the study, there was no justification for changing the critical Froude number for ice parcels to submerge or the erosion velocity of ice parcels. These values were kept at their default settings of 0.09 and 1.5 m/s, respectively. Table 3.5 contains the default values given in the *CRISSP2D* manual for each input parameter, the values tested, and the final values assigned to each variable. Tests were carried out on the critical velocity for freezing calculation and the ice parcel stoppage criterion over 72 hours with an initial ice concentration of 35% in order to attempt to simulate ice cover formation.

The parameter *VCRFRZ* allows freezing to take place at velocities greater than 0 m/s. To test the effects of this parameter on the model, a value of 0.001 m/s was first applied. This test resulted in the creation of exceptionally large thicknesses along the edges of border ice in several locations. In the next test, the smallest value that possible based on the spaces provided in the file, was used. This also resulted in extreme ice thicknesses that did not reflect reality. As a result, the value of this parameter was left at the default of 0.0 m/s.

**Table 3.5. Ice cover formation parameter defaults, values tested and final values used**

Physical Parameter	Units	Default value	Tested values	Final value used
Ice parcel stoppage criterion, <i>STPV</i>	m/s	0.0	1E-5, 1E-4, 1E-3, 1E-2	0.0
Critical Froude number for ice parcel to submerge, <i>CRIFR</i>	dimensionless	0.09	---	0.09
Erosion velocity of ice parcels, <i>UEROS</i>	m/s	1.5	---	1.5
Critical velocity for freezing calculation, <i>VCRFRZ</i>	m/s	0.00	0.001	0.00

In order to form a bridging point, the *CRISSP2D* model employs the use of a stopping criterion based on a velocity, *STPV*. This parameter was investigated in model testing (Section 3.3) and it was found that a value of 0.1 m/s was able to create a bridging point and initiate an ice cover. Shen *et al.*, (2000) used a value of 0.001 m/s as a stopping criterion in a 1-D viscous-plastic constitutive model. The value of 0.1 mm/s or 0.0001 m/s was used by Liu *et al.*, 2001, as a stopping criterion in the 2-D modeling of locks and dams using *DynaRICE*, a predecessor to *CRISSP2D*. Tests were carried out on each of these values using air temperatures and ice concentration as recorded on the Athabasca River.

In the first test, a value of 0.001 m/s was applied as the stopping criterion velocity. However, this resulted in an error as the density of ice parcels was exceeded. *CRISSP2D* places a limit to the amount of parcel interactions that can

take place in a domain per time step. In order to try to overcome this error, smaller values were tested. The stopping criterion velocity was set to 0.0001 m/s and 0.00001 m/s, which is the smallest value that can be entered into the file. However, in each case, the same density error occurred. The next attempts employed the use of a larger ice parcel size. Using a stopping criterion velocity of 0.001 m/s, 30 m long ice parcels and 60 m ice parcels (two times and four times the original length) were used. The width of the narrowest section in the reach is approximately 100 m, thus it would not make sense to test ice parcels of longer length. However, no combination of values aided the simulation and the same density error was encountered with every attempt. Since this error could not be avoided, the model could not form a bridging point and initiate an ice cover. Further testing may only be carried out when the problem of limited amount of ice parcels is resolved.

### **3.4.5 Border Ice Simulation**

Although it was not possible to simulate bridging and an ice cover formation, *CRISSP2D* was used to model the formation of border ice on the Athabasca River. Using all of the parameter values described above, ice processes were simulated for the freeze-up period from November 14<sup>th</sup> to November 19<sup>th</sup>, 2008. Figures 3.36 through 3.47 show the border ice output details at 12 hour intervals. These results were compared to the field observations wherever possible.

Figure 3.40 shows model results at 60 hours, which can be compared to the data in the ice map created for November 16<sup>th</sup>, 2008 in Figure 3.48. Throughout the majority of the reach, it was found that the model had simulated border ice formation well with respect to the shape and extent of ice cover.

In the area labeled A, located at the upstream end of the first sandbar, the model did not correlate well with observations. At this site, very little ice was simulated by the model, while more was observed in the field. In the areas labeled B through G, good agreement was found between what the model had simulated and

field observations. At the area labeled C, the sandbar in the middle of the channel was not modeled in its entirety. This may be due to the fact that this area was not well surveyed with the depth sounder or perhaps the shifting sands caused the sandbar to grow in size since the time the survey was carried out. Despite this, the ice that did form in the area is similar to what was seen in the field. At the area labeled E, the agreement was good at the downstream portion of the sandbar; however, the extent of the ice at the upstream portion was slightly different than what was observed in the field. There was less ice formed at the upstream portion of the sandbar and more border ice formed along the right bank just upstream of the sandbar, as compared to field observations. At the area labeled F, slightly more border ice was modeled than was observed in the field. Despite these details, the model still performed reasonably well, capturing the majority of the border ice formation in the area.

Figure 3.42 displays model output after 84 hours and can be compared to the ice map created for November 17<sup>th</sup>, 2008 in Figure 3.49. Once again, areas labeled A through G in the model output files are compared with the corresponding areas in the ice map. Since there is not much difference in the amount of border ice formation since the previous figure, similar observations are made as for November 16. Figures 3.50 through 3.56 show the corresponding photographs.

### **3.4.6 Validation**

Validating a model by running it with a different set of initial and boundary conditions is a useful step in confirming that a model was calibrated correctly. Freeze-up data was collected in both 2007 and 2008 in order to facilitate this. However, carrying out a validation proved to be difficult because freeze-up in 2007 was very similar to freeze-up in 2008.

Similar conditions were experienced over the freeze-up periods in 2007 and 2008. Throughout the freeze-up period, the average daily flows were very comparable (Figure 2.6). The majority of freeze-up, including bridging, occurred at

discharges of approximately 260 m<sup>3</sup>/s in 2007 and 250 m<sup>3</sup>/s in 2008. While air temperatures were slightly lower in 2008, they were very similar throughout most of the freeze-up period (Figure 2.7).

Looking at ice maps created from freeze-up in 2007 (Figures 2.15 through 2.18) and 2008 (Figures 2.19 through 2.22), it was found that despite bridging occurring in different areas, the border ice formation was very similar in both years. In both 2007 and 2008, constrictions were created at the upstream-most sandbar and the downstream-most sandbar in the detailed study reach. The minor differences observed in freeze-up patterns can be attributed to differences in the channel bed based on the fact that sand bed rivers shift each year. Because of this, there was little value in validating the model as the slight variations experienced would not make distinguishable impact on the results.

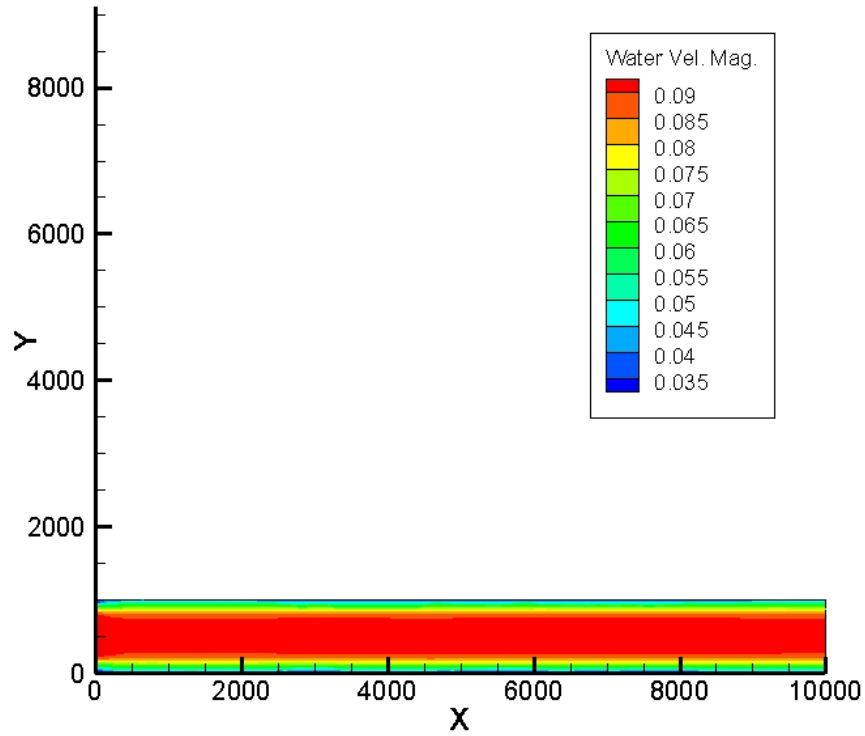


**Figure 3.1. Average channel velocity for a flow of 388.0 m<sup>3</sup>/s in a simple trapezoidal channel.**

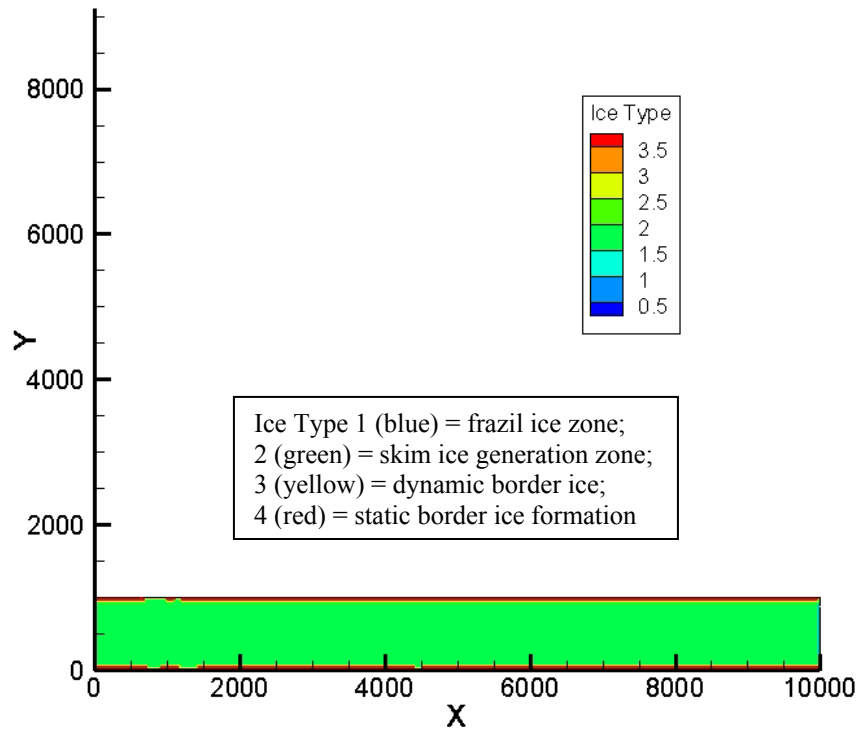


**Figure 3.2. Border ice formed in a simple trapezoidal channel with critical velocity above which skim ice will not form set to 0.05 m/s**

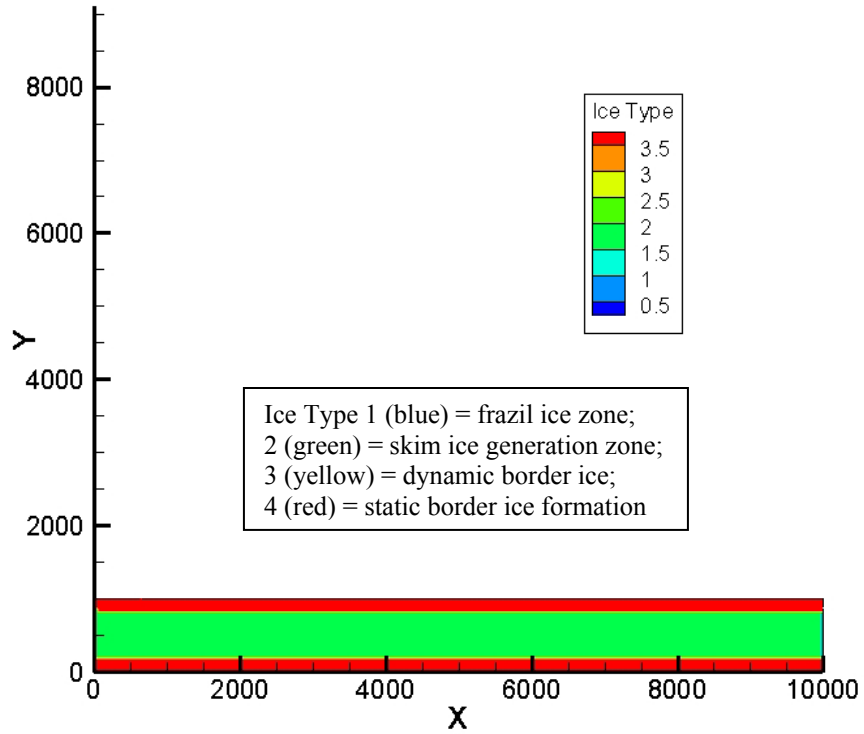


**Figure 3.3. Border ice formed in a simple trapezoidal channel with critical velocity above which skim ice will not form set to 0.08 m/s**

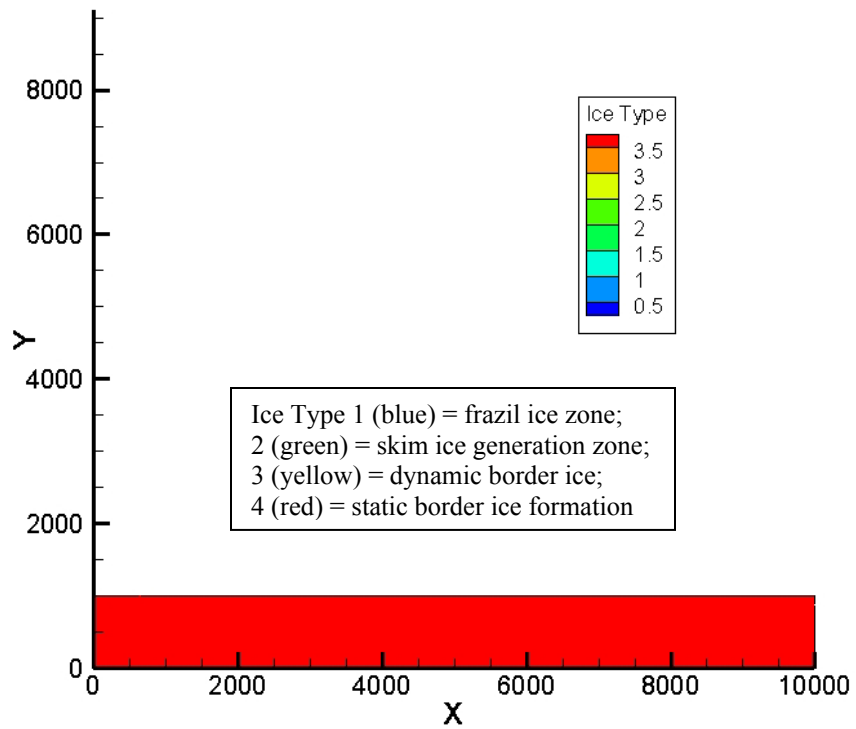


**Figure 3.4. Border ice formed in a simple trapezoidal channel with critical velocity above which skim ice will not form set to 0.10 m/s**

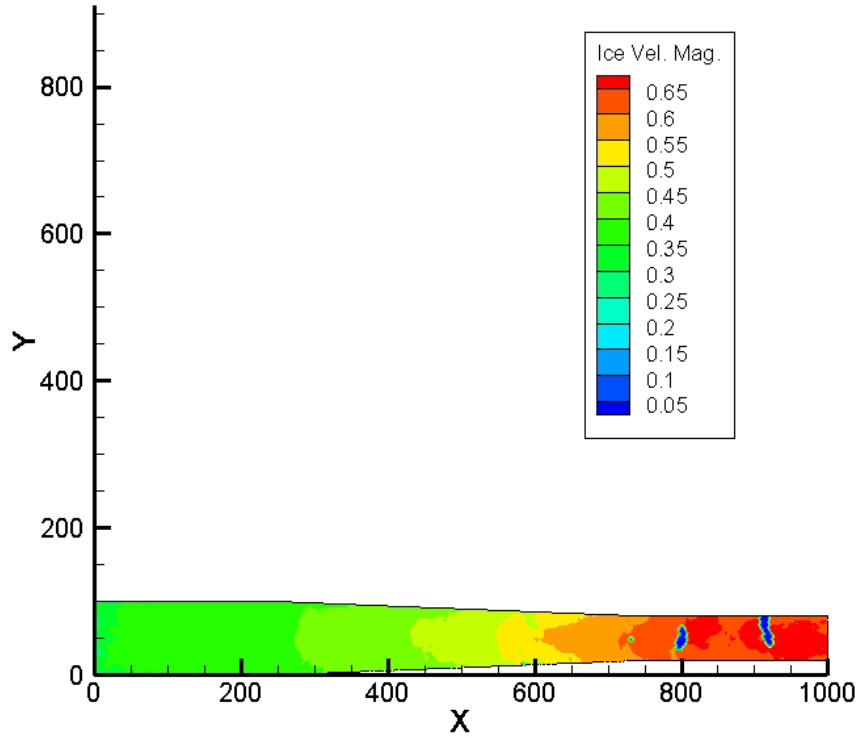


**Figure 3.5. Ice parcel velocity magnitude for a flow of  $25.2 \text{ m}^3/\text{s}$  in a simple rectangular channel**

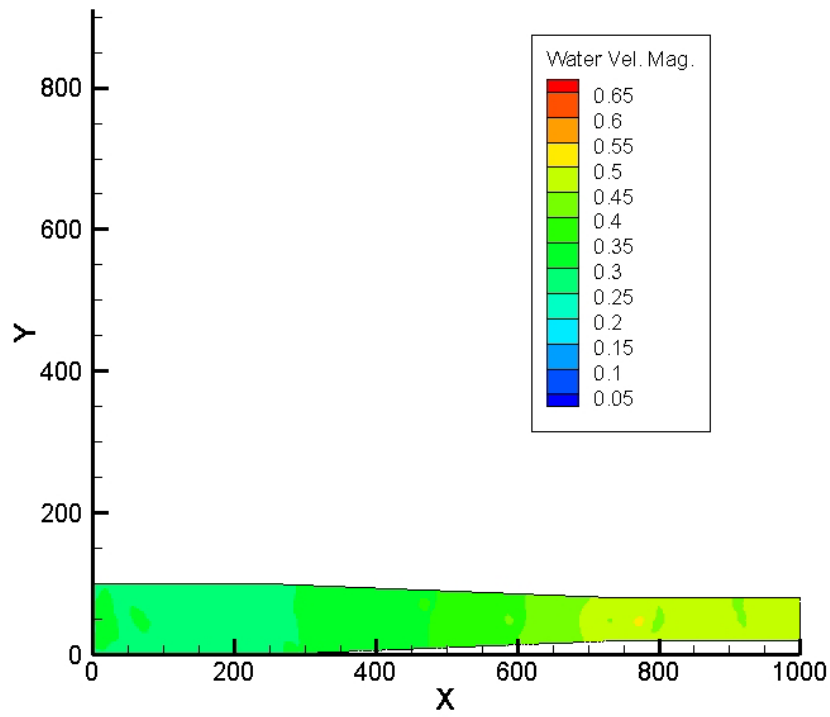


**Figure 3.6. Water velocity magnitude for a flow of  $25.2 \text{ m}^3/\text{s}$  in a simple rectangular channel**

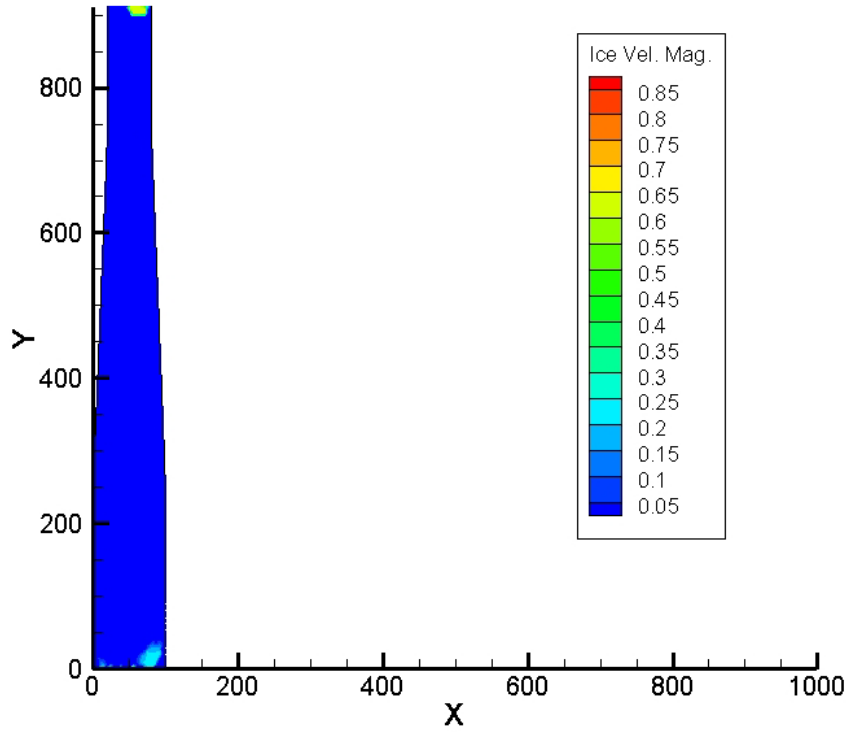


**Figure 3.7. Ice parcel velocity magnitude for a flow of 90.0 m<sup>3</sup>/s in a simple rectangular channel with a steep slope, stopping criterion velocity of 0.1 m/s**

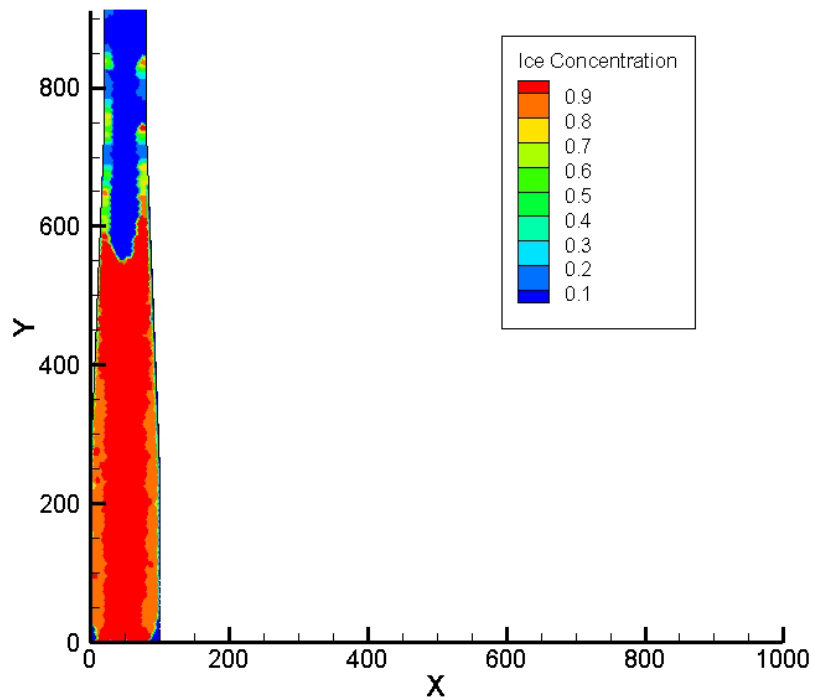


**Figure 3.8. Ice concentration for a flow of 90.0 m<sup>3</sup>/s in a simple rectangular channel with a steep slope, stopping criterion velocity of 0.1 m/s**

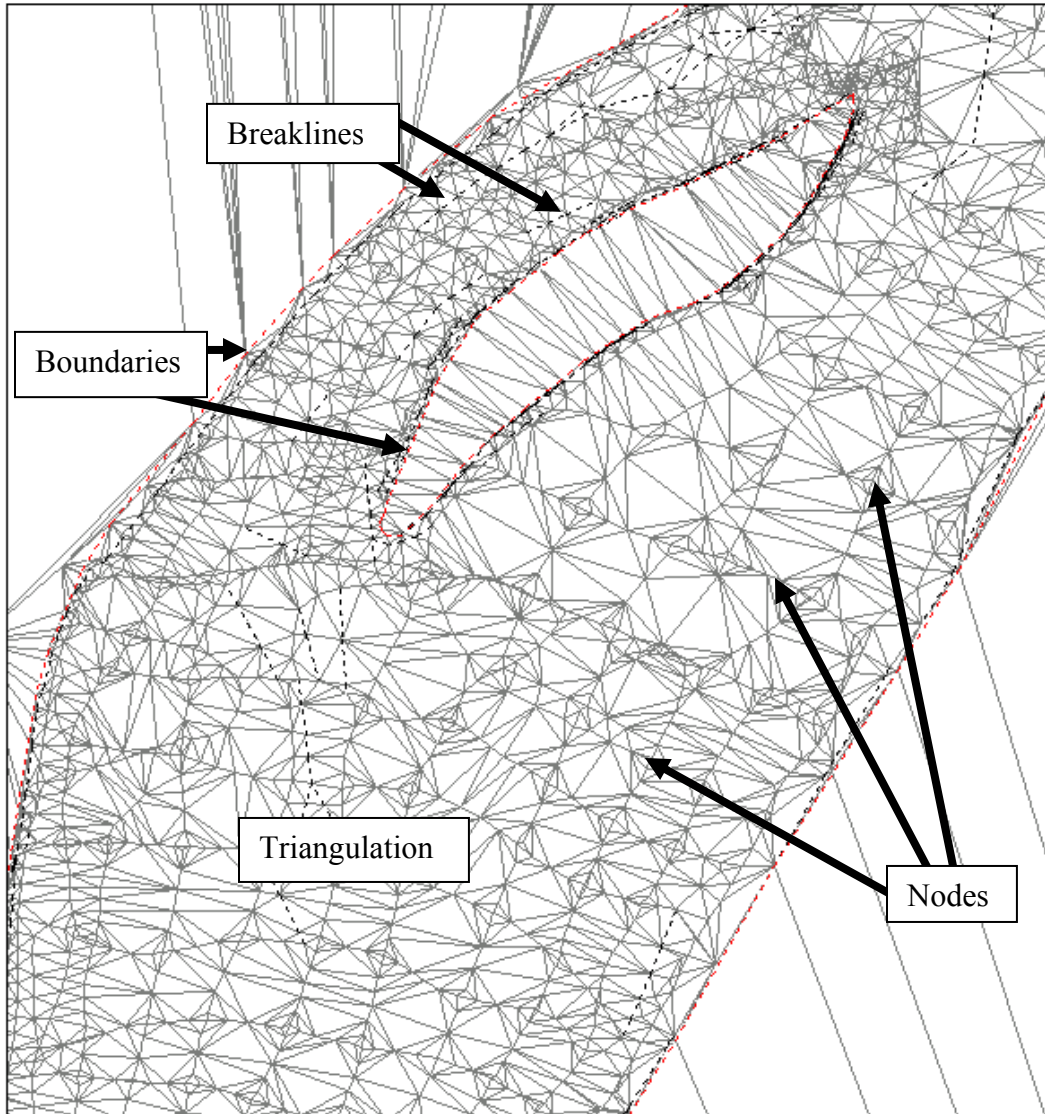


**Figure 3.9. Geometry mesh showing boundaries, nodes, triangulation and breaklines.**

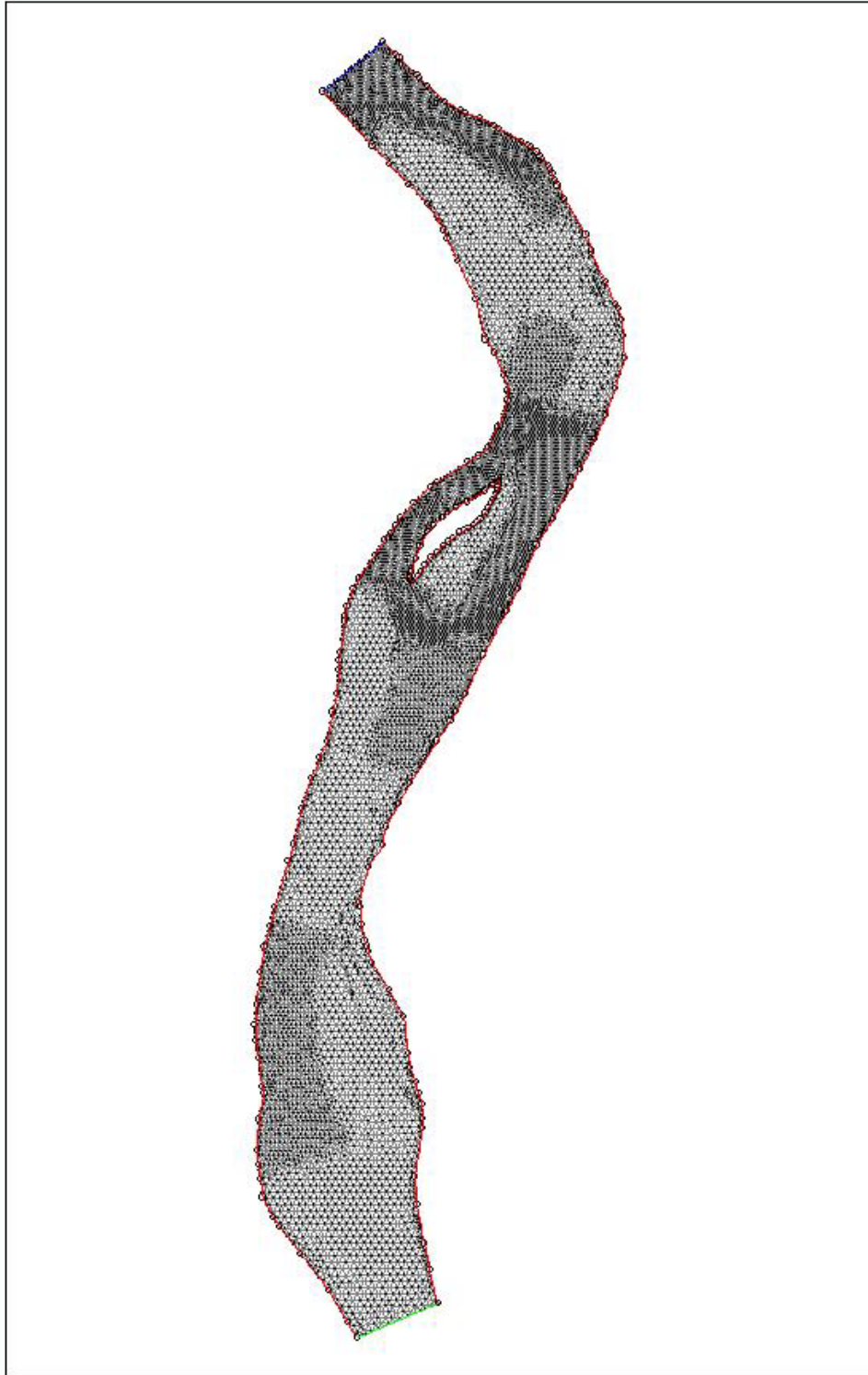


**Figure 3.10. Computational mesh, showing finer node spacing at narrow and shallow areas.**

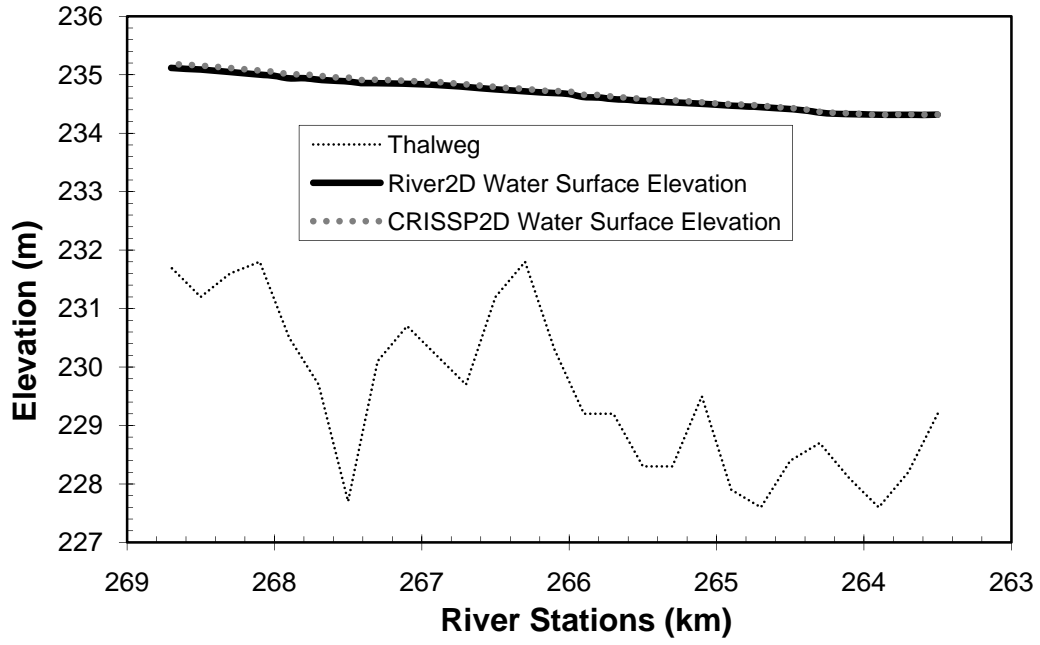
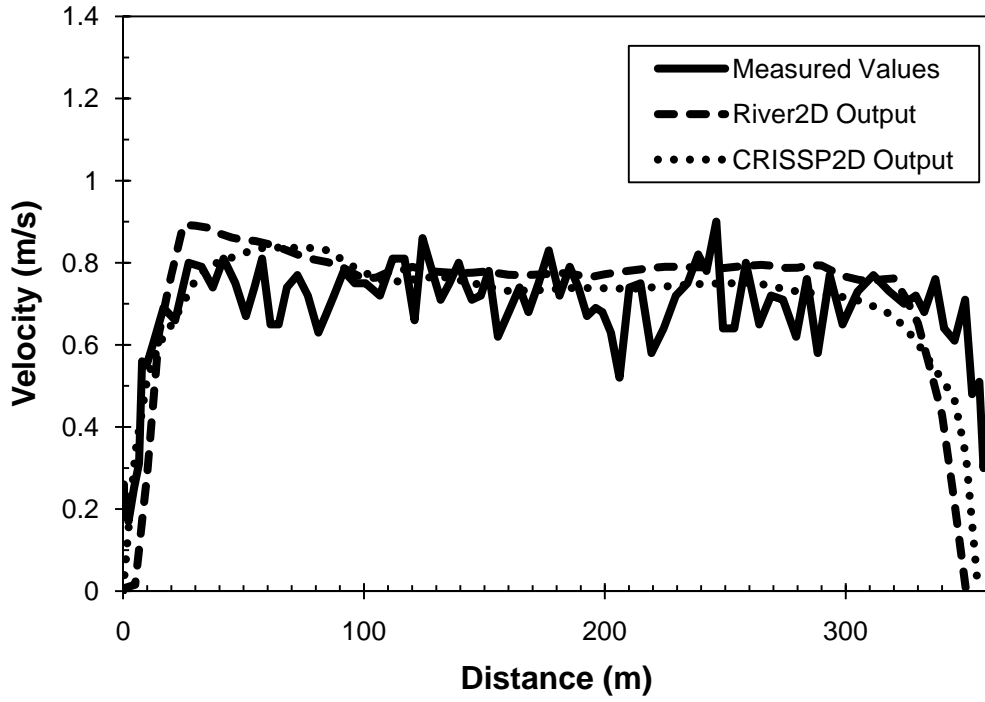


Figure 3.11. Water surface elevation profiles for *River2D* and *CRISSP2D*.

a)



b)

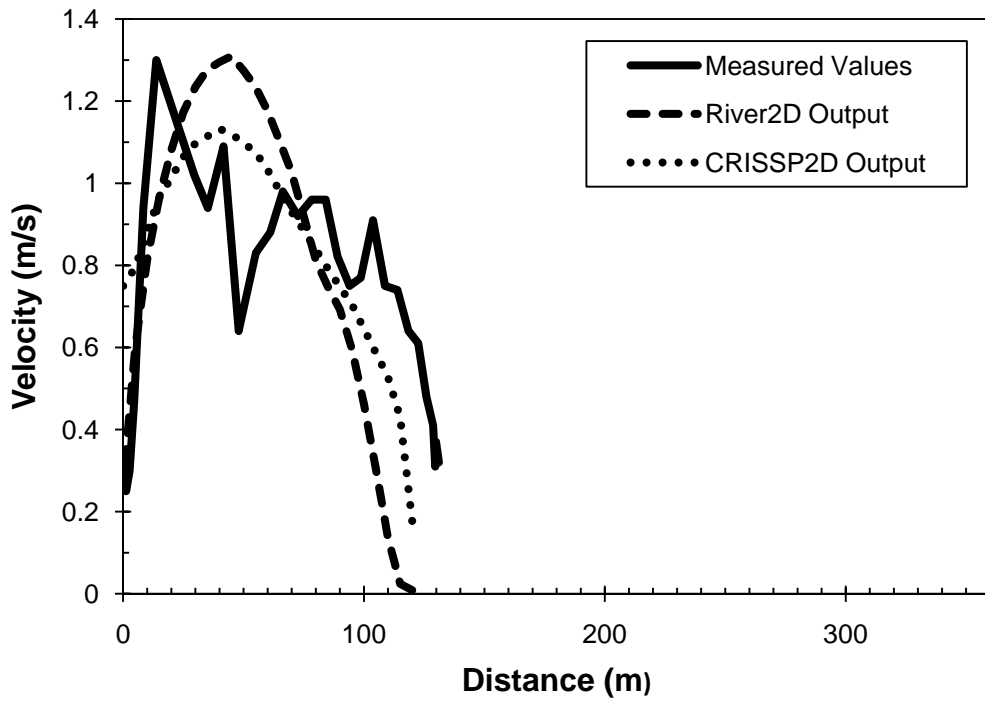
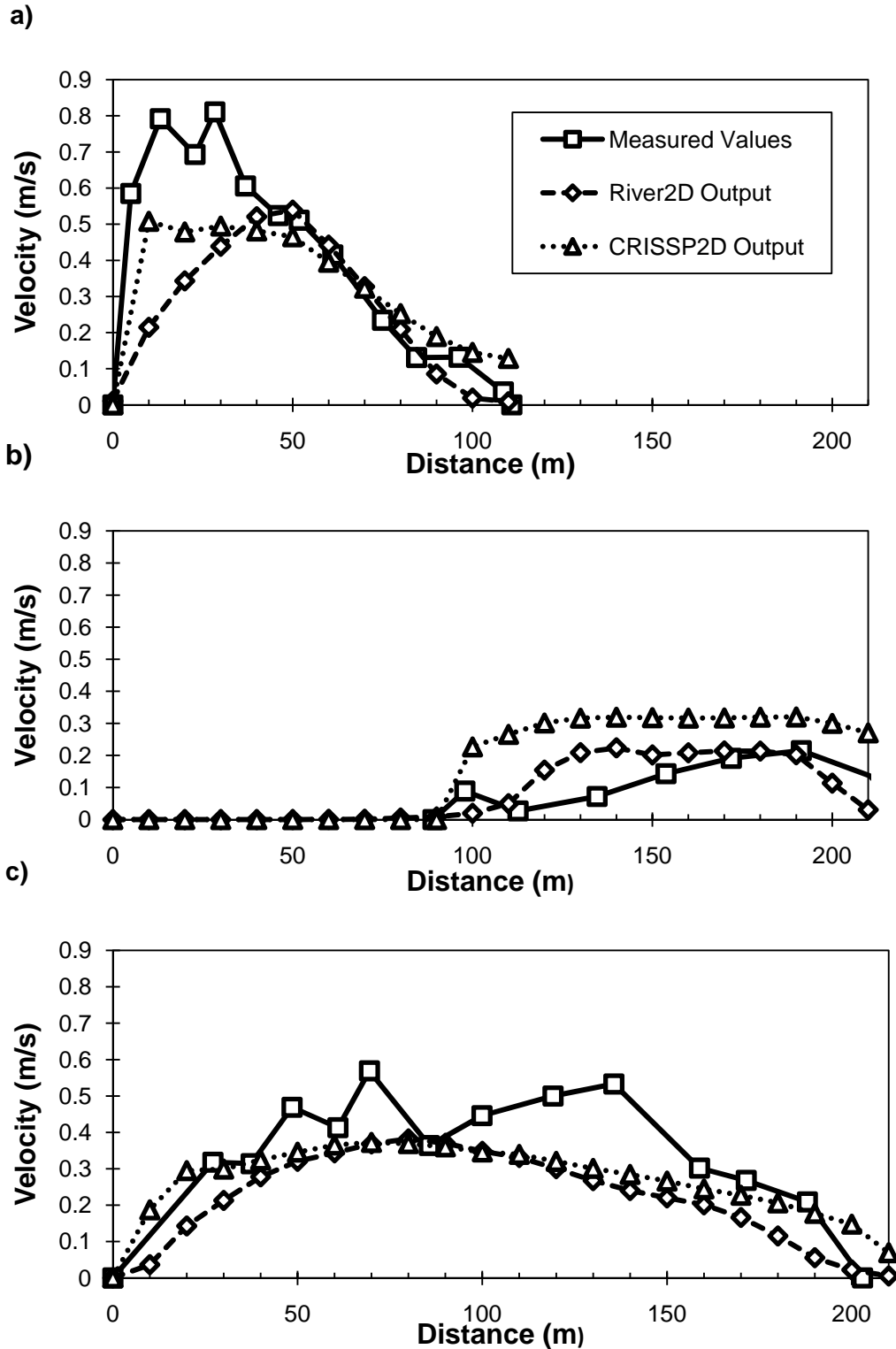


Figure 3.12. Velocity comparisons for open water conditions surveyed in July 2008 (a) Site 2 and (b) Site 3.



**Figure 3.13. Velocity comparisons for ice covered conditions surveyed in February 2009 (a) Site 3, (b) Site 4 and (c) Site 5.**

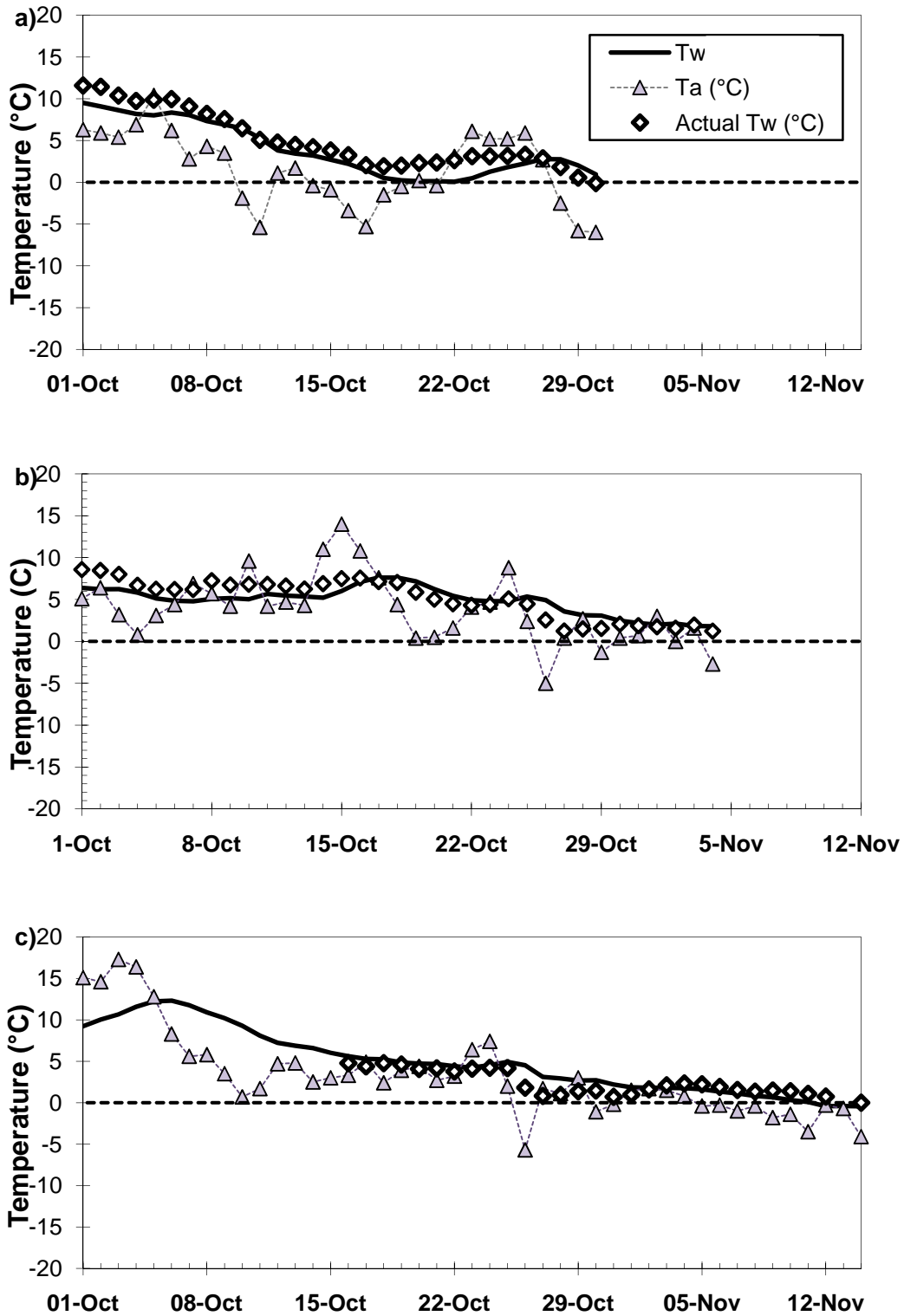
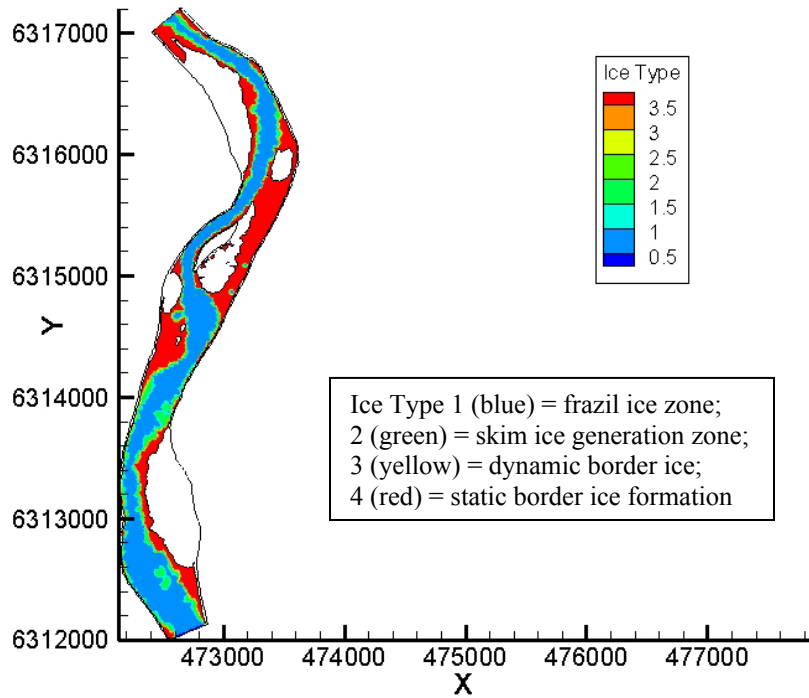
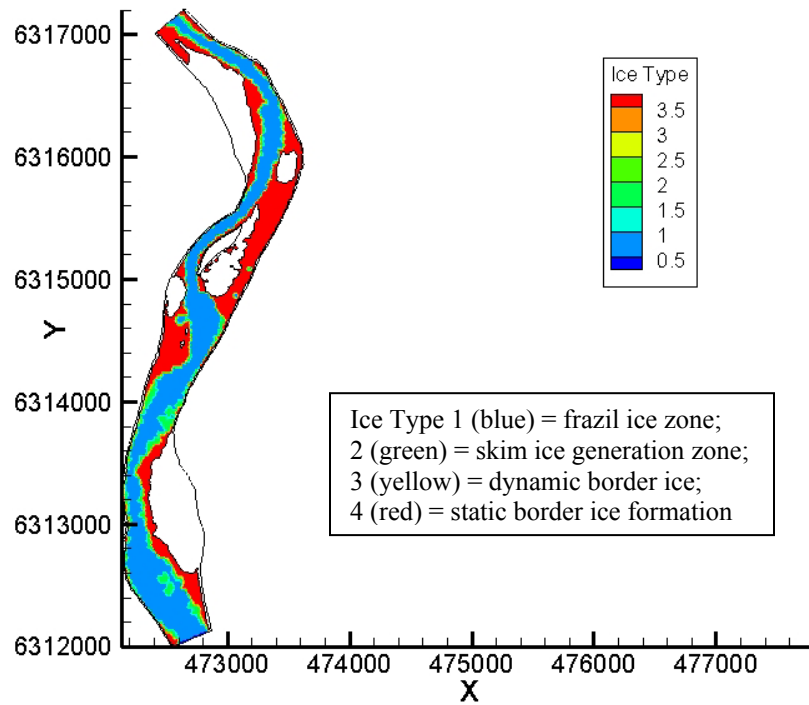


Figure 3.14. Air and water temperatures for the Athabasca River at Fort McMurray,  $h_{wa}=10 \text{ W/m}^2/^\circ\text{C}$  (a) 2006, (b) 2007 and (c) 2008.



**Figure 3.15. Ice formation in the channel at 72 hours after ice pans with an ice concentration of 35% have been introduced using a coupling time step of 60 s ( $T_a = -30^\circ\text{C}$ ).**



**Figure 3.16. Ice formation in the channel at 72 hours after ice pans with an ice concentration of 35% have been introduced using a coupling time step of 5 s ( $T_a = -30^\circ\text{C}$ ).**

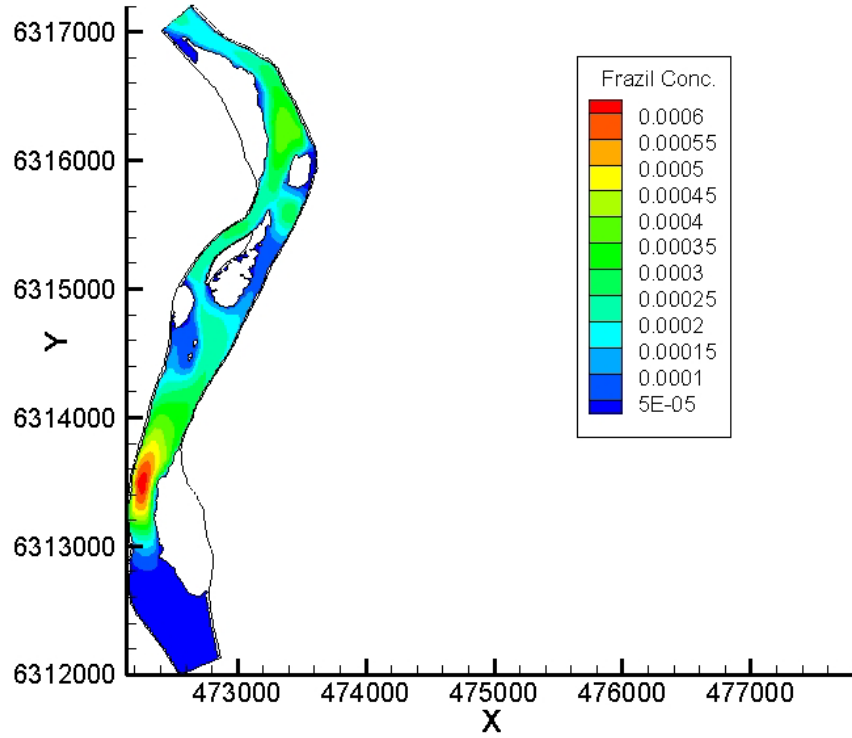


**Figure 3.17. Frazil concentration present in channel when initial water temperature is set to 0°C.**

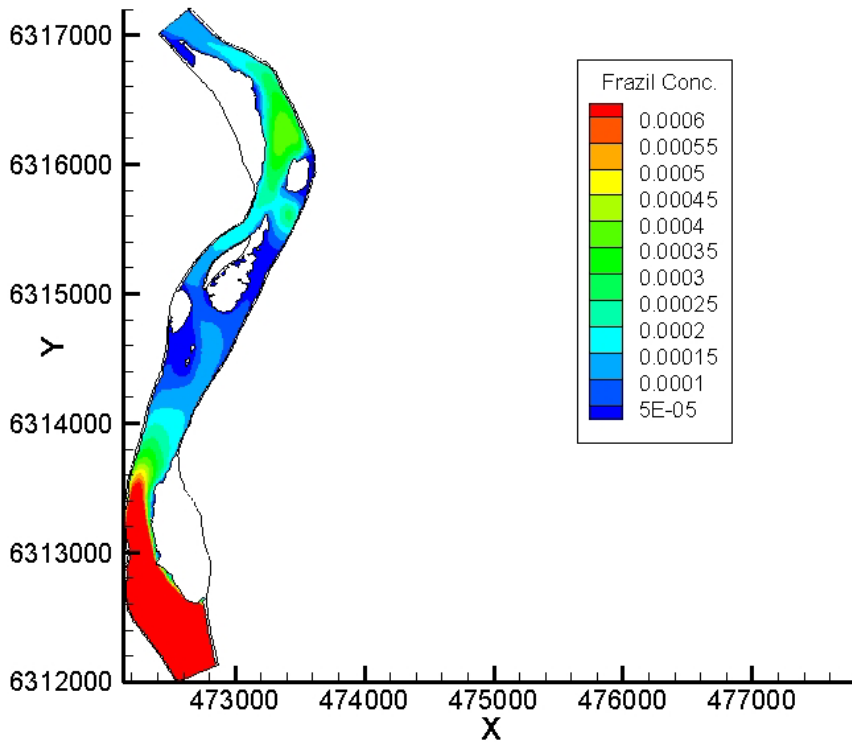


**Figure 3.18. Frazil concentration present in channel when initial water temperature is set to -0.1°C.**

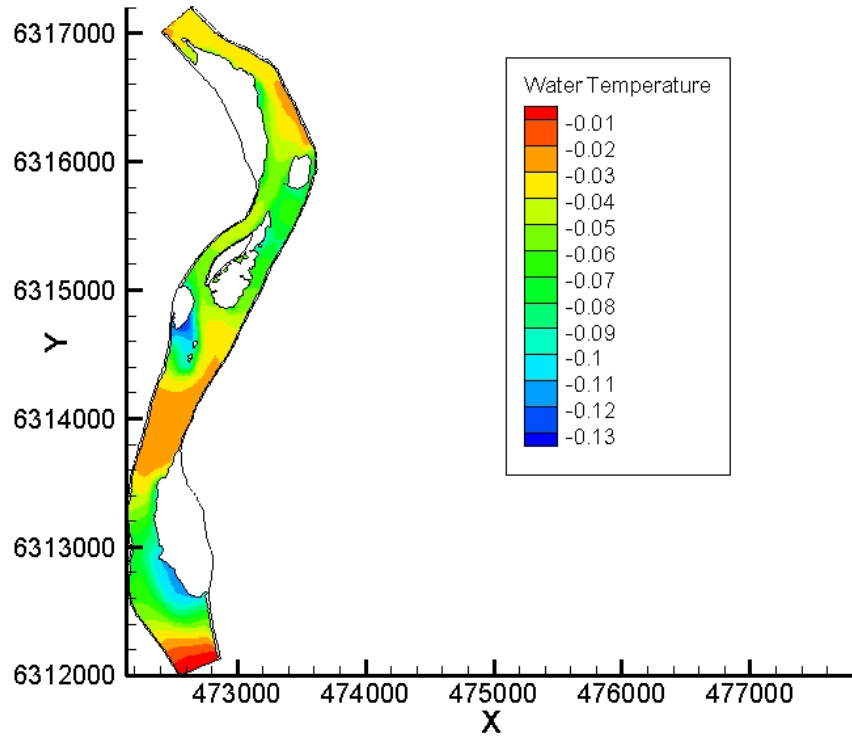


**Figure 3.19. Water temperature throughout the channel when initial water temperature is set to 0°C.**

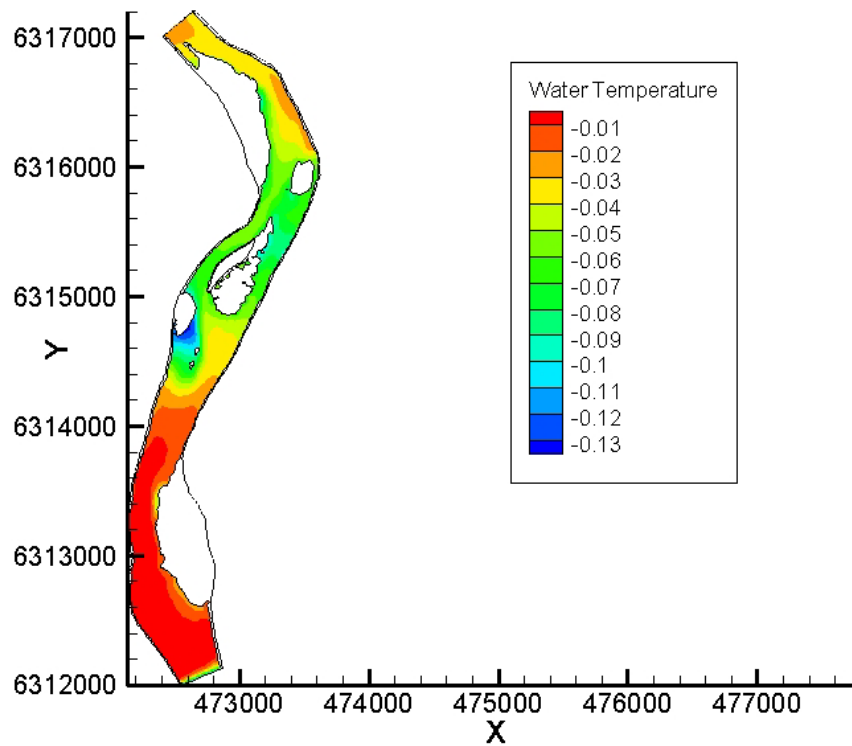


**Figure 3.20. Water temperature throughout the channel when initial water temperature is set to -0.1°C.**

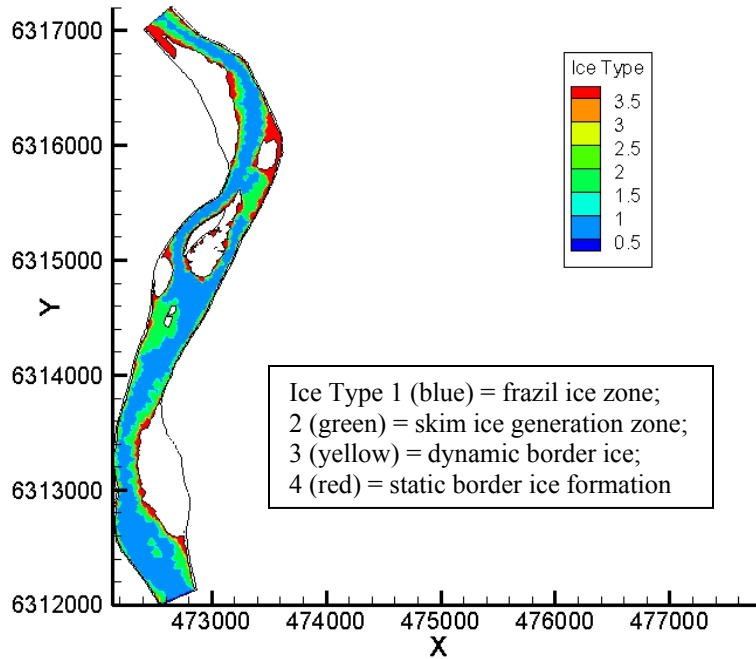


**Figure 3.21. Ice formation in the channel at 65 hours after ice pans with an ice concentration of 35% have been introduced with the critical velocity above which skim ice will not form set to 0.25 m/s ( $T_a = -30^\circ\text{C}$ ).**

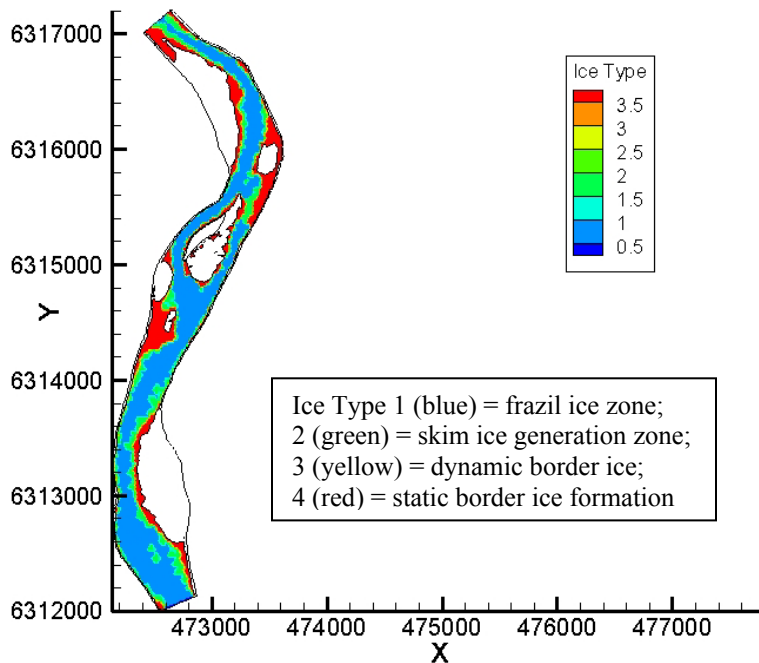


**Figure 3.22. Ice formation in the channel at 65 hours after ice pans with an ice concentration of 35% have been introduced with the critical velocity above which skim ice will not form set to 0.30 m/s ( $T_a = -30^\circ\text{C}$ ).**

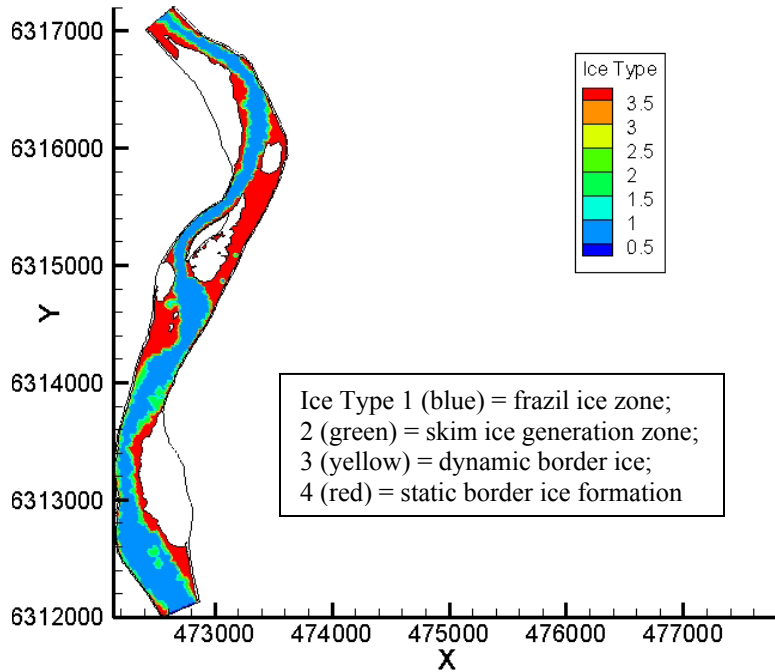


**Figure 3.23. Ice formation in the channel at 65 hours after ice pans with an ice concentration of 35% have been introduced with the critical velocity above which skim ice will not form set to 0.35 m/s ( $T_a = -30^\circ\text{C}$ ).**

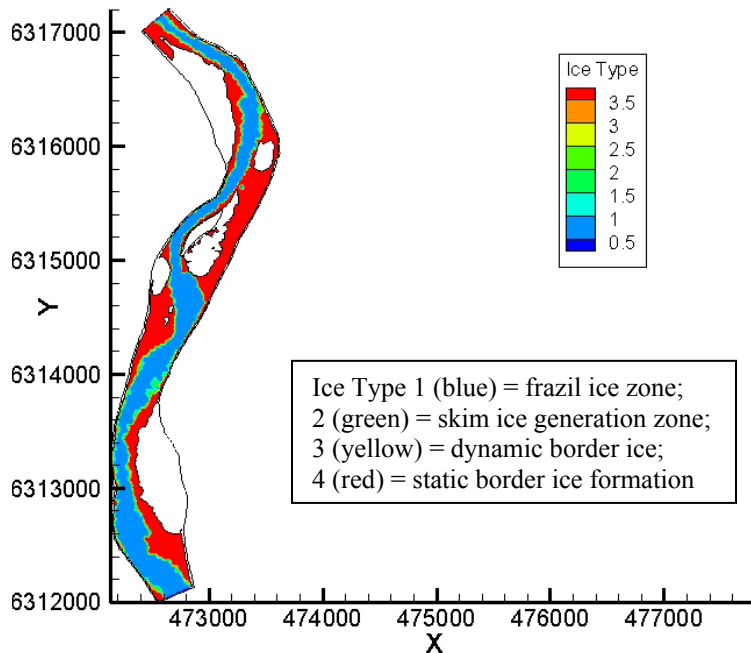


**Figure 3.24. Ice formation in the channel at 65 hours after ice pans with an ice concentration of 35% have been introduced with the critical velocity above which skim ice will not form set to 0.40 m/s ( $T_a = -30^\circ\text{C}$ ).**

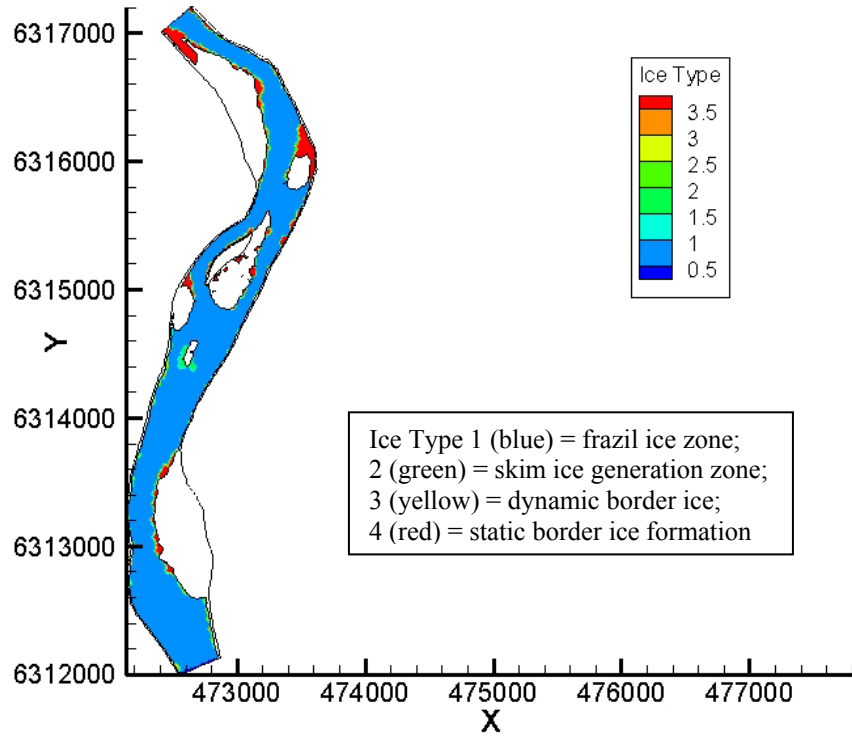


**Figure 3.25. Ice formation in the channel with the coefficient of heat flux for water to air set to  $10 \text{ W/m}^2/\text{°C}$  ( $T_a \sim$  of  $-5\text{°C}$  for 56 hours).**

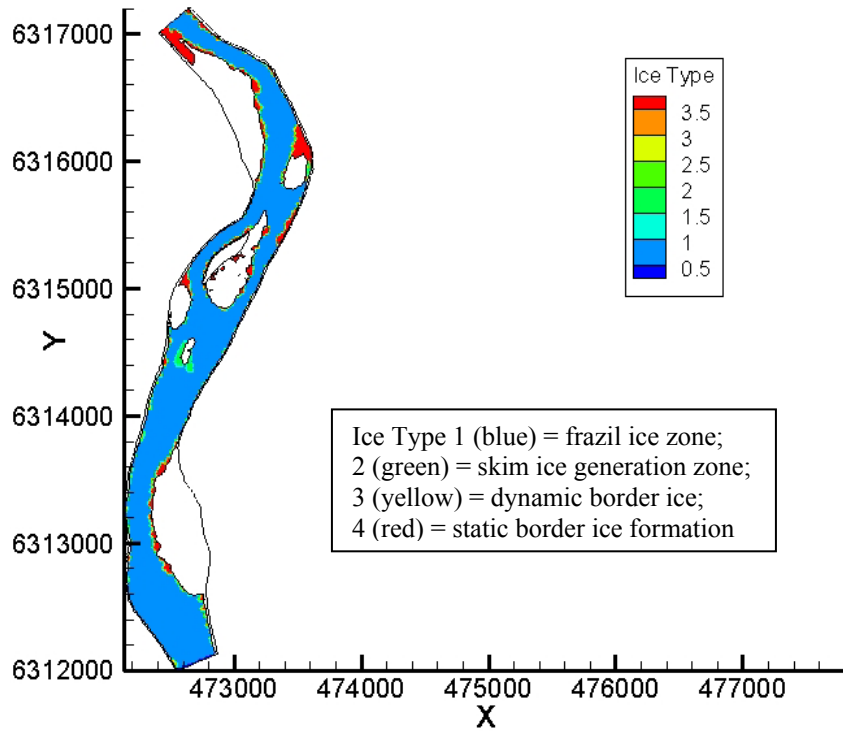


**Figure 3.26. Ice formation in the channel with the coefficient of heat flux for water to air set to  $15 \text{ W/m}^2/\text{°C}$  ( $T_a \sim$  of  $-5\text{°C}$  for 56 hours).**

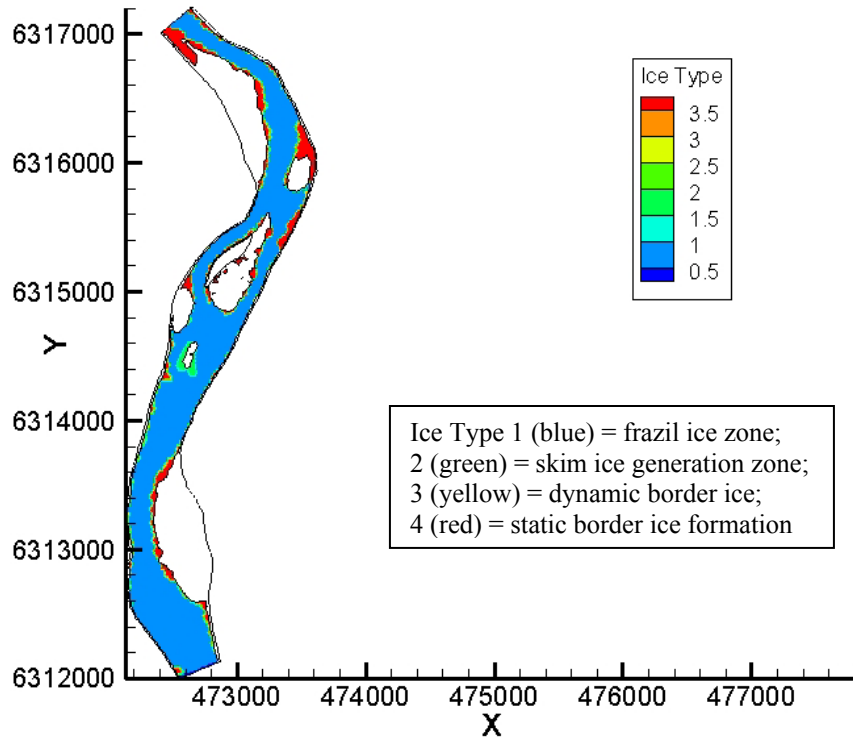


**Figure 3.27. Ice formation in the channel with the coefficient of heat flux for water to air set to  $20 \text{ W/m}^2/\text{°C}$  ( $T_a \sim$  of  $-5^\circ\text{C}$  for 56 hours).**

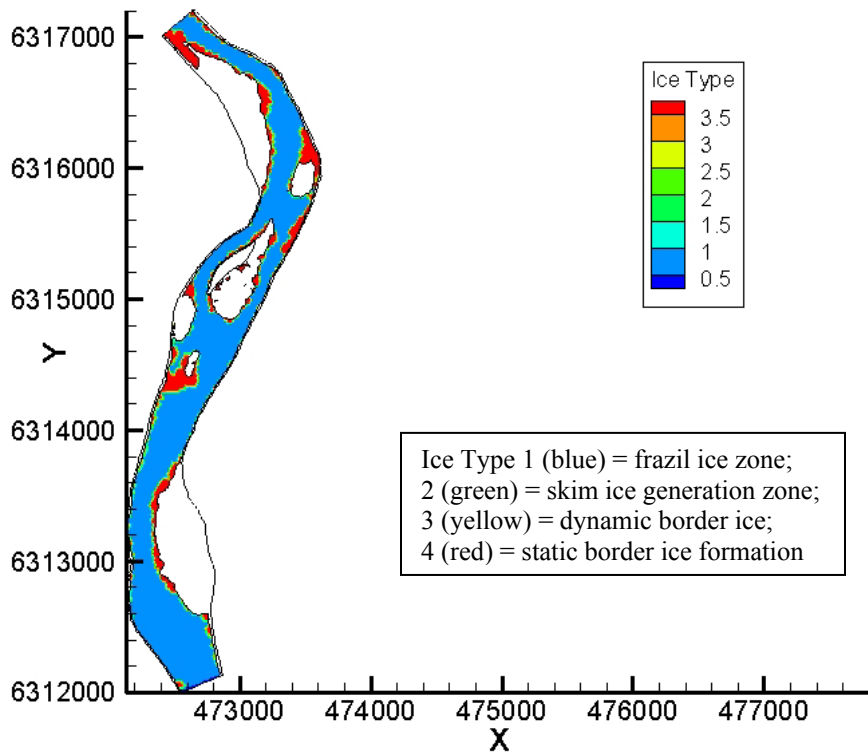


**Figure 3.28. Ice formation in the channel with the coefficient of heat flux for water to air set to  $25 \text{ W/m}^2/\text{°C}$  ( $T_a \sim$  of  $-5^\circ\text{C}$  for 56 hours).**

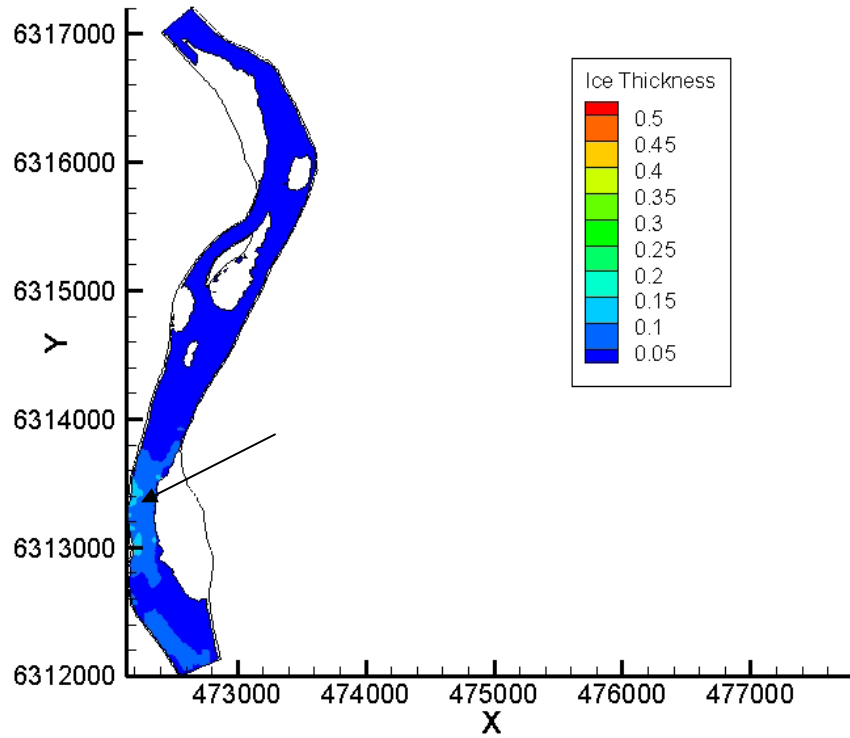


**Figure 3.29. Ice thickness in the channel at 1 hour after ice pans with an ice concentration of 5% have been introduced.**

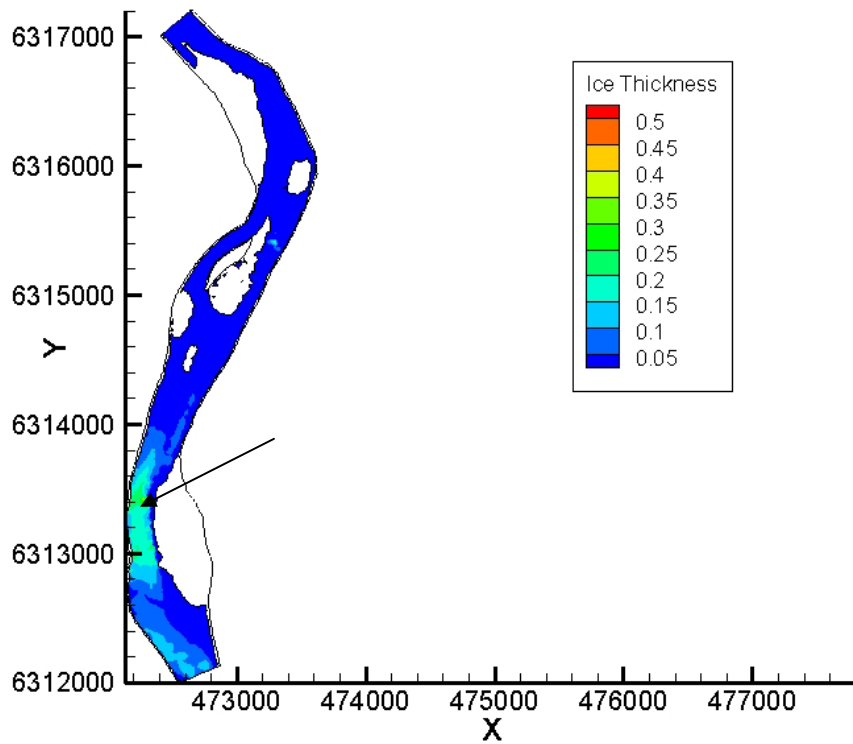


**Figure 3.30. Ice thickness in the channel at 1 hour after ice pans with an ice concentration of 35% have been introduced.**

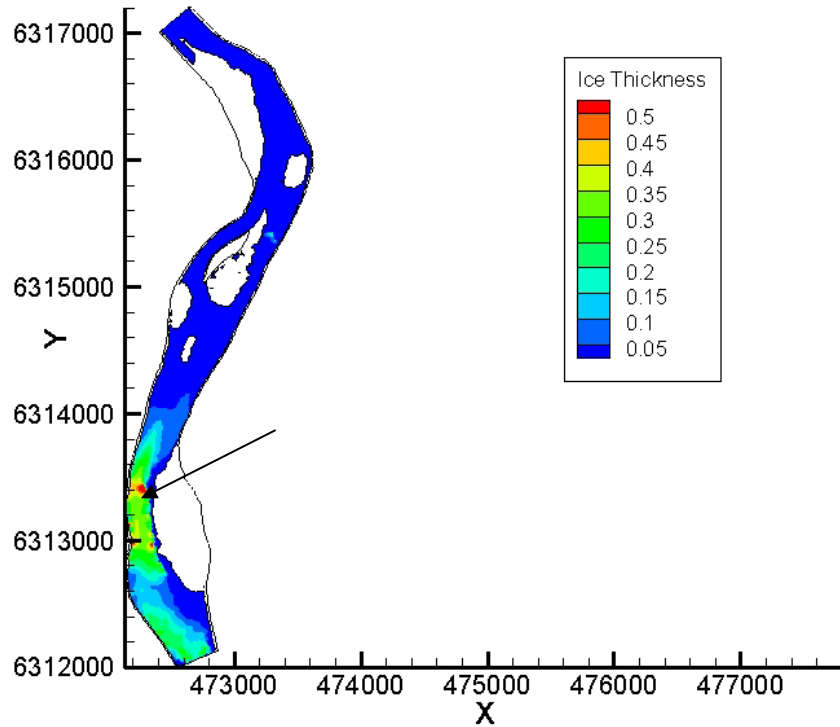


**Figure 3.31. Ice thickness in the channel at 1 hour after ice pans with an ice concentration of 70% have been introduced.**

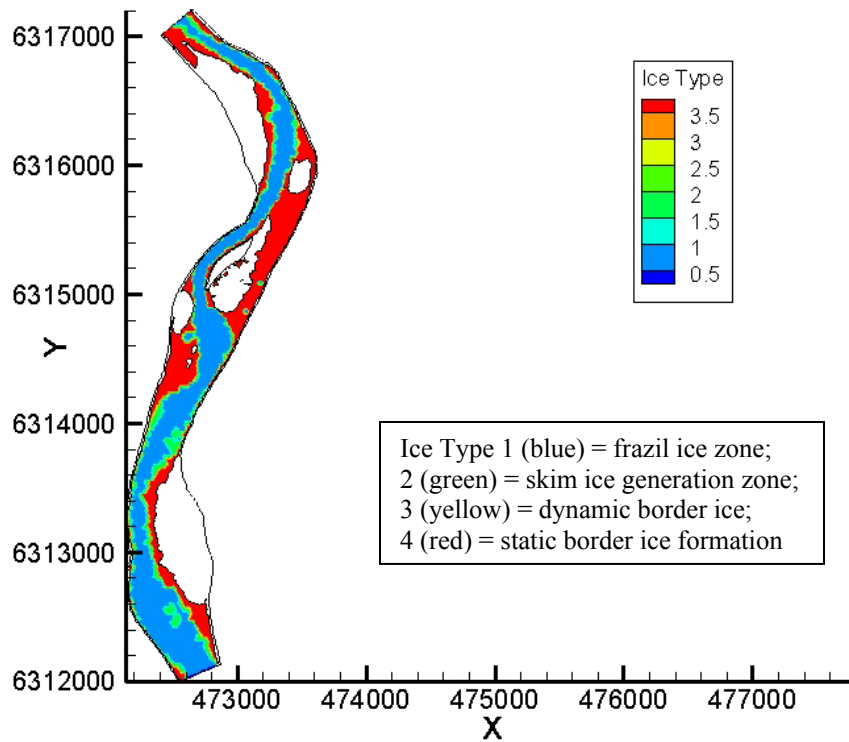


**Figure 3.32. Ice formation in the channel at 30 hours after ice pans with an ice concentration of 35% have been introduced ( $T_a = -30^\circ\text{C}$ ).**

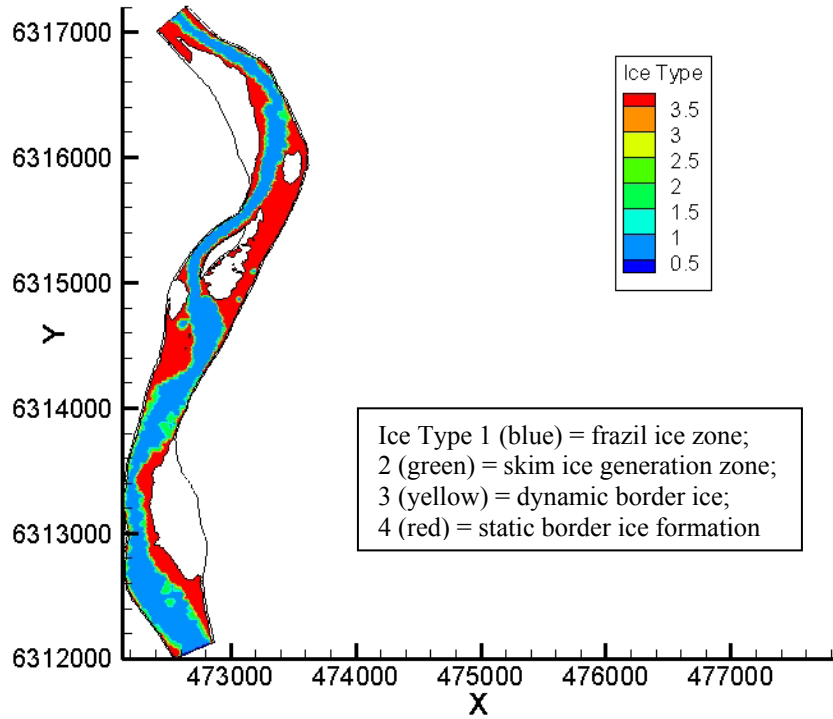


**Figure 3.33. Ice formation in the channel at 30 hours after ice pans with an ice concentration of 70% have been introduced ( $T_a = -30^\circ\text{C}$ ).**

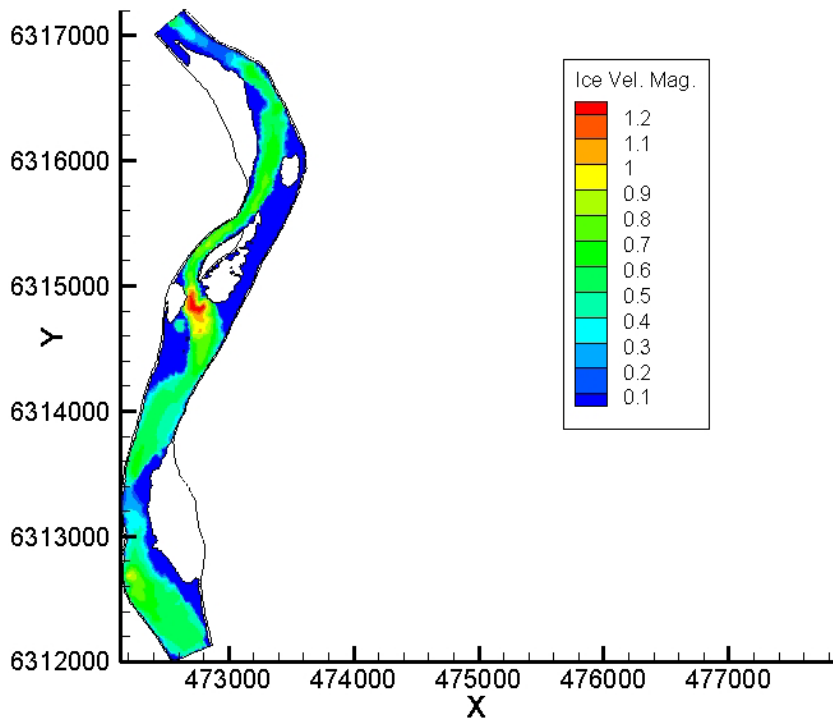


**Figure 3.34. Ice velocity magnitude in the channel at 30 hours after ice pans with an ice concentration of 70% have been introduced ( $T_a = -30^\circ\text{C}$ ).**

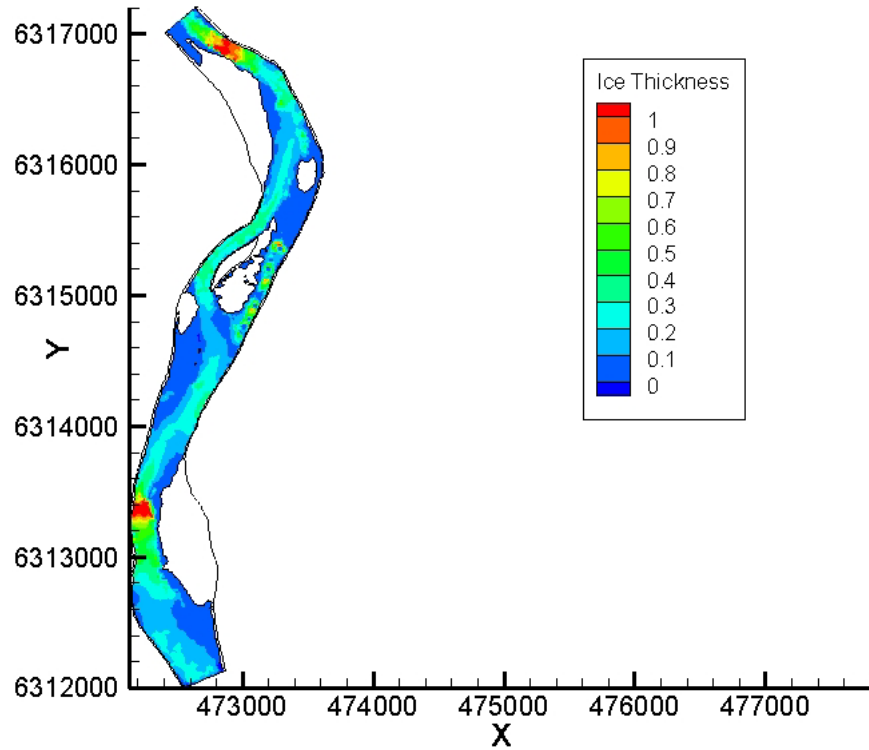


Figure 3.35. Ice thickness in the channel at 30 hours after ice pans with an ice concentration of 70% have been introduced ( $T_a = -30^\circ\text{C}$ ).

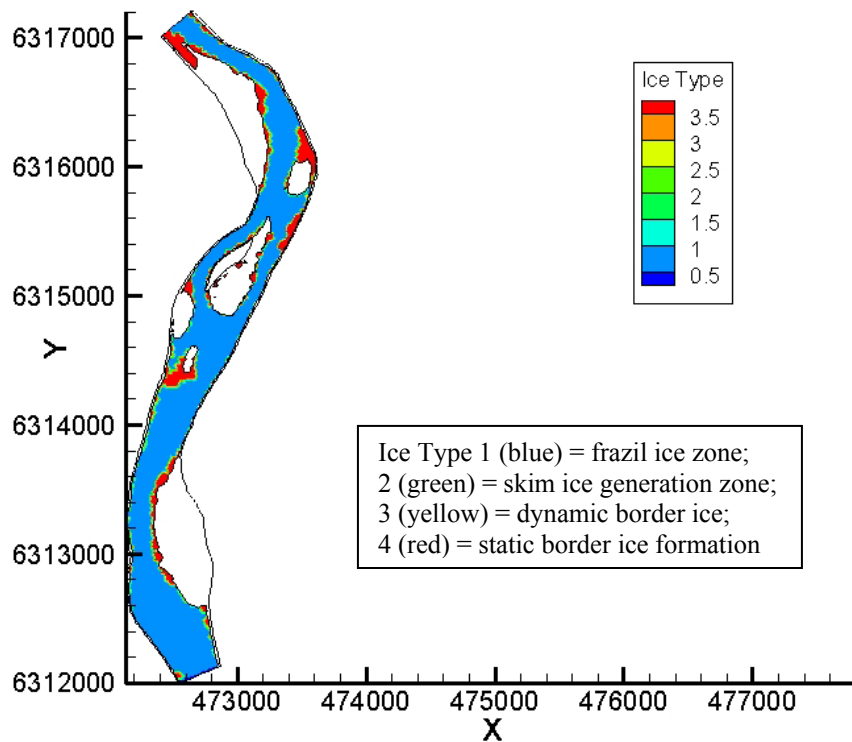


Figure 3.36. Ice formation on the Athabasca River after 12 hours.

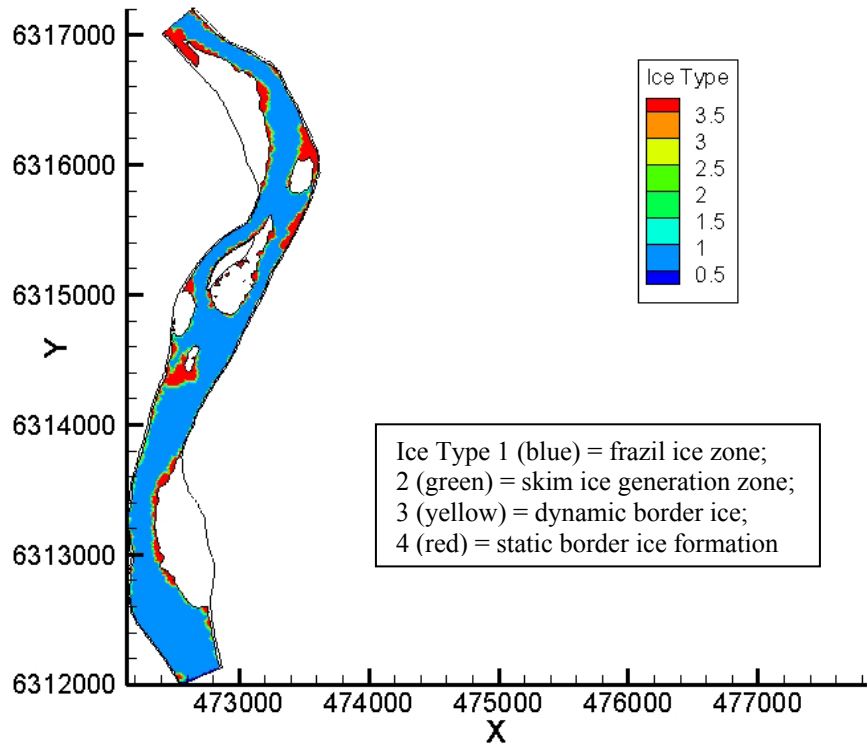


Figure 3.37. Modeled ice formation on the Athabasca River after 24 hours.

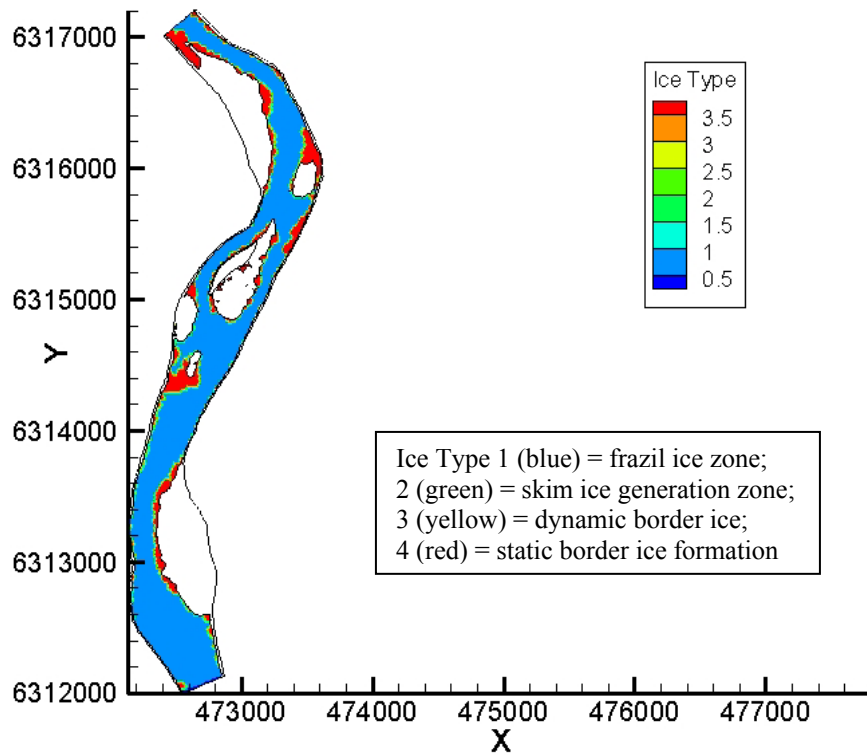


Figure 3.38. Modeled ice formation on the Athabasca River after 36 hours.

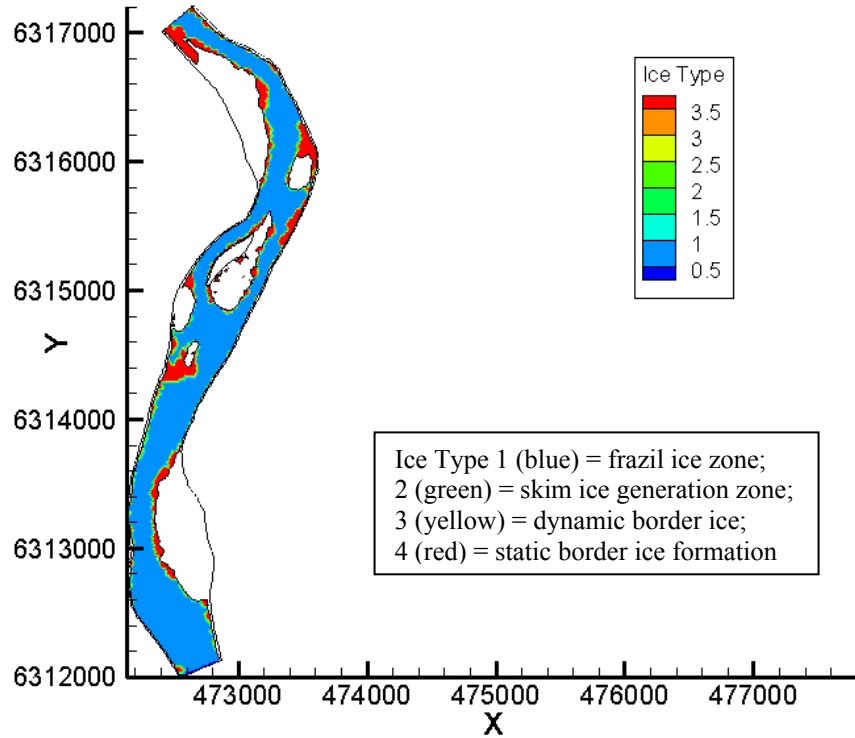


Figure 3.39. Modeled ice formation on the Athabasca River after 48 hours.

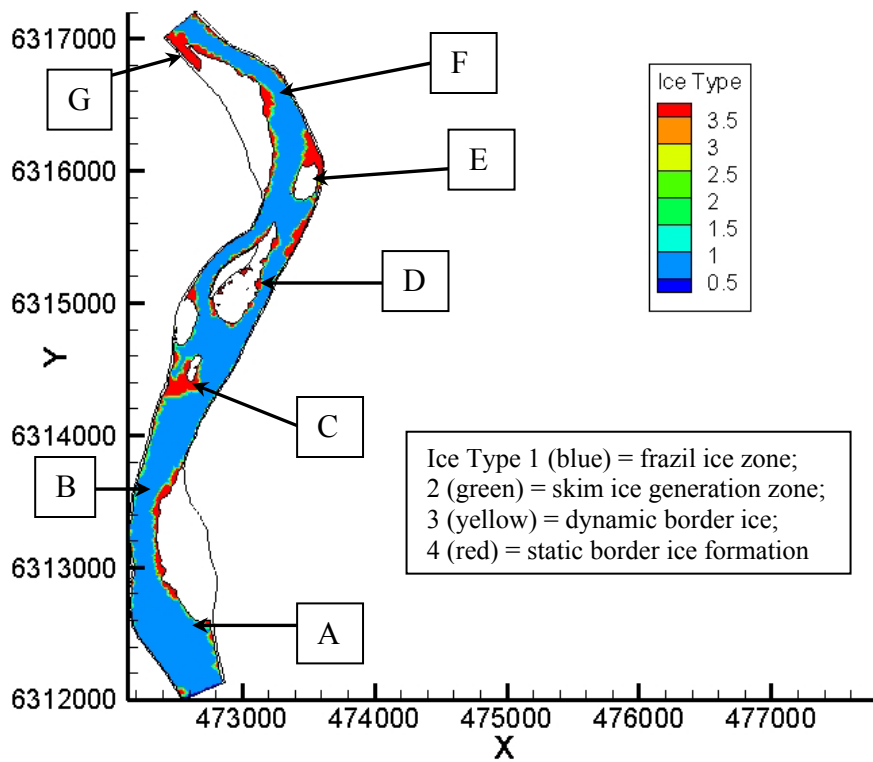


Figure 3.40. Modeled ice formation on the Athabasca River after 60 hours.

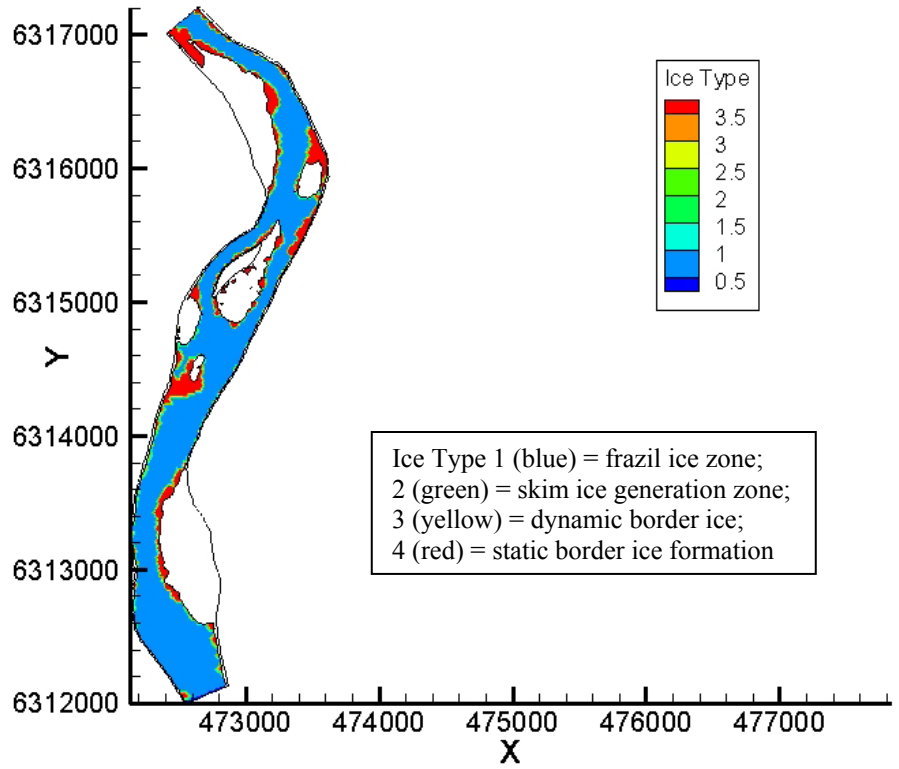


Figure 3.41. Modeled ice formation on the Athabasca River after 72 hours.

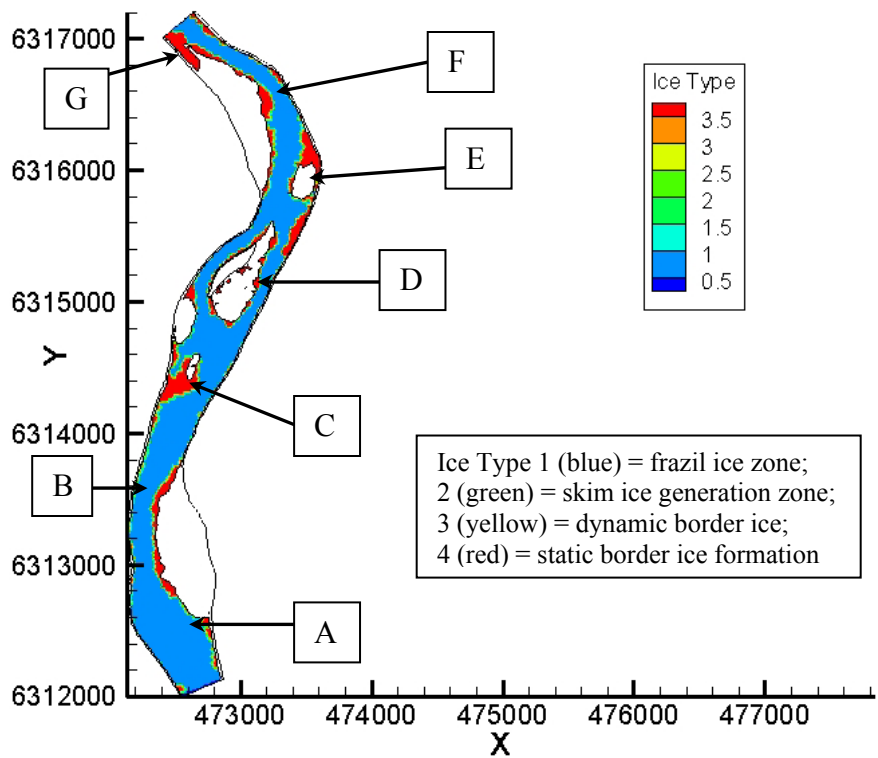
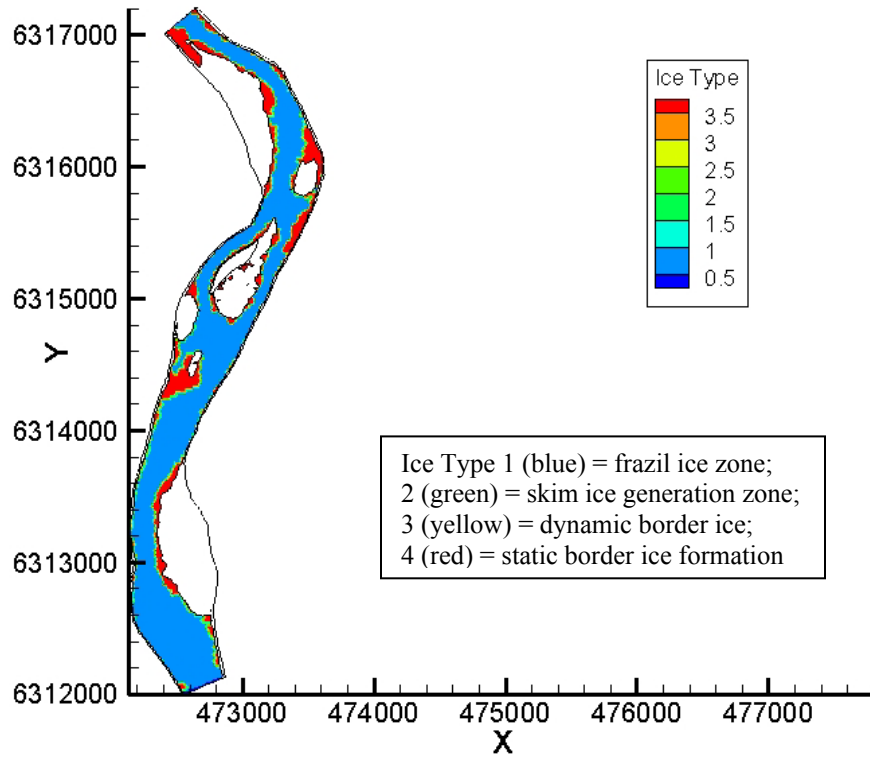
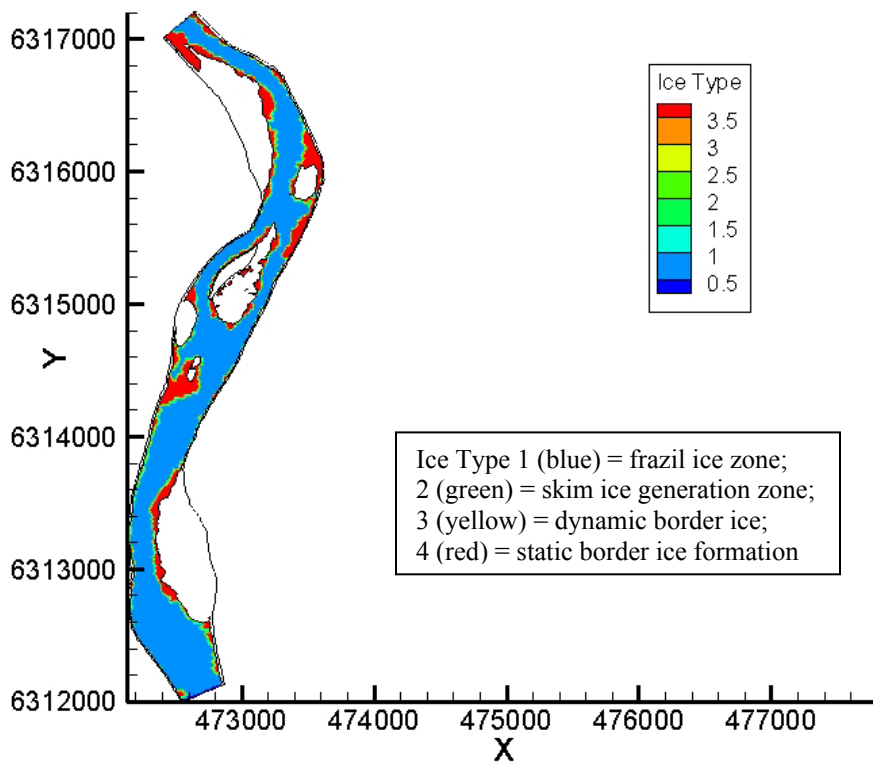


Figure 3.42. Modeled ice formation on the Athabasca River after 84 hours.



**Figure 3.43. Modeled ice formation on the Athabasca River after 96 hours.**



**Figure 3.44. Modeled ice formation on the Athabasca River after 108 hours.**

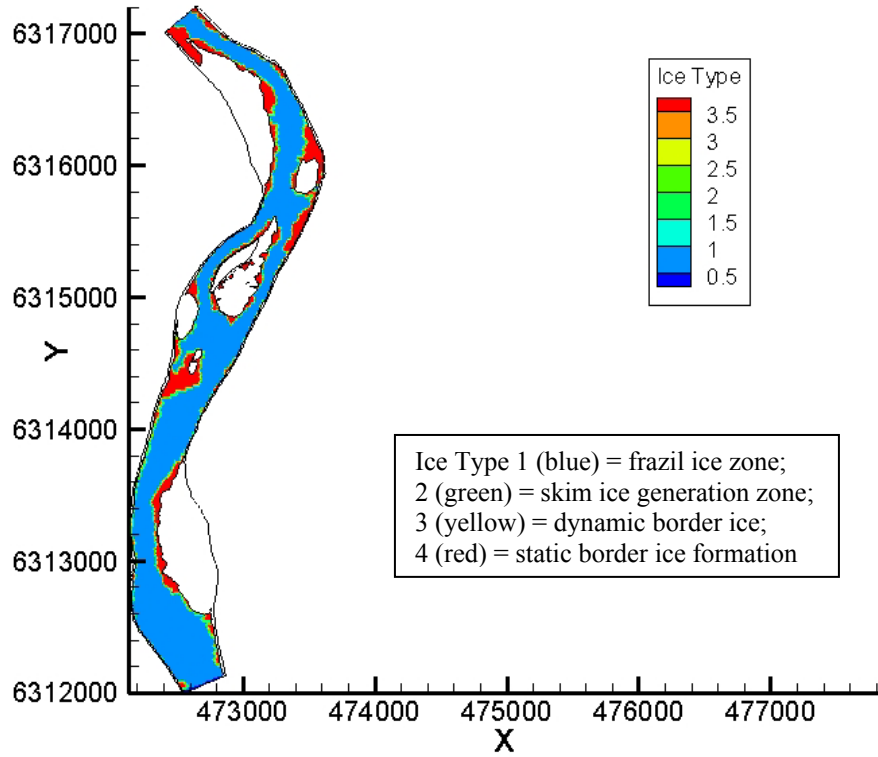


**Figure 3.45. Modeled ice formation on the Athabasca River after 120 hours.**

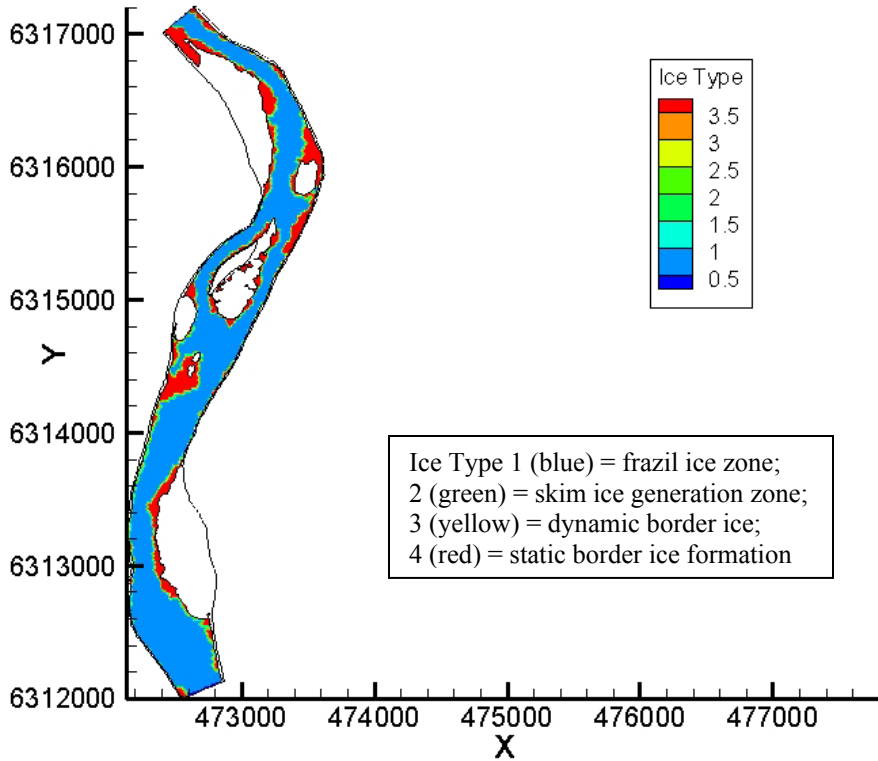


**Figure 3.46. Modeled ice formation on the Athabasca River after 132 hours.**

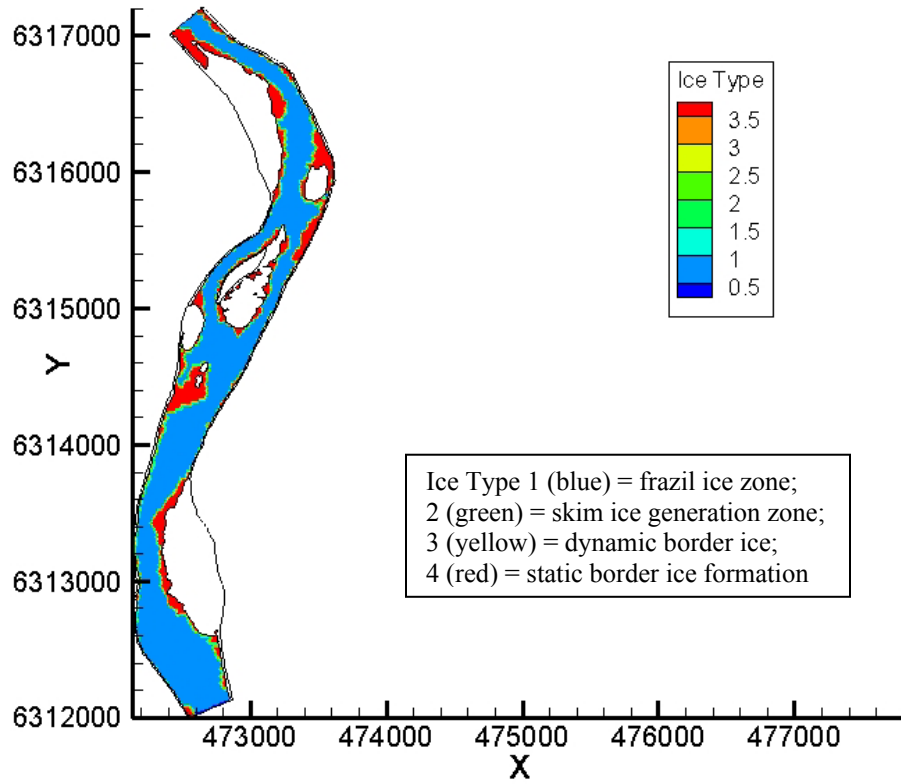


**Figure 3.47. Modeled ice formation on the Athabasca River after 144 hours.**

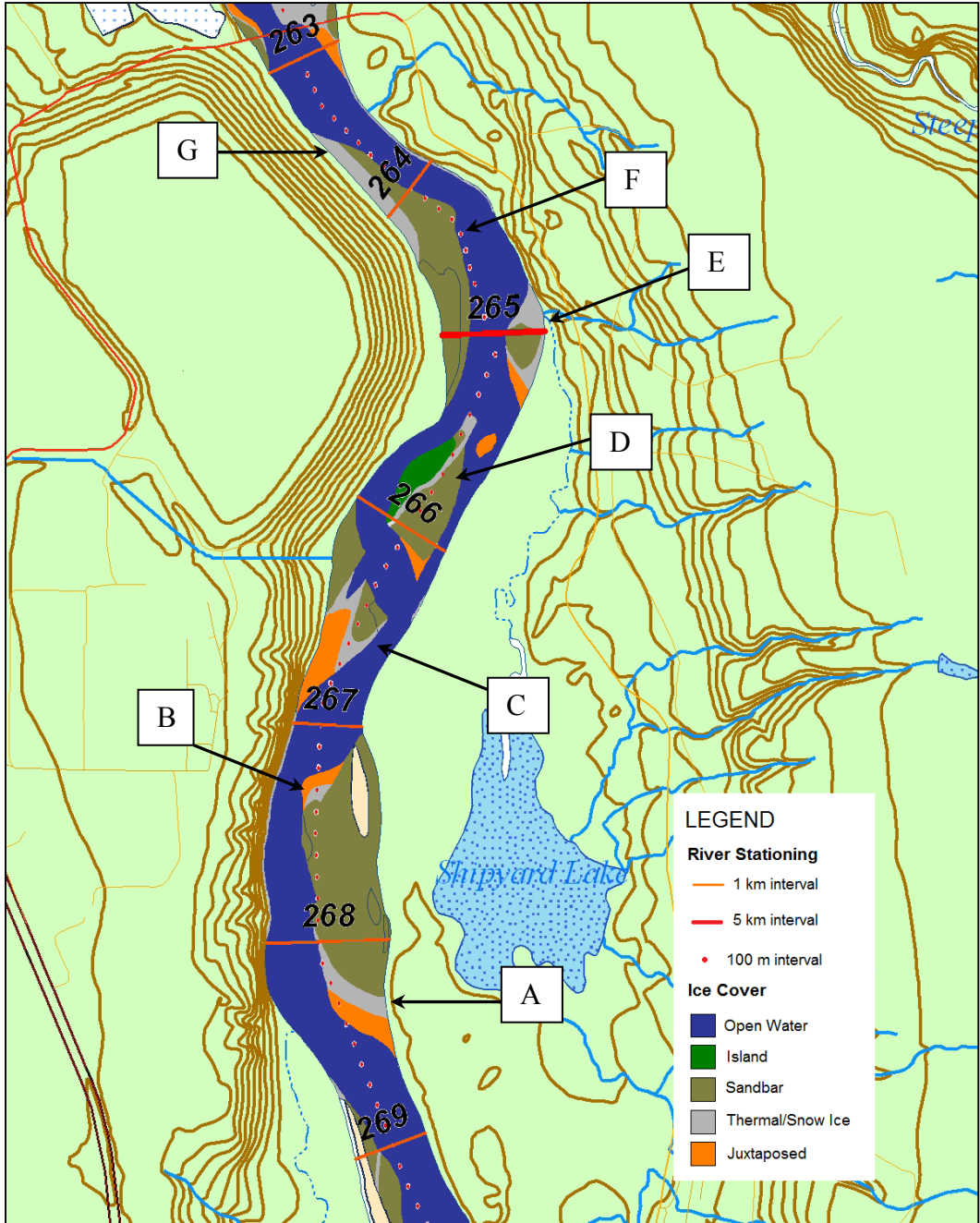


**Figure 3.48. Annotated ice map based on field observations made on November 16, 2008.**

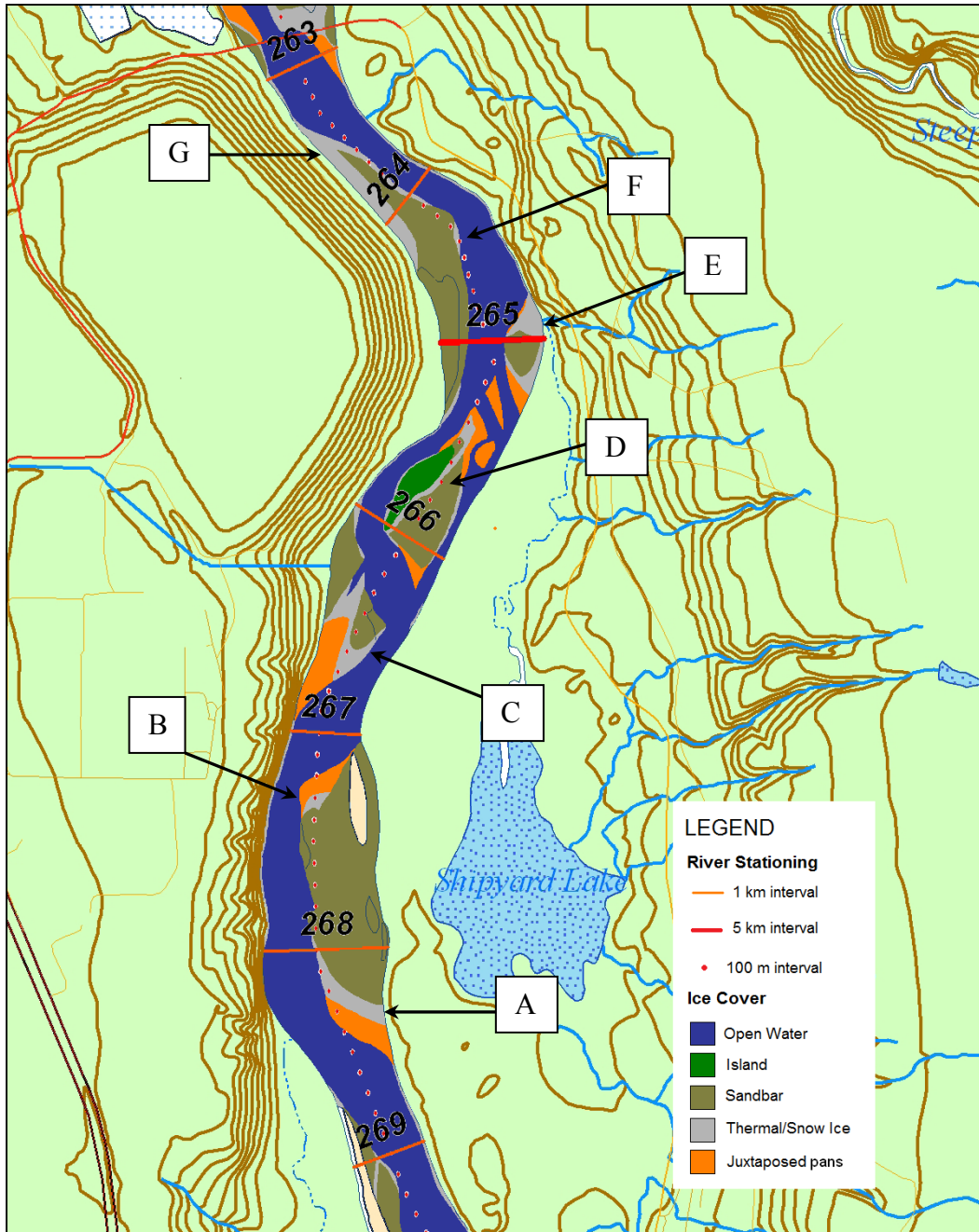


**Figure 3.49. Annotated ice map based on field observations made on November 17, 2008.**

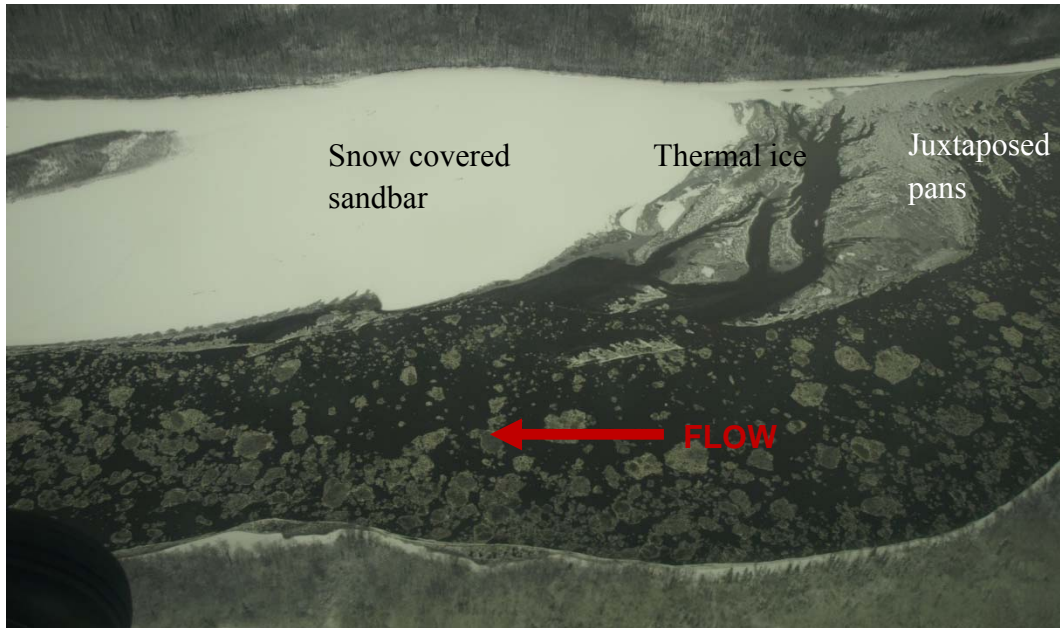


**Figure 3.50. Aerial photograph of Site A, view from west to east, November 17, 2008.**

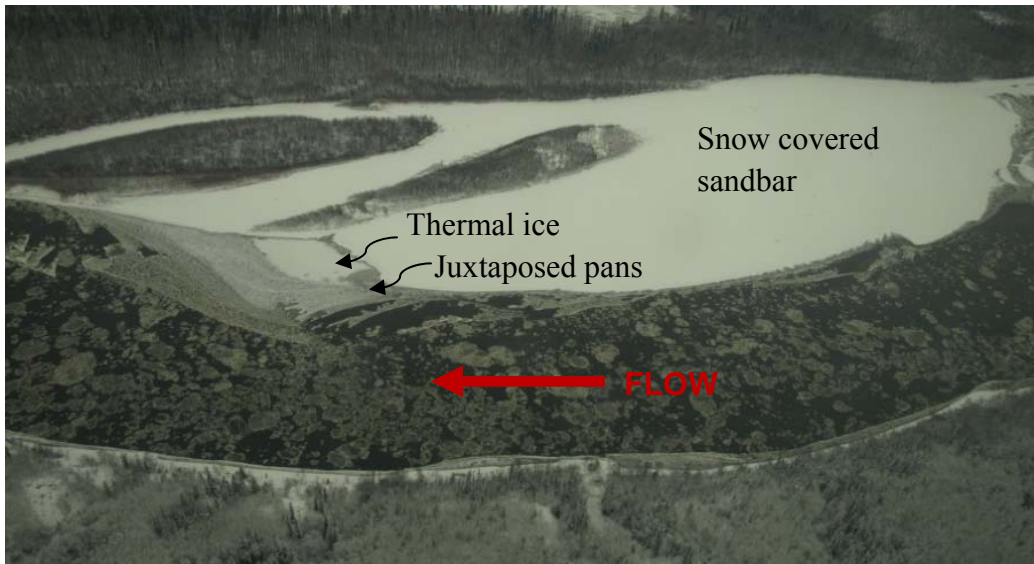


**Figure 3.51. Aerial photograph of Site B, view from west to east, November 17, 2008.**



**Figure 3.52. Aerial photograph of Site C, view northeast, November 17, 2008.**

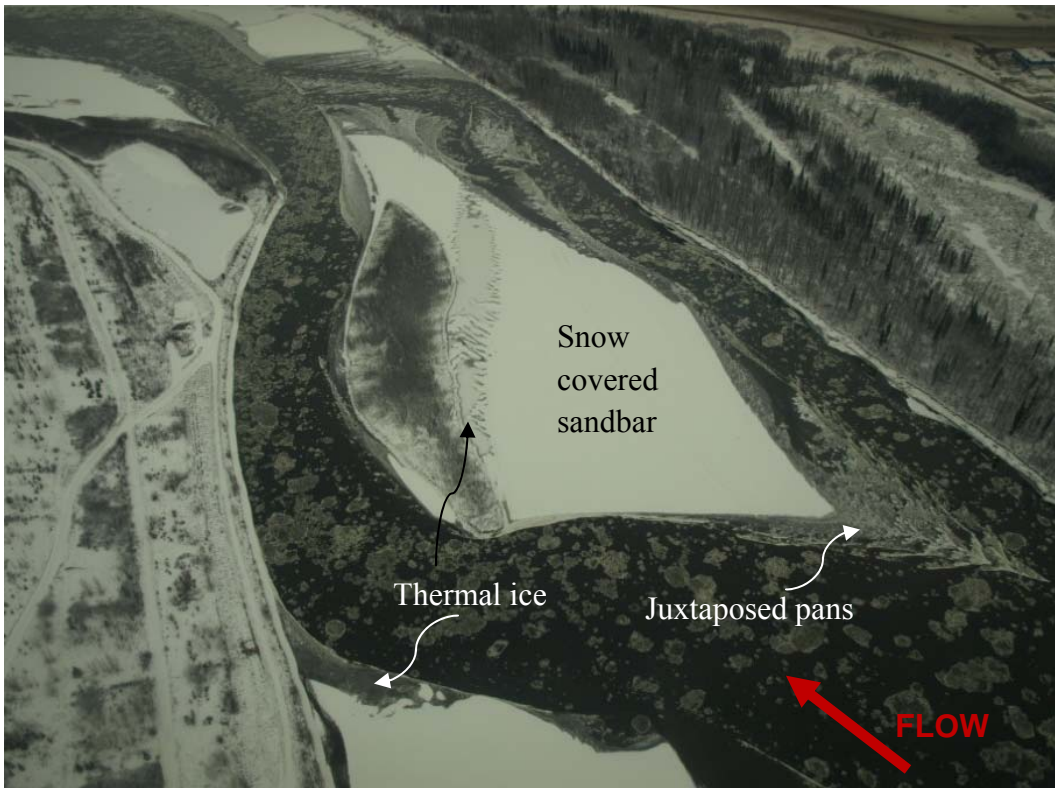


**Figure 3.53. Aerial photograph of Site D, view north, November 17, 2008.**

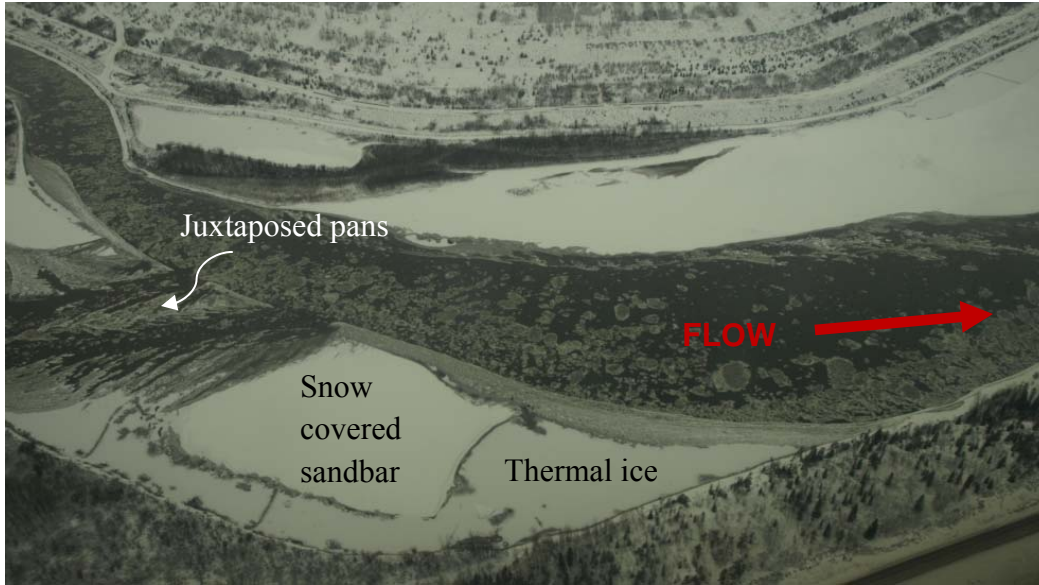


**Figure 3.54. Aerial photograph of Site E, view from east to west, November 17, 2008.**

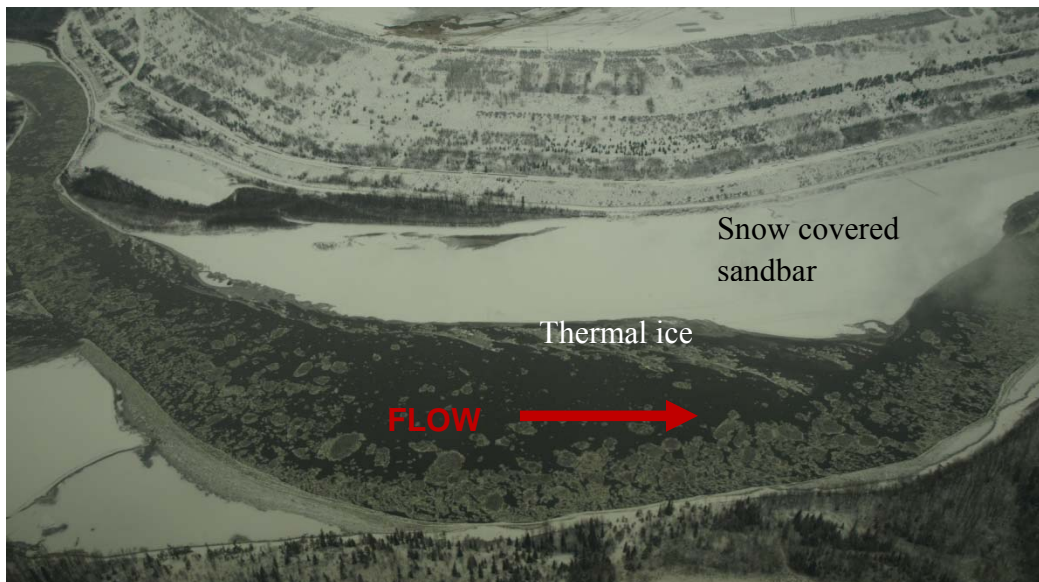


**Figure 3.55. Aerial photograph of Site F, view from east to west, November 17, 2008.**



**Figure 3.56. Aerial photograph of Site G, view south, November 17, 2008.**

#### **4. Summary and Recommendations**

This study is part of a three year project aimed to assess the effects of winter water withdrawals on the ice regime on the lower Athabasca River. The issue of adequate water supply on the Athabasca River arises as the demand for it increases due to the growing needs of various industrial projects. While various organizations are assessing the potential implications of water demand on the ecology of the area, one significant outstanding question involves the issue of river ice. This study was developed in order to further explore this topic through the application of a numerical model.

In order to obtain data for the numerical model, field work was carried out. Freeze-up monitoring was conducted along 80 km of the Athabasca River from Fort McMurray to Bitumont in the fall of 2007. Based on observations made that year and the previous year, a 5 km sub-reach was found that encompassed an area that experienced a full range of ice cover initiation processes. In 2008, a rigorous field program was conducted that included detailed bathymetric and water level surveys as well as discharge measurements in the summer, freeze-up monitoring in late fall and ice surveys in the winter.

In the summer of 2008, detailed bathymetric survey data was collected, water levels were surveyed and discharge measurements were carried out in the 5-km detailed reach. There was some difficulty in obtaining discharge measurements with an ADCP as sections of very shallow and deep water were encountered. A recommendation for a future study would be to use instruments that have a greater range of measurement to avoid such problems. Despite these issues, it was found that overall results were 10% those recorded at the WSC gauge station 07DA001 (Athabasca River below Fort McMurray). Discharge measurements carried out around the island showed that the flow split caused approximately 60% of the water to flow on the left side and 40% on the right side. Results from the surveys were used to create the geometry for a 2-D model. Water level data and discharge measurements were useful in calibration and validation of the model for open water conditions.

In the fall of 2007 and 2008, freeze-up monitoring was conducted, which included obtaining photographs from both remote camera stations and aerial flights, measuring water temperature, and obtaining air temperature data. Data collected was used to create ice cover maps as well as determine ice concentrations along the reach. In 2007, the freeze-up process was very similar to that in 2006 (Abarca, 2007). Bridging points were created in the same area, approximately 2 km upstream of the Suncor Bridge, and a juxtaposed ice cover formed upstream of these points with the remainder of the ice cover freezing thermally. In 2008, freeze-up occurred in a similar way than the two year prior; however, the bridging spot in this year was located at the Suncor Bridge. Discharges and air temperatures were very similar in both years, thus bedform movements were the likely cause of this change. This idea presents a great challenge for the modeling of sand bed rivers. Since bed movement can be frequent, multiple surveys would need to be conducted throughout the year in order to maintain accurate modeling data. This is neither practical nor feasible as conducting field work during freeze-up is very dangerous.

In the winter of 2009, detailed ice surveys were performed in the detailed 5 km reach. An ADV and an ADCP were used at the same sites in order to test out which piece of equipment was more effective for winter velocity and discharge measurements. The ADCP was more labor intensive to use; however, it provided the ability to view results in real-time. It was found that when velocities were in a low range, specifically below 0.3 m/s, the ADV consistently measured higher velocities than the ADCP. Both instruments displayed obvious error in measurement at several discrete points, highlighting the importance in taking multiple measurements at a site. The discharge measurements made in the winter were within 10% of those reported for the WSC gauge station 07DA001 (Athabasca River below Fort McMurray). Discharge measurements at the flow split showed that the majority of the water (80-90%) flowed in the left channel, while only approximately 10-20% of flow flowed in the right channel. It was not determined which piece of equipment was more effective than the other and further testing will need to be carried out to establish this. It is possible that one

instrument performs better in summer conditions while the other is best for winter conditions, so tests would need to be carried out at various times of the year.

The objectives of 2-D ice process modeling were to simulate the border ice formation, a bridging point and the formation of an ice cover. Using all of the data collected throughout the various field programs, a model of the Athabasca River study reach was set up using *River2D* and *CRISSP2D* and calibrated to observed conditions at the site. It was originally intended to use and compare both models; however, the ice process component of *River2D* was still under development at the time of writing the thesis; thus only *CRISSP2D* was used.

In order to select all of the appropriate parameters for the accurate modeling of freeze-up, a sensitivity analysis was performed. It was found that the key factors affecting border ice development were the critical velocity above which skim ice will not form,  $V_{CRSKM}$ , and the heat transfer coefficient between water and air,  $HWA$ . The parameter that did not affect the development of border ice was the critical velocity above which shore ice will not accumulate,  $V_{CRBOM}$ . Overall, it was found that the border ice formation patterns modeled agreed well with field observations. Since the domain length of a 2-D model is short in comparison with a 1-D model, there is no time in the reach to form, flocculate and float frazil to make pans. In this way, the amount of inflow surface ice concentration was nearly always the same as to the amount of surface ice concentration leaving the domain.

Once all of the parameters were selected to simulate border ice formation on the Athabasca River as accurately as possible, *CRISSP2D* was used to try to model a full ice cover formation. Unfortunately, this proved to be a major shortcoming of the model. The way in which a bridging point is created in *CRISSP2D* is through the use of a stopping velocity criterion. However, the model has a limit to the amount of parcel interactions possible in the domain and when this value is surpassed, the model fails. After various attempts, such as lowering the value of this parameter and increasing the ice parcel size, it was found that this error could

not be avoided. Without this critical step, the formation of an ice cover could not be simulated.

It is interesting to discuss the use of a stopping velocity as criterion for bridging. There are several problems that can be anticipated, even if this parameter were to stop the ice at a point. The first thing is that it would be very difficult to be able to accurately simulate the time frame in which an ice front progresses. While progression could be slowed down through the use of a smaller value for a stopping velocity criterion, this may not allow the user to have very good control over timing. Another potential problem is that once bridging is simulated and the ice front progresses upstream, the inflowing ice concentration may cause a jam to occur at the boundary, as was found in the simple case model. There would need to be a way for the program to acknowledge the formation of an ice cover and cut off the incoming ice parcel supply. A recommendation for a future study would be to use a boom to simulate an artificial bridging point and investigate how frontal progression occurs as well as the details of how an ice cover is formed. If this is successful, the model could be run over several weeks or months to see if ice thicknesses in the channel are similar to those measured in the field during the winter.

It was found that there were several other limitations to the *CRISSP2D* model that need to be overcome in order to make this model practical for ice process modeling. The first thing is that there is a maximum amount of nodes and elements that the model can handle. This affects the accuracy of results because a coarser mesh must be created in order to be able to run the model. It is interesting that given this limit, the model still requires a small time step in order to maintain stability. It was found that it took the model 1 hour of computational time to produce 1.5 hours of real time. Running multiple tests can take several days and running a long model would easily take weeks or even months.

Another disadvantage of the *CRISSP2D* model is that the user's manual lacks details and explanations needed to easily run the model. The user's and programmer's manuals describe each of the input parameters; however, the

explanations of many important functions are left out. Much was learned about the program through trial and error and this proved to be very time consuming. Also, it was found that there are many parameters in the model that simply cannot be calibrated by the user. Some of these parameters could be hard-coded into the model for the sake of ease.

Finally, the model is not a full package that allows the user to create, run and view the model. Input files are created with software that is not included in the program. The *CRISSP2D* model runs on a DOS-based interface and data can only be viewed at specified intervals through an expensive software package called Tecplot. Creating a suitable interface for this model would help to solve these issues and also allow the user to watch the simulation take place.

An excellent legacy data set on freeze-up processes and winter ice conditions was obtained through rigorous field studies. Through the application of this data set, an excellent parametric assessment was conducted on the *CRISSP2D* model. It was used to provide a good critical evaluation of the capabilities of the *CRISSP2D* model in simulating freeze-up processes on a natural unregulated river. It was found that currently no model exists that is capable of achieving full results. As advancements are made to *CRISSP2D* or when the ice process component of *River2D* is fully developed, it is intended that this data will be used for the future validation of 2-D ice process models. Once this is successfully carried out, various scenarios can be simulated to aid in answering the questions of how flow withdrawals affect the winter ice regime.

## 5. References

- Abarca, J N. (2007) Winter Ice Regime of the Lower Athabasca River. A thesis submitted to the Faculty of Graduate Studies and Research in partial fulfillment of the requirements for the degree of Master of Science in Water Resources Engineering. Department of Civil Engineering, University of Alberta, Edmonton, Alberta, 232 pp.
- Andrishak, R. and Hicks, F. (2008). Simulating the Effects of Climate Change on the Winter Regime of the Peace River. *Canadian Journal of Civil Engineering*, Vol. 35, 2008, 461-472.
- Andrishak, R., Abarca, J N., Wojtowicz, A., and Hicks, F. (2008). Freeze-up Study on the Lower Athabasca River (Alberta, Canada). *Proceedings of the 19th IAHR Ice Symposium, Vancouver, Canada*, 1:77-88.
- Beltaos, S. (Ed.). (1995). *River Ice Jams*. Colorado: Water Resources Publications, LLC.
- Conly, F.M., Crosley, R.W., and Headley, J.V. (2002). Characterizing Sediment Sources and Natural Hydrocarbon Inputs in the Lower Athabasca River, Canada. *Journal of Environmental Engineering and Science*, Volume 1, Number 3, June 2002, pp 187 – 199.
- Doyle, P. F. (1977). Hydrologic and Hydraulic Characteristics of the Athabasca River from Fort McMurray to Embarras. Report SWE 77-2, Transportation and Surface Water Engineering Division, Alberta Research Council, Edmonton.
- Healy, D., and Hicks, F. E. (2006). Experimental study of ice jam formation dynamics. *Journal of Cold Regions Engineering*, 20(4), 117-139.
- Hicks, F. E. and Steffler, P.M. (1990). Finite Element Modeling of Open Channel Flow. Water Resources Engineering Report No. 90-6. Department of Civil Engineering, University of Alberta. Edmonton, Alberta.

- Hicks, F. E. and Steffler P.M. (1992). A Characteristic-Dissipative-Galerkin Scheme for Open Channel Flow. *ASCE Journal of Hydraulic Engineering*, Vol. 118, No. 2, 337-352.
- Hicks, F. E. Chen, X. and Andres, D. (1995). Effects of ice on the hydraulics of Mackenzie River at the outlet of Great Slave Lake, N.W.T.: a case study. *Canadian Journal of Civil Engineering*, Vol. 22, 43-54 (1995).
- Katopodis, C. and Ghamry, H. (2005). Ice-covered hydrodynamic simulation: model calibration and comparisons for three reaches of the Athabasca River, Alberta, Canada. *Proceedings of the 13th Workshop on the Hydraulics of Ice Covered Rivers, Committee on River Ice Processes and the Environment, Hanover, New Hampshire*, 455-469.
- Kellerhals, R., Neil, C.R., and Bray, D.I. (1972). Hydraulic and Geomorphic Characteristics of Rivers in Alberta. *River Engineering and Surface Hydrology Report 72-1, Alberta Research Council, Edmonton, Alberta*.
- Liu, L., Tuthill, A. M., and Shen, H. T. (2001). Dynamic simulation of ice conditions in the vicinity of locks and dams. *Proceedings of the 11th Workshop on River Ice, Ottawa, Ontario, Canada*.
- Liu, L., Li, H., and Shen, H.T. (2006). A two-dimensional comprehensive river ice model. *Proceedings of the 18th IAHR Symposium on River Ice, Sapporo, Japan*.
- Malenchak, J, M Morris, HT Shen, and J Doering. (2006). Modeling Anchor Ice Growth at Sundance Rapids. *Proceedings of the 18th IAHR Symposium on River Ice, Sapporo, Japan*.
- Morse, B., and Richard, M. (2009). A field study of suspended frazil ice particles. *Cold Regions Science and Technology*, 55(1), 86-102.

- Robichaud, C. (2003). Hydrometeorological Factors Influencing Breakup Ice Jam Occurrence at Fort McMurray, Alberta. A thesis submitted to the Faculty of Graduate Studies and Research in partial fulfillment of the requirements for the degree of Master of Science in Water Resources Engineering. Department of Civil Engineering, University of Alberta, Edmonton, Alberta, 281 pp.
- Shen, H.T., Su, J., Liu, L., (2000). SPH simulation of river ice dynamics. *Journal of Computational Physics*, 165, 752–770.
- Shen, H. T. (2005a). CRISSP-2D User's Manual. CEATI Report No. T012700-0401. CEA Technologies Inc., Montreal.
- Shen, H. T. (2005b). CRISSP-2D Programmer's Manual. CEATI Report No. T012700-0401. CEA Technologies Inc., Montreal.
- Steffler, P. and Blackburn, J. (2002) River2D: Introduction to Depth Averaged Modeling and User's Manual, [www.river2D.ca](http://www.river2D.ca), 120 pp.
- Van der Vinne, G. and Andres, D. (1993). Winter Low Flow Tracer Dye Studies – Athabasca River. Athabasca to Bitumont, February and March, 1992 – Part I: Time of Travel, Northern River Basins Study Project Report No. 7. Edmonton, Alberta, June 1993.
- Wasantha Lal, A. M., and Shen, H. T. (1991). Mathematical model for river ice processes. *Journal of Hydraulic Engineering*, 117(7), 851-867.
- Woynillowicz, D., and Severson-Baker, C. (2006). Down to the Last Drop - The Athabasca River and Oil Sands, Oil Sands Paper No. 1, The Pembina Institute.
- Ye, S.Q. and J.C. Doering. (2003). A model for the vertical distribution of frazil ice. Proceedings of the 12th Workshop on River Ice, Edmonton, Alberta, Canada.

**Appendix A – Summer Discharge Measurement Output from the  
Acoustic Doppler Current Profiler**

**Discharge Measurement Summary**

Date July 24, 2008

<b>Station Information</b>		<b>Measurement Information</b>	
Station Number	ATH0803	Measurement No.	1
Station Name	Zone 1/2 Boundary	Compiled By	R Andrishak
Location	Athabasca R at Tar Island	Checked By	R Andrishak

<b>Personnel and Equipment</b>	
Party	R Andrishak / A Wojtowicz
Boat/Motor/Platform	C Krath / J Maxwell

<b>Rating Information</b>			
Gage Height	Rating Discharge	Rating No.	
GH Change	Index Velocity	Meas. Rating	
% Diff.	Rated Area	Control Code	
	0.0%		

<b>System Information</b>		<b>System Setup</b>			
Serial #	M509	# of Cells	25	Averaging Interval	5.0
System	3000 kHz	Cell Size	0.20	Magnetic Decl.	0.0
Frequency		Blanking Distance	0.20	Salinity	0.00
Firmware Version	9.6	Transducer Depth	0.06	Echo Sounder	Not Pres.
RiverSurveyor Ver	v4.50				

<b>Discharge Calculation Settings</b>					
Velocity Ref.	BTrack	Top Estimate	Power	Left Bank	Sloped
Track Ref.	BTrack	Bottom Est.	Power	Right Bank	Sloped
Depth Reference	ADP	Area Method	none	Orient. Profiles	all

<b>Computed Discharge Results</b>		<b>Diagnostic Files</b>	
Width	352.9	Moving Bed Test	
Area	875.3	Compass Cal	UA080724130224.compass
Mean Velocity	0.70	Pressure Cal	UA080724104625.pressure
Discharge	609.43	Depth Calibration	UA080724104712.depth
% Measured	72.0		
Adj. Mean	0		
Velocity			

<b>Measurement Results</b>																	
Tr#	Discharge						Distance			Area	Time		Mean Vel		#Profiles		
	Top	Middle	Bottom	Left	Right	Total	Left	Right	Total		Start	End	Boat	Water	Total	Bad	
1	L	96.929	433.64	70.736	0.48634	0.12131	601.92	4.1	1.9	347.5	860.3	13:17	13:24	0.83	0.70	82	0
2	R	97.372	438.14	70.384	0.35809	0.097518	606.35	4.1	1.9	352.3	877.2	13:24	13:32	0.72	0.69	96	0
3	R	99.899	437.97	73.85	0.44722	0.083334	612.25	4.1	1.9	355.6	884.8	13:39	13:47	0.81	0.69	87	0
4	R	99.701	445.1	72.042	0.26631	0.076885	617.19	4.1	1.9	355.2	876.9	13:53	14:00	0.86	0.70	81	0
<b>Mean</b>		98.475	438.71	71.753	0.38949	0.094761	609.43	4.1	1.9	352.9	875.3	<b>Total</b>	00:42	0.81	0.70	87	0
<b>SDev</b>		1.5426	4.7404	1.5695	0.098106	0.019685	6.5859	0.0	0.0	4.0	10.5			0.06	0.01		
<b>COV</b>		0.016	0.011	0.022	0.252	0.208	0.011	0.000	0.000	0.011	0.012			0.075	0.008		

Tr1=UA0807241318.ADP; Tr2=UA0807241325.ADP; Tr3=UA0807241340.ADP; Tr4=UA0807241354.ADP;

**Comments**

 Note: Units for the above parameters are: Distance (m), Velocity (m/s), Area (m<sup>2</sup>), Discharge (m<sup>3</sup>/s)

**Discharge Measurement Summary**

Date July 24, 2008

<b>Station Information</b>		<b>Measurement Information</b>	
Station Number	ATHISL1	Measurement No.	1
Station Name	Island Left Channel	Compiled By	R Andrishak
Location	Athabasca River at Tar Island	Checked By	R Andrishak

<b>Personnel and Equipment</b>		<b>Boat/Motor/Platform</b>	
Party	R Andrishak / A Wojtowicz	Boat/Motor/Platform	C Krath / J Maxwell

<b>Rating Information</b>			
Gage Height	Rating Discharge	Rating No.	
GH Change	Index Velocity	Meas. Rating	
% Diff.	0.0%	Rated Area	Control Code

<b>System Information</b>		<b>System Setup</b>			
Serial #	M509	# of Cells	19*	Averaging Interval	5.0
System	3000 kHz	Cell Size	0.30*	Magnetic Decl.	0.0
Frequency		Blanking Distance	0.20	Salinity	0.00
Firmware Version	9.6	Transducer Depth	0.06	Echo Sounder	Not Pres.
RiverSurveyor Ver	v4.50				

<b>Discharge Calculation Settings</b>					
Velocity Ref.	BTrack	Top Estimate	Power	Left Bank	Sloped
Track Ref.	BTrack	Bottom Est.	Power	Right Bank	Sloped
Depth Reference	ADP	Area Method	none	Orient. Profiles	all

<b>Computed Discharge Results</b>		<b>Diagnostic Files</b>	
Width	128.8	Moving Bed Test	
Area	415.3	Compass Cal	UA080724144314.compass
Mean Velocity	0.89	Pressure Cal	UA080724104625.pressure
Discharge	370.43	Depth Calibration	UA080724104712.depth
% Measured	73.5		
Adj. Mean Velocity	0		

<b>Measurement Results</b>																	
Tr#		Discharge					Distance			Area	Time		Mean Vel		#Profiles		
		Top	Middle	Bottom	Left	Right	Total	Left	Right		Total	Start	End	Boat	Water	Total	Bad
1	L	37.942	237.43	41.943	0.27926	0.37073	317.97	2.6	2.6	119.0	360.1	16:00	16:04	0.69	0.66	39	0
2	R	46.096	262.89	43.342	0.51247	0.35756	352.2	2.5	2.8	128.7	416.4	15:07	15:11	0.60	0.85	41	0
3	L	49.259	291.67	67.773	0.28303	0.35771	399.3	2.6	2.6	126.6	409.7	16:11	16:14	0.73	0.97	33	0
4	R	47.651	269.58	46.419	0.4705	0.314	364.43	2.5	2.8	126.5	391.4	15:14	15:17	0.76	0.93	32	0
5	L	49.514	263.61	62.126	0.20218	0.31074	375.76	2.5	2.8	129.9	408.4	15:17	15:19	0.78	0.92	32	0
6	R	46.326	276.94	50.151	0.17735	0.26653	373.86	2.5	2.8	130.6	417.0	15:19	15:23	0.64	0.90	35	0
7	L	45.738	297.38	61.937	0.30167	0.27862	396.63	2.6	2.6	131.8	436.2	16:23	16:29	0.32	0.92	76	0
8	R	45.136	293.89	49.314	-0.061671	0.23261	391.62	2.6	2.6	142.3	497.3	16:31	16:37	0.37	0.79	74	0
9	L	46.41	265.57	57.706	0.18135	0.31782	360.18	2.5	2.8	124.4	394.3	15:37	15:43	0.35	0.91	68	0
Mean		46.567	272.09	51.19	0.26178	0.31602	370.43	2.5	2.8	128.8	415.3	Total	00:42	0.57	0.89	46	0
SDev		3.5646	19.859	6.8958	0.16739	0.052027	25.835	0.0	0.0	6.2	36.1			0.18	0.05		
COV		0.076	0.073	0.136	0.639	0.165	0.070	0.000	0.000	0.048	0.087			0.315	0.061		

Tr1=UA0807241501.ADP; Tr2=UA0807241508.ADP; Tr3=UA0807241512.ADP; Tr4=UA0807241515.ADP; Tr5=UA0807241518.ADP; Tr6=UA0807241520.ADP; Tr7=UA0807241524.ADP; Tr8=UA0807241532.ADP; Tr9=UA0807241538.ADP;

**Comments**

Note: Units for the above parameters are: Distance (m), Velocity (m/s), Area (m2), Discharge (m3/s)

**Appendix B – Winter Discharge Measurement Output from the Acoustic  
Doppler Current Profiler**

Place your logo here (Put a logo.gif file in your Reports directory)

## Discharge Measurement Summary

Date Generated: Wed Mar 4 2009

### File Information

File Name UA0902271058.sds  
Start Date and Time 27/02/2009 11:01:09

### Site Details

Site Name Transect 4A  
Operator(s) Agata + Chris + Dave

### System Information

Sensor Type 3000 kHz ADP  
Serial # M509  
CPU Firmware Version 9.6  
Software Ver 1.20

### Units

Distance m  
Velocity m/s  
Area m<sup>2</sup>  
Discharge m<sup>3</sup>/s

### Discharge Uncertainty

Category	ISO	Stats
Accuracy	1.0%	1.0%
Depth	0.2%	7.1%
Velocity	0.4%	7.6%
Width	0.2%	0.2%
Method	0.2%	-
# Stations	3.6%	-
<b>Overall</b>	<b>3.8%</b>	<b>10.4%</b>

### Summary

Averaging Int.	60.0	Disch. Equation	Mid-Section
Start Edge	REW	Rated Discharge	150.00
Profile	33x0.15 cells	# Stations	14
Blanking Dist	0.20	Total Width	110.94
Salinity	0 ppt	Total Area	271.09
Azimuth	131.0 deg	Mean Depth	3.00
Start Stage	0.000	Mean Velocity	0.56
End Stage	0.000	<b>Total Discharge</b>	<b>151.59</b>

### Measurement Results

St	Clock	Loc	Depth	IceTh	IceD	Eff.Depth	Angle	MeanV	Area	Flow	%Q
1	11:01	0.00	0.000	0.600	0.600	-0.600	0.0	0.000	0.000	0.0000	0.0
2	11:01	2.35	0.922	0.500	0.460	0.460	59.1	0.029	3.395	0.0969	0.1
3	11:16	14.70	4.000	0.600	0.600	3.400	4.4	0.545	41.055	22.3911	14.8
4	11:03	26.50	1.463	0.550	0.550	0.910	22.8	0.148	9.704	1.4393	0.9
5	11:05	35.97	1.859	0.560	0.560	1.300	29.3	0.146	15.132	2.2109	1.5
6	11:09	49.79	2.433	0.690	0.700	1.730	18.2	0.205	20.069	4.1046	2.7
7	11:12	59.13	3.195	0.650	0.660	2.540	12.2	0.441	19.215	8.4781	5.6
8	11:14	64.95	3.721	0.600	0.580	3.140	9.6	0.513	23.448	12.0239	7.9
9	11:18	74.06	4.260	0.620	0.630	3.630	3.7	0.651	31.998	20.8185	13.7
10	11:20	82.58	4.524	0.540	0.530	3.990	7.0	0.735	28.055	20.6246	13.6
11	11:23	88.11	4.308	0.490	0.500	3.810	1.1	0.820	28.880	23.6903	15.6
12	11:26	97.75	4.059	0.550	0.560	3.500	1.3	0.792	31.230	24.7394	16.3
13	11:28	105.96	3.376	0.510	0.510	2.870	-4.1	0.581	18.902	10.9766	7.2
14	11:28	110.94	0.000	0.600	0.600	-0.600	0.0	0.000	0.000	0.0000	0.0

Report generated using SonTek Stationary Measurement software version 1.20

Place your logo here (Put a logo.gif file in your Reports directory)

# Discharge Measurement Summary

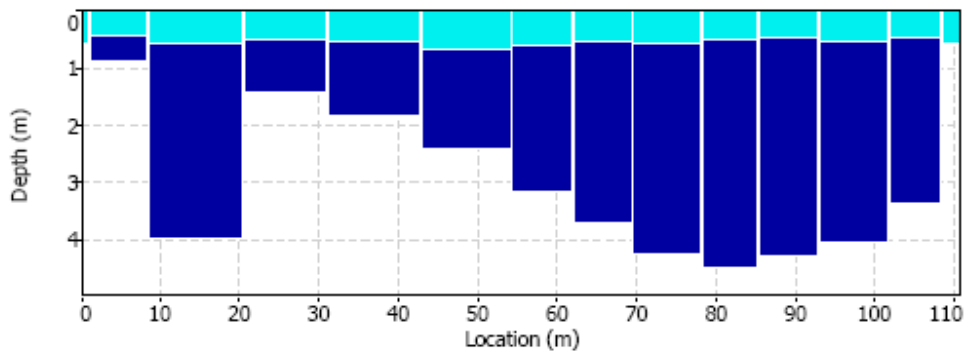
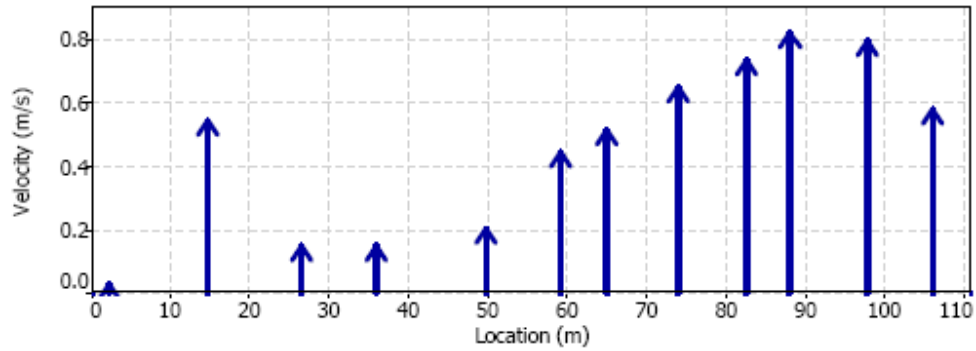
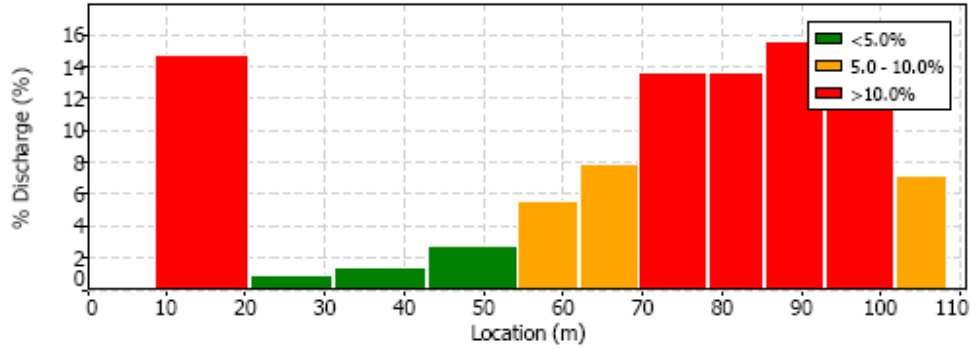
Date Generated: Wed Mar 4 2009

## File Information

File Name UA0902271058.sds  
Start Date and Time 27/02/2009 11:01:09

## Site Details

Site Name  
Operator(s) Agata + Chris + Dave  
Transect 4A



Report generated using SonTek Stationary Measurement software version 1.20

 Place your logo here (Put a logo.gif file in your Reports directory)

## Discharge Measurement Summary

Date Generated: Wed Mar 4 2009

### File Information

File Name UA0902271230.sds  
Start Date and Time 27/02/2009 12:36:10

### Site Details

Site Name Transect 4-A  
Operator(s) Agata + Chris + Dave

### System Information

Sensor Type 3000 kHz ADP  
Serial # M509  
CPU Firmware Version 9.6  
Software Ver 1.20

### Units

Distance m  
Velocity m/s  
Area m<sup>2</sup>  
Discharge m<sup>3</sup>/s

### Discharge Uncertainty

Category	ISO	Stats
Accuracy	1.0%	1.0%
Depth	0.2%	2.1%
Velocity	0.4%	4.0%
Width	0.2%	0.2%
Method	0.2%	-
# Stations	3.6%	-
<b>Overall</b>	<b>3.8%</b>	<b>4.7%</b>

### Summary

Averaging Int.	60.0	Disch. Equation	Mid-Section
Start Edge	REW	Rated Discharge	150.00
Profile	33x0.15 cells	# Stations	14
Blanking Dist	0.20	Total Width	110.94
Salinity	0 ppt	Total Area	274.86
Azimuth	131.0 deg	Mean Depth	3.04
Start Stage	0.000	Mean Velocity	0.52
End Stage	0.000	<b>Total Discharge</b>	<b>143.87</b>

### Measurement Results

St	Clock	Loc	Depth	IceTh	IceD	Eff.Depth	Angle	MeanV	Area	Flow	%Q
1	12:36	0.00	0.000	0.600	0.600	-0.600	0.0	0.000	0.000	0.0000	0.0
2	12:36	2.35	2.147	0.500	0.460	1.690	-65.9	0.036	12.401	0.4403	0.3
3	12:38	14.70	1.456	0.550	0.550	0.910	29.5	0.132	10.941	1.4409	1.0
4	12:40	26.50	1.839	0.560	0.560	1.280	37.7	0.131	13.598	1.7840	1.2
5	12:42	35.97	2.456	0.690	0.700	1.760	20.7	0.234	20.447	4.7759	3.3
6	12:45	49.79	3.212	0.650	0.660	2.550	23.7	0.415	29.552	12.2632	8.5
7	12:47	59.13	3.743	0.600	0.580	3.160	19.3	0.511	23.978	12.2636	8.5
8	12:49	64.95	3.939	0.600	0.600	3.340	23.8	0.524	24.923	13.0554	9.1
9	12:51	74.06	4.308	0.620	0.630	3.680	15.9	0.606	32.420	19.6385	13.7
10	12:58	82.58	4.079	0.550	0.560	3.520	10.7	0.811	24.722	20.0398	13.9
11	12:53	88.11	4.531	0.540	0.530	4.000	16.8	0.693	30.346	21.0366	14.6
12	12:56	97.75	4.283	0.490	0.500	3.780	14.3	0.792	33.761	26.7419	18.6
13	13:04	105.96	3.204	0.510	0.510	2.690	4.7	0.585	17.770	10.3874	7.2
14	13:04	110.94	0.000	0.510	0.510	-0.510	0.0	0.000	0.000	0.0000	0.0

Report generated using SonTek Stationary Measurement software version 1.20

Place your logo here (Put a logo.gif file in your Reports directory)

# Discharge Measurement Summary

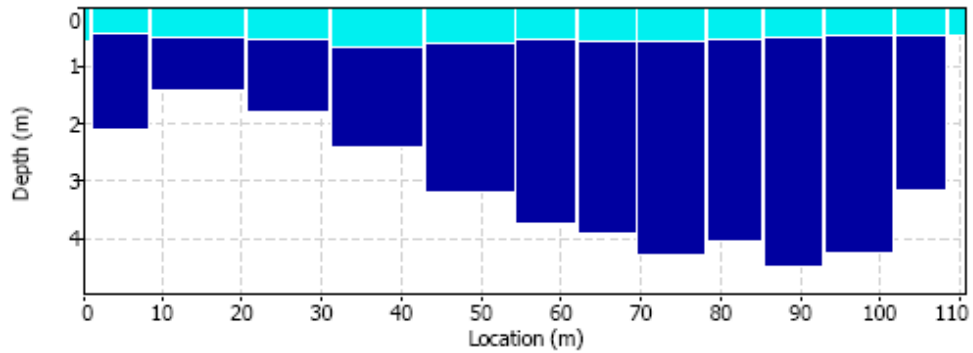
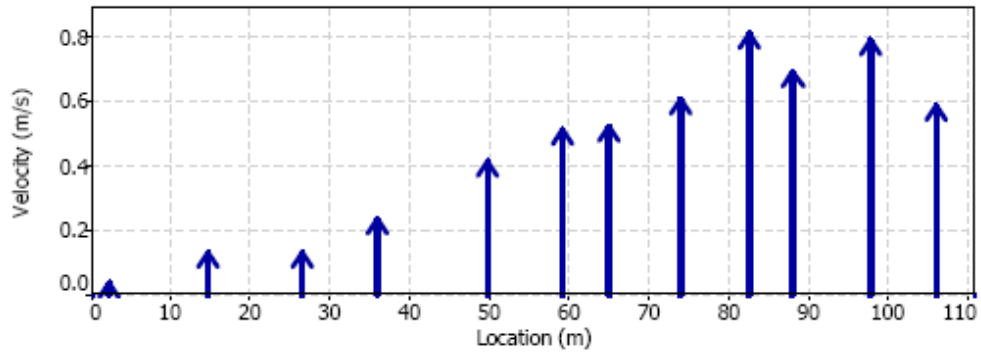
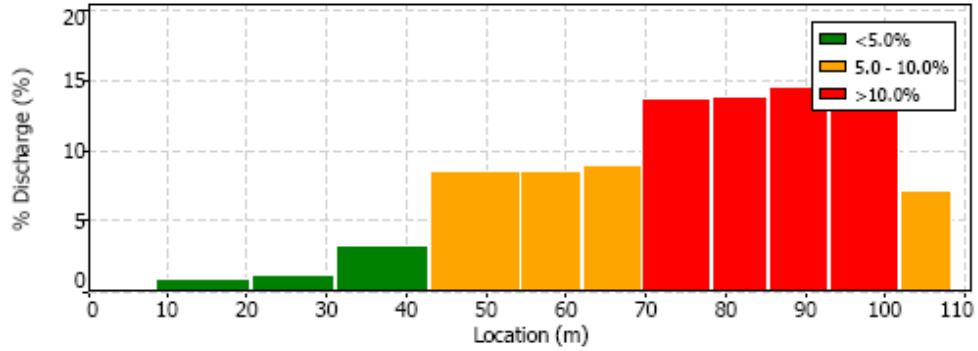
Date Generated: Wed Mar 4 2009

## File Information

File Name UA0902271230.sds  
Start Date and Time 27/02/2009 12:36:10

## Site Details

Site Name  
Operator(s) Agata + Chris + Dave  
Transect 4-A



Report generated using SonTek Stationary Measurement software version 1.20

 Place your logo here (Put a logo.gif file in your Reports directory)

## Discharge Measurement Summary

Date Generated: Wed Mar 4 2009

### File Information

File Name UA0902261314.sds  
Start Date and Time 26/02/2009 13:17:43

### Site Details

Site Name Transect 4 - B  
Operator(s) Agata + Chris + Dave

### System Information

Sensor Type 3000 kHz ADP  
Serial # M509  
CPU Firmware Version 9.6  
Software Ver 1.20

### Units

Distance m  
Velocity m/s  
Area m<sup>2</sup>  
Discharge m<sup>3</sup>/s

### Discharge Uncertainty

Category	ISO	Stats
Accuracy	1.0%	1.0%
Depth	0.2%	6.5%
Velocity	3.6%	8.2%
Width	0.2%	0.2%
Method	1.4%	-
# Stations	5.8%	-
<b>Overall</b>	<b>7.0%</b>	<b>10.6%</b>

### Summary

Averaging Int.	60.0	Disch. Equation	Mid-Section
Start Edge	LEW	Rated Discharge	25.00
Profile	14x0.15 cells	# Stations	9
Blanking Dist	0.20	Total Width	134.13
Salinity	0 ppt	Total Area	97.71
Azimuth	126.5 deg	Mean Depth	1.25
Start Stage	0.000	Mean Velocity	0.14
End Stage	0.000	<b>Total Discharge</b>	<b>13.83</b>

### Measurement Results

St	Clock	Loc	Depth	IceTh	IceD	Eff.Depth	Angle	MeanV	Area	Flow	%Q
1	13:18	0.00	0.000	0.600	0.600	-0.600	0.0	0.000	0.000	0.0000	0.0
2	13:18	8.86	1.184	0.530	0.540	0.640	50.8	0.089	7.617	0.6769	4.9
3	13:20	23.66	1.394	0.590	0.590	0.800	69.9	0.027	14.789	0.4049	2.9
4	13:26	45.64	0.855	0.530	0.530	0.320	45.3	0.072	6.676	0.4838	3.5
5	13:28	64.78	1.184	0.570	0.590	0.590	51.5	0.143	11.084	1.5870	11.5
6	13:30	82.95	1.460	0.550	0.570	0.890	50.4	0.191	16.745	3.2067	23.2
7	13:33	102.41	1.799	0.560	0.540	1.260	40.3	0.215	24.164	5.1906	37.5
8	13:35	121.34	1.699	0.640	0.650	1.050	45.6	0.137	16.631	2.2833	16.5
9	13:35	134.13	0.000	0.700	0.700	-0.700	0.0	0.000	0.000	0.0000	0.0

Report generated using SonTek Stationary Measurement software version 1.20

Place your logo here (Put a logo.gif file in your Reports directory)

# Discharge Measurement Summary

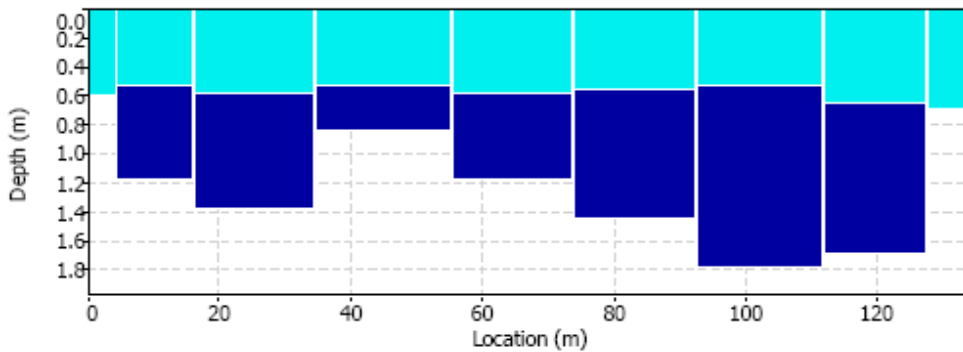
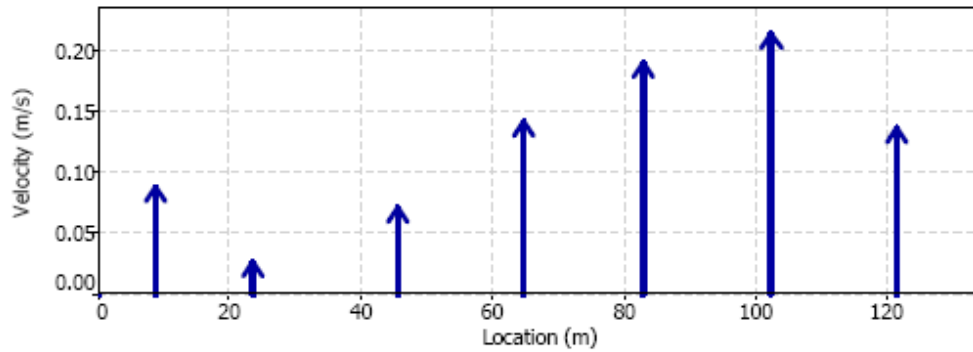
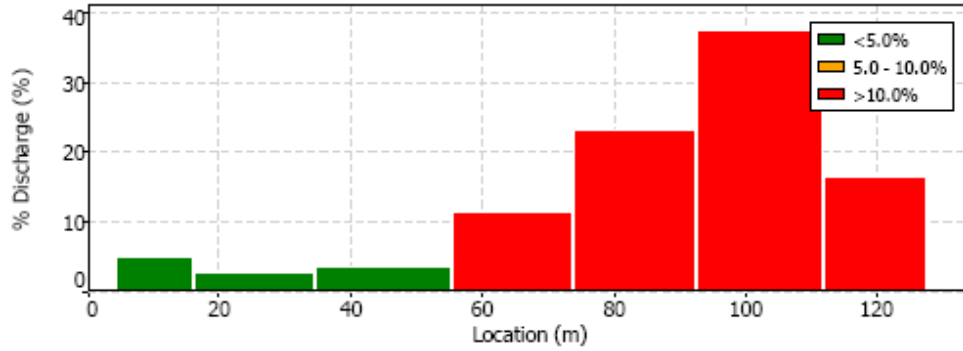
Date Generated: Wed Mar 4 2009

## File Information

File Name UA0902261314.sds  
Start Date and Time 26/02/2009 13:17:43

## Site Details

Site Name Transect 4 - B  
Operator(s) Agata + Chris + Dave



Report generated using SonTek Stationary Measurement software version 1.20

 Place your logo here (Put a logo.gif file in your Reports directory)

## Discharge Measurement Summary

Date Generated: Wed Mar 4 2009

### File Information

File Name UA0902261343.sds  
Start Date and Time 26/02/2009 13:47:21

### Site Details

Site Name Transect 4 - B  
Operator(s) Agata + Chris + Dave

### System Information

Sensor Type 3000 kHz ADP  
Serial # M509  
CPU Firmware Version 9.6  
Software Ver 1.20

### Units

Distance m  
Velocity m/s  
Area m<sup>2</sup>  
Discharge m<sup>3</sup>/s

### Discharge Uncertainty

Category	ISO	Stats
Accuracy	1.0%	1.0%
Depth	0.2%	4.8%
Velocity	3.4%	9.3%
Width	0.2%	0.2%
Method	1.3%	-
# Stations	5.8%	-
<b>Overall</b>	<b>6.9%</b>	<b>10.5%</b>

### Summary

Averaging Int.	60.0	Disch. Equation	Mid-Section
Start Edge	LEW	Rated Discharge	25.00
Profile	14x0.15 cells	# Stations	9
Blanking Dist	0.20	Total Width	134.13
Salinity	0 ppt	Total Area	101.00
Azimuth	126.5 deg	Mean Depth	1.28
Start Stage	0.000	Mean Velocity	0.15
End Stage	0.000	<b>Total Discharge</b>	<b>15.45</b>

### Measurement Results

St	Clock	Loc	Depth	IceTh	IceD	Eff.Depth	Angle	MeanV	Area	Flow	%Q
1	13:47	0.00	0.000	0.500	0.500	-0.500	0.0	0.000	0.000	0.0000	0.0
2	13:47	8.86	1.197	0.530	0.540	0.660	55.4	0.068	7.775	0.5279	3.4
3	13:50	23.66	1.390	0.590	0.590	0.800	17.8	0.063	14.712	0.9316	6.0
4	13:53	45.64	1.015	0.530	0.530	0.490	57.5	0.076	9.972	0.7615	4.9
5	13:55	64.78	1.181	0.570	0.590	0.590	46.2	0.205	11.027	2.2556	14.6
6	13:57	82.95	1.444	0.550	0.570	0.870	54.7	0.184	16.447	3.0320	19.6
7	13:59	102.41	1.819	0.560	0.540	1.280	49.2	0.192	24.559	4.7271	30.6
8	14:01	121.34	1.691	0.640	0.650	1.040	42.3	0.195	16.503	3.2122	20.8
9	14:01	134.13	0.000	0.700	0.700	-0.700	0.0	0.000	0.000	0.0000	0.0

Report generated using SonTek Stationary Measurement software version 1.20

Place your logo here (Put a logo.gif file in your Reports directory)

# Discharge Measurement Summary

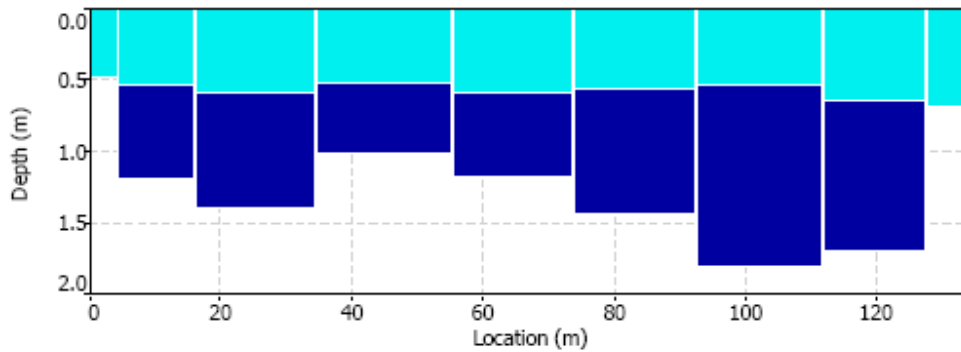
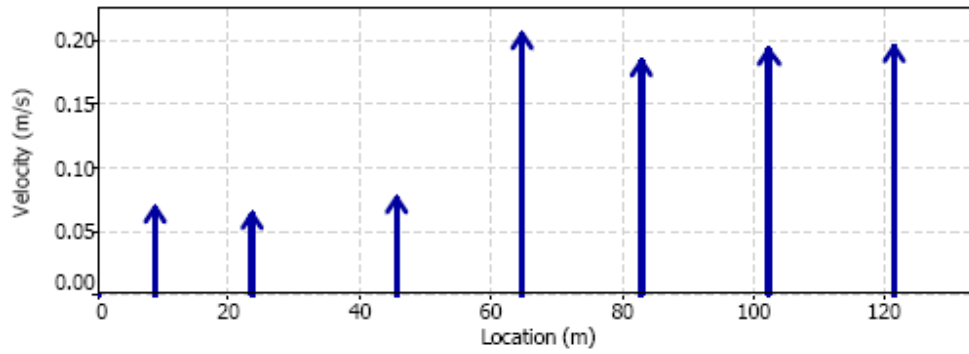
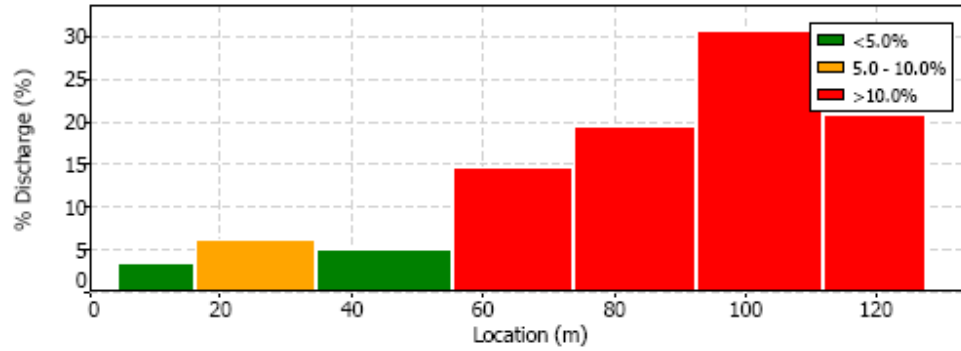
Date Generated: Wed Mar 4 2009

## File Information

File Name UA0902261343.sds  
Start Date and Time 26/02/2009 13:47:21

## Site Details

Site Name Transect 4 - B  
Operator(s) Agata + Chris + Dave



Report generated using SonTek Stationary Measurement software version 1.20

Place your logo here (Put a logo.gif file in your Reports directory)

## Discharge Measurement Summary

Date Generated: Wed Mar 4 2009

### File Information

File Name UA0902241416.sds  
Start Date and Time 24/02/2009 14:22:11

### Site Details

Site Name Transect 2  
Operator(s) Agata\_Chris\_Dave

### System Information

Sensor Type 3000 kHz ADP  
Serial # M509  
CPU Firmware Version 9.6  
Software Ver 1.20

### Units

Distance m  
Velocity m/s  
Area m2  
Discharge m3/s

### Discharge Uncertainty

Category	ISO	Stats
Accuracy	1.0%	1.0%
Depth	0.2%	5.8%
Velocity	0.6%	6.0%
Width	0.2%	0.2%
Method	0.3%	-
# Stations	3.6%	-
<b>Overall</b>	<b>3.8%</b>	<b>8.5%</b>

### Summary

Averaging Int.	60.0	Disch. Equation	Mid-Section
Start Edge	REW	Rated Discharge	150.00
Profile	33x0.15 cells	# Stations	14
Blanking Dist	0.20	Total Width	202.91
Salinity	0 ppt	Total Area	362.29
Azimuth	75.7 deg	Mean Depth	2.35
Start Stage	0.000	Mean Velocity	0.42
End Stage	0.000	<b>Total Discharge</b>	<b>152.57</b>

### Weather

sunny, -30, light wind

### Measurement Results

St	Clock	Loc	Depth	IceTh	IceD	Eff.Depth	Angle	MeanV	Area	Flow	%Q
1	14:22	0.00	0.000	0.500	0.500	-0.500	0.0	0.000	0.000	0.0000	0.0
2	14:22	14.91	1.224	0.490	0.540	0.680	8.9	0.209	10.758	2.2528	1.5
3	14:26	31.46	1.983	0.620	0.680	1.300	15.8	0.268	19.030	5.0985	3.3
4	14:29	44.13	2.457	0.720	0.740	1.720	12.9	0.302	30.768	9.2946	6.1
5	14:37	67.30	3.769	0.590	0.600	3.170	22.6	0.533	62.834	33.5104	22.0
6	14:42	83.78	2.651	0.630	0.640	2.010	25.4	0.500	35.888	17.9459	11.8
7	14:45	103.00	2.401	0.550	0.580	1.820	16.9	0.446	30.481	13.5965	8.9
8	14:49	117.25	2.163	0.550	0.610	1.550	28.9	0.364	23.657	8.6075	5.6
9	14:40	133.46	3.413	0.620	0.640	2.770	22.6	0.569	34.306	19.5223	12.8
10	14:31	141.99	2.651	0.500	0.570	2.080	17.9	0.413	21.786	9.0028	5.9
11	14:34	154.40	3.015	0.600	0.590	2.420	14.3	0.469	28.478	13.3547	8.8
12	14:51	165.48	2.424	0.600	0.640	1.780	21.4	0.314	19.111	5.9923	3.9
13	14:53	175.82	3.155	0.760	0.740	2.410	15.3	0.318	45.192	14.3921	9.4
14	14:53	202.91	0.000	0.600	0.600	-0.600	0.0	0.000	0.000	0.0000	0.0

Report generated using SonTek Stationary Measurement software version 1.20

Place your logo here (Put a logo.gif file in your Reports directory)

# Discharge Measurement Summary

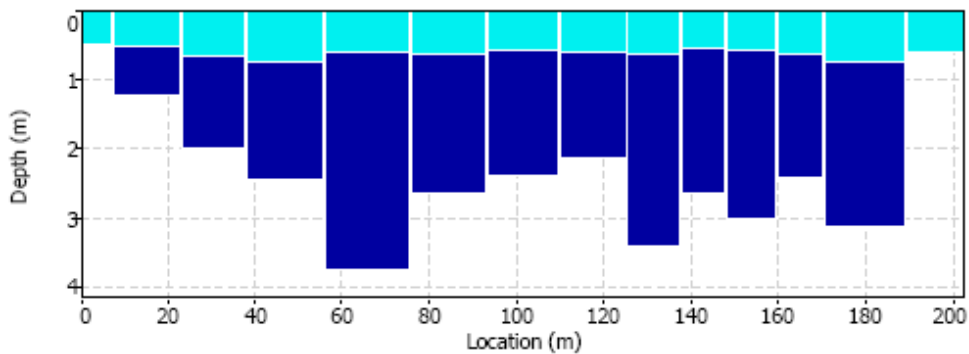
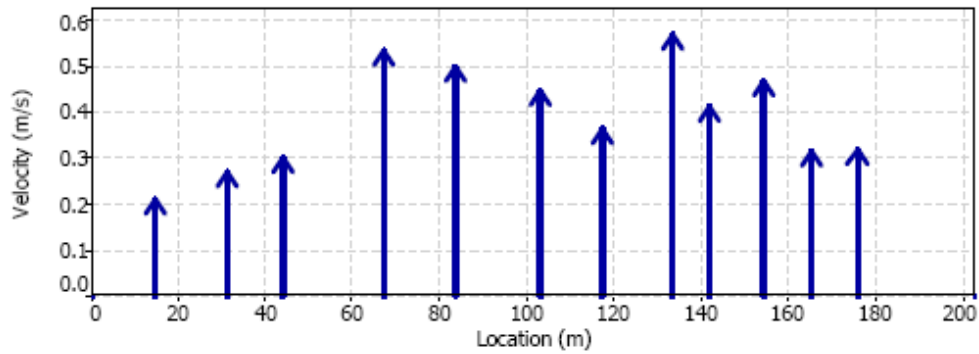
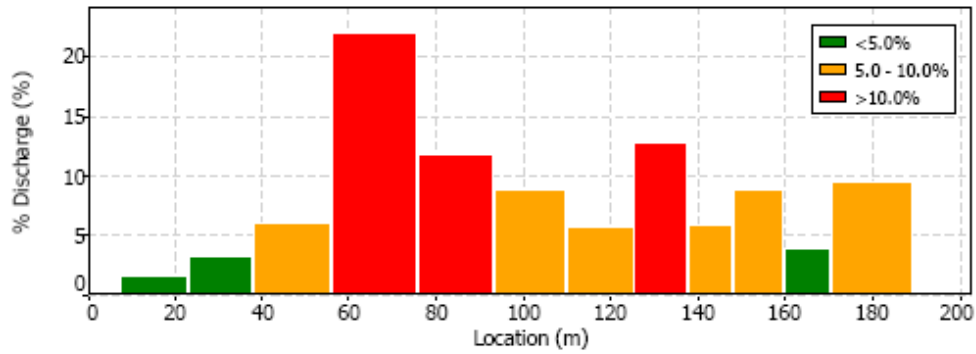
Date Generated: Wed Mar 4 2009

## File Information

File Name UA0902241416.sds  
Start Date and Time 24/02/2009 14:22:11

## Site Details

Site Name Transect 2  
Operator(s) Agata, Chris, Dave



Report generated using SonTek Stationary Measurement software version 1.20